MICROSTRUCTURE AND PROPERTIES OF ULTRA LOW CARBON BAINITIC STEEL WELD METAL FOR HSLA-100

Daya Singh

B.Tech. Institute of Technology, Banaras Hindu University, India, 1978

M.S. Indian Institute of Technology, Madras, India, 1984

A dissertation submitted to the faculty of
the Oregon Graduate Institute of Science & Technology
in partial fulfillment of the requirements for the degree of
Doctor of Philosophy
in
Materials Science and Engineering

January 1996

The dissertation ***"Microstructure and Properties of Ultra Low Carbon Bainitic Steel Weld Metal for HSLA-100"*** by Daya Singh has been examined and approved by the following Examination Committee:

Jack H. Devletian, Thesis Advisor
Professor

William E. Wood
Professor, Department Chairman

Paul Clayton
Professor

David G. Atteridge
Professor

James D. Parsons
Associate Professor

ACKNOWLEDGEMENT

I would like to acknowledge the U.S. Navy Manufacturing Technology Program, Office of Naval Research and the Oregon Graduate Institute of Science and Technology, for making this work possible. Thanks are due to my thesis committee members, Prof. Jack H. Devletian, Prof. William E. Wood, Prof. Paul Clayton, Prof. David G. Atteridge and Dr. James D. Parsons. Thanks are also due to the staff and students of the Materials Science and Engineering Department. Finally I wish to thank my wife Harvinder Kaur, without her patience and understanding I would not have been able to do this work.

TABLE OF CONTENTS

LIST OF TABLES

LIST OF FIGURES

ABSTRACT

Traditionally, carbon has been one of the most effective contributors to strength in structural steels. However, increasing the weld metal carbon content is known to increase; (1) the susceptibility to hydrogen assisted cracking (HAC) and (2) sensitivity to cooling rate. Similarly, for ultra low carbon contents, the weld metal strength does not decrease with increasing heat input. Steels with sufficiently low carbon levels are readily weldable without preheat, whereas, steels with similar carbon equivalent numbers, but higher carbon levels require preheating. The low carbon copper-precipitation strengthened HSLA-100 type steels can attain the strength and toughness levels of the higher carbon HY-100 quenched and tempered steels without the need for preheating. However, filler metals specifically designed to take advantage of welding without preheat for the HSLA-100 type steels have not yet been developed. The susceptibility of the weld metal to HAC in the current commercially available filler wires necessitates costly preheating.

The purpose of this work was to characterize the strength, toughness and microstructure of Ultra Low Carbon Bainitic (ULCB) steel weld metal deposits and to demonstrate that ULCB steel filler metal can be used to weld HSLA-100 without preheating, while meeting the stringent requirements for weld metal strength and toughness. Gas tungsten arc welding (GTAW) and gas metal arc welding (GMAW) was carried out on HSLA-100 using ULCB steel filler metal to evaluate the weld metal strength, toughness and microstructure. GTA welds were deposited on 12 mm (0.5 in) thick plates machined from 13 vacuum induction melted (VIM) ingots and

one argon oxygen decarburized (AOD) ingot using matching filler metal at 3.5 kJ/mm (90 kJ/in) and 2 kJ/mm (51 kJ/in) heat input, with cooling times from 800 to 500°C (t_{8-5}) of 35 s and 15 s, and cooling rates at 538°C (1000°F) of 6°C/s (11°F/s) and 18°C/s (32°F/s), respectively. Ar-5%CO_2, Ar and Ar-25%He were used as shielding gases. GMA welds on HSLA-100 plate and GTA welds on matching VIM plate were made using 1.6 mm (1/16 in.) diameter wires of three different compositions with Ar-5%CO_2 shielding gas. The GMA welding parameters were adjusted to attain same cooling rates as GTA welds.

Weld metal tensile, hardness and Charpy V notch (CVN) toughness testing as well as microstructural studies using transmission electron microscopy were conducted. GTA weld metal deposited with a 4.8 Ni-2.4 Mo alloy using Ar-5%CO_2 at 3.5 kJ/mm (90 kJ/in) attained a yield strength of 733 MPa (106 ksi) and an average CVN absorbed energy value of 73 J (53.8 ft-lb) at -51°C (-60°F). A second filler metal alloy (1.2 Mn-4.6 Ni-0.5 Mo) also met the mechanical property requirements for HSLA-100 weld metal. There was no significant variation in CVN toughness values of the GMA and GTA weld metal deposited using same shielding gas and filler wire under identical cooling rates. Depending on the alloy content, microstructures varied from granular bainite with no evidence of laths, to carbide free bainite with well developed laths. Laths traversed across the prior austenite grains but did not have an appreciable effect on the CVN toughness of the weld metal. Because ULCB weld metal was relatively insensitive to cooling rate, good strength and toughness could be maintained for a t_{8-5} as long as 35 seconds. No decrease in strength was

observed at the higher weld heat input. The absence of second phase particles and inclusions was found to be the most effective factor for maintaining high toughness. Unlike conventional high strength weld metals, the toughness and strength of ULCB weld metal did not have a strong dependence on either the grain size or the lath width, and the weld metal inclusions did not have a marked effect on austenite decomposition products.

In conclusion, ULCB steel weld metal is capable of achieving 690 MPa (100 ksi) yield strength and CVN toughness greater than 61 J (45 ft-lb) at -51°C (-60°F). In addition, no preheating is necessary to make sound welds and ULCB weld metal is insensitive to cooling rate. Additional work is needed to characterize and optimize ULCB filler metals for commercial application.

I. INTRODUCTION

Use of high strength steels results in substantial weight savings in structures. The martensitic quenched and tempered steels of HY-100 type have been extensively used in fabrication of ships and off shore structures. Since the strength of martensite is mainly controlled by the carbon content and its toughness by the tempering temperature, these steels require high carbon content to achieve strength and toughness.[1,2] However, increasing carbon in the weld metal as well as in the heat affected zone (HAZ) is known to increase the susceptibility to hydrogen assisted cracking (HAC). Steels with sufficiently low carbon levels are readily weldable with no or minimal preheat, where as steels with similar carbon equivalent numbers, but higher carbon levels require preheating.[3] The HY-100 type quenched and tempered steels with higher carbon levels have been gradually replaced by the lower carbon copper precipitation strengthened HSLA-100 type steels that can attain the strength and toughness levels of the HY-100 type quenched and tempered steels.[4]

Most filler wires for welding high strength steels were developed for quenched and tempered steels. These wires have a relatively limited heat input range and require preheating. Holsberg and Wong[5] carried out extensive weldability testing of HSLA-100 type steels using the HY-100 type consumables. They identified the susceptibility of the weld metal to HAC as, "the weak link of the weldment system." The strength of the weld metal deposited using the existing commercial filler wires was shown to increase linearly with decreasing heat input, thereby, imposing a limit on the useful heat input range. Limited heat input range and requirement of

preheating hamper productivity and increase the cost of fabrication. Welding consumables specifically designed to take advantage of lower or no preheat required for welding the HSLA-100 type steels have not yet been developed.

Tensile strength, and to a greater degree impact toughness of structural steel weld metal primarily depends on the weld metal microstructure,[6,7] which in turn is controlled by the final composition of the weld metal and the cooling rates attained for particular welding conditions.[8] Filler wire composition, extent of dilution from the parent plate and welding process determine the final composition of the weldmetal. Heat input, thickness of the plate and joint configuration determine the cooling rate.[9] In wrought steel plates, bainitic/martensitic microstructures and/or precipitation strengthening are utilized to attain high strength. Since steel plates can be subjected to mechanical and thermal processing, it is relatively easy to attain the required toughness. Weld metal can not be easily and economically subjected to such treatments.

Carbon is a major contributor to the carbon equivalent values, and increases the maximum attainable heat affected zone (HAZ) hardness. Carbon is also responsible for formation of martensite-austenite (M-A) islands and carbides, that are reported to have a deleterious effect on toughness.[10,11] At very low carbon levels, the ability to form martensite in low alloy steel is markedly reduced and the difference in strength between martensite and bainite becomes negligible.[12] As carbon level approaches very low values the bainite nose moves to the left, enabling formation of bainite in ultra low carbon bainitic (ULCB) steels over a wide range of

cooling rates. In wrought steel plates strength levels above 690 MPa (100 ksi) have been achieved by substitutional solid solution strengthening in virtual absence of carbon.[13,14] McEvily et al.,[13] emphasized the importance of low carbon and cleanliness for improving the toughness of wrought steel plates. One of their alloys with 3%Ni, 3%Mo, 0.7%Mn and 0.03%C achieved an as-rolled yield strength of 770 MPa (112 ksi). Garcia et al.,[14] have also attained strength levels above 690 MPa (100 ksi) in ultra low carbon bainitic (ULCB) wrought steel plates with 1%Mn, 3%Ni and 3%Mo as solid solution strengtheners. The high toughness of these steels was attributed to a low level of interstitial atoms, absence of second phase particles and fine grain size afforded by thermomechanical processing. Strengthening due to the dislocation substructure is reported to have a less deleterious effect on impact toughness.[15,16]

Ductile to brittle transition (DBT) in alpha iron is a function of grain size, the friction on a free dislocation, strength of dislocation locking and the degree of triaxiality of applied stress.[17] An addition of up to 0.02% carbon or nitrogen to iron causes a 55.5 MPa (8.05 ksi) increase in flow stress per 0.01 wt%, measured at 18°C. Carbon/nitrogen exhibit the strongest per wt% strengthening effect of all the conventional alloying elements in steel.[18] Petch,[17] demonstrated that strength of dislocation locking due to nitrogen is appreciably greater than that of the carbon, indicating a more deleterious effect of nitrogen on DBT temperature. Allen et al.,[19] reported that carbides appeared in air cooled steels with carbon levels above 0.013%, causing a rapid rise in the DBT temperature. Carbon and nitrogen help form

martensite-austenite (M-A) islands and carbonitrides in the matrix, that act as crack nucleation sites, adversely affecting the impact toughness.[20]

Acicular ferrite is capable of achieving high toughness. However, acicular ferrite is sensitive to alloy content and cooling rate, and requires a very precise balance of Al, Ti, B, O and N in the weld metal.[21,22] These limitations restrict the heat input range and also limit the maximum attainable yield strength of the weld metal.[23] The higher carbon bainitic/martensitic weld metal is also limited by it's susceptibility to HAC and its narrow heat input range.[5]

To overcome the limitations of commercially available consumables, a new approach, similar to the one employed for the design of ULCB wrought steels, comprising of a virtual absence of carbon and relatively higher substitutional alloying element content was adopted for steel weld metal with yield strength in excess of 690 MPa (100 ksi). Since an extremely low carbon level in the weld metal offers advantages in terms of high resistance to HAC, thereby eliminating the need for preheating and potential for improved toughness at low temperatures, ULCB steels remain relevant for weld metal applications where high strength and good low temperature toughness is required. The focus of this study was to characterize the microstructural features of ULCB steel weld metal and understand the relationships between various morphologies of bainite in ULCB weld metal and the mechanical properties viz., tensile strength and toughness.

One of the most important factors for improved toughness of ULCB steels is the absence of second phase particles (carbides and oxides). The conventional

shielding gases for GMAW of steels contain oxygen or CO_2 causing oxide inclusion formation in the weld metal. Thus the effect of different shielding gases on the toughness of ULCB weld metal was also studied.

The objectives of this investigation were to:

(1) Develop an ultra low carbon alloy system capable of meeting the following requirements in the GTA and GMA weld metal;

a. Yield strength levels of > 690 MPa (100 ksi).

b. Good low temperature toughness of > 61 J (45 ft-lb) at -51°C.

c. Insensitivity to cooling rate.

d. Good weldability with no preheating.

(2) Characterize the microstructure of ultra low carbon steel weld metal.

(3) Study the effect of microstructure on mechanical properties of ultra low carbon steel weld metal.

(4) Study the effect of shielding gas with nil oxygen potential on the toughness of ultra low carbon steel weld metal.

II. LITERATURE SURVEY

A review of the literature of relevance to the current work is given in this chapter. Weld metal solidification structure, austenite decomposition products viz, grain boundary ferrite and ferrite side plates, acicular ferrite and bainite, kinetics of bainitic transformation, mechanical properties and effects of alloying elements on mechanical properties of bainite are discussed in this section.

WELD METAL SOLIDIFICATION STRUCTURE

Generally in the case of low alloy welds, the base plate melts from austenite and after dilution with low carbon filler metal resolidifies as delta ferrite.[23-25] Reheating by subsequent passes does not alter the solidification structure i.e., has no effect on the segregation that occurs during solidification.[26] Solidification begins with epitaxial growth of delta ferrite from the grains of the parent plate, at the fusion line.[11,23] Large thermal gradients at the solid liquid interface result in cellular solidification with columnar delta ferrite grains having major axis roughly parallel to the direction of maximum heat flow.[27] Since the orientation of temperature isotherms changes with time due to a moving heat source, the major growth direction of the austenite is found to be somewhat different from that of delta ferrite grains.[28] Shape and size of austenite grains is of importance to the evolution of the final microstructure.[29] Although the factors controlling the austenite grain size in steel welds are not very clear,[30] it is believed that oxide inclusions in steel welds control the austenitic grain size by Zener pinning of the grain boundaries.[23,31-34] However

some researchers claim that austenite grain size is independent of the oxygen content of the weld metal.[11,35,36] Crystallographic texture of the plate also determines the austenitic grain size, grains with <100> direction parallel to the direction with maximum rate of heat flow grow rapidly. Austenitic grain size was found to be clearly different between two welds deposited on faces mutually at right angles on the same base plate.[37]

Austenite on further cooling may transform into various morphologies of ferrite, bainite, or martensite or a combination of these with some retained austenite.[38] According to Choi and Hill,[39] transformation temperatures for low alloy steels lie in the following general range.

a. Grain boundary nucleated ferrite forms between 1000 and 650°C.

b. Ferrite side plates (separated by low angle grain boundaries) form between 750 to 650°C, and are also nucleated at austenite grain boundaries

c. Fine grained acicular ferrite forms approximately below 650°C, within the austenite grains.

d. Lath microstructures, which can be a mixture of bainite and martensite, and have high dislocation densities, form below 650°C

All the above ranges show some dependence on composition.

GRAIN BOUNDARY FERRITE AND FERRITE SIDE PLATES

On cooling below Ar_3, primary ferrite is the first to form on the columnar austenite grain boundaries in low alloy welds. It quickly covers the grain boundary

surfaces, while subsequent growth into the grains is comparatively slower.[36,40] Dallam and Olson,[41] have shown that thickness of primary ferrite layers in welds does not depend on the austenite grain size. In parent steel plate it is reported to form with equilibrium carbon content but the growth rate is carbon diffusion controlled.[42,43] There is no change in the concentration of the substitutional alloying elements across the interface.[44] Ferrite side plates or Widmanstatten ferrite forms almost isothermally and extends into the austenite grains. The presence of boron on the austenite grain boundaries lowers the free energy of the grain boundaries and suppresses nucleation of primary ferrite.[45]

ACICULAR FERRITE

Acicular ferrite is commonly observed in low alloy steel welds. Relatively high strength and toughness makes it commercially important. If the conditions are favorable acicular ferrite may be the next phase to form. Acicular ferrite has the morphology of thin lenticular plates and two dimensional sections appear like sections of a plate typically about 10μm long and 1μm wide.[29] Acicular ferrite nucleates at the complex multiphase inclusions, entrapped at the delta ferrite interface during welding.[39,46-50] Bhadeshia and other workers have shown evidence of autocatalytic nucleation, and claim that one to one correspondence between inclusions and number of acicular ferrite plates is not expected.[48,51]

Ricks, et al.,[48] have reported that acicular ferrite grows by ledge mechanism from their observation of stepped growth fronts of the laths of acicular ferrite,

indicating nucleation and diffusion controlled growth, consistent with that of primary ferrite. Other workers claim that growth of acicular ferrite is diffusionless with carbon partitioning into austenite after the transformation has taken place; also, acicular ferrite is contained within the bainitic nose in T.T.T. diagrams.[7] Bhadeshia, et al.,[52] claim that bainite and acicular ferrite are identical and difference in morphology is because of difference in nucleation sites. Growth of acicular ferrite is stifled by impingement between plates nucleated independently. They have obtained bainite and acicular ferrite under identical isothermal transformation conditions in the same steel, with different grain sizes. Finer grained material formed bainite and coarser grained material formed acicular ferrite. Some work has been done on steels with controlled oxide additions (particle size 2μm), that are capable of forming acicular ferrite in the grain coarsened HAZ.[53,54] Finer austenite grains also mean higher amounts of grain boundary ferrite resulting in carbon enrichment of untransformed austenite which slows down the acicular ferrite nucleation rate leading to coarser acicular ferrite.[29]

Extensive work has been done by Evans[55] and others[33,56] on the effect of composition on the formation of acicular ferrite. The volume fraction of acicular ferrite goes through a maximum as a function of C, Cr, Mo. Since the carbon content of these steels is relatively low, effect of carbon may only be kinetic rather than thermodynamic. Other alloying elements (Mn, Ni, Mo, Cr, B) inhibit the formation of grain boundary ferrite thereby increasing the volume percent of acicular ferrite. Further increase in alloy content increases the hardenability suppressing the

formation of acicular ferrite. It is generally recognized that about 1.4-1.8% Mn, 3-5% Ni, up to 0.5%Mo, 0.2-0.3% Si help provide fine acicular ferrite microstructures with good CVN toughness values.

a. Role of Inclusions

Ricks, et al.,[48] have demonstrated theoretically that inclusions are less effective in nucleating ferrite compared to austenite grain boundaries and also larger inclusions are expected to be effective in nucleating ferrite. However nucleation of acicular ferrite is associated with inclusions and following four mechanisms are proposed in the literature

(i) Inclusions act as inert nucleation sites and nucleation at inclusions is followed by sympathetic nucleation.[48]

(ii) Nucleation takes place at inclusions having good lattice matching with ferrite.[57]

(iii) Inclusions cause local inhomogeneity in the austenite matrix which may cause nucleation of ferrite.[58]

(iv) The difference in thermal contraction between matrix and inclusions results in favorable array of dislocations or strain fields which act as nucleation sites for ferrite.[59]

b. Effect of Ti, Al, B, N, O

There is considerable circumstantial evidence that titanium oxides (TiO,TiO2,TiO3) are very potent in nucleating ferrite.[60] There must be some oxygen left over in the weld metal to form titanium oxides, after Al present in the weld metal has been oxidized. Aluminum content should be kept as low as possible to minimize the amount of oxygen required.[60,61] Some studies[62] indicate that nitrogen has no direct influence on the acicular ferrite content of the weld metal, whereas others[63] indicate alteration in microstructure as a function of nitrogen concentration. Hori et al.,[60] and others[64] indicate that nitrogen is not likely to influence microstructure in the absence of boron. Stoichiometry of Al,Ti,B,N,O should be maintained such that 3-5 ppm of boron is left uncombined to suppress the formation of grain boundary ferrite.[60] In larger grained steels Boron is reported to have adverse effect on the hardenability because more boron carbonitrides get trapped within the prior austenite grains.[45]

The amount of acicular ferrite formed shows a marked dependence on cooling rate. According to Harrison, et al.,[65] a reduction in cooling rate from 75°C/sec to 20°C/sec caused a 60% decrease in the amount of acicular ferrite. Although there exists an identifiable optimum level of major (C,Mn,Ni,Mo) and minor (Al,Ti,B,O,N) alloying elements for improved toughness of acicular ferrite, the dominant effect is that of the acicular ferrite lath size. The high angle grain boundaries between ferrite laths provide very small mean crack path.[32,66,67]

BAINITE

During the late twenties Davenport and Bain[68] discovered a new microstructure consisting of an "acicular dark etching aggregate". It was later named Bainite in the honor of Dr. E.C. Bain. Bainite transformed at higher temperatures was called Upper Bainite and the one transformed at lower temperatures was called Lower Bainite.[69] Both upper and lower bainite consist of bundles of plates or laths which are usually designated as sheaves or packets.[70,71] Aspect ratio (width/length) of packets decreases with decreasing temperature but is not sensitive to the amount of substitutional solid solution alloying elements for the majority of low alloy steels.[12,72,73] The packet width decreases with lower transformation temperature.[74,75] Laths are formed parallel to the close packed direction of ferrite which is approximately parallel to a close packed direction of the parent austenite.[76] It is not clearly understood why the laths form, however, lower transformation temperatures seem to favor the formation of laths.[76-82] Bainitic laths have low angle grain boundaries between them and may also be partly or completely separated from each other by an aggregate of retained austenite, martensite and/or carbides, or carbides and ferrite. Austenite grain size and the bainitic packet size do not have any effect on the lath width.[75,83] Laths do not cross the parent austenite grain boundaries.

No long range redistribution of substitution alloying elements (Cr, Mn, Mo, Ni, and Si) takes place during the growth of bainitic ferrite.[84-89] At transformation temperatures above 600°C some segregation of substitutional alloying elements in allotriomorphic ferrite has been reported.[84] Because of extremely fast diffusion

rates of interstitial atoms it is not possible to observe the behavior of carbon during the transformation. However, with decreasing transformation temperature, the amount of carbon associated with dislocations in bainitic ferrite increases, independent of the carbon concentration between 0.1 to 0.4 wt% carbon, because the dislocation density increases as the transformation temperature is lowered.[90] Carbon content of the bainitic ferrite after the transformation tends to be higher than equilibrium.[84-89]

Conventional terminology used to describe bainitic microstructures does not adequately describe the morphology of all the different bainitic microstructures observed. Habraken and Economopulous[91] were among the first to observe nonconventional bainitic microstructures and termed them *'carbide free acicular'* and *'massive or granular'* structures, although their paper was titled, "Bainitic Microstructures in Low-Carbon Alloy Steels and Their Mechanical Properties"; they do not seem to have specifically termed these structures as bainitic. These structures were later termed *'carbide free bainite'*[92] and *'granular bainite'*.[93] Other terminologies to describe all the morphologies of bainite have also been suggested,[82,94] however, upper bainite, lower bainite, granular bainite, carbide free bainite seem be most appropriate and comprehensive terms and are widely used in the literature. Carbide free and granular bainites form more readily during continuous cooling.[56]

a. Upper Bainite

No carbides are observed within the upper bainite laths, although enriched austenite between upper bainite platelets transforms to ferrite and cementite.[95] Carbide precipitation also takes place at austenite grain boundaries, effecting the mechanical properties, especially toughness.[96] Cementite is the carbide phase most often associated with upper bainite. Cementite in upper bainite is of the form of irregular ribbons in three dimensions and appears as particles parallel to the traces of habit planes of the bainitic ferrite laths.[97] Carbide precipitation becomes thermodynamically feasible when the concentration of carbon exceeds the equilibrium value given by the extrapolated *austenite/(austenite + cementite)* phase boundary.[98] Reaction mechanism for cementite precipitation from retained austenite for bainitic transformation is not fully understood. However the reaction sequence is likely to be similar to break down of austenite during second stage of martensite tempering. The sequence, according to Nakamura and Nagakura,[95] is as follows:

$$\text{Austenite}_{(\text{parent})} \rightarrow \text{Austenite}_{(\text{retained})} + \text{Bainite}_{(\text{supersaturated})}$$

$$\rightarrow \text{Bainite}_{(\text{unsaturated})} + \text{Austenite}_{(\text{retained, enriched})}$$

$$\rightarrow \text{Bainite}_{(\text{unsaturated})} + \text{Ferrite}_{(\text{intra lath, transformed from retained austenite})}$$

$$+ \text{Cementite}_{(\text{inter lath})}$$

This is different from the cooperative growth of ferrite and cementite during the pearlite formation in carbon steels and also with the pearlite formation in steels with substitutional alloy content where retained austenite differs in composition from the parent austenite in both interstitial and substitutional solute content.

Orientation relationship between cementite and ferrite are those established by Bagaryatski,[99] austenite and cementite follow the Pitsch orientation relationship.[100]

b. Lower Bainite

Carbides precipitation in lower bainite takes place within the laths, as well as, from the retained austenite trapped between the laths. Carbides within the laths usually occur in a single crystallographic direction and are oriented at an angle of 55-60° to the longitudinal axis of the bainite laths when viewed in a planar section.[101,102] Sharp edges of the bainitic laths are usually free of carbides and the carbides within the bainitic laths may or may not touch the sides of the laths.[103]

Carbides within the laths may be cementite or ϵ-carbide. Presence of ϵ-carbide in lower bainite was first discovered by Austin and Schwartz;[104] several other workers have since detected ϵ-carbide in lower bainite.[101,105-110] According to Matas and Hehemann,[108] ϵ-carbide precipitates first in hypoeuctectoid steels and is replaced by cementite on isothermal holding. Presence of ϵ-carbide in lower bainite indicates degree of supersaturation of carbon in bainitic ferrite up to an order of 0.25 wt%.[111] Rate of conversion of ϵ-carbide to cementite is higher at higher temperatures, while presence of relatively high Si ($\sim$2 wt%) significantly slows down the decomposition.[112-113] According to Miikhinen and Edmonds[75] Ni may help the precipitation of ϵ-carbide. High dislocation densities can mitigate the formation of ϵ-carbide. According to Kalish and Cohen,[114] free energy of the system is lowered by segregation of carbon atoms to the dislocations, and hence, ϵ-carbide may not be

observed in steels with sufficiently high dislocation density ($> 2 \times 10^{12}$ cm^{-2}).

Because carbides within the bainitic laths use up a part of the carbon, volume of retained austenite trapped between the platelets is less for lower bainite,[109] and consequently fewer inter lath carbides form, leading to a substantial improvement in toughness. Following is a summary of the precipitation reactions[52]:

a. For high dislocation density

$$\text{Austenite}_{(\text{parent})} \rightarrow \text{Austenite}_{(\text{retained})} + \text{Bainite}_{(\text{supersaturated})}$$

$$\rightarrow \text{Cementite}_{(\text{intra lath})} + \text{Bainite}_{(\text{unsaturated})} + \text{Austenite}_{(\text{retained, enriched})}$$

$$\rightarrow \text{Bainite}_{(\text{unsaturated})} + \text{Cementite}_{(\text{intra lath})} + \text{Cementite}_{(\text{inter lath})}$$

$$+ \text{Ferrite}_{(\text{intra lath, transformed from retained austenite})}$$

b. For low dislocation density

$$\text{Austenite}_{(\text{parent})} \rightarrow \text{Austenite}_{(\text{retained})} + \text{Bainite}_{(\text{supersaturated})}$$

$$\rightarrow \epsilon\text{-Carbide}_{(\text{intra lath})} + \text{bainite}_{(\text{unsaturated})} + \text{Austenite}_{(\text{retained, enriched})}$$

$$\rightarrow \text{Bainite}_{(\text{unsaturated})} + \epsilon\text{-Carbide}_{(\text{intra lath})} + \text{Cementite}_{(\text{inter lath})}$$

$$+ \text{Ferrite}_{(\text{intra lath, transformed from retained austenite})}$$

$$\rightarrow \text{Bainite}_{(\text{unsaturated})} + \text{Cementite}_{(\text{intra lath})} + \text{Cementite}_{(\text{inter lath})}$$

$$+ \text{Ferrite}_{(\text{intra lath, transformed from retained austenite})}$$

Orientation relationship between cementite and ferrite is same as that of upper bainite,[99] while austenite and cementite follow the Kurdjumov-Sach (K-S) orientation relationship.[115]

c. Carbide Free Bainite

Carbide free bainitic structures usually consist of laths with high dislocation density, that run across the prior austenite grains. The packets observed in the conventional upper and lower bainites may or may not be present in the carbide free bainite. Habraken and Economopoulos[91] were among the earliest researchers to have reported absence of packets in the "Carbide-Free Acicular Structures". Garcia et al.,[14] have also reported only one set of laths in each pancaked austenite grain of hot rolled steel. Some retained austenite and martensite may be present between the laths.[82,91,105] Morphology similar to that of lower bainite with no intra lath carbides have also been reported for carbide free bainitic microstructures.[92] Austenite and ferrite observe the Nishiyama-Wasserman (N-W) orientation relationship and martensite and retained austenite follow the K-S orientation relationship.[115,116]

d. Granular Bainite

Granular bainite has been known for more than 30 years,[93] and yet it probably is still the least understood among the different morphologies of bainite.[117] Granular bainite occurs in the form of highly dislocated massive ferrite, with some martensite-austenite (M-A) islands. Volume fraction of M-A islands may depend on carbon content, cooling rate and dislocation density.[92,93] Granular bainite forms during transformation temperature range of approximately 550°C-400°C and is generally lath free. Lath formation is favored at higher cooling rates, and mixed

morphology may occur at intermediate cooling rates.[92,117] It is postulated that because of the relatively slow cooling rates, lesser number of dislocations are generated at the interface, hence fewer atoms of carbon get trapped in the dislocations at the transformation front, and also, there is time for long range diffusion of interstitial atoms. This leads to formation of regions rich in imperfections and interstitial atoms within the untransformed austenite along the octahedral planes. These regions subsequently give rise to M-A islands within the bainitic ferrite.[93] According to Bojarski et al.,[92] bainitic transformation during continuous cooling can be divided into three temperature dependent stages

- preliminary stage (just before the transformation)
- the transformation itself
- the final stage (second activity of transformation)

Some workers[93,118] believe there is advance segregation of carbon in the austenite above B_s. Ko and Cotrell[119] claim that segregation is coincident with the transformation start. According to Christian,[120] segregation precedes the transformation only in the case of upper bainite. Bojarski and Bold[92] did extensive hot stage spectrographic analysis under varying continuous cooling rates on a steel containing 0.18% C, 0.5% Mn, 2.4% Cr, 1.4% Ni, 0.4% Mo and 0.003% B. They have reported formation of centers with higher and lower carbon concentrations in the unstable austenite. Carbon segregation starts just below Ar_3 and continues below B_s. The lower carbon centers act as ferrite nuclei, and start growing only below B_s, this has been contributed to the presence of boron and higher substitutional alloy content.

The centers were considered to be of microscopic size since they did not effect the width and shape of austenite diffraction lines. Changes in austenite lattice constant at B_s showed that austenite is enriched in carbon during the transformation indicating long range diffusion of carbon, and, since no carbides form in the austenite, long range diffusion alone is accountable for lower carbon concentration in bainitic ferrite. Since untransformed austenite is not uniform in carbon concentration, the higher carbon regions transform into martensite on further cooling giving rise to M-A islands. Some carbon further diffuses from the martensite to austenite. Carbon concentration of bainitic ferrite is reported not to exceed 0.01%. The orientation relationships in granular bainite are the same as those in carbide free bainite.[116]

According to Yang and Bhadeshia[121] acicular ferrite is also a bainitic microstructure, and is formed because of difference in nucleation and growth conditions that are primarily controlled by grain size and the availability of nucleation sites in the form of inclusions within the prior austenite grains. Acicular ferrite with inter lath carbides and/or M-A constituent is considered equivalent of upper bainite and with intra lath carbide is considered lower bainite. Positive identification of low carbon bainites is difficult, owing to the morphological similarities between Widmanstätten ferrite, bainite and martensite. It is not possible to reliably distinguish between carbide free bainitic laths and low carbon martensite laths.[31,32]

KINETICS OF BAINITIC TRANSFORMATION

Similarities between bainite and martensite on one hand and between bainite and Widmanstatten ferrite on the other hand have been recognized since the discovery of bainite. Some workers claim that bainite is formed by diffusion [122,123] and others claim that bainite is formed by shear transformation.[124] Surface relief associated with invariant plane strain (IPS) has been observed in bainitic microstructures,[122] however, Dahmen[125] and Aaronson[123] claim that surface relief of IPS can be observed in diffusion controlled transformations also.

Size, shape and growth rate of bainitic plates have been reported to conform to that expected by diffusion controlled transformation by a number of workers.[123,126,127] Others have reported conformance to that of transformation controlled by shear.[118,128] Proponents of shear theory have shown that solute atoms are evenly distributed with no segregation across the interface.[129] Others have shown redistribution of Cr and Mo.[130] Behavior of interstitial elements like carbon is difficult to asses because the diffusion rates of carbon are relatively high at bainitic transformation temperatures.[131] Bhadeshia[86] has shown higher carbon concentration in dislocated ferrite.

All the experimental evidence gathered by various workers is based on steels with varying compositions subjected to diverse experimental conditions, making direct comparisons difficult and conclusions uncertain.

MECHANICAL PROPERTIES

Morphology of bainitic structures varies widely depending on their chemical composition, thermal history and mechanical processing. Bainitic structures may vary from featureless prior austenite grains with high dislocation density to fine laths that may form packets or run across the prior austenite grains without forming packets. Volume fraction and morphology of carbides depends on the carbon content and cooling conditions. Mechanical properties of bainites have been related to morphological features like; lath size, packet size and carbide distribution.[90,132-133]

a. Yield Strength

Four major contributors to the strength of bainitic steels are (*i*) substitutional and interstitial solid solution, (*ii*) dislocation substructure, (*iii*) slip band length, controlled by packet size and lath width and (*iv*) dispersion hardening due to carbides.[126,135,136] With the exception of interstitial solid solution strengthening factors (*i*), (*ii*) and (*iii*) are likely to be the major contributors to strength in ULCB steels. Dislocation density and lath width are controlled by the B_s temperature[74] which in turn depends on substitutional and interstitial alloy content and cooling rate. Therefore effect of each of these individual factors is, at best, difficult to isolate.[126] In granular bainite, an increase in volume fraction of M-A islands increases strength.[102,137]

Carbon has been the main stay of high strength quenched and tempered martensitic steels, however, deleterious effects of carbon on weldability are very well

documented. For bainitic steels where very little carbon remains in solid solution, and also when 'as cooled' strength and toughness is desired, substitutional solid solution strengthening with the use of other alloying elements becomes important. Mn, Ni and Mo are the most commonly used substitutional solid solution alloying elements, with Mo being, by far, the most effective contributor to solid solution strengthener of the three. McEvily et al.,[13] reported that 3% Mo contributes about 20,000 psi to the yield strength in a 111 ksi yield strength steel.

Very low carbon supersaturation is expected in bainitic ferrite because of the high mobility of carbon throughout the bainitic transformation temperature range.[138] Atom probe measurements using field ion microscopy have measured carbon levels on the average of the order of 0.01 wt percent. These studies also report non random carbon atom distribution in the bainitic ferrite, indicating that the carbon atoms are associated with the dislocation substructure. At 0.01 wt percent carbon can cause 55 MPa (8 ksi) increase in flow stress.[139] However for vacuum melted ULCB steels strengthening due to interstitial solid solution strengthening is expected to be negligible.

Strengthening due to dislocation substructure is one of the largest factors contributing to the yield strength of bainitic steels. Dislocation density of bainitic ferrite is greater than polygonal and Widmanstatten ferrite. Dislocations in bainitic ferrite are reported to be of three types, (*i*) in the bainitic lath boundaries, (*ii*) uniform distribution within the laths and (*iii*) in a network, larger in scale than the lath width. The first two types of dislocation are a direct result of the plastic shear

strain associated with the bainitic transformation and the third type of dislocation distribution is believed to be the remanents of dislocations in austenite prior to decomposition.[14,140] McEvily et al.,[13] reported a 40 ksi increase in yield strength of a 3%Ni-3%Mo steel which was isothermally transformed at 650°C (1200°F) and then water quenched compared to the steel subjected to air cooling after the isothermal transformation, with the increase in yield strength being attributed to the dislocation substructure.

For lath martensite, effect of dislocation density is given by the following equation:

$$\sigma_d = \alpha \mu \mathbf{b} \, (\rho)^{1/2} \qquad (2.1)$$

where: σ_d is the dislocation strengthening, α is a proportionality constant, μ is the elastic modulus, **b** is the burgers vector, ρ is the dislocation density. Extensive data to generate such empirical correlations for bainitic steels does not exist yet. Bainitic ferrite can have dislocation densities of the order of 10^{14} m^{-2} which can increase the yield strength by 145 MPa.[141]

Early research applied the methods used for rationalizing the strength of ferritic/pearlitic steels, to bainitic steels.[12,16,90,133,142,143] Following is the most common relationship used:

$$\sigma = K + k_y \, D^{-1/2} \qquad (2.2)$$

where: σ is the flow stress, K is a material constant and k_y is analogous to Hall-Petch parameter. The material constant K in these equations was considered to be composed of lattice friction stress term, solid solution strengthening term, and a term

to account for the flow stress increase due to transformation structure, which could be considered to include a lath strengthening component and a dislocation strengthening component.[144] Another typical example is:

$$YS = YS_o + \Delta YS_s + \Delta YS_p + \Delta YS_t + \Delta YS_d + \Delta YS_c + k_y D_F^{-1/2} \qquad (2.3)$$

where: YS is the measured yield strength, YS_o is the lattice friction stress and ΔYS_s, ΔYS_p, ΔYS_t, ΔYS_d and ΔYS_c are contributions to the strength due to solid solution, precipitation, texture, dislocations and bulk second phase, ie., carbides, respectively. The term $k_y D_F^{-1/2}$, is the contribution to strength by ferritic grain size.[143]

According to Langford and Cohen[145,146] in case of very fine grain size, slip plane dimensions are too small to allow the existence of dislocation pileups. In this case yielding is determined by the stress necessary to expand a dislocation loop across a slip plane. Flow stress in this case is expected to vary with the inverse of grain size. The changeover from Hall-Petch to Langford-Cohen relationship is expected to occur when the slip plane dimensions are of the order of 1 μm.[147] Based on the Langford-Cohen relationship, Brozzo et al.,[136] established the following relationship between lath width and strength:

$$\sigma = \sigma_o + \sigma_{subss} + \sigma_{intss} + k''_y(l)^{-1} \qquad (2.4)$$

where: l is the average lath width. They did not find a strong relationship between packet size and strength. Yield strength has been associated to both lath width and packet size by other researchers.[83,148-150] The studies that used lath size as the primary parameter contributing to the yield strength agree that flow stress varies with the reciprocal of some characteristic lath dimension that conforms to Langford-Cohen

relationship and not as the Hall-Petch inverse square root relationship. Since 25% of all the possible slip systems are parallel to the lath axis there is a possibility that there is some contribution from the packet size which is equal to the lath length. One study[135] has postulated that yield strength is controlled by the slipband length and has shown that yield strength is a function of both lath and packet size, and derived the following expression:

$$\sigma = (\sigma_o + \sigma_{ss} + \sigma_{cem}) + K''' M^{-1} \quad (2.5)$$

where M is a geometrical parameter relating average slipband length to both lath width and packet size. M is defined by the equation:

$$M = 2/\pi[l \ln \tan\{0.5 \arccos(l/D) + 0.25\pi\} + 0.5\pi D - D \arccos(l/D)] \quad (2.6)$$

where l is the lath width and D is the packet size.

However, it must be stressed that it is not possible to completely isolate the contribution of lath and packet size to yield strength from the effect of solid solution strengthening, because higher alloy content results in lower B_s temperatures which in turn increases the dislocation density and refines the lath and packet size.

Since the carbides formed at lath boundaries in upper bainite are coarse they are not likely to contribute to strength. They may impede the dislocation movement to some degree, but the effect is likely to be secondary. Finer intralath distribution of carbides makes a significant contribution.[142,151] The strengthening effect of carbide dispersion strengthening has been described by the Ashby-Orowan type expression:[152]

$$\sigma_{cem} = C (n_e)^{1/2} \ln D/(n_e)^{1/2} \quad (2.7)$$

where: C and D are material constants and n_e is the number of effective intralath carbides per unit area.

b. Toughness

There are two aspects of toughness of steels. The first is a ductile to brittle transition (DBT) which is affected by temperature and strain rate dependence of the yield strength, σ_y, of body centered cubic (bcc) metals. The second is the energy absorbed during crack propagation, which does undergo a change with DBT because of the change in fracture mode, but is also controlled by the microstructure of the ferrite and the morphology and distribution of carbides.

According to an expression first stated by Stroh,[153] a crack containing n dislocations will propagate as a cleavage crack if σ, the stress at the crack front, is sufficient to satisfy the following equation;

$$nb\sigma(1+1/\sqrt{2}) = 4\gamma' \qquad (2.8)$$

where: b is the burgers vector and γ' is the effective surface energy associated with crack growth. By taking into account σ_o, the stress required to overcome the friction on an unlocked dislocation, and relating it to the slip plane length in the Hall-Petch relationship, Petch[17] developed another expression for the stress required to cause crack propagation;

$$\sigma \approx 4\mu\gamma'/k^*l^{1/2} \qquad (2.9)$$

where μ is the modulus of rigidity, l is the slip plane length and k^* is a constant.

Increase in grain size favors cleavage fracture because larger slip bands allow larger dislocation pileups. Temperature dependence of transition is due to the σ_o part of σ, which is the resistance to the motion of a free dislocation. Cracknell and Petch[154] have shown that σ_o has two parts; 1) σ_o^* is independent of temperature and is

due to the resistance to dislocation movement offered by random solute atoms, fine precipitates, and lattice defects and is about 2 ksi for an annealed mild steel, at lower yield point; and 2) $\sigma_o^{\dagger}$ is dependent on temperature and represents appreciable Peierls-Nabarro stress. $\sigma_o^{\dagger}$ varies from about 2 ksi at room temperature to 24 ksi at -196°C for normal strain rates.[155] Petch[17] developed the following expression for the transition temperature T_c.

$$\epsilon T_c = \sigma_o^* + C - \left(\frac{4q\mu\gamma'}{k^*} - k^* \right) \qquad (2.10)$$

where: C and ϵ are constants and q represents stress concentration factor. The expression is derived assuming; 1) operative slip plane is at 45° to the applied stress and direction of crack propagation is normal to the applied stress; and 2) entire σ_o obeys the temperature dependence relationship of $\sigma_o^{\dagger}$ since σ_o^* is small, and the temperature dependence of $\sigma_o^{\dagger}$ is linear.

From the expression describing T_c, transition temperature is function of; grain size, friction on an unlocked dislocation, the strength of dislocation locking and the degree of triaxiality of applied stress.

Brittle fracture in structural steels usually occurs by transgranular cleavage i.e., separation along one or more crystallographic planes; Cleavage is considered as the propagation of a dislocation induced micro crack as a Griffith crack. Sensitive techniques like strain gauges[156] and etch pitting[157] indicate that microplastic deformation occurs before cleavage in iron and steel. Crack nucleation may be

caused by dislocation pile up or at second phase particles and inclusions. A series of edge dislocations blocked at a grain boundary or a second phase particle is the simplest example.[158] Cotrell[160] postulated that two active interacting (110) slip planes in bcc materials generate a cleavage micro crack on the common (100) plane. This is supposed to happen when two leading dislocations from the intersecting (110) planes react to form a sessile dislocation which serves as an obstacle to the dislocation flow. According to Zener,[159] n, the number of dislocations in a pile up increases as they coalesce at the tip of the pile up to nucleate a micro crack. Cracks can also nucleate due to particle matrix separation or particle cracking.[161] Intersecting twin bands generated by deformation twinning are also known to cause crack nucleation when the resolved normal stress on the cleavage plane is high.[162-165]

The crack nucleus is of the order of a few microns and before it grows into a final fracture it must grow to the grain boundary or another obstacle like second phase particle or inclusion. Crack growth may or may not be stopped by the obstacle. If the elastic energy released is of sufficient magnitude to equal the surface energy of the new surfaces and all additional fracture work at the new obstacle, the crack may continue to grow; lacking sufficient energy release it will be arrested. Experimental work shows that cleavage strength is independent of temperature,[166-168] which means that effective surface energy and the other factors that influence the cleavage process are independent of temperature. Petch[17] had reached the same conclusion based on the fact that the slope of the lower yield point (σ_{lyp}) versus the inverse square root of grain size ($l^{-½}$) plot did not change with temperature. Therefore, cleavage can occur

when the maximum nominal stresses are larger than or equal to cleavage strength, as verified by experimentation.[168-172] Ductile fracture, on the other hand, is accompanied by extensive plastic deformation. Here the microcracks do not grow as in cleavage, with the growth of microcracks (microvoids) now controlled by the plastic flow of the matrix material. Eventually these microvoids join up with each other resulting in fracture.[173]

Cleavage facet size is recognized as an important structural unit effecting toughness.[74,174-177] Refined packet and lath size, as well as prior austenite grain size improve toughness. Major deviation in the direction of crack propagation occurs at packet boundaries.[83,135,150,174,178-181] Increase in carbon content refines the microstructure but decreases toughness, indicating the strong influence of the shape and size of carbides on toughness.[178] Toughness of upper bainite is significantly lower than that of lower bainite, mainly due to the morphology of carbides.[91,179,182]

In case of granular bainite where packets and laths do not exist toughness is controlled by the M-A constituent.[137] Polygonal ferrite and bainitic ferrite do not offer intrinsic resistance to growing cleavage crack.[183] Therefore, in ultra low carbon bainitic steels, regardless of granular or lath morphology, prior austenite grain size may be the controlling factor for toughness.

INFLUENCE OF ALLOYING ELEMENTS ON STRENGTH AND TOUGHNESS

Carbon, Mn, Ni, Mo and Si are the most common alloying elements in steel weld metal; Al, Ti, B are also presents in small amounts either as carry overs from

the steel making process or are specifically added to control microstructure. Most of the oxygen in the weld metal usually comes from the shielding gas or the flux depending on the welding process, and the nitrogen levels are also dependent on the welding process.

CARBON

Solid solution strengthening effect of carbon (and nitrogen) is the highest among the alloying elements in steel. However retention of carbon in solid solution in steel weld metal is of the order of 0.01%. Nevertheless carbon does have a marked strengthening effect in as deposited weld metal. Moll and Stout[184] have reported a rate of increase of 800 $MNm^{-2}/\%$ over a range of 0.08%-0.16% in multiple pass GTAW welds on C-Mn steels. They also reported an increase in the volume fraction of carbides and a refinement of grain size with increasing carbon. Carbon is a major contributor to the carbon equivalent values and increases the maximum attainable hardness in the heat affected zone.

Interstitial carbon has a high dislocation locking strength[17] which causes an increase in DBT temperature. Cleanliness has a strong effect on the toughness. Hard particles (carbides, inclusions, M-A islands) can act as nuclei for cleavage cracks; reduction or total elimination of these particles improves toughness.[20,184] During multiple pass welding of carbon steels, regions heated below Ac_3 lose strength and toughness due to carbon diffusion and formation of carbides respectively.[51] A loss in toughness of the weld metal due to coarsening of the microstructure at carbon

levels below 0.07% has been reported, however it is not clear if all the other variables were kept constant.[26] Virtually no data are available on the effects of ultra low carbon levels on the weld metal.

MANGANESE

Mn has a moderate solid solution strengthening effect in steels, Pickering[16] has reported a solid solution strengthening effect of about 30 $MNm^{-2}/\%$ on yield strength, while Lacy and Gensamer[186] have reported 40 $MNm^{-2}/\%$. In weld metal strengthening effects between the values of 50 to 150 $MNm^{-2}/\%$ have been reported.[187-192] Most of the toughness data for Mn in the weld metal has been reported with respect to acicular ferrite. Morigaki et al.,[193] reported that toughness peak occurs at lower Mn levels as the Ni content of the weld metal increases. Similar results have been reported by Taylor and Evans.[194] Ito and Nakanishi[195] reported maximum toughness with Mn levels between 0.7-1.5%. They also reported that up to about 0.1-0.2% Si at 1% Mn improves toughness; further increase in Si with increasing Mn caused degradation in toughness. Mn is reported to significantly increase the martensite hardenability, i.e., promotes the formation of mixed microstructures consisting of bainite and martensite. Therefore higher levels of Mn may not be suitable in high strength steel weld metals.[196]

NICKEL

The solid solution strengthening effect of Ni is not significant. Ni is the only conventional alloying element that improves impact toughness of steel. Morrison and Cameron[197] reported the beneficial effect of Ni additions on low temperature impact properties of steel in 1927. Hodge et al.,[198] reported that Ni also reduces the grain size thereby improving impact toughness. Nunes and Larsen[199] reported that Ni increased the fracture strain at low temperature and decreased the temperature dependence of yield stress. Davies and Ku[200] reported that Ni makes cross slip less difficult in steel, from their observation of random dislocation configuration in 6% Ni steel. Wullart[201] postulated that Ni may reduce the stress required to move a dislocation (Peierls-Nabbarro Force) through a perfect lattice. Nickel is reported to raise the stacking fault energy of bcc iron thereby promoting cross slip and also may spread the shear misfit of $<100>$ edge dislocations making them less effective as crack nuclei.[202] Leslie, et al.,[202,203] have attempted to relate toughness of Ni bearing steels to Engel-Brewer concept [204] of electron configuration and have postulated that Ni changes the nature of inter atomic bonding in steels because the Ni atom has a large excess of *d* electrons, thereby promoting cross slip at high strain rates and low temperatures. Up to 5% Ni in the weld metal is reported to improve low temperature toughness of the weld metal.[205]

MOLYBDENUM

Molybdenum is a strong inhibitor of formation of high temperature products, i.e., ferrite and pearlite during continuous cooling, thus moving the ferrite nose in a continuous cooling transformation (CCT) diagram to the right. Mo also inhibits the formation of martensite, i.e., moves the bainite nose of a CCT diagram to the left, which creates a considerably wide range of cooling rates where bainite is the major product of austenite decomposition on continuous cooling.[206] A 0.5% concentration of Mo in a series of steels containing 0.17 to 0.93% carbon is reported to form bainite in air cooled bars ranging from 0.5 to 10 in. in diameter.[207] Mo is reported to be very effective in lowering the B_s temperature which results in higher average dislocation densities in the austenite decomposition products. McEvily et al.,[13] have reported a 75% contribution to strength due to Mo in substitutional solid solution and substructure strengthening in an ultra low carbon steel containing 3% Ni and 3% Mo. They have found that a steel containing 9% Ni and 3% Mo has sufficiently high hardenability to exhibit no change in yield strength in air cooled or water quenched condition. Garcia et al.,[14] have attained strength levels above 690 MPa (100 ksi) in ULCB wrought steel plates containing 1% Mn, 3% Ni and 3% Mo as solid solution strengtheners. Mo is reported to increase the austenite grain coarsening temperature.[206]

SILICON

Silicon is a strong deoxidizer and can also act as solid solution strengthener, however, it is reported to have adverse effect on toughness of the weld metal when present at concentrations greater than ~0.5% in the weld metal. To maintain good electrode operating characteristics Si levels greater than ~0.3% are considered essential.[208] Evans[209,210] reported a decrease in Charpy toughness of MMA weld metal with an increase of Si content from 0.2 to 0.9%. For submerged arc weld metal, Hannerz[211] determined an optimum Si range from 0.25 to 0.35% in the weld metal. Terashima and Hart[212,213] found weld metal toughness to be independent of Si content. According to Boniszewski,[208] when strong deoxidants are added to the coating or are present in the flux the optimum Si content required for good toughness may be lower than 0.2%.

BORON

Boron promotes formation of bainite in hypoeutectoid steels by inhibiting the nucleation of allotriomorphic ferrite on the austenite grain boundaries and has been extensively used to improve the hardenability of steels. Solubility of boron in austenite is very low, it is estimated to be about 0.001% at 912°C.[214] The solubility in ferrite is essentially zero, but is reported to be influenced by the impurities in steel.[215] Due to low solubility of boron in austenite it tends to be highly concentrated on the prior austenite grain boundaries. Boron reduces the free energy of austenite grain boundaries, thereby, suppressing the nucleation of ferrite.[216,217] Hardenability

effect of boron is reduced by increasing carbon content.[218]

Boron has to be in solid solution to be effective. In the weld metal boron is always added in conjunction with Ti and Al because of its strong carbide and nitride forming ability. Carbon also tends to segregate to the grain boundaries in low carbon steels, but Ti can tie up some of the carbon also leaving the grain boundaries free for boron. MnS and Al_2O_3 inclusions in the welds metal tend to act as heterogenous nucleation sites for BN and $M_{23}C_6$ during welding, this in turn reduces the boron in solid solution.[219,220] According to Hori[60] about 0.0003 to 0.0005% boron should be in the weld metal and sufficient amounts of Ti and Al should be added to tie up the nitrogen and oxygen in the weld metal.

III. TECHNICAL APPROACH

This research effort was designed to overcome the limitations of the commercially available high strength steel filler wires, resulting from the current philosophy of the weld metal alloy design, listed below:

- Susceptibility to HAC.
- Narrow welding parameter window.
- Necessity of preheating.
- Dependence on complex stoichiometry of Al, Ti, O, N and B in the weld metal to maintain adequate toughness

A new approach to high strength steel weld metal alloy design consisting of following salient features is proposed:

- No intentional addition of carbon. (ultra low carbon)
- Increased contribution to strength from substitutional solid solution strengthening and transformation induced dislocations. (modified CCT behavior making it possible to generate bainitic microstructures over a wide range of cooling rates and low B_s temperatures)
- Minimum possible concentration of N and O in the weld metal with low levels of interstitial atoms and low volume fraction of second phase particles, leading to a high level of cleanliness in the weld metal. (achieved by vacuum induction melting)

Carbon is the traditional strengthening element in quenched and tempered steels. It is a major contributor to the carbon equivalent values and increases the

maximum attainable hardness in the heat affected zone. Multiple pass welds regions heated below Ar_3 lose strength and toughness due to carbon diffusion and formation of carbides.[51] Low Ar_3 in the weld metal is desirable because it will cause higher volume fraction of reheated weld metal to transform to austenite, which will then transform to a microstructure similar to the primary microstructure, retaining its strength and toughness.

Nominal compositions of some of the commercially available filler wires and HSLA-80 and HSLA-100 steel plate are given in Table I. HAZ hardness is regarded as a rough index of susceptibility to hydrogen cracking. A hardness value of 350 HV is often specified as maximum allowable HAZ hardness.[221] With the exception of HSLA-80 and HSLA-100 steel plates, all compositions in Table I have maximum calculated[222] hardness close to or above 350 HV.

Lowering the carbon levels is the most effective means to reduce maximum attainable hardness in the weld metal, because hardness of martensite depends on its carbon content, however, lowering the carbon levels leads to reduction in yield strength. To attain high yield strength levels in ultra low carbon steels major contribution to strength of the weld metal must come from substitutional solid solution strengthening and dislocation substructure, which means that the phase transformation of austenite must result in extensive shear deformation and the transformation must occur at a low enough temperature so that the resulting substructure of dislocation arrays and cells does not anneal out during further cooling. This necessitates relatively higher alloy content compared to that of the wrought material of comparable

strength and lower B_s temperature for the filler metal. Considering the beneficial effect of Ni on toughness, ability of Mo to promote the formation of bainite over a wide cooling rate, and relatively strong strengthening effect of Mn; Ni, Mo, Mn were chosen as the alloying elements to increase yield strength by dislocation and substitution solid solution strengthening. Strengthening by dislocation substructure is reported to affect toughness to a lesser degree than interstitial solid solution strengthening, which means lower B_s temperatures are desirable.[15,16]

Cleanliness has a strong effect on the toughness. Hard particles (carbides, inclusions, M-A islands) can act as nuclei for cleavage cracks; reduction or total elimination of these particles improves toughness.[20,185] The deleterious effect of interstitial solute atoms on toughness of steel has been recognized for a long time, removal of interstitial solute atoms from the matrix is reported to eliminate most of the grain size dependence of impact transition temperature.[203] Because of the higher heat input levels required for greater productivity, there is very little control over the grain size of weld metal. Thus bainitic weld metal must be free of carbonitrides, inclusions and interstitial elements. Vacuum induction melting (VIM) process was selected to reduce nitrogen and oxygen content to levels as low as possible and to ensure cleanliness in the steels.

IV. EXPERIMENTAL PROCEDURES

Materials used as filler metals during this investigation, welding procedures, weld metal cooling rate determination, weld metal mechanical property evaluation, microstructural analysis using electron and optical microscopy, inclusion analysis, fractography using SEM, CCT diagram determination using Gleeble 1500, and acoustic emission testing are described in this chapter.

MATERIALS

Weld metal of sixteen different steel alloys was tested and analyzed for this investigation. The chemical composition of the steels are given in Table II. Thirteen of the steel alloys numbered 1 through 9 and 12 through 15 were vacuum induction melted (VIM) by Precision Cast parts Corporation. Alloys 12 through 15 had B additions. The VIM ingots were approximately 11 cm (4.5 in.) in diameter and 50 cm (18 in.) long weighing about 25 kg (55 lb) each. Two of the alloys numbered 10 and 11 were provided by ESAB Group Inc., in the form of 1/16 in. (1.6 mm) diameter wire. Alloy 16 was a 900 kg (2000 lb) ingot melted by ESCO Corp., using the argon oxygen decarburization (AOD) process.

WELDING PROCEDURES

Gas tungsten arc (GTA) welds were deposited on matching base plates for Alloys 1 through 9 and 12 through 16 and GTA weld metal using Alloy 10 and Alloy 11 filler was deposited on Alloy 8 and Alloy 5 base plates respectively. GTA weld

metal of Alloy 7 was also deposited on HSLA-100 and HY-130 base plates. Commercial filler wires of MIL-100S-1 and MIL-120S-1 type were used to deposit GTA weld metal on HSLA-100 base plate for comparison. Gas Metal Arc (GMA) weld metal for Alloys 7, 10 and 11 was deposited on HSLA-100 base plate. The welding parameters for GMA welds were adjusted to attain cooling rates identical to the GTA welds. Details of the GTA welds are given in Table III and those of GMA weld are given in Table IV.

GTA Welding

The VIM ingots and the AOD ingot were sectioned to produce 12 mm (0.5 in.) thick plates. One and a half millimeter (0.06 in.) thick slices cut from the ingots and sheared into 1.5 X 3 mm (0.06 X 0.12 in.) cross section rods were used as filler metal. Double U grooves were machined on the 12 mm (0.5 in.) thick plates for Charpy V notch (CVN) test samples and single U groove for tensile test samples; the groove geometries are shown in Fig. 1. The welds were made using a GTAW torch mounted on a motor driven head which traversed along a beam. The filler was fed into the weld pool by hand. Double U groove joints were welded using one autogenous pass followed by another pass with matching filler metal on each side. Single U grooves were welded using one autogenous pass and three passes with matching filler metal. Details of GTA welding conditions are given in Table III.

To reproduce the chemical interactions of GMA welds, GTA welds were made using the standard GMAW shielding gas viz, Ar-5%CO_2. Ar and Ar-25%He

shielding gases were used for comparison. Ar-5%CO_2 welds were made at 3.5 kJ/mm (90 kJ/in.) and 2 kJ/mm (51 kJ/in.) heat input. Ar welds were made at 3.2 kJ/mm (82 kJ/in.) heat input. Higher heat input levels could not be attained with Ar due to the lower arc voltage. A mixture of Ar-25%He achieved 3.5 kJ/mm (90 kJ/in.) heat input, Ar-25%He welds were also made at 3.2 kJ/mm. Welding grade shielding gases were used to make all the welds.

GMA Welding

GMA welds were made using Alloy 7, 10 and 11 filler wires and HSLA-100 base plates. Weld metal was deposited in a 60° V groove machined on 16 mm (0.6 in.) thick plates. GMAW welds were made at 2.5 kJ/mm (64 kJ/in.) and 1.9 kJ/mm (48 kJ/in.) heat input with Ar-5%CO_2 shielding gas. Three passes were required for 2.5 kJ/mm (64 kJ/in.) heat input welds and the 1.9 kJ/mm (48 kJ/in.) heat input welds were completed with four passes each. Alloy 7 weld metal was also deposited with Ar-25%He shielding gas at 2.5 kJ/mm (64 kJ/in.) heat input on HSLA-100 base plate. GMA welds at 2.5 kJ/mm (64 kJ/in.) heat input were made with 150°C (300°F) preheat. Welding parameters for GMAW at 2.5 kJ/mm (64 kJ/in.) and 1.9 kJ/mm (48 kJ/in.) heat input were adjusted to attain the cooling rates identical to those of the 3.5 kJ/mm (90 kJ/in.) and 2 kJ/mm (51 kJ/in.) heat input GTA welds. Details of GMA welding conditions are given in Table IV, and the groove geometries are shown in Fig. 1.

WELD METAL COOLING RATE MEASUREMENT

W-5%Re/W-26%Re thermocouples, having a 0.5 mm (0.02 in.) diameter, were used to determine the cooling rate of 2 kJ/mm and 3.5 kJ/mm welds. Thermocouples were plunged at mid length of a typical groove weld and moved along with the molten weld pool for 3 seconds to allow the thermocouple to warm up. Movement of the thermocouple was then stopped to allow the weld metal around the thermocouple to solidify. The thermocouple output was recorded on a computer, and time to cool from 800 to 500° C (t_{8-5}) as well as cooling rates at 538° C (1000° F) were determined. Several cooling cycles were recorded for each heat input. GMAW parameters were adjusted to attain cooling rates identical to those of GTA welds.

MECHANICAL TESTING

Tensile tests were carried out on all-weld-metal samples in the as-welded condition using standard 6.3 mm (0.250 in.) bars in accordance with ANSI/ASTM E8-79a standard. Rockwell hardness tests were performed on the transverse cross sections of the weld metal. Charpy V notch impact test bars were machined transverse to the weld in order to ensure crack propagation along the weld axis during testing. The CVN bars were then cut and surface ground to final dimensions in accordance with ASTM standard E23. The bars were etched with 10% nital to correctly place the notch at the exact center of the weld. CVN tests were performed at -51° C (-60° F), -18° C (0° F) and 25° C (77° F).

METALLOGRAPHIC EXAMINATION

Metallographic samples were cut transverse to the weld axis, polished samples were etched with 2% nital for optical microscopy, and LePera's etchant was used to reveal borocarbides at the prior austenite grain boundaries. Specimens for transmission electron microscopy (TEM) studies were cut into 0.3 mm (0.01 in.) thick slices using an abrasive parting wheel and were further thinned to 0.15 mm (0.005 in.) by grinding. Three millimeter (0.12 in.) round discs were punched out of the slices and electropolished using 5% perchloric acid solution in methanol at -40°C (-40°F). A TEM operated at 100kV was used to study the weld metal microstructure.

For inclusion analysis, polished and unetched samples were observed in a SEM in the backscatter mode; 25 fields at a magnification of 500X were collected and analyzed for each specimen. A quantitative image analysis program was used to measure inclusion volume fraction and size distribution. Fracture surfaces of the CVN test samples were also studied using the SEM.

CCT CURVE DETERMINATION

CCT curves were determined using all-weld metal round bars 10 mm (0.4 in.) in diameter and 10 cm (4 in.) long for slow cooling rates with 'Gleeble 1500'. For the faster cooling rates the bar diameter was reduced to 6 mm (0.23 in.) in the center over a length of 15 mm (0.6 in.) and the samples were cooled with forced flow of Argon through the 6.5 mm (2.6 in.) diameter 4 cm (1.5 in.) long holes drilled at each

end of the bar. The specimens were austenitized at 825°C for three minutes to minimize the grain coarsening and alterations in the weld metal microstructure. Change in diameter due to cooling as well as phase transformation was monitored using a strain gage with 0.00025 mm (0.000001 in.) resolution. Transformation start and finish temperatures were determined for cooling rates varying from 0.015°C/s to 100°C/s. CCT diagrams were plotted using the software available on the 'GLEEBLE 1500'.

ACOUSTIC EMISSION TESTING

Acoustic emission testing was performed on 0.5 X 0.2 in. cross section all-weld metal tensile specimens machined out of Alloy 8 weld metal deposited at 3.5 kJ/mm (90 kJ/in.) heat input with Ar-5%CO_2 and Ar-25%He shielding gases. The specimens were tested using universal testing machine with a load capacity of 20,000 lb. A piezoelectric transducer with a resonant frequency of 375 kHz and a sensitivity -70 dB was attached to the tensile specimens to detect acoustic emission signals. The transducer was connected to the system mainframe via a preamplifier with a fixed gain of 60 dB and total gain in the system was 94 dB. Acoustic emission from the specimen was monitored using the AET 5500 system. A schematic diagram of the experimental setup is given in Fig. 2.

V. RESULTS AND ANALYSIS

Chemical compositions of the VIM ingots and weld metals, results from the optical and transmission electron microscopy, inclusion analysis, acoustic emission tests, the tensile, hardness and CVN impact toughness tests are described in this section.

VIM INGOT COMPOSITION

The chemical compositions of the VIM ingots, two 1/16 in. diameter wire alloys and the AOD alloy are given in Table II. The most significant characteristic of these VIM alloys is the extremely low levels of C (<0.02%), N (<5 ppm), O (<60 ppm), S (<0.01%), P (<0.01%). C levels were maintained at or below 0.03% level with the exception of Alloy 4 having 0.055% C for reference. Alloys 12-15 had B addition varying from 0.0018 to 0.0022%. Alloys 10 and 11 are the alloys provided by the ESAB Group Inc. Alloy 16 is the AOD alloy. Carbon levels in the VIM Alloys varied from 0.001% in Alloy 2 to 0.055% in Alloy 4, Mn from 0.93% in Alloy 2 to 1.52% in Alloy 5, Ni from 2.23% in Alloy 1 to 5.59% in Alloy 10 and Mo from 0.47% in Alloy 1 to 2.40% in Alloy 8. Lowest oxygen level in the VIM alloys was 10 ppm in Alloy 10 and the highest level was 57 ppm in Alloy 6. Lowest nitrogen level was 1 ppm and the highest was 5 ppm in Alloy 6.

Because of the difficulties experienced in adding Mn, B and Ti to small sized 25 kg (50 lb) heats the compositions of the VIM ingots were different from the originally designed matrix of alloys. The desired levels of Ni and Mo were easy to

achieve. Difficulty was experienced in achieving Mn levels above 0.9 wt.%, because of evaporation of Mn during melting in the VIM furnace. Ti levels were too low for accurate determination with the exception of Alloy 8. Excessive levels of B were added to Alloys 12 through 15 due to inadequate control over B additions in small heats.

WELD METAL COMPOSITIONS

The chemical compositions of the GTA weld metal deposited on the plates cut from the VIM ingots using Ar-5%CO_2 and matching filler metal at 3.5 kJ/mm (90 kJ/in.) heat input are given in Table V. There was an increase in the C content and loss of Mn, Ti and Al from the weld metal, Ni and Mo transferred to the weld metal without any change. Carbon levels in the GTA weld metal of VIM steels varied from 0.013% in Alloy 5 to 0.064% in Alloy 4, Mn from 0.65% in Alloy 2 to 1.23 in Alloy 11, Ni from 2.23% in Alloy 1 to 5.59% in Alloy 10 and Mo from 0.48% in Alloy 1 to 2.40% in Alloy 8. Lowest oxygen level in the VIM alloy weld metal was 180 ppm and the highest level was 317 ppm. In addition to oxygen from the shielding gas the weld metal also showed an increase in N level, picked up from the atmosphere during welding. Lowest nitrogen level in the GTA weld metal was 4 ppm and the highest was 9 ppm. Because of the more violent nature of the arc, the nitrogen levels in the GMA weld metal were higher compared to those in the GTA weld metal, nitrogen level was 27 ppm for the Alloy 10 and 51 ppm for Alloy 11 GMA weld metal.

The CEN values, maximum attainable hardness of martensite, as welded hardness and hardness with no martensite in the weld metal calculated using Yurioka's[222] model and the B_s temperatures calculated after Steven and Hayens[43] for the weld metal deposited at 3.5 kJ/mm (90 kJ/in.) heat input using Ar-5%CO_2 shielding gas are given in Table VI. Alloy 7 weld metal deposited on matching plate at 3.5 kJ/mm (90 kJ/in.) using Ar-5%CO_2 shielding gas had the highest CEN value at 0.44 and the lowest B_s temperature at 451°C, Alloy 1 weld metal deposited under same conditions had the lowest CEN value at 0.20 and the highest B_s temperature at 559°C, Alloy 1 also had the lowest as welded weld metal hardness values.

TRANSFER EFFICIENCIES

Transfer efficiencies of alloying elements through the welding arc were determined by comparing the compositions of the VIM ingots given in Table II and the compositions of the corresponding weld metals given in Table V. Experimentally observed transfer efficiencies are given in Table VII.

Ni and Mo transferred from filler metal to the weld metal with virtually no change indicating a transfer efficiency of 1. Other elements were affected by the presence of oxygen in the arc plasma resulting from the dissociation of CO_2. Average transfer efficiency of Mn was found to be about 0.74.

Due to very low Ti levels in the VIM ingots, transfer efficiency of Ti could not be determined. However empirical data from the GMAW work done at Electric

Boat indicates a transfer efficiency of 0.25 for Ti.[223]

Because of the extremely low levels of C in the VIM ingots, the weld metal picked up C from the arc plasma resulting in a higher C levels in the weld metal with respect to those of the corresponding VIM ingots. Average transfer efficiency for C was determined to be about 1.4.

WELD METAL COOLING RATES

Weld metal cooling rates were measured using W-5%Re/W-26%Re thermocouples. Thermocouples were plunged into the weld pool at about half way point along the length of a typical groove weld and allowed to warm up for about 3 seconds by trailing the arc while still immersed in the weld pool. Thermocouple motion was then stopped while the weld pool solidified around it.

Several cooling cycles were recorded for both 3.5 kJ/mm (90 kJ/in.) and 2 kJ/mm (51 kJ/in.) heat input GTA welds. The Thermocouple output was stored in a computer. The GMA welding parameters were varied to match the cooling rates of the GTA welds. Representative time versus temperature plots for GTA and GMA welds are given in Fig. 3 and 4 respectively. The weld metal cooling rates for GTA and GMA welds computed from the recorded data are given in Table VIII.

Average cooling rate for 3.5 kJ/mm (90 kJ/in.) GTA weld at 538°C (1000°F) was 6°C/s (11°F/s) with a corresponding cooling time from 800 to 500°C (t_{8-5}) of 35 s; GMA welds deposited at 2.5 kJ/mm (64 kJ/in.) heat input on a 15 mm (0.6 in.) thick plate with a preheat of 150°C (300°F) attained same cooling rates as 3.5 kJ/mm

(90 kJ/in.) GTA welds. Average cooling rate for 2.5 kJ/mm (51 kJ/in.) GTA welds at 538°C (1000°F) was 17.8°C (32°F/s) with a corresponding t_{8-5} of 15 s, while GMA welds deposited at 1.9 kJ/mm (48.3 kJ/in.) heat input on a 15 mm (0.6 in.) thick plate attained the same cooling rates as 2 kJ/mm (51 kJ/in.) GTA welds.

Commercial filler wires currently available are capable of attaining good CVN toughness values within a narrow window of cooling rates (welding variables). CVN toughness of weld metal deposited at a cooling rate of 10°F is known to be poor. Hence a cooling rate of 6°C (11°F/s), as used in this study, is close to the lower limit and will be a true test of the inherent toughness of the ULCB steel weld metal. U.S. military specifications[224] requires toughness tests for high cooling rate weld metal indicating that for some commercially available weld metal systems achieving required toughness values can be a problem at high cooling rates also, further narrowing the welding parameter window.

CCT DIAGRAMS

CCT diagrams were determined for GTA weld metal of Alloys 5 and 16 deposited at 3.5 kJ/mm (90 kJ/in.) heat input with Ar-5%CO_2 shielding gas using 'Gleeble 1500', Fig. 5 and 6. The CCT diagrams indicate that B_s temperature does not undergo a great change over a wide range of cooling rates. With a change in t_{8-5} from 35 s to 14 s for Alloy 5 weld metal, the change in B_s temperature is negligible, Fig. 5. However, the B_s did decrease with increase in cooling rate over the entire test range.

MICROSTRUCTURAL ANALYSIS

Optical and transmission electron microscopy was carried out to characterize the microstructure of the ULCB weld metal. Optical microscopy was found to be of only limited use in describing the ULCB weld metal microstructures. Following are the results of optical and transmission electron microscopy analysis.

Optical Microscopy

Due to ultra low C levels of the GTA weld metal deposited on the VIM ingots very little detail could be observed in the optical micrographs. Micrographs of GTA weld metal of Alloy 7 deposited on matching base plates at 3.5 kJ/mm (90 kJ/in.) and 2 kJ/mm (51 kJ/in.) using Ar-5%CO_2 are shown in Fig. 7(a) and (b) respectively. In the B containing alloys borocarbides decorated the prior austenite grain boundaries. Micrograph of GTA weld metal of Alloy 15 deposited on matching plate at 3.5 kJ/mm (90 kJ/in.) using Ar-5%CO_2 shielding gas shows the concentration of borocarbides on the prior austenite grain boundaries, Fig. 8. There was a reduction in the prior austenite grain size with decrease in heat input. A comparison of the optical micrograph of GTA weld metal of Alloy 7 deposited on matching base plate at 3.5 kJ/mm (90 kJ/in.) and 2 kJ/mm (51 kJ/in.) shown in Fig. 7(a) and (b), respectively, indicates the reduction in prior austenite grain size with decreasing heat input.

Microstructures of the GMA weld metal deposited on HSLA-100 base plate with Alloy 11 filler using Ar-5%CO_2 shielding gas at 2.5 kJ/mm (64 kJ/in.) and

1.9 kJ/mm (48.3 kJ/in.) heat input are shown in Fig. 9 and 10. Microstructure of the last pass is shown in Fig. 9(a) and 10(a). The reheated region in the GMA weld metal shown in Fig. 9(b) and 10(b) exhibited finer microstructures, however, the finer details differentiating these structures could not be observed with the optical microscope.

Macrographs of GTA weld metal of Alloy 7 deposited at 3.5 kJ/mm (90 kJ/in.) heat input with Ar-5%CO_2 shielding gas on a matching base plate and GMA weld metal of Alloy 11 deposited at 2.5 kJ/mm (64 kJ/in.) are shown in Fig. 11 and 12, respectively. GMA weld metal has a large area of the previous pass that has been heated above Ac_3, where as the reheated region heated above Ac_3 in the GTA weld metal is relatively small.

Transmission Electron Microscopy

Transmission electron microscopy revealed a range of microstructures from granular bainite with no laths to carbide free bainite with well developed laths. GTA Weld metal of Alloy 1 deposited at 3.5 kJ/mm (90 kJ/in.) with Ar-5%CO_2 shielding gas on a matching base plate exhibited granular bainite microstructure, Fig. 13. GTA weld metal of Alloys 5, 6, 8 and 9 deposited at 3.5 kJ/mm (90 kJ/in.) with Ar-5%CO_2 shielding gas on matching base plate exhibited mixed morphologies having areas of well developed laths as well as areas of granular bainite with no laths, Fig. 14. Alloy 4 and 7 exhibited carbide free bainite microstructures with laths running across the prior austenite grains, Fig. 15. Uniformly sharp lath boundaries

were observed in weld metals with high alloy content, Fig. 16(a), while relatively diffuse lath boundaries were observed in the weld metals exhibiting mixed morphologies, i.e., weld metals containing areas of well developed laths as well as areas of granular bainite, Fig. 16(b). Alloy 5, 6 and 8 tended to form cellular dislocation tangles in the areas where no laths were present, Fig. 16(c). In the relatively small area observed under the TEM no martensite-austenite (M-A) islands in granular bainite were observed, also no retained austenite could be found between the laths of carbide free bainite. Lath size of the GTA weld metal deposited at 2 kJ/mm (51 kJ/in.) heat input was finer compared to that of the 3.5 kJ/mm (90 kJ/in.) weld metal, Fig. 17. Because of the profile of the GTA weld metal, shown in Fig. 11, and the fact that relatively small quantities of filler wire could be added resulting in almost complete remelting of the previous pass, the region heated above the Ac_3 was very small.

TEM micrographs of the GMA weld metal last pass of Alloy 11 deposited at 1.9 kJ/mm (48 kJ/in.) and 2.5 kJ/mm (64 kJ/in.) heat input are shown in Fig. 18 and 19. The last pass of GMA weld metal of Alloys 10 and 11 also had carbide free bainite microstructures, however, unlike the GTA weld metal of Alloys 4 and 7, Alloys 10 and 11 had packets within the prior austenite grains. No carbides, M-A constituent or retained austenite was found in the GMA weld metal also. The low heat input welds had finer substructure. The GMA weld metal had large regions reheated above Ac_3. The reheated regions exhibited mixed morphology, i.e., areas containing laths and areas with no laths, Fig. 20(a) to (c).

Increasing weld metal alloying element content lead to an increasing tendency for lath formation. Alloy 1 weld metal with the lowest alloying element content and Yurioka's CEN value of 0.20 had granular bainite microstructure with no evidence of lath formation, and Alloy 7 with the highest alloying element content and Yurioka's CEN value of 0.44 had carbide free bainite microstructure with well defined laths.

TEM analysis of the GTA and GMA weld metal indicated that inclusions generally had no effect on the austenite decomposition products. Only in the case of GTA weld metal of Alloy 5 deposited at 3.5 kJ/mm (90 kJ/in.) using Ar-5%CO_2 shielding gas some inclusion were associated with ferrite nucleation, Fig. 21.

INCLUSION ANALYSIS

Inclusion analysis was carried out on GTA weld metals of Alloy 7 deposited at 3.5 kJ/mm (90 kJ/in.) heat input using Ar-5%CO_2 and Ar-25%He shielding gases on matching base plate. Results of the inclusion analysis are given in Table IX, and the inclusion size distribution is shown in Fig. 22. The weld metal deposited using Ar-5%CO_2 shielding had five times the inclusion volume fraction of the weld metal deposited using Ar-25%He. Average inclusion diameter for the weld metal deposited using Ar-5%CO_2 shielding gas was 0.65 μm and for the Ar-25%He weld metal it was 0.36 μm. More than 75% of the total inclusions in the Ar-5%CO_2 weld metal were greater than 0.43 μm in diameter whereas in the Ar-25%He only about 6% of the inclusions were over 0.43 μm in diameter. This indicates that most of the inclusions in the weld metal are formed due to the presence CO_2/O_2 in the shielding gas.

ACOUSTIC EMISSION TESTS

Acoustic emission tests were carried out on flat tensile samples machined out of GTA weld metal of Alloy 8 deposited using Ar-5%CO_2 and Ar-25%He shielding gases at 3.5 kJ/mm (90 kJ/in.) heat input on a matching base plate. The results of the acoustic emission tests are shown in Fig. 23 and 24. Acoustic signals generated by the weld metal deposited using Ar-5%CO_2 shielding gas during the tensile test were significantly greater than those generated by the weld metal deposited using Ar-25%He shielding gas under identical testing conditions. Peak amplitude for the Ar-5%CO_2 weld metal was about 2000 db and for Ar-25%He weld metal it was 175 db. The results indicate that the number of microvoids generated in the weld metal during the test, due to either matrix interface separation or particle cracking, were greater in the Ar-5%CO_2 than those generated in the Ar-25%He weld metal, Fig. 24.

HARDNESS AND TENSILE TESTS

Hardness testing was carried out on all the welds made. The hardness values for 3.5 kJ/mm (90 kJ/in.) GTA weld metal deposited on 12 mm (0.5) in thick plates cut from the VIM ingots using Ar-5%CO_2 shielding gas are given in Table X. The hardness values for 2 kJ/mm (51 kJ/in.) weld metal deposited under similar condition are given in Table XI. The hardness values of the GMA weld metal deposited on HSLA-100 base plate are given in Table XII. The hardness values of GTA welds made using Ar and Ar-25%He shielding gases and the hardness values of GTA weld

metal deposited on HSLA-100 and HY-130 base plates are given in Appendix I and Appendix II, respectively. Hardness values for weld metals deposited at 3.5 kJ/mm (90 kJ/mm) and 2 kJ/mm (51 kJ/mm) for each alloy did not change significantly with heat input, Fig. 25 (a) and (b).

GTA weld metal deposited on Alloy 7 with matching filler at 3.5 kJ/mm (90 kJ/in.) using Ar-5%CO_2 shielding gas had average hardness of 23 HRC, Table X. The GMA weld metal of Alloy 11 deposited on HSLA-100 base plate at 2.5 kJ/mm (64 kJ/in.) heat input using Ar-5%CO_2 shielding gas had average hardness value of 21.4 HRC, Table XII. GTA weld metal deposited on HY-130 base plate using Alloy 7 filler metal at 90 kJ/mm heat input with Ar-5%CO_2 shielding gas had the highest weld metal hardness at 32.7 HRC, Appendix II. Variation in the hardness of 3.5 kJ/in. (90 kJ/in.) and 2 kJ/mm (51 kJ/in.) GTA weld metal deposited using Ar-5%CO_2 shielding gas, with Yurioka's CEN values was approximately linear, Fig. 26. Also from Fig. 26 it is apparent that the difference between the hardness of 3.5 kJ/mm (90 kJ/in.) weld metal and the corresponding 2 kJ/mm (51 kJ/in.) weld metal was extremely small. This indicates that ULCB weld metal is insensitive to cooling rate and exhibits little change in yield strength values over a range of cooling rates.

Results of the tensile tests are shown in Table XIII and Fig. 27. For Alloys 1 to 9 and 12 to 16 tensile testing was carried out on GTA weld metal deposited at 3.5 kJ/mm (90 kJ/in.) heat input with Ar-5%CO_2 shielding gas on matching base plate. Tensile properties for GMA weld metal of Alloys 10 and 11 deposited at

2.3 kJ/mm (60 kJ/in.) heat input with Ar-5%CO_2 shielding gas on HY-100 plate are also reported in Table XIII.

Variation in yield strength of the GTA weld metal deposited at 3.5 kJ/mm (90 kJ/mm) with Ar-5%CO_2 shielding gas on matching base plate with Yurioka's CEN values was approximately linear, as shown in Fig. 28. Among the GTA weld metal of VIM alloys deposited at 3.5 kJ/mm (90 kJ/in.) heat input with Ar-5%CO_2 shielding gas on matching base plate, the weld metal of Alloy 1 with lowest CEN value, 0.20, had the lowest yield strength at 465 MPA (67.5 ksi) and the corresponding weld metal of Alloy 7 with the highest CEN value, 0.44, attained the highest yield strength at 733 MPa (106.3 ksi).

The tensile properties of the GMA weld metal of Alloys 10 and 11 deposited at 1.41 to 2.3 kJ/mm (36 to 60 kJ/in.) heat input with Ar-5%CO_2 shielding gas on HY-100 base plate are given in Table XIV;[223] the calculated cooling rates vary from 5°C/s (9°F/s) to 35.5°C/s (64°F/s) at 538°C (1000°F). The tensile properties of the GMA weld metal of Alloys 10 and 11 deposited at 1.33 and 3.2 kJ/mm (34 and 82.5 kJ/in.) heat input with Ar-5%CO_2 shielding gas on HY-100 base plate are given in Table XV; the calculated cooling rates are 3.5°C/s (6.4°F/s) and 36°C/s (64.5°F/s) at 538°C (1000°F) respectively.[225] There is an increase of 89.5 MPa (13 ksi) in the yield strength with an increase in cooling rate from 5°C/s (9°F/s) to 35.5°C/s (64°F/s) at 538°C (1000°F) for Alloy 11 weld metal, Fig. 29. The data reported in Table XV indicates an increase of 90 MPa (13 ksi) in yield strength of GMA weld metal of Alloy 11 with an increase in cooling rate from 3.5°C/s (6.4°F/s) to 36°C/s (64.5°F/s)

at 538°C (1000°F), Fig. 30. In commercially available filler wires the increase in yield strength over the same range is approximately 152 MPa (22 ksi), and a minimum cooling rate of 11°C/s (20°F/s) at 538°C (1000°F) is required to attain a minimum yield strength of 703 MPa (102 ksi).[5]

Yield strength also varied linearly with the Hardness. Fig. 31 shows the variation of yield strength with Rockwell C hardness (HRC) for the higher strength weld metals, and Fig. 32 shows the variation of yield strength with Rockwell B hardness (HRB) for lower strength weld metals. Empirical linear relationship between yield strength (YS) and HRC is given by the equation:

$$YS\ (ksi) = 1.54\ (HRC) + 70.4 \qquad (5.1)$$

and between YS and HRB is given by:

$$YS\ (ksi) = 1.54\ (HRB) - 60.2 \qquad (5.2)$$

Using these empirical relationships a reasonably accurate estimate of yield strengths for ULCB weld metals can be attained from their hardness values.

GTA weld metal deposited on Alloy 7 plate using matching filler at 3.5 kJ/mm (90 kJ/in.) using Ar-5%CO_2 shielding gas attained a yield strength of 733 MPa (107 ksi), Table XIII and Fig. 27(a). Based on the hardness values, the GMAW weld metal of Alloy 11 deposited on HY-100 base plate at 2.3 kJ/mm (60 kJ/in.) heat input using Ar-5%CO_2 shielding gas attained average yield strength of 734 MPa (106.5 ksi), Table XIV and Fig. 29.

GMA weld metals deposited using Alloy 10 and Alloy 11 filler wires on HSLA-100 base plate at 2.5 kJ/mm (64 kJ/in.) heat input using Ar-5%CO_2 shielding

gas attained yield strengths of 710 MPA (103 ksi) and 712.4 MPa (103.3 ksi), respectively, calculated using equation 5.1 and the weld metal hardness values. The differences in the respective hardness values of GMA weld metal deposited with Alloys 10 and 11 on HSLA-100 base plate at 2.5 kJ/mm (64 kJ/in.) and 1.9 kJ/mm (48 kJ/in.) heat input using Ar-5%CO_2 shielding gas were negligible (Table XII and Fig. 33) illustrating the insensitivity of ULCB weld metal to cooling rate.

IMPACT TOUGHNESS

Weld metal Charpy V notch (CVN) toughness testing was carried out at 25°C (77°C), -18°C (0°F) and -51°C (-60°F). For the weld metal of Alloy 11 deposited at 2.5 kJ/mm (64 kJ/in.) heat input with Ar-5% CO_2 shielding gas, on HSLA-100 base plate, the CVN tests were carried out at 150°C (303°F), 25°C (77°F), -18°C (0°F), -51°C (-60°F), -100°C (148°F) and -196°C (-321°F) in order to determine a full transition curve. Results of the CVN toughness tests are shown in Tables XVI to XXXVIII and Fig. 34 (a) to (f). GTA weld metal of Alloy 1, with the lowest CEN value, 0.20, deposited using Ar-5%CO_2 at 2 kJ/mm (51 kJ/in.) on matching plate had the highest CVN absorbed energy values. All the samples tested at room temperature and -18°C (0°F) and one sample at -51°C (-60°F) had absorbed energy values of 355 J (262 ft-lb), which is the upper limit of the CVN impact testing machine, Table XVI, Fig. 34(a). GTA weld metal of Alloy 4, with the highest C content (0.064% C), deposited at 3.5 kJ/mm (90 kJ/in.) heat input on matching base plate had average CVN absorbed energy values of 45 J (32 ft-lb) at -51°C (-60°F),

Table XIX and Fig. 34(b). These are the lowest CVN absorbed energy values for GTA weld metal of the VIM ingots with no B addition. SEM fractographs of the CVN test carried out at -51°C (-60°F), on the weld metal of Alloy 4, deposited at 3.5 kJ/mm (90 kJ/in.) heat input on matching base plate with Ar-5%CO_2 and Ar-25%He shielding gases, Fig. 35 (a) and (b) respectively, show a cleavage fracture.

The variation of CVN absorbed energy with Yurioka's CEN values for GTA weld metal deposited at 3.5 kJ/mm (90 kJ/in.) and 2 kJ/mm (51 kJ/mm) tested at -18°C (0°F) and -51°C (-60°F) is shown in Fig. 36(a) and (b), with the absorbed energy values decreased with increasing CEN values. The slower cooling 3.5 kJ/mm (90 kJ/in.) GTA weld metal and 2.5 kJ/mm (64 kJ/mm) GMA weld metal with identical cooling rate had lower CVN toughness values than the corresponding faster cooling 2 kJ/mm (51 kJ/in.) GTA weld metal and 1.9 kJ/mm (48 kJ/in.) GMA weld metal.

GTA weld metal of Alloy 7 deposited at 3.5 kJ/mm (90 kJ/in.) heat input with Ar-5%CO_2 shielding gas on matching base plate with 733 MPa (106 ksi) yield strength, Table XIII and Fig. 27(a), had average CVN absorbed energy values of 87 J (64 ft-lb) at -18°C (0°F) and 73 J (54 ft-lb) at -51°C (-60°F), Table XXII and Fig. 34(d), meeting the mechanical property requirements for HSLA-100 weld metal.[226] SEM fractographs of the CVN test carried out at -51°C (-60°F) on the weld metal of Alloy 7 with Ar-5%CO_2 shielding gas, Fig. 37, show ductile dimples on the fracture surface indicating a ductile fracture. The GTA weld metal of Alloy 7 deposited using identical welding conditions and Ar-25%He shielding gas instead of

Ar-5%CO_2 had average CVN absorbed energy values of 233 J (172 ft-lb) at -18°C (0°F) and 193 J (142 ft-lb) at -51°C (-60°F), Table XXII and Fig. 34(d) and 38. Similarly the GTA weld metal deposited on HSLA-100 plate with Alloy 7 filler using Ar-5%CO_2 shielding gas had average CVN absorbed energy values of 84 J (62 ft-lb) at -18°C (0°F) and 42 J (31 ft-lb) at -51°C (-60°F), and the GTA weld metal deposited under identical conditions using Ar-25%He shielding gas had CVN absorbed energy values of 240 J (177 ft-lb) at -18°C (0 °F) and 136 J (100 ft-lb) at -51°C (-60°F), Table XXXV and Fig. 39. This substantial increase in CVN absorbed energy values is attributed to reduction in inclusion volume fraction of the weld metal, the effect of inclusions on the CVN toughness is analyzed in detail later on in this chapter.

The GTA weld metal of Alloy 11 deposited on Alloy 5 base plate using Ar-5%CO_2 and 3.5 kJ/mm (90 kJ/in.) heat input had a yield strength of 599 MPa (86.8 ksi), calculated using the weld metal hardness and equation 5.2, and average CVN absorbed energy value of 60 J (81 ft-lb) at -51°C (-60°F), Table XXVI and Fig. 34(e). The GMA weld metal of Alloy 11 deposited at 2.5 kJ/mm (64 kJ/in.) heat input (to match the cooling rate of 3.5 kJ/mm (90 kJ/in.) GTA welds) with Ar-5%CO_2 shielding gas on a HSLA-100 base plate had CVN absorbed energy values of 127 J (94 ft-lb) at -18°C (0°F) and 84 J (62 ft-lb) at -51°C, Table XXXIV, and had a yield strength of 712 MPa (103 ksi) calculated using equation 5.1 and the weld metal hardness value from Table XII, thus meeting the mechanical property requirements for HSLA-100 weld metal.[226] Fig. 40 shows the comparison of GTA and GMA weld metal for Alloy 11 deposited at identical cooling rates. For the same

cooling rate the GTA and GMA weld metal did not exhibit a great variation in CVN toughness values.

GMA weld metal of Alloy 11 deposited on HSLA-100 base plate at 2.5 kJ/mm (64 kJ/in.) heat input using Ar-5%CO_2 shielding gas did not exhibit a sharp transition temperature. The CVN absorbed energy values dropped gradually over a temperature range from 25°C (77°F) to -125°C (-193°F), as shown in Fig. 41. SEM fractographs of the fractured surfaces of the CVN bars of the GMA weld metal of Alloy 11 deposited at 2.5 kJ/mm (64 kJ/in.) with Ar-5%CO_2 shielding gas on HSLA-100 base plate are shown in Fig. 42-45. At -18°C (0°F) the fracture is completely ductile, showing the classic dimples, Fig. 42. At -51°C (-60°F) the fracture surface is still predominantly ductile, however, there are a few areas where cleavage fracture seems to have occurred, Fig. 43 (a) and (b). At -100°C (-148°F), Fig. 44, there is a substantial increase in the area of cleavage fracture and at -196°C (-321°F, liquid nitrogen) the fracture is entirely cleavage, Fig. 45.

The GTA welds deposited at 3.5 kJ/mm (90 kJ.in) heat input with Ar-5%CO_2 shielding gas on HSLA-100 and HY-130 base plates using Alloy 7 filler had lower CVN absorbed energy values compared to those of the corresponding Alloy 7 weld metal deposited on a matching base plate, Fig. 46. The CVN absorbed energy values of the GTA weld metal deposited at 3.5 kJ/mm (90 kJ/in.) heat input with Ar-5%CO_2 shielding gas on HSLA-100 base plate with commercial filler wires of MIL-100S and MIL-120S type were lower than the corresponding weld metal of Alloy 7 deposited on HSLA-100 base plate, Fig. 47. The ULCB weld metal

maintains better CVN toughness values compared to those of the commercial filler wires under identical welding conditions.

GMA weld metal of Alloy 7 deposited at 2.5 kJ/mm (64 kJ/in.) heat input with Ar-5%CO_2 and Ar-25%He shielding gases on HSLA-100 base plate had poor CVN toughness values, Table XXXII. This is attributed to the lubricant trapped in the wire during the wire swaging and drawing process. A micrograph of the cross section of the Alloy 7 filler wire is shown in Fig. 48.

GTA weld metal of Alloys 12 through 15 deposited at 3.5 kJ/mm (90 kJ/in.) heat input with Ar-5%CO_2 shielding gas on matching base plate exhibited poor low temperature CVN toughness values because of the higher than ideal B content for the very clean VIM steels. GTA weld metal of Alloys 1 and 12 have almost identical chemical composition except for 0.0021 wt% B in Alloy 12, similarly Alloys 2 and 14 have almost identical chemical composition except for the 0.0027 wt% B addition in Alloy 14, Table IV and V. Comparison of CVN impact toughness of GTA weld metal deposited at 3.5 kJ/mm (90 kJ/in.) heat input using Ar-5%CO_2 shielding gas on matching base plate for alloys 1 and 12 and alloys 2 and 14 shown in Fig. 50(a) and (b) illustrates the embrittling effect of excessive B in ULCB weld metal. An optical micrograph showing the presence of borocarbides at the grain boundaries is shown in Fig. 8.

EFFECT OF MICROSTRUCTURE ON MECHANICAL PROPERTIES

A wide variety of microstructures were observed ranging from granular bainite

with no laths to carbide free bainite with well developed laths. Virtually no difference was observed in the hardness values of GTA weld metal of Alloy 7 deposited at 3.5 kJ/mm (90 kJ/in.) heat input resulting in coarser grain size and lath width and the 2 kJ/mm (51 kJ/in.) weld metal, with finer prior austenite grain size and lath width, Fig. 7 and 17. Lath size of the 3.5 kJ/mm (90 kJ/in.) weld metal for Alloy 7 was approximately three times that of the 2 kJ/mm (51 kJ/in.) weld metal. Thus, grain size and lath width did not have a pronounced effect on the strength of the ULCB weld metal. A comparison of harness values of 3.5 kJ/mm (90 kJ/in.) and 2 kJ/mm (51 kJ/in.) GTA weld metal deposited on matching base plates using Ar-5%CO_2 shielding gas for Alloys 1-16 is shown in Fig. 25 (a) and (c).

Laths per se and the lath width did not seem to have an effect on the toughness of the ULCB weld metal. Alloy 4, 6 and 9 have similar yield strength levels. Alloy 4 with a well developed lath structure had lower CVN absorbed energy values than Alloys 6 and 9 with mixed morphologies, Fig. 50. Lower CVN impact toughness of Alloy 4, even though it had well developed lath structure was attributed to higher C level in the alloy. Alloy 1 with granular bainitic microstructure had substantially higher CVN absorbed energy values than those of Alloys 4 and 7 with well developed lath structure, Fig. 51. Although Alloy 1 has a lower yield strength, the laths in Alloys 4 and 7 did not help increase the CVN absorbed energy values and the absence of laths in Alloy 1 did not lower the CVN absorbed energy values. There was very little difference in the CVN absorbed energy values of Alloy 7 welds made at 3.5 kJ/mm (90 kJ/in.) and 2 kJ/mm (51 kJ/in.) heat input, Fig. 38. The lath

width for the 2 kJ/mm (51 kJ/in.) welds was approximately three times finer than the 3.5 kJ/mm (90 kJ/in.) welds, Fig. 17. The results indicate that the presence laths as well as the lath width does not have a pronounced effect on the CVN impact toughness of the ULCB weld metal.

Alloy 4, with well developed laths, had lower CVN absorbed energy values compared to Alloy 6 with a mixed morphology. Both alloys had a comparable yield strength, indicating that laths did not affect ULCB steel weld metal toughness. Similarly Alloy 4 and Alloy 7 had well developed laths, but Alloy 7 with higher yield strength had higher CVN absorbed energy values. Since Alloy 6 with mixed morphology and Alloy 7 with well developed laths had good CVN impact toughness, ULCB weld metal toughness may be independent of prior austenite grain size and the substructure within the grains.

CVN absorbed energy values for the GTA weld metal deposited at 2 kJ/mm (51 kJ/in.) using Ar-5%CO_2 shielding gas were greater than those of the 3.5 kJ/mm (90 kJ/mm) heat input weld metal of the same alloy deposited under identical conditions. However, the increase in CVN absorbed energy values for GTA weld metal deposited at 3.5 kJ/mm (90 kJ/in) heat using Ar-25%He shielding gas was considerably greater than the increase due to lower heat input, indicating that finer prior austenite grain size and smaller lath width were less effective in increasing the CVN absorbed energy values than a cleaner shielding gas which results in lower inclusion volume fraction in the weld metal. Effect of inclusions on the CVN absorbed energy values of ULCB weld metal is discussed in the next section.

EFFECT OF INCLUSIONS ON CVN TOUGHNESS

The volume fraction of inclusions in the GTA weld metal of Alloy 7 deposited at 3.5 kJ/mm (90 kJ/in.) heat input with Ar-5%CO_2 shielding gas on a matching base plate averaged five times that of the GTA weld metal deposited at identical heat input using Ar-25%He shielding gas, and the average inclusion size in the Ar-5%CO_2 weld metal was two times that of the Ar-25%He weld metal. Inclusion analysis and the particle size distribution results for GTA weld metals of Alloy 7 deposited at 3.5 kJ/mm (90 kJ/in.) using Ar-5%CO_2 and Ar-25%He shielding gases are shown in Table IX and Fig. 22(a) and (b). X ray analysis of inclusions in the TEM samples showed that inclusions contained oxides of Mn, Si and Fe. Results of the EDAX analysis is shown in Fig. 52.

Comparison of CVN absorbed energy values of the GTA weld metal deposited with different shielding gases and heat inputs on matching base plates for Alloys 4-7 are shown in Fig. 38 and 53-55. GTA weld metal deposited at 3.5 kJ/mm (90 kJ/in.) and 2 kJ/mm (51 kJ/in.) heat input using Ar-5%CO_2 shielding gas exhibited lower CVN absorbed energy values than those of the GTA weld metal deposited at 3.2 kJ/mm (82 kJ/in.) and 3.5 kJ/mm (90 kJ/in.) heat input using Ar and Ar-25%He shielding gases, respectively, for the same Alloy. The Ar and Ar-25%He welds made at 3.2 and 3.5 kJ/mm heat inputs, respectively, had higher CVN absorbed energy values than the Ar-5%CO_2 welds made at 2 kJ/mm heat input. Ar and He used were welding grade. The higher CVN absorbed values of the GTA weld metal deposited using Ar and Ar-25%He shielding gases compared to those of the weld

metal deposited using Ar-5%CO_2 shielding gas on the same Alloy was due to the lower inclusion volume fraction and smaller average inclusion diameter of the Ar and Ar-25%He weld metals, Table IX.

Comparable CVN absorbed energy values at -51°C (-60°F) for 3.5 kJ/mm (90 kJ/in.) welds of Alloy 4 (Fig. 54), regardless of the shielding gas, were attributed to the relatively higher C content (0.064%) of Alloy 4 weld metal. SEM fractograph of the fracture surfaces of CVN test samples of Alloy 4 GTA weld metal deposited at 3.5 kJ/mm (90 kJ/in.) using Ar-5%CO_2 and Ar-25%He shielding gases on matching base plate and tested at -51°C (-60°F), show a cleavage fracture surface indicating brittle failure, Fig. 35.

The CVN absorbed energy values of GTA weld metal samples tested at room temperature did not always follow the trend observed by the samples tested at -18°C (0°F) and -51°C (-60°F) as shown in Fig. 53 and 55. Since only one sample each was tested at room temperature, this is attributed to scatter. The filler wire was hand fed into the weld pool. Care was taken to maintain a uniform feed rate, however, minor variations can not be ruled out. That could vary the cooling rates in different welds leading to some scatter in CVN impact toughness values. The important inference made from this data is that when the fracture is controlled by microvoid coalescence and growth, the Ar-25% He welds show consistently higher CVN absorbed energy values compared to those of the Ar-5% CO_2 weld metal, regardless of the heat input.

The CVN absorbed energy values of the GTA weld metal deposited with Ar at

3.2 kJ/mm and with Ar-25%He at 3.5 kJ/mm are consistently higher than those of the corresponding welds made with Ar-5%CO_2 at 2 kJ/mm, Fig. 38, 53-55. This indicates that the increase in CVN absorbed energy due to the finer grain size (caused by lower heat input) is much smaller than the increase in CVN absorbed energy resulting from the lower inclusion density in the weld metal. Therefore, a reduction in inclusion density (due to a cleaner shielding gas) is a more effective approach compared to finer grain size for improving ULCB weld metal CVN toughness.

EFFECT OF CARBON ON WELD METAL PROPERTIES

The role of C in increasing the susceptibility to cold cracking is well documented. Increase in C content of the weld metal increases the hardness of martensite making the weld metal more prone to hydrogen assisted cracking. Hardness of martensite is the maximum possible hardness a steel weld metal can have, however, in relatively higher carbon steels with carbon levels above the solid solubility limit of carbon in ferrite, excess carbon can form areas with carbon concentrations much greater than the average concentration, leading to a great increase in the hardness of martensite in the carbon enriched areas, increasing the susceptibility of the weld to HAC. Hardness of martensite for each weld metal calculated using Yurioka's[222] model are given in Table VI. Weld metal of Alloy 4 with highest C has the maximum attainable hardness value at 351 VHN.

GTA weld metal of Alloys 2 and 4 have identical composition with exception of C concentration. Alloy 2 weld metal has a C level of 0.017% and Alloy 4 has a

C level of 0.064%. Comparison of the yield strengths of the GTA weld metal of the Alloys 2 and 4, Fig. 56(a) and Table XIII, deposited at 3.5 kJ/mm (90 kJ/in.) with Ar-5%$C0_2$ shielding gas on matching plate shows that a 0.047% increase in C content of the weld metal caused an increase of 60 MPa (8.7 ksi) in the yield strength. Yurioka's CEN value for Alloys 4 and 9 is 0.31. Alloy 4 has 0.044% more C than Alloy 9, which caused a very small 17.5 Mpa (2.5 ksi) increase in yield strength of Alloy 4 compared to that of Alloy 9, Fig. 56(b) and Table XIII.

A decrease in C content, however, caused a substantial improvement in the CVN toughness of the weld metal. Comparisons of the CVN absorbed energy values for the GTA weld metal of Alloys 2 and 4 deposited at 3.5 kJ/mm (90 kJ/in.) and 2 kJ/mm (51 kJ/in.) with Ar-5%CO_2 shielding gas on matching base plate are shown in Fig. 57(a). The low C Alloy 2 weld metal has CVN absorbed energy values more than two times as high as those of the high C Alloy 4 weld metal at -51°C (-60°F), at 3.5 kJ/mm (90 kJ/in.) as well as 2 kJ/mm (51 kJ/in.) heat input. Similarly a comparison between the CVN absorbed energy values of Alloys 4 and 9, Fig. 57(b), with identical CEN value of 0.31 and different C levels illustrates the deleterious effect of C on CVN toughness. GTA weld metal of Alloy 9 with higher C deposited at 3.5 kJ/mm (90 kJ/in.) and 2 kJ/mm (51 kJ/in.) heat input with Ar-5%CO_2 shielding gas on matching base plate has consistently lower CVN absorbed energy values compared to those of the corresponding GTA weld metal of low C Alloy 9. A plot of CVN absorbed energy values versus heat input for Alloys 2 and 4 shown in Fig. 58 illustrates that there is no increase in CVN absorbed energy values of the

weld metal with decreasing heat input in case of high carbon Alloy 4 weld metal, whereas, the weld metal of low carbon Alloy 2 shows an increase in CVN absorbed energy values with decreasing heat input.

EFFECT OF BORON ON WELD METAL PROPERTIES

GTA weld metals of B containing Alloys 12-15 deposited on matching base plate using Ar-5%CO_2 shielding gas at 3.5 kJ/mm (90 kJ/in.) had poor low temperature CVN toughness values, Table XXVII to XXX and Fig. 34(e) and (f). Alloys 1 and 12, and Alloys 2 and 14 have identical compositions with the exception of B concentration. Alloys 1 and 2 have no intentional B added to them, and Alloys 12 and 14 have 0.0021 and 0.0027 wt.% B added to them. The GTA weld metal of Alloy 12 showed a 59 MPa (8.5 ksi) increase in yield strength compared to that of Alloy 1, and GTA weld metal of Alloy 14 showed a 79 MPa (11.4 ksi) increase in yield strength compared to that of Alloy 2, Fig. 59.

Boron, however, had a strong deleterious effect on the CVN toughness of the GTA weld metal. Comparisons of CVN absorbed energy values of the GTA weld metals deposited on matching plate at 3.5 kJ/mm (90 kJ/in..) using Ar-5%CO_2 shielding gas for Alloys 1 and 12 and Alloys 2 and 14 are shown in Fig. 49(a) and (b). Addition of B causes a reduction of more than 100 J (73.7 ft-lb) in CVN absorbed energy values is -51°C (-60°F) in both the cases. The lower CVN toughness was attributed to a large excess of boron over the ideal concentration of 0.0005%, which is reported to have a beneficial effect on CVN toughness.[60]

EFFECT OF O, N, Al and Ti ON MICROSTRUCTURE AND TOUGHNESS

Inclusions did not have a noticeable effect on the prior austenite decomposition products, only in Alloy 5 were some of the inclusions associated with ferrite nucleation. The morphology of the ferrite nucleated at the inclusions in Alloy 5 was not that of acicular ferrite, Fig. 21.

Although the Al and Ti levels in the weld metal were low because of the difficulties encountered by the melter in adding small controlled amounts of Al and Ti in 25 kg (55 lb) heats, one significant role Al and Ti are likely to play in the ULCB weld metal is that of gettering the nitrogen and oxygen imparted to the weld metal by the shielding gas and dilution. Because of the low levels of Al and Ti in the weld metal their effects could not be assessed. The effect of inclusions, primarily caused by oxygen in the shielding gas, on the CVN toughness of the ULCB weld metal has been discussed in the section titled "Effects of Inclusions on CVN Toughness".

The role of nitrogen is very similar to that of C. Since nitrogen has three times the dislocation locking strength of C it is likely to have a greater deleterious effect on the CVN toughness of the weld metal.[17] Therefore the level of nitrogen was kept as low as possible.

ALLOYING WITH Mn, Ni and Mo

Mn, Ni and Mo were the primary substitutional solid solution strengthening alloys used. Their addition increased the CEN and lowered the calculated B_s temperature, Table V and VI. Lower B_s temperature results in higher dislocation

density due to the increase in transformation induced dislocations, which translates into higher yield strength with increasing alloy content.

Ni is the conventional alloying element used for improving toughness of steels. A comparison of CVN toughness of the GTA weld metal of Alloys 7 containing 4.8% Ni and 8 containing 3% Ni indicates that 1.8% increase in Ni caused a substantial increase in CVN absorbed energy values of GTA weld metal of Alloy 7 at -51°C (-60°F) and -18°C (-0°F) as shown in Fig. 60. GTA weld metal of Alloy 6 deposited at 3.5 kJ/mm (90 kJ/in.) using Ar-5%CO_2 containing 0.034% C and 4.4% Ni had lower CVN absorbed energy values than the corresponding weld metal of Alloy 3 containing 0.017% C and 2.6% Ni, Fig.61. This indicates that higher C content neutralized the beneficial effect of higher Ni content in the weld metal. Increasing Mo content caused a drop in the CVN absorbed energy values and increased the yield strength of the GTA weld metal for Alloys 1, 3, 8 and 9, as shown in Fig. 62.

Effect of Mn on strength and toughness could not be determined due to the problems encountered by the melter in producing ingots with Mn levels greater than 1%. However, a comparison was made between GTA weld metals of Alloy 5 containing 1.2% Mn and Alloy 2 containing 0.65% Mn. Within this limited range Mn had no effect on the CVN absorbed energy values as shown in Fig. 63, but did increase yield strength.

VI. DISCUSSION

The microstructures, strength and hardness, impact toughness and the effect of inclusions on the toughness of the ULCB weld metal is discussed in this section. The discussion is based on the available literature and the results obtained during this investigation.

MICROSTRUCTURE

The only standard terminology for classification of bainitic microstructures available in the literature is for classical upper and lower bainite. The nonclassical forms of bainite viz, bainite exhibiting lathy morphology with no intralath carbides but with or without interlath M-A constituent and bainite with no laths again with or without M-A islands do not have a universally accepted terminology capable of defining and distinguishing the various non classical forms of bainite.

Ohmori[82] divided bainite into three different forms: (a) BI-carbide free bainite formed between 600° and 500°C, during isothermal transformation. (b)-BII lath bainite with inter lath carbides formed between 500° and 450°C, during isothermal transformation. (c) BIII-bainite with carbide morphology similar to that of lower bainite and formed between 500°C and M_s, during isothermal transformation. This terminology does not account for the continuous cooling transformation products and also it can be difficult to determine the transformation temperature by merely observing a micrograph. Bramfit and Speer[94] have proposed a similar terminology consisting of: (a) Class 1 bainite, B_1, with intralath carbides. (b) Class 2 bainite, B_2,

with interlath carbides. (c) Class 3 bainite, B_3, with discrete regions of retained austenite or M-A constituent. This terminology is also by no means comprehensive, besides both B_1 and B_2 can have retained austenite or M-A constituent. For the present investigation microstructures of the ULCB metals were termed 'carbide free bainite' and 'granular bainite' according to subsequent developments of the terminology first employed by Habraken and Economopoulos.[91-93]

The 3.5 kJ/mm GTA weld metal of Alloy 1 with the lowest alloying element content (Table V) and lowest Yurioka's CEN value at 0.20 (Table VI), had granular bainite microstructure with no laths. Alloys 5, 6, 8 and 9 with Yurioka's CEN values varying from 0.27 to 0.41 exhibited mixed morphology. Alloy 7 with highest Yurioka's CEN value at 0.44 had well developed laths exhibiting a carbide free bainite microstructure. Alloy 4 with highest carbon content at 0.064% also exhibited carbide free bainite microstructure with well developed laths although the CEN value (0.31) for Alloy 4 is in the intermediate range. The GMA weld metal of Alloys 10 and 11 also had well developed laths with CEN values at 0.31 and 0.32. It is postulated that higher carbon in Alloy 4 and higher nitrogen levels in the Alloy 10 and Alloy 11 weld metal might have promoted the lath formation, even though the reasons and mechanism for lath formation during the austenite decomposition are not well established.[227] The finer lath width due to faster cooling rate can be accounted for by the fact that with decreasing B_s temperature the critical nucleus size is lowered because the increase in the free energy change accompanying the transformation.[227]

No M-A islands were found by the TEM observation. Extremely low

carbon levels and the relatively fast cooling rates during welding lower the amount of carbon able to diffuse to the lattice defects in austenite ahead of the transformation front thereby number and size of the stabilized islands of austenite and retained austenite in between the laths is significantly reduced. Thus given the very small sampling area of a TEM specimen probability of locating and observing retained austenite under such conditions is very small. Therefore, even though it may be present, no carbides or retained austenite could be observed in the small sampling area of the TEM specimens. However, because the free energy of the system is lowered by the segregation of carbon to the dislocations,[114] it is possible that in the ULCB weld metal with high dislocation density and extremely low carbon levels all the available carbon atoms diffuse to the dislocations and do not have a high enough concentration anywhere in the matrix to form M-A islands or carbides.

Since there are no observable carbides in these microstructures, positive identification of these microstructures is extremely difficult, as there is no sure way to tell the difference between the martensitic laths and the bainite laths without observation of carbide morphology. Even in the presence of carbides differentiating between tempered martensite and bainite can be a challenge. However, considering the cooling rates encountered during welding and the work by Garcia et al.,[14] who have termed the microstructures of steels with similar compositions as bainite, the weld metal microstructures for the steels in this work can be termed bainitic. Also the transformation start temperature in the CCT diagram for Alloy 5 kept steadily dropping from a cooling rate of 0.02°C/sec to 75°C/sec, Fig. 5. This indicated that

martensite formation in ULCB weld metals did not start even at cooling rates as fast as 75°C/sec. All the measured hardness values of the weld metal are lower than the hardness values of martensite predicted by Yurioka's model, Table VI, again indicating that the microstructures are probably bainitic. There is sufficient circumstantial evidence to term the microstructures for these ultra low carbon steel weld metals as bainitic with a degree of certainty.

STRENGTH AND HARDNESS

GTA weld metal of Alloy 7 with 0.015% C (Table V) attained a yield strength of 733 MPa (106.3 ksi), Table XIII, proving that strength levels above 690 MPa (100 ksi) can be attained in the virtual absence of carbon and without any help from the dislocation substructure generated by thermomechanical processing. Most conventional steels show a strong effect of grain size on strength, however, grain size was not found to be a critical factor in controlling the strength, as is evidenced by a very small change in hardness with the change in cooling rate, Fig. 26. Similar results have been reported by Brownrigg[228] in the case of low carbon martensite. The results clearly indicate that the contribution of grain size and lath width to yield strength is minor in ULCB steel weld metal. Transformation induced dislocations due to low B_s temperatures coupled with increased substitutional solid solution strengthening due to increasing alloying element content were responsible for significant increases in strength. From the two CCT diagrams, Figs. 5 and 6, it is evident that there is an across the board difference of approximately 100°C (180°F) in

B_s temperature at corresponding cooling rates for the GTA weld metal of Alloy 5 with a CEN value of 0.27 and that of Alloy 16 with a CEN value of 0.43. The increase in yield strength for the CEN and B_s change is 233 MPa (33.3 ksi). Therefore successful design of ULCB weld metal for high strength applications must depend on substitutional solid solution strengthening and the accompanying lower B_s resulting in higher transformation induced dislocation densities.

Alloys 10 and 11 have CEN values of 0.31 and 0.32 respectively, Table VI, GTA weld metal of these alloys deposited at 3.5 kJ/mm (90 kJ/in.) heat input with Ar-5%CO_2 shielding gas had hardness values of 99.2 and 95.6 HRB (Table X) respectively, which are comparable in the general range of hardness values expected from the GTA weld metal of other ULCB alloys. Hardness of the GTA weld metal of Alloy 10 is a little higher than that of Alloy 11 because the base plate for the GTA weld was that of Alloy 8 containing 2.4% Mo, thus the excess Mo accumulation in the weld metal, due to excessive dilution involved in the GTA welds. Higher Mo in the Alloy 10 weld metal resulted in an increase in the hardness of Alloy 10 GTA weld metal. However the GMA weld metal of Alloys 10 and 11 deposited on HSLA-100 base plate had average hardness values of 21.2 and 21.4 HRC, Table XII, which are significantly higher than the GTA weld metal hardness values. Yield strength of GMA weld metal of Alloy 10 is 748 MPa (108.5 ksi), Table XIII, and yield strength of the corresponding GTA weld metal calculated using the weld metal hardness, Table X, and equation 5.2 is 644.6 MPa (93.5 ksi), representing an increase of 103 MPA (15 ksi). Similarly for the weld metal of Alloy 10 the change from GTAW to

GMAW resulted in an increase of 135 MPa (19.5 ksi).

GMA weld metal of Alloy 10 contains 0.0027% nitrogen and that of alloy 11 contains 0.0051% nitrogen and the nitrogen content of the GTA weld metal is an order of magnitude smaller. Carbon and nitrogen atoms associated with dislocations in the steel matrix have a relatively large effect on the strength. According to Brozzo et al.,[136] contribution to strength by C and N in interstitial solid solution is given by:

$$\sigma_{ssi} = 1900\ [(C+N)_{wt\%}]^{1/2} \qquad (7.1)$$

Where σ_{ssi} is the contribution of interstitial solid solution strengthening to the strength of the steel. From the above equation there is a contribution of 99 MPa (14.3 ksi) and 135.6 MPa (19.6 ksi) to the GMA weld metal of Alloy 10 and Alloy 11 respectively, which is almost exactly the same as the differences in the yield strengths physically observed. The nitrogen content is the only significant difference between the two kinds of weld metals for each alloy. It is assumed that this is due to the inherently violent nature metal transfer in the GMAW process which causes air to be entrained into the shielding gas. The increase in yield strength of the GMA weld metal is therefore attributed to the increase in nitrogen content of the weld metal. It is interesting to note that the Yurioka's CEN values do not reflect the effect of these apparently small changes in nitrogen content. The measured hardness values did vary linearly with the Yurioka's CEN values, however the predicted hardness values of the weld metal, Table VI, were higher than the measured hardness values, Tables X and XI. It is possible that the empirical relationships developed for the Yurioka's

model are not entirely valid for the ULCB steel weld metals.

Carbon, as expected, also has a strong effect on strength, the GTA welds made on HY-130 base plate with Alloy 7 filler metal and Ar-5%CO_2 shielding gas had the highest average hardness value at 32.7 HRC, Appendix II, which translates to a calculated yield strength of 832 MPa (120.7 ksi). The results also indicate the inadequacy of the commercially available MIL-100S-1 and MIL-120S-1 type filler wires. The GTA weld metal of both these wires deposited on HSLA-100 base plate had hardness values of 94.8 and 99.4 HRB respectively, which translates to a yield strength of 591 MPa (85.8 ksi) for the MIL-100S-1 wire and 640 MPa (92.8 ksi) for the MIL-120S-1 wire. The CVN toughness values for these wires were also lower than the requirements.[226] Impact toughness of the ULCB steel weld metal is discussed in the next section.

IMPACT TOUGHNESS

According to Naylor et al.,[74] an increase in toughness can be realized by decreasing both the lath width and the packet size. They showed ductile brittle transition (DBT) to be a logarithmic function of the inverse square root of the product of lath width and packet size. As discussed in the section on microstructures, no packets were observed in the ULCB weld metals, and the laths ran across the prior austenite grain boundaries. It is clear from the comparison of the CVN absorbed energy values of Alloys 4, 6 and 9, Alloys 4 and 7, and 3.5 kJ/mm (90 kJ/in.) and 2 kJ/mm (51 kJ/in.) weld metal of Alloy 7, shown in Figs. 50, 51 and 38 respectively, that laths and the lath width was not found to be a controlling factor for the toughness

of the ULCB weld metal.

The packets have high angle grain boundaries between them and hence the cleavage planes in the packets intersect at large angles causing a sharp change in the direction of crack propagation, which requires greater energy, consequently improving toughness. Laths, however, have low angle grain boundaries between them and hence can not provide a sharp deviation in the crack path, which is probably the reason why finer lath size did not improve the toughness of the ULCB weld metal.

Insensitivity of CVN toughness to the microstructure also translates to insensitivity to cooling rate indicated by a relatively small improvement in CVN absorbed energy values of the welds made at 2 kJ/mm (51 kJ/in.) representing t_{8-5} of 35 s compared to those of the corresponding welds made at 3.5 kJ/mm (90 kJ/in.) weld metal with t_{8-5} of 15 s. Refinement in the prior austenite grain size resulting from lower heat input did not significantly increase the impact toughness of the weld metal, Figs. 38, 53, 54 and 55. According to Leslie et al.,[203] removal of interstitial solute atoms from bcc iron removes most of the grain size dependence of DBT temperature. They have reported an increase of 3°C in the DBT temperature per ASTM grain size for Fe-0.15% Ti alloy. CVN absorbed energy values of the GMA and GTA weld metal of Alloy 11 deposited at identical cooling rates with Ar-5%CO_2 shielding gas were comparable, Fig. 36. This indicates that, for a given cooling rate and shielding gas, switching from the GTAW to GMAW process has no effect on the toughness of the weld metal.

Ni:Mo ratio may have some effect on the CVN toughness of the ULCB weld

metal at higher strength levels. GTA weld metal deposited at 3.5 kJ/mm (90 kJ/in.) with Ar-5%CO_2 shielding gas for Alloy 7 with a Ni:Mo ratio of 2 and that of Alloy 9 with a Ni:Mo ratio of 1.8 had average CVN toughness values of 73 J (54 ft-lb) and 58 J (47 ft-lb) respectively, at -51°C (-60°F). Alloy 8 with a Ni:Mo ratio of 1.2 and lower yield strength than that of Alloy 7, had average CVN toughness values of 36 J (29.2 ft-lb) at -51°C (-60°F) for 3.5 kJ/mm (90 kJ/in) welds made with Ar-5%CO_2 (Tables XXII-XXIV). Thus, it appears that the Ni:Mo ratio of about 2 or higher may be essential to maintain adequate CVN absorbed energy values for ULCB weld metal. However, this is based on just three alloys, thus work needs to be done on a series of alloys with varying Ni and Mo to establish this. GTA weld metal for Alloy 10 with 5.59% Ni and 0.7% Mo deposited on Alloy 8 base plate with 3.07% Ni and 2.4% Mo at 3.5 kJ/mm (90 kJ/in.) with t_{8-5} of 34 s had lower CVN absorbed energy values compared to the GMA weld metal of Alloy 10 deposited on HSLA-100 base plate with heat input adjusted to match the cooling rate of the GTA weld. This indicates that the increase in Mo content in the weld metal due to the dilution from the base metal was deleterious to toughness, further indicating that a balance between Ni and Mo may be required to maintain good toughness levels particularly at high strength levels.

The GTA weld metal of the commercial MIL-100S-1 and MIL-120S-1 type deposited under exactly the same conditions as that of Alloy 7 on HSLA-100 base plate had lower CVN absorbed energy values, Fig. 47. Both strength (discussed in the previous section) and toughness of the weld metal of commercial filler wires were

lower than those of the Alloy 7 weld metal deposited under identical conditions. The results prove that the current commercial filler wires for high strength steels are inferior in performance to the experimental ULCB steel filler wires and can only attain the desired strength and toughness levels under a very limited set of welding conditions.

Carbides and other second phase particles in the matrix act as crack initiators. The greater number of crack initiating second phase particles reduce the area a microvoid has to grow in the form of a dimple till it intersects with other growing microvoids, effectively reducing the energy required for fracture. Ultra low carbon levels coupled with absence of carbides and second phase particles was considered to be the reason for relative insensitivity of CVN absorbed energy values to the microstructural features of the ULCB weld metal. Inclusions in the weld metal generated due to the presence of CO_2 in the shielding gas had a marked effect on the toughness of the GTA weld metal, this is discussed in detail in the next section.

EFFECT OF INCLUSION ON CVN IMPACT TOUGHNESS

Inclusion density and size distribution are reported to have a strong influence on toughness. Nucleation of internal cavities, the first stage of dimpled rupture, can be caused by particle-matrix interface separation or by particle cracking. Nucleation can also be caused by blocked slip bands, in absence of second phase particles.[158] Passoja and Hill,[229] in a study of C-Mn steel weld metal, established a correspondence between the number of dimples on a fracture surface and inclusion

density measured on a plane polished surface. The greater number of inclusions in the Ar-5%CO_2 weld metal, Tables IX and Fig. 22, reduced the weld metal CVN absorbed energy values, compared to those of the weld metal deposited using Ar and Ar-25%He shielding gas, regardless of the heat input, Figs. 38, 39, 53-55.

The stress required to initiate microcracking is reported to increase with decreasing inclusion size.[230-32] From Fig. 22 it can be seen that for the GTA weld metal of Alloy 7 deposited at 3.5 kJ/mm (90 kJ/in) heat input using Ar-25%He shielding gas, more than 90% of the particles were below 0.6 μm^2 area (0.87 μm dia.), whereas, for the corresponding Ar-5%CO_2 weld metal only about 18% were that small. Hence, microvoid nucleation was easier in Ar-5%CO_2 weld metal, because it had greater number of inclusions with higher diameter (Fig. 22). Argon et al.,[161] have suggested that 10 nm may be the lower inclusion size limit that can act as a void nucleation site. Palmer et al.,[233] have concluded that there may be no lower limit to the size of the particle that can act as a site for void nucleation.

Acoustic emission test results taken during tensile testing (Figs. 23 and 24), show that the number of events (each event indicates noise generated due to inclusion matrix interface separation) and the peak amplitude is far greater in the case of weld metal deposited using Ar-5%CO_2 shielding gas than that of Ar-25%He shielding gas, which directly translates into the number of microvoids generated. Since no cracked inclusions could be observed in any of the SEM and TEM micrographs, it is reasonable to assume that particle matrix interface separation was the dominating mechanism for microvoid initiation.

Void growth is controlled by the plastic flow of the matrix material, surrounding the inclusions. According to Shockey et al.,[173] more than 87% of the energy absorbed during dimple rupture of a high strength steel is used up by void growth. Birkle et al.,[234] related fracture toughness to spacing between inclusions using extraction replica techniques. Considering the available literature and the results obtained during this investigation, the lower toughness of the GTA weld metal deposited using Ar-5%CO_2 shielding gas can be attributed to the higher volume fraction and greater average size of inclusions in the weld metal deposited using Ar-5%CO_2 shielding gas.

Nucleation of microvoids required less applied stress due to the greater average diameter of inclusions and the voids generated at the inclusions had to grow smaller distances to coalesce with other microvoids due to higher inclusion volume fraction, resulting in lower absorbed energy during CVN testing of the weld metal deposited using Ar-5%CO_2 shielding gas. Because the improvement in CVN toughness of the weld metal deposited at 3.5 kJ/mm (90 kJ/in.) using Ar-25%He shielding gas is two to three times that of the corresponding weld metal deposited at 2.5 kJ/mm (51 kJ/in.) heat input with Ar-5%CO_2 shielding gas, cleaner shielding gas resulting in lower inclusion volume fraction was found to be more effective in improving the CVN toughness of the weld metal than the finer grain size resulting from lower heat input.

VII. CONCLUSIONS

From the testing and analysis of the GTA and GMA welds made using the vacuum induction melted ultra low carbon steels, the following conclusions can be drawn:

1. ULCB steel weld metal achieved yield strength levels above 690 MPa (100 ksi). Steel weld metal can attain these strength level in virtual absence of carbon and without the strengthening effects of thermomechanical processing as in the case of wrought steels. Major contribution to strength was thought to be from substitutional solid solution strengthening and dislocation strengthening due to transformation induced dislocations afforded by low B_s temperatures.
2. Grain size and lath width did not have a strong influence on the yield strength of ULCB steel weld metal.
3. ULCB steel weld metal was found to be capable of maintaining CVN impact toughness values greater than 61 J (45 ft-lb) at -51°C (-60°F).
4. Impact toughness of ULCB weld metal was not strongly dependent on the microstructure. Laths and the lath width did not have any effect (beneficial or deleterious) on the CVN impact toughness. Finer prior austenite grain size, resulting from lower heat input, also had a very weak beneficial effect on the CVN impact toughness.

5. ULCB weld metal was weldable over a wide range heat inputs (thereby, eliminating the need for preheating). Good low temperature toughness was maintained over a wide range of cooling rates without a significant change in the strength values.

6. The weld metal inclusions did not have an appreciable effect on the austenite decomposition products.

7. A greater increase in CVN impact toughness was realized by reduction in inclusion density of the weld metal compared to the increase resulting from the finer prior austenite grain size.

8. Impact toughness of ULCB weld metal was independent of the welding process. Weld metal deposited by the GTAW and GMAW processes under identical welding conditions had comparable CVN impact toughness values.

9. Formation of laths in the ULCB weld metal microstructure was found to be a function of alloy content. Also, higher alloy content promoted sharp lath boundaries.

10 Performance of weld metal deposited using the commercially available high strength steel welding wires was found to be inferior to that of the experimental ULCB steel weld metal under identical welding conditions.

REFERENCES

1. Grange, R.A., Hribal, C.R. and Porter, L.F.: "Hardness of Tempered Martensite in Carbon and Low-Alloy Steels," *Metall. Trans. A*, 1977, Vol. 8A(11), pp 1775-1785.

2. Grossman, M.A. and Bain, E.C.: *Principles of Heat Treatment*, 5th Ed., ASM, Metals Park OH, 1964, pp 48-49.

3. Granville, B.A.: "Cold Cracking in Welds in HSLA Steels," *Welding of HSLA (Microalloyed) Structural Steels*, Proc. Intl. Conf., Nov. 1976, Rome Italy, ASM, Metals Park, OH, 1978, pp 85-101.

4. Holsberg, P.W., Gudas J.P. and Caplan, I.L.: "Metallurgical Design and Processes in The U.S. Navy High Strength Steel Welding," *Recent Trends in Welding Science and Technology*, Eds. S.A. David and J.M. Vitek, ASM Intl., Metals Park, OH, 1990, pp 593-605.

5. Holsberg, P.W. and Wong, R.J.: "Welding of HSLA-100 Steel for Naval Applications," *Weldability of Materials*, Eds. R.A. Patterson and K.W. Mahin, ASM Intl., Metals Park, OH, 1990, pp 219-239.

6. Ito, Y., Nakanishi, M. and Komizo, Y.: "Crack Opening Displacement Properties on submerged Arc Weld Metal." *Sumitomo Search*, 1979, Vol. 21(5), pp 52-67.

7. Ito, Y., Nakanishi, M. and Komizo, Y.: "Effects of Oxygen on Low Carbon Steel Weld Metal." *Metal Constr.*, 1982, Vol. 14(9), pp 472-478.

8. Harrison, P.L. and Farrar, R.A.: "Application of Continuous Cooling Diagrams for Welding of Steels," *Intl. Mater. Rev.*, 1989, Vol. 34, pp 36-50.

9. Graville, B.A.: "Weld Cooling Rates and Heat Affected Hardness in a Carbon Steel," *Weld. J.*, 1973, Vol. 54, pp 377s-385s.

10. Crawford, D.G. and T.N. Baker, T.N.: "Microstructure and Toughness of Low Carbon Steel Weld Metal," *Mater. Sci. and Engg.*, Vol A131, 1991, pp 255-263.

11. Savage, W.F., Lundin, C.D. and Aronson, A.H.: "Weld Metal Solidification Mechanics." *Weld. J.* 1965, Vol 44(4), pp 175s-181s.

12. Irvine, K.J. and Pickering, F.B.: "High Carbon Bainitic Steels," Special Report, No: 93, *Iron and Steel Inst.*, London, 1965, pp 110-125.

13. McEvily, A.J., Davis, R.D., Magee, C.L., and Jhonston, T.C.: "Structure, Hardenability and Toughness of Low-Carbon High Strength Steels," *Proc. Symp., Transformations and Hardenability in Steels*, Climax Molybdenum Co., 1967, pp 179-194.

14. Garcia, C.I., Lis, A.K. and DeArdo, A.J.: "The Physical Metallurgy of Ultra-Low Carbon Bainitic Plate Steels," *Metallurgy of Vacuum Degased Steel Products,* Ed. R. Pradhan, The Minerals and Metals Soc., 1990, pp 451-467.

15. Burns, K.W. and Pickering, F.B.: "Deformation and Fracture of Ferrite-Pearlite Structures," *J. Iron Steel Inst.*, 1964, Vol. 202, pp 899-906.

16. Pickering. F.B.: "High-Strength, Low-Alloy Steels - A Decade of Progress," *Microalloying '75,* Proc. Int. Symp., Washington DC, Union Carbide Corp., New York, NY, 1977, pp 9-31.

17. Petch, N.J.: "The Ductile-Cleavage Transition in Alpha-Iron,' *Fracture*, Eds. B.L. Averbach, D.K. Felbeck, G.T. Hahn and D.A. Thomas, The MIT Press, Cambridge, Massachusetts, 1959, pp 54-67.

18. Pickering, F.B. and Gladman, T.: "An Investigation into Some Factors which Control the Strength of carbon Steels," *Metallurgical Developments in Carbon Steel,* BISRA Report 81, 1963, pp 10-25.

19. Allen, W.P., Rees, W.P., Hopkins, B.E. and Tipler, B.R.: "Tensile and Impact Properties of High-Purity Iron-Carbon and Iron-Carbon-Manganese Alloys of Low Carbon Content," *J. Iron Steel Inst.*, 1953, Vol. 174, pp 108-120.

20. McMohan, C.J., Jr.: *Fundamental Phenomenon in the Material Science,* Plenum, New York, Vol 4, 1967, pp 247-284.

21. Shinada, K., Horii, Y., and Yurioka, N.: "Development of Weld Metal with High Toughness and Low Hardenability." *Weld. J.*, 1992, Vol. 71(7), pp 253s-262s.

22. Farrar, R.A. and Harrison, P.L.: "Acicular Ferrite in Carbon-Manganese Weld Metals: an Overview." *J. Mater. Sci.*, 1987, Vol. 22, pp 3812-3820.

23. Davies, G.J., Garland, J.G: "Solidification Structure and Properties of Fusion Welds." *Intl. Metal. Rev.*, 1975, Vol. 20(6), pp 83-106.

24. Savage, W.F.: "1980 Houdermont Lecture. Solidification Segregation and Weld Imperfections," *Weld. World*, 1980, Vol. 18(5/6), pp 89-114.

25. Savage, W.F.: "Solidification, Segregation and Weld Defects," *Physical metallurgy and Failure Phenomenon,* Proc. 5th Bolton Landing Conf, Eds. R.J. Christoffel et al., pp 1-18, 1979.

26. Abson, D.J. and Pargeter, R.J., "Factors Influencing As-Deposited Strength, Microstructure, and Toughness of Manual Metal Arc Welds Suitable for C-Mn Steel Fabrications," *Int. Metals Rev.*, 1986, Vol. 31, pp 141-94.

27. Calvo, F.A., Bentley, K.P., and Baker, R.G.: *Studies of the Welding Metallurgy of Steels*, British Welding Research Association, 1963, Abington, Cambridge.

28. Dadian, M.: "The Contribution of Welding to the Understanding of Metallurgical Phenomena." *Advances in the Science and Technology of Welding*, Gatlinburg, Tennessee, USA, Ed. S.A. David, ASM, Metals Park, OH 44073, 101-117, 1986.

29. Bhadeshia, H.K.D.H.: "Control of Weld Metal Microstructure and Properties," *Conf. Proc. The Metallurgy, Welding, and Qualification of Microalloyed (HSLA) Steel Weldments*, Houston, TX, AWS, Florida, 1990, pp 34-69.

30. Bhadeshia, H.K.D.H.: "Modeling the Microstructure in the Fusion Zone of Steel Welds," *Recent Advances in the Science and Technology of Welding*, Eds. S.A. David and J. Vitek, ASM International, Ohio 1989, pp 189-198.

31. Gloor, K., Christensen, N., Maehle, G. and Simonsen, T.: *"Nonmetallic Inclusions in Weld Metal,"* 1963, IIW DOC II-A-106-63.

32. Fleck , N.A., Grong, O., Edwards, G.R., and Matlock, D.K.: "Filler Metal Wire and Flux Effects in SMA Weld Metal Transformation Kinetics," *Weld. J.*, 1986, Vol. 65, 113s-121s.

33. Harrison, P.L. and Farrar, R.A.: "Influence of Oxygen-Rich Inclusions on the τ-α Phase Transformation in High-Strength Low-Alloy (HSLA) Steel Weld Metals." *J. Mater. Sci.*, 1981, Vol 16(8), pp 2218-2226.

34. Cochrane, R.C.: "Trends in Steels and Consumables for Welding," The Welding Institute, Abington, pp 661-673, 1979.

35. Bhadeshia, H.K.D.H., Svensson, L.E., and Gretoft, B.: "The Austenitic Grain Structure of Low Alloy Steel Weld Deposits," *J. Mat. Sci.*, 1986, Vol. 21, pp 3947-3941.

36. Bhadeshia, H.K.D.H., Svensson, L.E., and Gretoft, B.: "A Model for the Prediction of Microstructure in Fusion Zone of Steel Welds," *Acta. Met.*, 1985, Vol. 33, pp 1271-1283.

37. Babu, S. and Bhadeshia, H.K.D.H.: "Crystallographic Texture and the Austenitic Grain Structure of Low-Alloy Steel Weld Deposits," *Jnl. Mat. Sci. Let.*, 1990 Vol. 10(3) pp 142-144.

38. Cochrane, R.C.: "Weld Metal Microstructures - a State of the Art Review," *Weld. World*, 1983, Vol. 21(1-2), pp 16-24.

39. Choi, C.L. and Hill, D.C.: "A Study of Microstructural Progression in As-Deposited Weld Metal," *Weld. J.*, 1978, Vol. 57(8), pp 232s-236s.

40. Bhadeshia, H.K.D.H.: "Diffusional Formation of Ferrite in Iron and its Alloys," *Prog. in Mat. Sci. Lett.*, 1985, Vol. 29, pp 231-386.

41. Dallam, C.B., and Olson, D.L.: "Stress and Grain Size Effects on Weld Metal Ferrite Formation," *Weld. J.*, 1989, Vol. 68, pp 198s-205s.

42. Bhadeshia, H.K.D.H.: "Diffusion-Controlled Growth of Ferrite Plates in Plain Carbon Steel." *Mater. Sci. Tech.*, 1985, Vol. 1(7), pp 497-504.

43. Steven, W. and Haynes, A.G.: "The Temperature of Formation of Martensite and Bainite in Low-Alloy Steels -- Some Effects of Chemical Composition," *JISI*, 1956, Vol. 83, pp 349-359.

44. Hultgren, A.: "Isothermal Transformation of Austenite," *Trans. ASM*, 1947, Vol. 39, 915-1005.

45. Ohmori, Y. and Yamanaka, K.: "Hardenability of Boron-Treated Low Carbon Low Alloy Steels," *Conf. Proc. Boron in Steels*, Eds. S.K. Banerji and J.E. Morral, The Met. Soc. of AIME, Milwaukee, Wisconsin, 1979, pp 44-60.

46. Barbaro, F.J., Kranklis, P. and Easterling, K.E.: "The Composition and Morphology of Non-Metallic Inclusions in Hsla Steel Weld Metals," *Proc. 7th Australian X-Ray Analysis Association AXAA-88*, U. of Western Aust., pp 1-14., 1988.

47. Kluken, A.O. and Grong, O.: "Mechanism of Inclusion Formation in Al-Ti-Si-Mn Deoxidized Steel Weld Metals," *Met. Trans.*, 1989, Vol. 20A, pp 1335-1349.

48. Ricks, R.A., Howell, P.R., and Barrite, G.S.: "The Nature of Acicular Ferrite in HSLA Steel Weld Metals," *J. Mat. Sci.*, 1982, Vol. 17, pp 732-740, 1982.

49. Ferrante, M. and Farrar, R.A.: "Properties and Microstructure of Stress Relieved Submerged-Arc Weld Metal Containing Niobiium," *J. Mater. Sci.*, 1982, Vol. 17(8), pp 2405-2412.

50. Ohkita, S., Homma, H., Tsushima, S. and Mori, N.: "The Effect of Oxide Inclusion on Micro-structure of Ti-B Containing Weld Metal." *Aust. Weld. J.*, 1984, Vol. 29(3), pp 29-36.

51. Bhadeshia, H.K.D.H. and Svenson, L.-E.: "The Microstructure of Submerged Arc Weld Deposits for High-Strength Steels," *J. of Mat. Sci.*, 1986, Vol. 24, pp 3180-3188.

52. Bhadeshia, H.K.D.H., and Christian, J.W.: "Bainite in Steels," *Met. Trans.*, 1990, Vol. 21A, pp 767-797.

53. Nishioka, K. and Tamehiro, H.: "High Strength Ti Oxide Bearing Line Pipe Steel for Low Temperature Service", *Microalloying '88 ASM Intl.*, Chicago, 1988, pp 1-9.

54. Imagumbai, M., Chijiiwa, R. and Aikawa, N.: "Advanced Steel for Low-Temperature Service," *HSLA Steels: Metallurgy and Applications*, Beijing, Peoples Republic of China, 4-8 Nov. 1985, Eds. J.M. Gray, et al., ASM Int., Cleveland, OH, 1986, pp 557-566.

55. Evans, G.M.: "Effect of Electrode Diameter on the Microstructure and Properties of Carbon and Manganese Containing Pure weld metals," *Oerlikon Schweissmitt*, Vol. 39, pp 4-17, 1980.

56. Baily, N.: "The Establishment of Safe Welding Procedures for Steel." *Weld. J.*, 1972, Vol. 51(4), pp 169s-177s.

57. North, T.H., Bell, H.B., Koukabi, A. and Craig, I.: "Notch Toughness of Low Oxygen Content Submerged Arc Deposits," *Weld.J.*, 1979, Vol. 58(12), pp 343s-354s.

58. Farrar, R.A. and Watson, M.N.: "Effects of Oxygen and Manganese on SA Weld Metal Microstructure." *Metal Const.*, 1979, Vol. 11(6), pp 285-286.

59. Devillers, L., et al.: *The Effects of Residual Impurity and Microalloying Elements on Weldability and Weld Properties*, Abington, The Welding Institute, pp 1-11, 1984.

60. Horii, Y., "Development of Welding Materials for Low Temperature Service," *Nippon Steel Report*, May 1986.

61. Thewlis, G.: "Pipeline Welds- Effect of Pipe Material and Consumables Composition," *Joining and Materials*, 1989, Vol. 2(1-3), pp 25-31 and 125-129.

62. Kawabata, F., Matsuyama, J.-Y., Nishiyama, N. and Tanaka, T.: "Progress in Productivity and Weld Quality of UOE Pipes by Four-Wire Submerged Arc Welding," *Trans. ISIJ*, 1986, Vol. 26(5), pp 395-402.

63. Okabe, R., et.al.: "Improvement in Toughness of Weld Joint of Steel Plate for Large Heat Input Welding," *Trans. ISIJ*, 1983, Vol. 23, p. 390.

64. Lau, T.W., Sandowski, M.M. North, T.H. and Weatherly, G.C.: "Effect of Nitrogen on Properties of Submerged Arc Weld Metal," *Mater. Sci. Technol.*, 1988, Vol. 4(1), pp 52-61.

65. Harrison, P.L. and Farrar, R.A.: "Microstructural Development and Toughness of C-Mn and C-Mn-Ni Weld Metals I. Microstructural Development." *Metal Const.*, 1987, Vol. 19(7), pp 392R-599R.

66. Terashima, H. and Hart, P.H.M.: "Effect of Aluminium on C-Mn-Nb Steel Submerged Arc Weld Metal Properties." *Weld. J.*, 1983, Vol. 63(8), p 173s-183s.

67. Abson, D.J. and Dolby, R.E., *Welding Inst. Res. Bulletin, 19*, pp 202, 1979.

68. Davenport, E.S. and Bain, E.C.: "Transformation of Austenite at Constant Subcritical Temperatures," *Trans. TMS-AIME*, Vol. 90, 1930, pp 117-154.

69. Mehl, R.F.: *'Hardenability of Alloy steels,'* ASM, Cleveland, OH, 1990, p 1.

70. Aaronson, H.I. and Wells, C.: "Sympathetic Nucleation of Ferrite", *Trans. AIME*, 1956, Vol. 206(10), pp 1216-1223.

71. Chilton J.M., Barton C.J. and Speich, G.R.: "Martensite Transformation in Low-Carbon Steels." JISI, 1970, Vol. 208(2), pp 184-193.

72. Speich, G.R.: "The Decomposition of Austenite by Diffusional Processes," Eds. Zackay, D.F. and Aaronson, H.I., Interscience, New York, NY, 1962, pp 359-369.

73. Hawkins, M.J. and Barford, J.: "Experimental Kinetics of Bainite Formation." *JISI*, 1972, Vol. 210, pp 97-105.

74. Naylor, J.P. and Krahe, P.R.: "The Effect of Bainite Packet Size on Toughness," *Metal. Trans A.*, 1974, Vol. 5A, pp 1699-1701.

75. Miihkinen, V.T.T. and Edmonds, D.V.: "Fracture Toughness of Two Experimental High-strength Bainitic Low-alloy Steels Containing Silicon," *Mater. Sci. Tech.*, 1987, Vol. 3, pp 441-449.

76. Davenport, A.T., "The Crystallography of Upper Bainite," *Republic Steel Research Report on Project 12051*, Feb. 1974, pp 1-35.

77. Oblak, J.M., Goodenow, R.H. and Hehemann, R.F.: "Morphology of Bainite in Hypoeutectoid Steels." *Trans. TMS AIME*, 1964, Vol. 230(2), pp 258-259.

78. Srinivasan, G.R. and Wayman, C.M.: "Transmission Electron Microscope Study of the Bainite Transformation in Iron-Chrome-Carbon Alloys." *Acta Metall.*, 1968, Vol. 16(5), pp 609-620.

79. Srinivasan, G.R. and Wayman, C.M.: "The Crystallography of the Bainite Transformation." *Acta Metall.*, 1968, Vol. 16(5), pp 620-636.

80. Bhadeshia, H.K.D.H. and Edmonds, D.V.: "The Mechanism of Bainite Formation in Steels." *Acta Metall.*, 1980, Vol. 28(8), pp 1265-73.

81. Ohmori, Y. and Honeycombe, R.W.K.: "The Isothermal Transformation of Plain Carbon Austenite," *Proc. ICTIS, Suppl. to ISIJ*, 1971, Vol. 11, pp 1160-1165.

82. Ohmori, Y., Ohtani, H. and Kunitake, T.: "The Bainite in Low Carbon Low Alloy High Strength Steels,: *Trans. ISIJ*, 1971, Vol. 11, pp 250-259.

83. Lonsdale, D. and Flewitt, P.E.J.: "The Role of Grain Size on the Ductile-Brittle Transition of a 2.25 pct Cr-1 pct Mo Steel," *Metall. Trans. A*, 1978, Vol. 9A, pp 1619-1623.

84. Aaronson, H.I. and Domain, H.A.: "Partition of Alloying Elements Between Austenite and Proeutectoid Ferrite or Bainite." *Trans. TMS-AIME*, 1966, Vol. 236(5), pp 781-96.

85. Bhadeshia, H.D.K.H. and Waugh, A.R.: *Proc. International Conf. on Solid→Solid Phase Transformations*, Pittsburgh, PA, ASM, Metals Park, OH, 1981, pp 993-998.

86. Bhadeshia, H.K.D.H. and Waugh, A.R.: "Bainite: an Atom Probe Study of the Incomplete Reaction Phenomenon," *Acta Metall.*, 1982, Vol. 30, pp 775-784.

87. Stark, I., Smith, G.D.W. and Bhadeshia, H.K.D.H.: "The Element Redistribution Associated with 'the Incomplete-Reaction Phenomenon' in Bainitic Steels: An Atom Probe Investigation," *Phase Transformations '87,* [Conf. Proc.], Inst. of Metals, London, 1988, pp. 211-215.

88. Stark, I., Smith, G.D.W. and Bhadeshia, H.K.D.H.: "The Distribution of Substitutional Alloying Elements During the Bainite Transformation," *Metall. Trans. A*, 1990, Vol. 21A(4), pp 837-844.

89. Josifsson, B. and Anderson, H.O.: *Proc. 35th Int. Field Emissions Symp.*, Oak Ridge, TN, July 18-22, 1988.

90. Pickering, F.B.: "The Structure and Properties of Bainite in Steels," *Proc. Symp., Transformation and Hardenability in Steels*, Climax Molybdenum Co., Ann Arbor, MI, 1967, pp 109-129.

91. Habraken, L.J. and Economopoulous, M.: "Bainitic Microstructures in Low Carbon Alloy Steels and their Mechanical Properties," *Proc. Symp., Transformations and Hardenability in Steels*, Climax Molybdenum Co., 1967, pp 69-106.

92. Bojarski, Z. and Bold, T.: "Structure and properties of Carbide-Free Bainite," *Acta Met.*, 1974, Vol. 22, pp 1223-1234.

93. Habraken, L.: "Some Special Aspects of the Bainitic Structure," *Proc. 4th Congress on Electron Microscopy*, Vol. 1, Springer - Verlag, 1958, pp 621-628.

94. Bramfit, B.L. and Speer, J.G.: "A Perspective on the Morphology of Bainite," *Metall. Trans. A*, 1990, Vol. 21A, pp 817-29.

95. Nakamura, T. and Nagakura, S.: "Decomposition of Retained Austenite During the Tempering of Martensitic High Carbon Steel Studied by In Situ Electron Microscopy." *Intl. Conf. on Martensitic Transformations. ICOMAT-86,* The Japan Inst. of Metals Sendai 980, Japan, 1986, pp 1057-1065.

96. Pickering, F.B.: *Proc. Intl. Conf. on Electron Microscopy*, Springer-Verlag OHG, Berlin, 1958, pp 628-637.

97. Fisher, R.M.: *Proc. Intl. Conf. on Electron Microscopy*, Springer-Verlag OHG, Berlin, 1958, pp 579-588.

98. Kriesement, O. and Wever, F.: "The Mechanism of Phase Transformation in Metals," *Monograph and Report Ser. No. 18*, Institute of Metals, London, 1956, pp 253-255

99. Shackelton and Kelly: "Physical Properties of Martensite and Bainite," *Special Report, I.S.I.*, vol. 93, p. 126, 1962.

100. Pitsch, W.: "Der Orientierungszusdmmenhang Zwischen Zementit und Austenit," *Acta Met.*, 1962, Vol. 10, pp 897-900.

101. Sandvik, B.P.J.: "The Bainite Reaction in Fe-Si-C ALLOYS: The Primary Stage," *Metall. Trans.*, 1982, Vol. 13A, pp 777-787.

102. Bush, M.E. and Kelly, P.M.: "Strengthening Mechanisms in Bainitic Steels," *Acta Met.*, 1971, Vol. 19(12), pp 1363-1371.

103. Bhadeshia, H.K.D.H.: "The Lower bainite transformation and the Significance of Carbide precipitation." *Acta Metall.*, 1980, Vol. 28(8) pp 1103-1114.

104. Austin, A.E. and Schwartz, C.M.: "Electron-Diffraction Study of Iron Carbides in Bainite and Tempered Martensite," *Proc. ASTM*, 1952, Vol. 52, pp 592-596.

105. Oblak, J.M.,and Heheman, R.F.: "Structure and Growth of Widmanstätten ferrite and Bainite," *Proc. Symp., Transformation and Hardenability in Steels*, Climax Molybdenum Co., Ann Arbor, MI, 1967, pp 15-30.

106. Sandvik, B.P.J.: "The Bainite Reaction in Fe-Si-C Alloys: The Secondary Stage," *Metall. Trans. A*, 1982, Vol. 13A, pp 789-800.

107. Lai, G.Y.: "On the Precipitation of Epsilon-Carbide in Lower Bainite," *Metall. Trans. A*, 1975, Vol. 6A, pp 1469-1471.

108. Matas, S.J. and Hehemann, R.F.: "The Structure of Bainite in Hypoeutectoid Steels." *Trans. TMS-AIME*, 1961, Vol. 221(2), pp 179-185.

109. Hehemann, R.F.: "The Bainite Transformation," *Phase Transformations*, ASM, Metals Park, OH, 1970, pp 397-432.

110. Der-Hung-Huang and Thomas, G.: "Metallography of Bainitic Transformation in Silicon Containing Steels." *Metall. Trans. A*, 1977, Vol. 8A(11), pp 1661-1674.

111. Roberts, C.S., Averbach, B.L. and Cohen, M.: "The Mechanism and Kinetics of the First Stage of Tempering." *Trans. ASM*, 1953, Vol. 45, pp 576-604.

112. Owen, W.S.: "The Effect of Silicon on the Kinetics of Tempering," *Trans. ASM*, 1954 Vol. 46, pp 812-829.

113. Gordine, J. and Codd, I.: "The Influence of Silicon Up to 1.5 wt-% on the Tempering Characteristics of a Spring steel." *JISI*, 1969, Vol. 207(4) pp 461-467.

114. Kalish. D. and Cohen, M.: "Structural Changes and Strengthening in the Strain Tempering of Martensite," *Mater. Sci. Eng.*, 1970, Vol. 6, pp 156-166.

115. Kurdjumow, G.K. and Sachs, G.: "Ümber den Mechanismus der Stalhärtung," *Z. Physik*, 1930, Vol. 64, 1930, pp 325-343.

116. Lee, J.-L., Hon, M.-H.: "The Structure and Microphases in a Bainitic Transformation Product," *Scripta Met.*, 1987, Vol. 21, pp 293-298.

117. Guoqing, K. and Weixun, Y.: "An Investigation of Granular Bainite in a Low Carbon Mn-Mo-V Steel," *Proc. Int. conf. on HSLA Steels, Metallurgy and Application*, Beijing, China, 1985, pp 369-372.

118. Entin, R.I.: "The Elementary Reaction in the Austenite-Pearlite and the Austenite Bainite Transformations," *Decomposition of Austenite by Diffusional Processes*, Eds. Zackay, V.F. and Aaronson, H.J., Interscience, New York, NY, 1962, pp 295-311.

119. Ko, T. and Cottrell, S.A.: "The Formation of Bainite," *JISI*, 1952, Vol. 172(11), pp 307-313.

120. Christian, J.W.: "Physical Properties of Martensite and Bainite," *Iron and Steel Institute, London, Special Report 93*, 1965, pp 1-9.

121. Yang, J.R. and Bhadeshia, H.K.D.H.: "Thermodynamics of the Acicular Ferrite Transformation in Alloy-Steel Weld Deposites," *Advances in Welding Science and Technology*, Ed. S.A. david, ASM, Metals Park, OH, 1986, pp 187-191.

122. Heheman, R.F., Kinsman, K.R. and Aaronson, H.I.: "A Debate on the Bainitic Reaction," *Metall. Trans A.*, 1972, Vol. 3A, pp 1077-1094.

123. Aaronson, H.I. and Reynolds, W.T.Jr.: "Reply to a Discussion by J.W. Christian and D.V. Edmonds of Papers by Aaronson and Co-workers on the Proeutectoid Ferrite and Bainite Reaction" *Scripta Metall.*, 1988, Vol. 22, pp 567-572.

124. Bhadeshia, H.K.D.H. and Edmonds, D.V.: "The Bainite Transformation in Silicon Steel," *Metall. Trans. A*, 1979, Vol. 10A, pp 895-907.

125. Dahmen, U.: "Surface Relief and the Mechanism of Phase Transformation," *Scripta Met.*, 1987, Vol. 21 pp 1029-1034.

126. Edmonds, D.V. and Cochrane, R.C.: "Structure Property Relationships in Bainitic Steels," *Metall. Trans.*, 1990, Vol 21A, pp 1527-1540.

127. Aaronson, H.I., Rigsbee, J.M. and Trivedi, R.K.: "Comments on an Overview of the Bainite Reaction," *Scripta Met.*, 1986, Vol. 20(9), 1986, pp 1299-1304.

128. Bhadeshia, H.K.D.H.: "Solute-Drag, Kinetics and the Mechanisms of the Bainite Reactions in Steels," *Intl. Conf. on Phase Transformation in Ferrous Alloys*, Eds. A.R. Marder and J.I. Goldstein, ASM, Cleveland, OH, 1984, pp 335-340.

129. Bhadeshia, H.K.D.H.: "Diffusional Displacive Transformation," *Scripta Met.*, 1987, Vol. 21, pp 1017-1022.

130. Bach, P.W., et.al., "Atom Probe Analysis of Bainite Phase Boundaries in Low Alloyed Cr Mo steel," *Scripta Met.*, 1980, Vol. 14, pp 205-210.

131. Hsu, T.Y. and Xuemin, Li: "Diffusion of Carbon During the Formation of Low-Carbon Martensite," *Scripta Met.*, 1983, Vol. 77, pp 1285-1288.

132. Owen, W.S. and Wilson, E.A.: "Physical Properties of Martensite and Bainite," *Iron and Steel institute, London, Special Report 93*, 1965, pp 53-55.

133. Gladman, T., Holems, B. and McIvor, I.D.: "The Effect of Second Phase Particles on the Mechanical Properties of Steels," *Iron and Steel Institute*, London, 1971, pp 68-78.

134. Edmonds, D.V.: "The relationship Between Structure and Properties in Bainitic Steels," *Iron and Steel Maker*, 1990, Vol. 17(11), pp 75-84.

135. Naylor, G.P.: "The Influence of the Lath Morphology on the Yield Stress and Transition Temperature of Martensitic-Bainitic Steels," *Metall. Trans. A*, 1979, Vol. 10A, pp 861-873.

136. Brozzo, P., Buzzichelli, G., Mascanzoni, A. and Mirabile, M.: "Microstructure and Cleavage Resistance of Low-Carbon Bainitic steels" *Met. Sci.*, 1977, Vol. 11, pp 123-129.

137. Xu, Y.B., Liu, G.J. and Zhang, T.Y.: "Granular Product in a High Strength, Low Alloy Containing Molybdenum and Niobium," *Metall. Trans.*, 1987, Vol. 18A, pp 1923-1928.

138. Kinsman, K.R. and Aaronson,H.I.: "Discussion of Structure and Growth of Widmanstätten Ferrite and Bainite," *Transformation and Hardenability in Steels [Symposium]*, Ann Arbor, Michigan, USA, Climax Molybdenum Co., 1967, pp. 33-38.

139. F.B. Pickering and T. Gladman: "Metallurgical Developments in Carbon Steel," *BISRA Report 81*, 1963, pp 9-31.

140. Edwards, R.H. and Kennon, N.F.: "The Morphology and Mechanical Properties of Bainite Formed from Deformed Austenite," *Metall. Trans. A*, 1978, Vol. 9A, pp 1801-9.

141. Yang, J.R., Ph.D. Dissertation, University of Cambridge, 1987.

142. Irvine, K.J. and Pickering, F.B.: "The Metallography of Low-Carbin Bainitic Steels," *J. Iron Steel Inst.*, 1958, Vol. 188, pp 101-112.

143. Gladman, T., Dulieu, D. and McIvor, I.D.: "Structure-Property Relationships in High-Strength Microallyed Steels," *Microalloying '75*, Union carbide Corp., New York, NY, 1977, pp 32-55.

144. Whiteman, J.A.: "The Contribution of Physical Metallurgy to the Development of Low Carbon Steels," *Low Carbon Structural steels for the Eighties, Inst. of Metallurgists*, Plymouth, UK, 1977, pp 11-17.

145. G. Langford and M. Cohen: "Strain Hardening of Iron by Severe Plastic Deformation," *Trans. ASM*, 1969, Vol.62, pp 623-638.

146. G. Langford and M. Cohen: "Calculation of Cell-Size Strengthening of Wire Drawn Iron," *Metall Trans A*, 1975, Vol. 6A, pp 901-910

147. H.K.D.H. Bhadeshia: *Bainite in Steels,* The Inst of Metals, London, 1992, pp 295-296.

148. Kunitake, T.: "On the Yield Strength of Quenched and Tempered Structures of Low-Carbon Low-Alloy Steel," *Trans. ISIJ*, 1967, Vol. 7, pp 254-262.

149. Roberts, M.J., "Effect of Transformation Substructure on the Strength and Toughness of Fe-Mn Alloy," *Metall. Trans. A*, 1970, Vol 1A, pp 3287-3294.

150. Naylor, J.P. and Blondeau, R.: "The Respective Roles of the Packet Size and Lath Width on Toughness." *Metall. Trans. A*, 1976, vol. 7A(6), pp 891-894

151. Pickering, F.B.: "The Structure and Properties of Bainite in Steels (discussion)," *Proc. Symp., Transformations and Hardenability in Steels*, Climax Molybdenum Co., 1967, pp 130-132.

152. McIvor, I.D.: *British Steel Research Report, No. PROD/PM/6498/-/72/A*, British Steel, London, 1972.

153. Stroh, A.N.: "A Theory of the Fracture of Metals," *Advances in Physics*, 1957, Vol. 6(10), pp 418-465.

154. Cracknell, A. and Petch, N.J.: "Frictional Forces on Dislocation Arrays at the Lower Yield Point in Iron." *Acta Met.*, 1955, vol. 3(2), pp 186-189.

155. Heslop, J. and Petch N.J.: "The Stress to Move a Free Dislocation in Alpha Iron'" *Phil. Mag.*, 1956, Vol. 1(9), pp 866-873.

156. Richards, C.E., Reed, C.N. and Smallman, R.E.: "Intergranular Fracture Strength of High Purity Iron," *Intl. Conf. on Strength of Metals and Alloys*, Japan Institute of Metals, Tokyo, 1967, Vol. 517, pp 961-969.

157. Worthington, P.J. and Smith, E.: "Slip Twinning and Fracture in Polycrystalline 3% Silicon-Iron," *Acta Met.*, 1966, Vol. 14, pp 35-41.

158. Vanstone, R.H., Low, J.R. and Shanon, J.L., Jr.: "Investigation of the Fracture Mechanism of Ti-5Al-2.5Sn at Cryogenic Temperatures," *Metall. Trans. A*, 1978, Vol. 9A, pp 539-52.

159. Zener, C.: "Micro Mechanisms of Fracture," *Fracture of Metals*, ASM, Cleveland, OH, 1949, pp 3-31.

160. Cottrell, A.H.: "Theory of Brittle Fracture in Steels and Similar Metals," *Trans. AIME*, 1958, vol. 212, pp 192-203.

161. Argon, A.S., Im, J. and Safoglu, R.: "Cavity Formation from Inclusions in Ductile Fracture," *Metall. Trans. A*, 1975, vol. 6A(4), pp 825-837.

162. Hull, D.: "Twinning and Fracture of Single Crystals of 3% Silicon Iron," *Acta Met.*, 1960, Vol. 8, pp 11-18.

163. Hull, D.: "Twinning and Nucleation of Cracks in B.C.C. Metals," *Fracture of Solids*, Eds. Drucker and Gilman, Interscience, New York, NY, 1963, pp 417-453.

164. Reid, C.N.: "A Review of Mechanical Twinning in Body-Centered Cubic Metals and it's Relation to Brittle Fracture," *J. Less Common Metals*, 1965, Vol. 9, pp 105-122.

165. Hording, J: "The Yield and Fracture Behavior of High Purity Iron Single Crystals at High Rates of Strain," *Proc. Royal Soc.*, A299, 1967, pp 469-90.

166. Knott, J.F: "On Stress Intensification in Specimen of Charpy Geometry Prior to General Yield," *J. Mech. Phys. Solids*, 1967, Vol. 15, 1967, pp 97-103.

167. Wilcox, B.A. and Gilbert, A: "Fracture Initiation and Propagation In Polycrystalline Molybdenum," *Conference on Refractory Metals and Alloys*, Eds. Jaffee, R.I. et al., Gordon and Breach, New York, NY, 1969, Vol. 4, p 95.

168. Tetelman, A.S: Wilshaw, T.R. and Rau, C.A: "The Critical Tensile Stress Criterion for Cleavage," *Intl. J. of Fracture Mech.*, 1968, Vol 4, pp 147-157.

169. Wilshaw, T.R., Rau, C.A., and Tetelman, A.S: "A General Model to Predict the Elastic-Plastic Stress Distribution and Fracture Strength of Notched Bars in Plain Strain Bending," *Engineering Fracture Mechanics*, 1968, Vol. 1, pp 191-211.

170. Hendrickson, J.A., Wood, D.S. and Clark, D.S: "Prediction of Transition Temperature in Notched Bar Impact Tests," *Trans. ASM*, 1959, Vol. 51, pp 629-641.

171. Knott, J.F. and Cottrell, A.A: "Notch Brittleness in Mild Steel," *J. Iron Steel Inst.*, 1963, Vol. 201, pp 249-60.

172. Wilshaw, T.R. and Pratt, P.L: "The Effect of Temperature and Strain Rate on the Deformation and Fracture of Mild Steel Charpy Specimens," *Proc. of the First Int. Conf. on Fracture*, Sendai, Japan, B.III, 1965, Vol. 2, pp 973-985.

173. Shockey, D.A., Seaman, L., Dao, K.C. and Curan, D.R: "A Computational Fracture Model for SA533, Brade B, Class 1 Steel Based on Microfracture Processes," *EPRI, Report NP-701-SR*, 1978, Palo Alto, CA.

174. Ohtani, H., F. Terasaki and T. Kunitake: "The Microstructure and Toughness of High Tensile Strength Steels," *Trans ISIJ*, 1972, Vol. 12, pp 118-127.

175. Matsuda, S., T. Inoue, H. Mimura and Y. Okamura: "Toughness and Effective Grain Size in Heat-Treated Low-Alloy High Strength Steels," *Trans ISIJ*, 1972, Vol. 12, pp 325-33.

176. Ohmori, Y., H. Ohtani and T. Kunitake, "Tempering of the Bainite and the Bainite/Martensite Duplex Structure in a Low-Carbon Low-Alloy Steel," *Metal. Sci.*, 1974, Vol. 8, pp 357-66.

177. Tanaka, S., S. Tani and C. Ouchi: "Low Temperature Toughness of Water-Cooled and Tempered Low Carbon Manganese Steel," *Trans. ISIJ*, 1975, Vol. 15, pp 19-26.

178. Kamada, A. N. Koshizuka and T. Funakoshi: "Effect of Austenite Grain Size and C Content on the Substructure and Toughness of Tempered Martensite and Bainite," *Trans. ISIJ*, 1976, Vol. 16, pp 407-416.

179. Irvine, K.J. and Pickering, F.B.: "The Impact Properties of Low Carbon Bainitic Steels," *JISI*, 1963, Vol. 201, pp 518-31.

180. Tomita, Y.: "Effect of Microstructure on Plane-Strain Fracture Toughness of AISI 4340 Steel," *Metall. Trans. A*, 1988, Vol. 19A, pp 2513-2521.

181. Inoue, T., Matsuda, S., Okamura, Y. and Aoki, K.: "The Fracture of Low Carbon Tempered Martensite," *Trans, Japan Inst. of Metals*, 1970, Vol. 11, pp 36-43.

182. Der-Hung-Huang and Thomas, G: "Structure and Mechanical Properties of Tempered Martensite and Lower Bainite in Fe-Ni-Cr Steels," *Metall. Trans. A*, vol. 2A, 1971, pp 1587-1598.

183. Hahn, C.T., Averbach, B.L., Owen, W.S. and Cohen, M.: "Initiation of Cleavage Microcracks in Polycrystalline Iron and Steel." *Fracture*, Wiley, New York, 1959, pp 91-116.

184. Moll, R.A. and Stout, R.D.: "Composition Effects in Iron-Base Weld Metal." *Weld. J.*, 1967, Vol. 46(12), pp 551s-561s.

185. Coldren, A.P.: et al., *Proc. Steel Strengthening Mechanisms*, (Zurich), Climax Molybdenum Co., Greenwich, 1969, pp 17-46.

186. Lacy, C.E. and Gensamer, M: *Trans. ASM*, 1944, Vol. 32, pp 88-110.

187. Evans, G.M.: "Effect of Manganese on the Microstructure and Properties of All-Weld-Metal deposites," *IIW Doc. IIA-432-77*, 1977.

188. Evans, G.M.: "Effect of Manganese on the Microstructure and Properties of All-Weld-Metal Deposits." *Weld. J.*, 1980, Vol. 59(3), pp 67s-75s.

189. Sakai, H: *J. Jpn. Weld. Rev.*, vol. 29, 1960, pp 478-84.

190. Evans, G.M.: "Effect of Interpass Temperature on The Microstructure and Properties of C-Mn All-Weld-Metal Deposits," *IIW Doc. IIA-460-78*, 1978.

191. Evans, G.M.: "Factors Affecting the Microstructure and Properties of C-Mn All Weld Metal Deposits. 1-Inter Pass Temperature," *Weld. Rev.*, 1982, Vol. 1(1), pp 14-20.

192. Bosward, I.G. and John, R: "Trends in Steel and Consumable Welding," *The Welding Institute*, Abington, UK, 1979, pp 135-50.

193. Morigaki, O., Tanigaki, T., Kuwabara, M., Fujibayashi, K. and Otawa, M: "Development of a Covered Electrode for Steel Structures in Low Temperature Service," *IIW Doc. II-746-75*, 1975.

194. Steel, A.C.: "The Effects of Sulphur and Phosphorous on Toughness of Steel Weld Metal," *Weld. Res. Intl.*, 1972, Vol. 2(3), pp 37-76.

195. Ito, Y. and Nakanishi, M: *Sumitomo Search*, 1967, vol. 15, pp 42-62

196. Bain, E.C. and Paxton, H.W.: *Alloying Elements in Steel*, ASM, Metals Park, Ohio, 1966, pp 125-127.

197. Morrison, I.F. and Cameron, A.E: *Proc. Second Triennial Empire Mining Congress* (Edmonton, Alberta, 1927), Part IV, p. 533.

198. Hodge, J.M. et al.: *Trans. AIME*, Vol. 185, 1949, pp 233.

199. Nunes, J. and Larson, F.R.: "Tensile Flow and Fracture Temperature Dependence of some Iron-Base Alloys," *Trans. AIME*, 1963, Vol. 227(6), pp 1369-1377.

200. Davies, R.G. and Ku, R.C.: "Solid Solution Strengthening in Iron-Base Alloys." *Trans. AIME*, 1966, Vol. 236(12), pp 1691-1696.

201. Wullart, R.A: "*The Effect of Nickel on the Microstructural and Mechanical Properties of Ferritic Steels*," Ph. D. Thesis, Stanford U., 1969.

202. Leslie, W.C: *The Physical Metallurgy of Steels*, McGraw-Hill Book Co., 1981.

203. Leslie, W.C, Sober, R.J., Babcock, S.G. and Green, S.J.: "Plastic Flow in Binary Substitutional Alloys of BCC Iron - Effects of Strain Rate, Temperature and Alloy Content," *Trans. ASM.* 1969, Vol. 62, pp 690-710.

204. Brewer, L: "Bonding and Structure of Transition Metals," *Science*, 1968, Vol. 161, pp 115-161.

205. McHenry, H.I. and Reed, R.P: "Fracture Behavior of the Heat-Affected Zone in 5% Ni Steel Weldments," *Weld. J.*, 1977, Vol. 58, pp 104s-111s.

206. Bain, E.C. and Paxton, H.W.: *Alloying Elements in Steel*, ASM, Metals Park, Ohio, 1966, pp 274-275.

207. Irvine, K.J. and Pickering, F.B.: "Low Carbon Bainitic Steels," *J. Iron Steel Inst.*, 1957, Vol. 187(12), pp 292-309.

208. Boniszewski, T.: "Manual Metal Arc Welding - Old Process, New Developments. 1 - Introductory Considerations," *Metall. Mater. Technol.*, 1979, Vol. 11(10), pp 567-74, 640-43 and 697-705.

209. Evans, G.M: "The Effect of Silicon on the Microstructure and Properties of C-Mn All-Weld-Metal Deposites," *IIW Doc. II-A-630-84*, 1984.

210. Evans, G.M: "The Effect of Silicon on the Microstructure and Properties of Carbon-Manganese All-Weld Metal Deposit," *Oerlikon Schweissmitt*, Vol. 44, 1986, pp 19-33.

211. Hannerz, N.E: "The Influence of Silicon on the Mechanical Properties and on the Weldability of Mild and High Tensile Structural Steels - Literature Survey and Own Experimental Studies," *IIW Doc. IX-1169-80*, 1980.

212. Terashima, H. and Hart, P.H.M: "Effect of Aluminium in C-Mn steels on Microstructure and Toughness of Submerged Arc Weld Metal - A Progress Report," *Research Report 186/1982*, The Welding Institute, Abington.

213. Terashima, H. and Hart, P.H.M: *64th Annual AWS Convention*, Philadelphia, PA, April 1983, Paper 26C.

214. Brown, A., Garnish, J.D., Honeycombe, R.W.K.: "Distribution of Boron in Pure Iron." *Met. Sci.*, 1974, Vol. 8(10), pp 317-324

215. Lucci, A., Della Gatta, D., Venturello, G: "On the Solubility of Boron in High-Purity Alpha-Iron," *Met. Sci. J.*, vol. 3, 1969, pp 14-17.

216. Mortimer, D.A. and Nicolas, M.G.: "Surface and Grain Boundary energies of AISI 316 Stainless Steel in the Presence of Boron." *Met. Sci.*, 1976, Vol. 10(9), pp 326-332.

217. Morral, J.E. and Cameron, T.B.: "A Model for Ferrite Nucleation Applied to Boron Hardenability." *Metall. Trans. A.* 1977, Vol. 8A(11), pp 1817-1819.

218. Grange, R.A. and Mitchell, J.B.: "On the Hardenability Effect of Boron in Steel," *Trans. ASM*, 1961, Vol. 53, pp 157-185.

219. Saeki, M., Kurosawa, F. and Matsuo, M.: "Micro and State Analysis as the Bases for Microalloying Techniques." *Trans. Iron Steel Inst. Jpn.*, 1986, Vol. 26, 1986, 1017-1035.

220. Dionne, S., Krishnadev, M.R., Collins, L.E. and Boyd, J.D.: "Influence of Processing and Cooling Rate on the Transformation Kinetics and Microstructure of Boron HSLA Steels," *Conf. Proc. Accelerated Cooling of Rolled Steel*, Eds. Ruddle, G.E. and Crawley, A.F., Pergamon Press, Maxwell House, New York, NY, 1988, pp 71-84

221. Nakawugi, H. et al.: *Alloys for the 80's* Climax Molybdenum Co., Ann Arbor, MI, p 213, 1979.

222. Yurioka N.: "Weldability of Modern Steels," *Nippon Steel Report*, Nippon Steel Corporation, R&D Laboratories-II, Fuchinobe 5-10-1, Sagamihara, 229, Japan, 1978.

223. Data provided by Ms. Marie A. Quintana, from the Electric Boat Division of General Dynamics Corporation, Groton, CT, May 1994.

224. Military Specification, "Electrodes, Welding, Bare, Solid, Nickel - Manganese - Chromium - molybdenum Alloy Steel for Producing HY-130 Weldments for As-Welded Applications." MIL-E-24355B (16 Apr 1982).

225. Data Provided by Ms. Susan R. Fiore, from the ESAB Group, Inc. Hanover, PA, May 1994.

226. Military Specification MIL-E-23765/2A.

227. Private communication with Prof. H.I. Aaronson, Naval research Labs, Washington DC, July 1994.

228. Brownrigg, A: "The Effect of Austenite Grain Size on the Strength of Low Carbon martensite," *Scr. Met.*, 1973, Vol. 7, pp 1139-1142.

229. Passoja, D.E. and Hill, C.H.: "Comparison of Inclusion Distributions on Fracture Surface and in the Bulk of Carbon-Manganese Weldments," *Fractography-Microscopic Cracking Processes*, Eds. Beachem, C.D. and Warke, W.R., STP 600, 1976, ASTM, Philadelphia, PA. pp 30-46.

230. Cox, T.B., and Low, J.R., Jr.: "An Investigation of the Plastic Fracture of AISI 4340 and 18 Ni-200 Grade Maraging Steels," *Metall. Trans. A*, 1974, Vol. 5A. pp 1457-1470.

231. Tanaka, J.P., Pampillo, C.A., and Low, J.R., Jr.: "Fractographic Analysis of the Low-Energy Fracture of an Aluminum Alloy," *Review of Developments in Plain Strain Fracture Toughness Testing*, Ed. Brothers, A.J., STP 463, 1970, ASTM, Philadelphia, PA, pp 191-215.

232. Van Stone, R.H., Merdrant, R.H., and Low, J.R., Jr.: "Investigation of the Plastic Fracture of High-Strength Aluminum Alloys," *Fatigue and Fracture Toughness-Cryogenic Behavior*, Eds. Hickey, C.F., Jr., and Broadwell, R.G., STP 556, 1973, ASTM, Philadelphia, PA, pp 93-124.

233. Palmer, I.G., Smith, G.C., and Warda, R.D.: "Some Aspects of Ductile Fracture in Metals," *Physical Basis of Yield and Fracture*, Ed. Strickland, A.C. Ed., 1967, The Physical Society, London, pp 53-59.

234. Birkle, A.J., Wei, R.P., and Pellissier, G.E.: "Analysis of Plain-Strain Fracture in a Series of 0.45C-Ni-Cr-Mo Steels with Different Sulfur Contents," *Trans ASM.*, 1966, Vol. 59, pp 981-990.

Table I: **Nominal Chemical Composition of some Commercial Filler Wires, HSLA-80 and HSLA-100 Wrought Steels (wt%).**

Material	C	Mn	Si	Ni	Mo	Cu	Cr	CEN	HM	B_s (°C)
WIRE-1	0.06	1.65	0.35	1.75	0.35	--	0.1	0.31	347	528
WIRE-2	0.07	1.55	0.35	2.40	0.55	--	0.45	0.38	356	513
WIRE-3	0.11	1.60	0.35	2.60	0.90	--	0.70	0.62	391	490
HSLA-80	0.04	0.55	0.30	0.90	0.20	1.20	0.70	0.26	329	556
HSLA-100	0.04	0.90	0.25	3.5	0.40	1.60	0.60	0.40	329	514

Table II: Chemical Composition of the VIM Ingots, 1/16 in. Diameter Wires, AOD Alloy and HSLA-100 (wt%).

Alloy	C	Mn	Si	Ni	Mo	Ti	Al	B	O	N	S	P
1	0.003	1.00	0.23	2.23	0.47	0.011	0.10	--	0.0028	0.0001	0.002	0.001
2	0.001	0.93	0.24	3.07	0.63	0.008	0.011	--	0.0018	0.0001	0.002	0.001
3	0.002	0.98	0.23	2.24	0.62	0.006	0.011	--	0.0019	0.0001	0.001	0.001
4	0.055	1.19	0.25	3.61	0.58	<0.001	0.008	--	0.0059	0.0002	0.008	0.002
5	0.013	1.52	0.25	3.63	0.55	<0.001	0.008	--	0.0032	0.0001	0.009	0.003
6	0.029	1.15	0.26	4.36	0.59	<0.001	0.009	--	0.0057	0.0005	0.008	0.003
7	0.012	0.94	0.25	4.81	2.36	<0.001	0.030	--	0.0030	0.0002	0.008	0.007
8	0.010	1.11	0.26	3.07	2.40	0.006	0.032	--	0.0017	0.0003	0.008	0.007
9	0.013	0.96	0.23	2.79	1.50	<0.001	0.017	--	0.0030	0.0002	0.006	0.002
10*†	0.020	0.99	0.35	5.59	0.70	0.017	0.002	--	0.0010	0.0004	0.002	0.004
11*‡	0.020	1.66	0.35	4.89	0.61	0.021	0.004	--	0.0011	0.0003	0.002	0.004
12	0.007	1.00	0.24	2.04	0.49	0.010	0.009	0.0022	0.0044	0.0001	0.001	0.001
13	0.016	1.03	0.24	2.23	0.49	0.012	0.009	0.0018	0.0018	0.0001	0.001	0.001
14	0.004	1.02	0.23	3.13	0.62	0.006	0.011	0.0018	0.0028	0.0001	0.002	0.001
15	0.033	1.04	0.24	3.17	0.63	0.012	0.010	0.0021	0.0026	0.0001	0.001	0.002
16§¡	0.033	0.99	0.41	5.41	0.55	0.001	0.014	--	0.0526	0.0042	0.007	0.004
HSLA-100¿	0.025	0.78	0.25	3.30	0.59	0.002	0.028	0.001	0.0131	0.0125	0.003	0.004

* 1/16 in. dia filler wire from ESAB. † Cr-0.26%. ‡ Cr-0.01%.
§ Argon Oxygen Decarburized ingot melted by ESCO Corp. ¡ Cr-1.38%. ¿ Cu-1.47, Cr-0.54

Table III: Welding Variables for the GTA Welds.

No:	Heat Input kJ/mm (kJ/in)	Shielding Gas	Welding Voltage (V)	Welding Current (A)	Travel Speed mm/min (in/min)
1	3.5 (90)	Ar-5%CO_2	21	355	127 (5)
2	2.0 (51)	Ar-5%CO_2	17	300	153 (6)
3	3.2 (82)	Ar	16	425	127 (5)
4	3.2 (82)	Ar-25%He	19	360	127 (5)
5	3.5 (90)	Ar-25%He	19	390	127 (5)

Table IV: Welding Variables for The GMA Welds.

No:	Heat Input kJ/mm (kJ/in.)	Shielding Gas	Welding Voltage (V)	Welding Current (A)	Travel Speed mm/min (in/min)
1	2.5 (64)	Ar-5%CO_2	32	300	229 (9)
2	1.9 (48)	Ar-5%CO_2	31	260	254 (10)
3	2.5 (64)	Ar-25%He	32	300	229 (9)

Table V: **Chemical Composition of the GTA Weld Metal Deposited on Matching Base Plates at 3.5 kJ/mm (90 kJ/in.) Heat Input using Ar-5%CO_2 Shielding Gas (wt%).**

Alloy	C	Mn	Si	Ni	Mo	Ti	Al	B	O	N	S	P
1	0.017	0.71	0.16	2.66	0.48	<0.001	0.005	--	0.0250	0.0004	0.006	0.001
2	0.017	0.65	0.16	3.65	0.61	<0.001	0.007	--	0.0290	0.0006	0.007	0.001
3	0.017	0.73	0.17	2.63	0.60	<0.001	0.007	--	0.0310	0.0008	0.007	0.001
4	0.064	0.83	0.14	3.66	0.60	<0.001	0.007	--	0.0300	0.0009	0.008	0.003
5	0.013	1.21	0.16	3.56	0.59	<0.001	0.007	--	0.0250	0.0006	0.008	0.003
6	0.039	0.82	0.16	4.43	0.60	<0.001	0.007	--	0.0197	0.0009	0.008	0.003
7	0.015	0.68	0.15	4.79	2.36	<0.001	0.028	--	0.0180	0.0005	0.007	0.006
8	0.014	0.85	0.18	3.04	2.40	<0.001	0.028	--	0.0200	0.0005	0.007	0.007
9	0.020	0.69	0.13	2.79	1.50	<0.001	0.015	--	0.0240	0.0007	0.006	0.002
10*†	0.029	0.82	0.30	5.06	0.61	<0.001	0.007	--	0.0368	0.0027	0.007	0.001
11*‡	0.03	1.23	0.29	4.64	0.54	<0.001	0.008	--	0.0388	0.0051	0.007	0.002
12	0.018	0.71	0.16	2.71	0.49	<0.001	0.006	0.0021	0.0315	0.0008	0.006	0.001
13	0.018	0.75	0.17	2.72	0.49	<0.001	0.006	0.0027	0.0310	0.0006	0.006	0.001
14	0.020	0.76	0.17	3.79	0.62	<0.001	0.007	0.0027	0.0304	0.0005	0.007	0.001
15	0.039	0.66	0.10	3.51	0.65	<0.001	0.001	0.0020	0.0303	0.0004	0.003	0.002
16	0.032	0.74	0.32	5.22	0.54	<0.001	0.012	--	0.0510	0.0051	0.007	0.007

* GMA Weld Metal, Heat Input 2.5 kJ/mm (64 kJ/in.), HSLA-100 Base Plate. † 0.327 %Cr. ‡ 0.164 %Cr.

Table VI: **CEN Values and Hardness of Martensite, As Welded and Nil Martensite Hardness Calculated using Yurioka's[222] Model and B_s Values Calculated using Steven and Hayen's[43] Equation for the GTA Weld Metal Deposited at 3.5 kJ/m Heat Input and Ar-5%CO_2 Shielding Gas.**

Alloy	CEN (YURIOKA)	HARDNESS OF MARTENSITE (HV)	AS WELDED HARDNESS (HV)	HARDNESS WITH NIL MARTENSITE (HV)	B_s (°C)
1	0.20	309	227	217	559
2	0.23	309	257	235	540
3	0.21	309	238	227	552
4	0.31	351	302	251	533
5	0.27	305	283	254	523
6	0.29	328	307	254	522
7	0.44	307	312	274	451
8	0.41	306	311	274	468
9	0.31	312	302	267	517
10	0.31	320	308	258	491
11	0.32	321	307	258	495
12	0.21	310	228	218	557
13	0.21	310	231	220	555
14	0.25	312	270	243	533
15	0.41	328	271	241	497
16	0.43	322	322	268	456
HSLA-100	0.35	316	313	265	487

Table VII: Transfer Efficiencies of Alloying Elements during GTAW.

ELEMENT	C	Mn	Ni	Mo	Si	Ti	Al	O	N
TRANSFER EFFICIENCY	1.4	0.7	1.00	1.00	0.60	0.25	0.8	5-6	1.2

Table VIII: Cooling Rates for the GTA and GMA Welds.

No:	Welding Procedure	Heat Input kJ/mm (kJ/in.)	Plate Thickness mm (in.)	Cooling Rate at 1000°F (°F/sec)	Preheat Temp. °C (°F)	Cooling Time 800-500°C (seconds)
1	GTAW	3.5 (90)	12 (0.5)	11	—	35
2	GTAW	2 (51)	12 (0.5)	32	—	14
3	GMAW	2.5 (64)	16 (0.6)	11	150 (300)	35
4	GMAW	1.9 (48)	16 (0.6)	32	—	14

Table IX: Results of the Inclusion Analysis for Alloy 7 Weld Metal.

SHIELDING GAS	Ar-5%CO_2	Ar-25%He
Total Area (mm^2)	0.94	0.79
Total Incl. Area (μm^2)	5297	1123
Inclusion Density (mm^{-2})	4185	3416
Std. Deviation	0.88	1.12
Ave. Incl. Dia. (μm)	**0.65**	**0.36**
Incl. Vol. Fraction	**0.05%**	**0.01%**

Table X: Hardness of GTA Weld Metal Deposited at 3.5 kJ/mm (90 kJ/in.) Heat Input using Ar-5%CO_2 Shielding Gas for Alloys 1 to 16.

ALLOY	HRB	AVERAGE
1	87.5, 85, 87.5, 89, 88, 88.5, 88	87.6
2	83.7, 90.5, 89, 87.5, 87.5, 90, 84, 85.5,	87.2
3	89, 88.4, 85, 84, 88, 88, 84	86.6
4	91, 92, 93.5, 94.5, 91	92.5
5	83.3, 89.5, 89, 85, 90, 85, 84, 90, 87	87.0
6	88.8, 94, 93, 93.2, 93.8, 97, 89, 76.5, 93, 95.7, 97, 96, 91, 93.5, 95, 92	92.4
7	23, 25, 24.7, 25.3, 22, 23, 27, 23.5, 17.5, 22.7, 20.8, 23.7, 19.8, 23, 23, 24, 22.3	22.9(HRC)
8	97.3, 97.5, 99, 100, 99.2, 96.8, 96.2, 95, 93, 96, 96, 99.2, 100, 99.5, 99.8	97.6
9	96.7, 96.5, 95.5, 96.3, 96, 95, 97.3, 95, 95.5, 95, 96.5, 95.2, 93.5, 94.5, 92, 96, 93	95.3
10†	100, 101, 99, 99, 96.5, 99.5, 99, 97.5, 101, 100	99.2
11‡	97, 96.5, 97, 94.5, 98, 94.5, 93.5, 94	95.6
12	84, 86.5, 91.5, 88.5, 80, 83.5, 85.5, 87	85.8
13	91.5, 88.5, 93.5, 88, 93, 93, 93, 88	91
14	86, 86.5, 88.5, 89.5, 89, 90.5, 87.5, 87.5	88.1
15	90, 91, 91, 93, 92, 91.5, 92.5, 92	91.6
16	24.5, 25, 23, 23.5, 23, 25, 24, 24	24

† Alloy 8 base plate.
‡ Alloy 5 base plate.

Table XI: Hardness of GTA Weld Metal Deposited at 2 kJ/mm (51 kJ/in.) Heat Input using Ar-5%CO_2 Shielding Gas for Alloys 1 to 16.

ALLOY	HRB	AVERAGE
1	95, 91.7, 91.5, 91, 76, 70, 90, 90, 86.5, 90, 89.5, 90, 80, 87, 89, 87.5, 77	86.6
2	91, 92, 87.5, 90.5, 87.5, 86, 87.5, 84	88.7
3	90, 86, 89.7, 87.5, 90, 86.5, 80, 80	86.2
4	96, 96, 94, 95, 93, 97, 95, 95, 97, 99.5	95.7
5	93, 97, 94, 93, 92, 92, 93, 92	93.2
6	94, 97, 98, 93.2, 96, 95, 97, 93.8, 97.2, 94	95.5
7	22, 20.2, 21.5, 22, 21.8, 20.5, 22.5, 23	21.9(HRC)
8	98, 98.5, 100.5, 100.5, 99.7, 100.5, 100.5, 98.5	99.6
9	91.7, 92, 93, 92, 90, 90, 93.6, 91	91.6
10†	99, 98, 100, 100, 100, 100, 100, 102	99.8
11‡	96.5, 99, 95, 92.5, 98, 95.5, 94, 89, 96.5, 98, 97	95.5
12	92, 85, 91, 89, 88.5, 92, 90.5, 91.5, 91.5, 88.5, 93.5, 88, 93, 93, 93, 88	90.5
13	92.2, 92.5, 89.9, 90, 88.5, 93.5, 90.5, 90.5	91.0
14	86, 86.5, 88.5, 89.5, 89, 90.5, 87.5, 87.5	88.1
15	90.5, 90, 91.7, 90, 91.8, 94, 91.5, 91	91.3
16	23, 28.5, 25.5, 28, 28, 21.5, 29.5, 23.5	26 (HRC)

† Alloy 8 base plate.
‡ Alloy 5 base plate.

Table XII: Hardness Values for GMA Weld Metal of Alloys 7, 10 and 11 Deposited on HSLA-100 Base Plate with Ar-5%CO_2 Shielding Gas.

FILLER METAL	SHIELDING GAS	HEAT INPUT kJ/mm (kJ/in)	HARDNESS (HRC)	AVERAGE (HRC)
Alloy 7	Ar-5%CO_2	2.5 (64)†	24, 23, 25, 23, 24,23	23.6
Alloy 7	Ar-25%He	2.5 (64)†	29.5, 25, 28, 26, 24, 24.5	26.1
Alloy 10	Ar-5%CO_2	2.5 (64)†	20, 21, 22, 22, 21	21.2
Alloy 10	Ar-5%CO_2	1.9 (48.3)‡	20.5, 22.5, 21, 20, 22.5	21.3
Alloy 11	Ar-5%CO_2	2.5 (64)†	22, 22, 22, 21, 20	21.4
Alloy 11	Ar-5%CO_2	1.9 (48.3)‡	20, 20, 21, 22.5, 20, 20	20.6

† Cooling rate adjusted to match that of the 3.5 kJ/mm (90 kJ/in.) GTA welds.
‡ Cooling rate adjusted to match that of the 2 kJ/mm (51 kJ/in.) GTA welds.

Table XIII: Tensile Properties of GTA Weld Metal deposited on matching Base Plate at 3.5 kJ/mm (90 kJ/in.) Heat Input with Ar-5%CO_2 Shielding Gas.

ALLOY	Yield Strength MPa (ksi)	Tensile Strength MPa (ksi)	ELONGATION % (in 1")	R.A.% (0.25"DIA)
1	465 (67.5)	574 (83.2)	22.1	77.2
2	504 (73.1)	640 (92.8)	23.0	74.9
3	483 (70)	582 (84.4)	21.9	75.3
4	564 (81.8) 565 (81.9)	699 (101.4) 694 (100.6)	19.0 20.0	70.0 67.5
5	508 (73.7)	643 (93.3)	24.5	75.0
6	566 (82.1)	695 (100.8)	18.5	63.5
7	733 (106.3)	898 (130.3)	15.5	64.0
7(a)	758 (109.9)	928 (134.6)	16	63
8	656 (95.2)	784 (113.7)	17.0	71.5
9	542 (78.6) 552 (80.1)	691 (100.2) 685 (99.3)	20.0 21.0	72.0 70.0
10†	748 (108.5)	834 (121)	18	68
11†	734 (106.5)	824 (119.5)	19.5	68
12	524 (76.0)	615 (89.2)	19.3	74.1
13	555 (80.5)	624 (90.5)	21.0	73.9
14	583 (84.5)	692 (100.4)	17.1	66.8
15	567 (82.3)	628 (91.1)	9.8	37
16	738 (107)	972 (141)	16	63.5

† GMA weld metal, Heat Input 2.3 kJ/mm (60 kJ/in.), Cooling Rate 9°F/1000°F, HY-100 Base Plate, Data from Electric Boat.

7(a): GTA weld metal with Alloy 7 filler metal on HSLA-100 base late.

Table XIV: Tensile Properties of GMA Weld Metal of Alloys 10 and 11 Deposited at 1.41 kJ/mm (36 kJ/in.) to 2.3 kJ/mm (60 kJ/in.) heat input with Ar-5%CO_2 Shielding gas on HY-100 base Plate (Data from Electric Boat).

ALLOY	No:	HEAT INPUT kJ/mm (kJ/in)	COOLING RATE (°F/s at 1000°F)	Y. S. MPa (ksi)	U.T.S. MPa (ksi)	El. (%)
10	1	2.3 (60)	9	748 (108.5)	834 (121)	18
	2	1.7 (45)	20	779 (113)	841 (122)	20.5
	3	1.57 (40)	30	786 (114)	858 (124.5)	18
	4	1.57 (40)	46	800 (116)	865 (125.5)	18
	6	1.41 (36)	65	824 (119.5)	876 (124)	16
11	1	2.3 (60)	9	734 (106.5)	824 (119.5)	19.5
	2	1.7 (45)	20	758 (110)	827 (120)	21
	3	1.57 (40)	30	793 (115)	851 (123.5)	19.5
	4	1.57 (40)	46	817 (118.5)	876 (124)	19
	5	1.41 (36)	64	824 (119.5)	889 (129)	16

Table XV: Tensile Properties of GMA Weld Metal of Alloys 10 and 11 Deposited at 1.33 kJ/mm (34 kJ/in.) and 3.2 kJ/mm (82.5 kJ/in.) heat input with Ar-5%CO_2 Shielding gas on HY-100 base plate (Data from ESAB).

ALLOY	No:	HEAT INPUT kJ/mm (kJ/in)	COOLING RATE (°F/s at 1000° F)	Y. S. MPa (ksi)	U.T.S. MPa (ksi)	EL (%)
10	1	3.2 (82.5)	6.4	686 (99.5)	870 (126.2)	19
	2	1.33 (34)	64	797 (115.6)	856 (124.1)	14
11	1	3.2 (82.5)	6.4	629 (91.2)	818 (118.7)	21
	2	1.33 (34)	64	786 (114)	851 (123.5)	16

Table XVI: CVN Impact Toughness Values for GTA Weld Metal of Alloy 1 Deposited on Matching Base Plate.

HEAT INPUT kJ/mm (kJ/in)	SHIELDING GAS	TEMP. °C (°F)	IMPACT TOUGHNESS J (ft-lb)	AVERAGE J (ft-lb)
3.5 (90)	Ar-5%CO_2	25 (77)	214 (158)	214 (158)
		-18 (0)	149 (110), 225 (166), 225 (166)	199 (147)
		-51 (-60)	203 (150), 183 (135), 80.5 (109)	165 (122)
2 (51)	Ar-5%CO_2	25 (77)	355 (262)‡	355 (262)
		-18 (0)	355 (262)‡, 355 (262)‡	355 (262)
		-51 (-60)	282 (208), 355 (262)‡	318 (235)

‡ upper limit of CVN impact testing machine.

Table XVII: CVN Impact Toughness Values for GTA Weld Metal of Alloy 2 Deposited on Matching Base Plate.

HEAT INPUT kJ/mm (kJ/in)	SHIELDING GAS	TEMP. °C (°F)	IMPACT TOUGHNESS J (ft-lb)	AVERAGE J (ft-lb)
3.5 (90)	Ar-5%CO_2	25 (77)	140 (103)	140 (103)
		-18 (0)	103 (76.2), 98 (72.5)	101 (74.2)
		-51 (-60)	138 (102), 115 (85), 62 (45.5)	105 (77)
2 (51)	Ar-5%CO_2	25 (77)	264 (195)†	264 (195)
		-18 (0)	142 (105)†	142 (105)
		-51 (-60)	162 (120)†	162 (120)

† weld defects observed in the broken CVN bar.

Table XVIII: CVN Impact Toughness Values for GTA Weld Metal of Alloy 3 Deposited on Matching Base Plate.

HEAT INPUT kJ/mm (kJ/in)	SHIELDING GAS	TEMP. °C (°F)	IMPACT TOUGHNESS J (ft-lb)	AVERAGE J (ft-lb)
90 (3.2)	Ar-5%CO_2	25 (77)	225 (166)	225 (166)
		-18 (0)	226 (167), 133 (98), 197 (145)	185 (136)
		-51 (-60)	206 (152), 150 (111), 160 (118.2), 155 (114.3)	168 (124)
2 (51)	Ar-5%CO_2	25 (77)	355 (262)‡	355 (262)
		-18 (0)	355 (262)‡, 194 (143)†	273 (202.5)
		60 (-51)	355 (262)‡, 162 (120)†	259 (191)

‡ upper limit of CVN impact testing machine.
† weld defects observed in the broken CVN bar.

Table XIX: CVN Impact Toughness Values for GTA Weld Metal of Alloy 4 Deposited on Matching Base Plate.

HEAT INPUT kJ/mm (kJ/in)	SHIELDING GAS	TEMP. °C (°F)	IMPACT TOUGHNESS J (ft-lb)	AVERAGE J (ft-lb)
3.5 (90)	Ar-5%CO_2	25 (77)	128 (95)	128 (95)
		-18 (0)	71 (52.5), 85 (62.5)	78 (57.5)
		-51 (-60)	59.7 (44), 50.2 (37), 38 (28)	49 (36)
2 (51)	Ar-5%CO_2	25 (77)	116 (86)	116 (86)
		-18 (0)	80 (59), 62 (46), 39 (29)	61 (45)
		-51 (-60)	58.3 (43), 56.9 (42), 37 (27)	51 (37)
82 (3.2)	Ar	25 (77)	257 (190)	257 (190)
		-18 (0)	209 (154), 195 (144)	202 (149)
		-51 (-60)	161 (119), 129 (95)	145 (107)
3.5 (90)	Ar-25%He	25 (77)	271 (200), 285 (210)	278 (205)
		-18 (0)	164 (121), 224 (165), 123 (91), 154 (114), 108 (80)	155 (114)
		-51 (-60)	47 (35), 38 (28), 46 (34)	44 (32)
82 (3.2)	Ar-25%He	25 (77)	220 (162.5)	220 (162.5)
		-18 (0)	201 (148), 149 (110), 202 (149)	184 (136)
		-51 (-60)	107 (79), 106 (78), 46 (34), 16 (11.5)	69 (51)

Table XX CVN Impact Toughness Values for GTA Weld Metal of Alloy 5 Deposited on Matching Base Plate.

HEAT INPUT kJ/mm (kJ/in)	SHIELDING GAS	TEMP. °C (°F)	IMPACT TOUGHNESS J (ft-lb)	AVERAGE J (ft-lb)
3.5 (90)	Ar-5%CO_2	25 (77)	171 (126)	171 (126)
		-18 (0)	114 (84), 94 (69)	104 (76.5)
		-51 (-60)	16 (11.5), 76 (56), 95 (70)	62 (46)
2 (51)	Ar-5%CO_2	25 (77)	209 (154)	209 (154)
		-18 (0)	206 (152), 168 (124), 217 (160)	197 (145)
		-51 (-60)	138 (102), 127 (94), 160 (118), 130 (96)	139 (102.5)
82 (3.2)	Ar	25 (77)	298 (220)	298 (220)
		-18 (0)	229 (169), 291.5 (215)	260 (192)
		-51 (-60)	192.5 (142), 198 (146)	195 (144)

Table XXI: CVN Impact Toughness Values for GTA Weld Metal of Alloy 6 Deposited on Matching Base Plate.

HEAT INPUT kJ/mm (kJ/in)	SHIELDING GAS	TEMP. °C (°F)	IMPACT TOUGHNESS J (ft-lb)	AVERAGE J (ft-lb)
3.5 (90)	Ar-5%CO_2	25 (77)	133 (98)	133 (98)
		-18 (0)	88 (65), 79 (58)	83 (61.5)
		-51 (-60)	64 (47), 69 (51)	66 (49)
2 (51)	Ar-5%CO_2	25 (77)	138 (102)	138 (102)
		-18 (0)	117 (86), 125 (92)	121 (89)
		-51 (-60)	81 (60), 102 (75)	91.5 (67.5)
82 (3.2)	Ar	25 (77)	328 (242)	328 (242)
		-18 (0)	187 (138), 271 (200)	229 (169)
		-51 (-60)	149 (110), 197 (145), 168 (124)	171 (126)
3.5 (90)	Ar-25%He	25 (77)	312 (230)	312 (230)
		-18 (0)	296 (218), 251 (185), 289 (214)	279 (206)
		-51 (-60)	202 (149), 206 (152), 207 (153)	205 (151)
82 (3.2)	Ar-25%He	25 (77)	301 (222)	301 (222)
		-18 (0)	306 (226), 272 (201), 312 (230)	297 (219)
		-51 (-60)	167 (123), 184 (136), 252 (186)	201 (148)

Table XXII: **CVN Impact Toughness Values for GTA Weld Metal of Alloy 7 Deposited on Matching Base Plate.**

HEAT INPUT kJ/mm (kJ/in)	SHIELDING GAS	TEMP. °C (°F)	IMPACT TOUGHNESS J (ft-lb)	AVERAGE J (ft-lb)
3.5 (90)	Ar-5%CO_2	25 (77)	90 (67)	90 (67)
		-18 (0)	76 (56), 89 (66), 96 (71)	87 (64)
		-51 (-60)	72 (53), 84 (62), 90 (67), 46 (34)	73 (54)
2 (51)	Ar-5%CO_2	25 (77)	126 (93)	126 (93)
		-18 (0)	109 (81), 88 (65)), 106 (78)	101 (75)
		-51 (-60)	70 (52), 86 (64), 68.5 (51)	75 (55)
3.5 (90)	Ar-25%He	25 (77)	274 (202)	274 (202)
		-18 (0)	217 (160), 237 (175), 244 (180)	233 (172)
		-51 (-60)	168 (124), 247 (182), 163 (120)	193 (142)

Table XXIII: **CVN Impact Toughness Values for GTA Weld Metal of Alloy 8 Deposited on Matching Base Plate.**

HEAT INPUT kJ/mm (kJ/in)	SHIELDING GAS	TEMP. °C (°F)	IMPACT TOUGHNESS J (ft-lb)	AVERAGE J (ft-lb)
3.5 (90)	Ar-5%CO_2	25 (77)	157 (116)	157 (116)
		-18 (0)	53 (39), 113 (83), 18 (13), 13 (10), 50 (37)	49 (36)
		-51 (-60)	99 (73), 9 (6.5), 11 (8)	40 (29)
2 (51)	Ar-5%CO_2	25 (77)	230 (170)	230 (170)
		-18 (0)	150 (111), 160 (118), 75 (56), 179 (132)	141 (104)
		-51 (-60)	160 (118), 45 (33), 113 (83)	106 (78)

Table XXIV: CVN Impact Toughness Values for GTA Weld Metal of Alloy 9 Deposited on Matching Base Plate.

HEAT INPUT kJ/mm (kJ/in)	SHIELDING GAS	TEMP. °C (°F)	IMPACT TOUGHNESS J (ft-lb)	AVERAGE J (ft-lb)
3.5 (90)	Ar-5%CO_2	25 (77)	176 (130)	176 (130)
		-18 (0)	125 (92), 124 (91.5), 94 (69)	114 (84)
		-51 (-60)	17 (12.5), 47 (35), 115 (84.5), 118 (87), 21 (15.5)	64 (47)
2 (51)	Ar-5%CO_2	25 (77)	179 (132)	179 (132)
		-18 (0)	171 (126), 163 (120), 152 (112)	162 (119)
		-51 (-60)	155 (114), 133 (98.5), 104 (77)	131 (96.5)

Table XXV: CVN Impact Toughness Values for GTA Weld Metal of Alloy 10 Deposited on Alloy 8 Base Plate.

HEAT INPUT kJ/mm (kJ/in)	SHIELDING GAS	TEMP. °C (°F)	IMPACT TOUGHNESS J (ft-lb)	AVERAGE J (ft-lb)
3.5 (90)	Ar-5%CO_2	25 (77)	117 (86)	117 (86)
		-18 (0)	76 (56), 61 (45), 64 (47)	66 (49)
		-51 (-60)	45 (33), 77 (57), 43 (32), 42 (31)	52 (38)
2 (51)	Ar-5%CO_2	25 (77)	156 (115)	156 (115)
		-18 (0)	114 (84), 144 (106), 141 (104)	133 (98)
		-51 (-60)	76 (56), 46 (34), 54 (40)	58 (43)

Table XXVI: CVN Impact Toughness Values for GTA Weld Metal of Alloy 11 Deposited on Alloy 5 Base Plate.

HEAT INPUT kJ/mm (kJ/in)	SHIELDING GAS	TEMP. °C (°F)	IMPACT TOUGHNESS J (ft-lb)	AVERAGE J (ft-lb)
3.5 (90)	Ar-5%CO_2	25 (77)	108 (80)	108 (80)
		-18 (0)	88 (65), 81 (60), 145 (107)	104 (77)
		-51 (-60)	89 (66), 95 (70), 58 (43)	81 (60)
2 (51)	Ar-5%CO_2	25 (77)	165 (122)	165 (122)
		-18 (0)	156 (115), 159 (117), 144 (106)	153 (113)
		-51 (-60)	81 (60), 88 (65), 106 (78)	92 (68)

Table XXVII: CVN Impact Toughness Values for GTA Weld Metal of Alloy 12 Deposited on Matching Base Plate.

HEAT INPUT kJ/mm (kJ/in)	SHIELDING GAS	TEMP. °C (°F)	IMPACT TOUGHNESS J (ft-lb)	AVERAGE J (ft-lb)
3.5 (90)	Ar-5%CO_2	25 (77)	154 (114)	154 (114)
		-18 (0)	98 (72), 122 (90), 122 (90)	114 (84)
		-51 (-60)	8.8 (6.5), 23.7 (17.5)	16 (12)

Table XXVIII: CVN Impact Toughness Values for GTA Weld Metal of Alloy 13 Deposited on Matching Base Plate.

HEAT INPUT kJ/mm (kJ/in)	SHIELDING GAS	TEMP. °C (°F)	IMPACT TOUGHNESS J (ft-lb)	AVERAGE J (ft-lb)
3.5 (90)	Ar-5%CO_2	25 (77)	197 (145), 168 (124)	183 (135)
		-18 (0)	17 (13), 32.5 (24)	25 (18)
		-51 (-60)	5.4 (4)	5.4 (4)

Table XXIX: CVN Impact Toughness Values for GTA Weld Metal of Alloy 14 Deposited on Matching Base Plate.

HEAT INPUT kJ/mm (kJ/in)	SHIELDING GAS	TEMP. °C (°F)	IMPACT TOUGHNESS J (ft-lb)	AVERAGE J (ft-lb)
3.5 (90)	Ar-5%CO_2	25 (77)	110 (81)	110 (81)
		-18 (0)	20 (14.5), 15 (11)	17 (13)
		-51 (-60)	10 (7.5)	10 (7.5)

Table XXX: CVN Impact Toughness Values for GTA Weld Metal of Alloy 15 Deposited on Matching Base Plate.

HEAT INPUT kJ/mm (kJ/in)	SHIELDING GAS	TEMP. °C (°F)	IMPACT TOUGHNESS J (ft-lb)	AVERAGE J (ft-lb)
3.5 (90)	Ar-5%CO_2	25 (77)	163 (120)	163 (120)
		-18 (0)	10 (13.5), 22 (30)	22 (16)
		-51 (-60)	6.4 (9)	9 (6.4)
2 (51)	Ar-5%CO_2	25 (77)	159 (117)	159 (117)
		-18 (0)	264 (195), 176 (130)†	220 (162.5)
		-51 (-60)	49.5 (36.5)†, 22 (16)	36 (26)

† weld defects observed in the broken CVN bar.

Table XXXI: CVN Impact Toughness Values for GTA Weld Metal of Alloy 16 Deposited on matching Base Plate.

HEAT INPUT kJ/mm (kJ/in)	SHIELDING GAS	TEMP. °C (°F)	IMPACT TOUGHNESS J (ft-lb)	AVERAGE J (ft-lb)
3.5 (90)	Ar-5%CO_2	25 (77)	64 (47)	64 (47)
		-18 (0)	39 (29), 53 (39), 66 (49)	53 (39)
		-51 (-60)	50 (37), 60 (44), 43 (32)	51 (37)
2 (51)	Ar-5%CO_2	25 (77)	68 (50)	68 (50)
		-18 (0)	73 (54), 58 (43)	66 (49)
		-51 (-60)	41 (31), 37 (27)	39 (29)

Table XXXII: CVN Impact Toughness Values for GMA Weld Metal of Alloy 7 Deposited on HSLA-100 Base Plate.

HEAT INPUT kJ/mm (kJ/in)	SHIELDING GAS	TEMP. °C (°F)	IMPACT TOUGHNESS J (ft-lb)	AVERAGE J (ft-lb)
2.5 (64)†	Ar-5%CO_2	25 (77)	77 (56.5)	77 (56.5)
		-18 (0)	34 (25), 39 (29), 47 (35)	40 (30)
		-51 (-60)	28 (21), 14 (10), 26 (19)	23 (17)
2.5 (64)†	Ar-25%He	25 (77)	47 (35)	47 (35)
		-18 (0)	39 (29), 28 (21), 26 (19)	31 (23)
		-51 (-60)	9 (7), 13 (10), 26 (19)	20 (15)

† welding parameters adjusted to attain the cooling rate of 3.5 kJ/mm (90 kJ/in.) GTA welds.

Table XXXIII: CVN Impact Toughness Values for GMA Weld Metal of Alloy 10 Deposited on HSLA-100 Base Plate.

HEAT INPUT kJ/mm (kJ/in)	SHIELDING GAS	TEMP. °C (°F)	IMPACT TOUGHNESS J (ft-lb)	AVERAGE J (ft-lb)
2.5 (64)†	Ar-5%CO_2	25 (77)	129 (95)	129 (95)
		-18 (0)	94 (69), 118 (87), 115 (85)	109 (80)
		-51 (-60)	52 (39), 83 (61), 79 (58)	72 (53)
1.9 (48.3)‡	Ar-5%CO_2	25 (77)	122 (90)	122 (90)
		-18 (0)	119 (88), 121 (89), 121 (89)	120 (89)
		-51 (-60)	112 (83), 108 (80), 102 (75)	107 (79)

† welding parameters adjusted to attain the cooling rate of 3.5 kJ/mm (90 kJ/in.) GTA welds.
‡ welding parameters adjusted to attain the cooling rate of 2 kJ/mm (51 kJ/in.) GTA welds.

Table XXXIV: CVN Impact Toughness Values for GMA Weld Metal of Alloy 11 Deposited on HSLA-100 Base Plate.

HEAT INPUT kJ/mm (kJ/in)	SHIELDING GAS	TEMP. °C (°F)	IMPACT TOUGHNESS J (ft-lb)	AVERAGE J (ft-lb)
2.5 (64)†	Ar-5%CO_2	150 (302)	146 (108), 134 (99)	140 (103.5)
		25 (77)	136 (100), 125 (92)	130 (96)
		-18 (0)	129 (95), 122 (90), 130 (96)	127 (94)
		-51 (-60)	85 (63), 79 (58), 91 (67)	84 (62)
		-100 (-148)	23 (17), 34 (25)	28 (21)
		-196 (-321)	6.7 (5)	6.7 (5)
1.9 (48.3)‡	Ar-5%CO_2	25 (77)	130 (96)	130 (96)
		-18 (0)	126 (93), 132 (97), 129 (95)	129 (95)
		-51 (-60)	92 (68), 113 (83), 108 (80)	103 (76)

† welding parameters adjusted to attain the cooling rate of 3.5 kJ/mm (90 kJ/in.) GTA welds.
‡ welding parameters adjusted to attain the cooling rate of 2 kJ/mm (51 kJ/in.) GTA welds.

Table XXXV: CVN Impact Toughness Values for GTA Weld Metal of Alloy 7 Deposited on HSLA-100 Base Plate.

HEAT INPUT kJ/mm (kJ/in)	SHIELDING GAS	TEMP. °C (°F)	IMPACT TOUGHNESS J (ft-lb)	AVERAGE J (ft-lb)
3.5 (90)	Ar-5%CO_2	25 (77)	134 (99)	134 (99)
		-18 (0)	80 (59), 92 (68), 58 (43)	84 (62)
		-51 (-60)	41 (30), 47 (35), 39 (29)	42 (31)
3.5 (90)	Ar-25%He	25 (77)	241 (178)	241 (178)
		-18 (0)	241 (178), 237 (175), 241 (178)	240 (177)
		-51 (-60)	76 (55), 163 (120), 171 (126)	136 (100)

Table XXXVI: CVN Impact Toughness Values for GTA Weld Metal of Alloy 7 Deposited on HY-130 Base Plate.

HEAT INPUT kJ/mm (kJ/in)	SHIELDING GAS	TEMP. °C (°F)	IMPACT TOUGHNESS J (ft-lb)	AVERAGE J (ft-lb)
3.5 (90)	Ar-5%CO_2	25 (77)	58 (43)	58 (43)
		-18 (0)	35 (26), 22 (16)	26 (19)
		-51 (-60)	12 (9), 12 (9)	12 (9)
3.5 (90)	Ar-25He	25 (77)	117 (86)	117 (86)
		-18 (0)	60 (44), 38 (28), 37 (27)	45 (33)
		-51 (-60)	9 (7), 30 (22), 50 (37)	30 (22)

Table XXXVII: CVN Impact Toughness Values for GTA Weld Metal Deposited using Commercial MIL-100S-1 type wire on HSLA-100 Base Plate.

HEAT INPUT kJ/mm (kJ/in)	SHIELDING GAS	TEMP. °F (°C)	IMPACT TOUGHNESS J (ft-lb)	AVERAGE J (ft-lb)
3.5 (90)	Ar-5%CO_2	25 (77)	89 (66)	89 (66)
		-18 (0)	40 (30), 38 (28), 47 (35)	42 (31)
		-51 (-60)	18 (14), 24 (18), 27 (20)	23 (17)

Table XXXVIII: CVN Impact Toughness Values for GTA Weld Metal Deposited using Commercial MIL-120S-1 type wire on HSLA-100 Base Plate.

HEAT INPUT kJ/mm (kJ/in)	SHIELDING GAS	TEMP. °C (°F)	IMPACT TOUGHNESS J (ft-lb)	AVERAGE J (ft-lb)
3.5 (90)	Ar-5%CO_2	25 (77)	84 (62)	84 (62)
		-18 (0)	39 (29), 34 (25), 49 (36), 52 (39), 64 (47)	48 (35)
		-51 (-60)	24 (18), 26 (20), 17 (13)	23 (17)

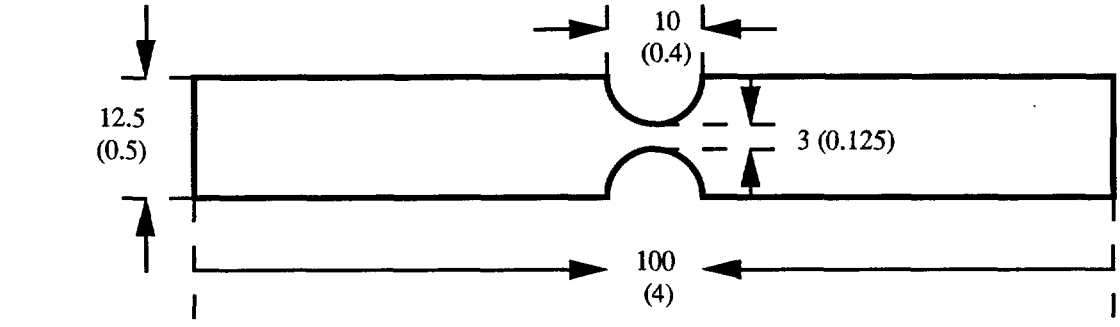

(a)

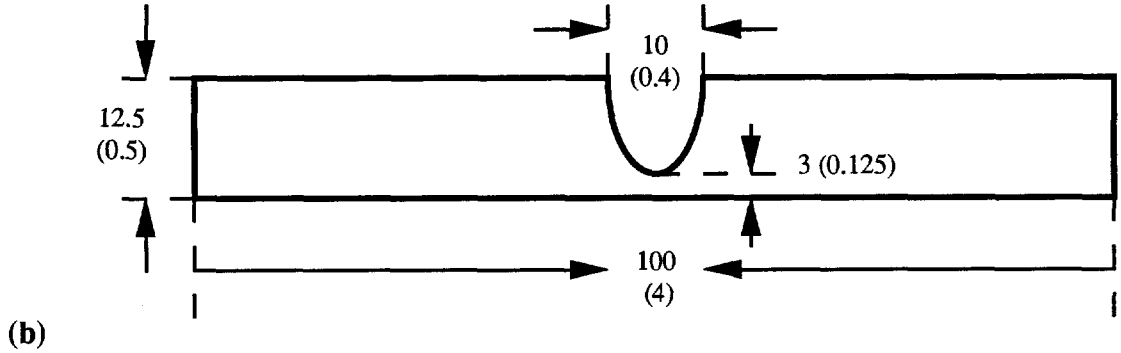

(b)

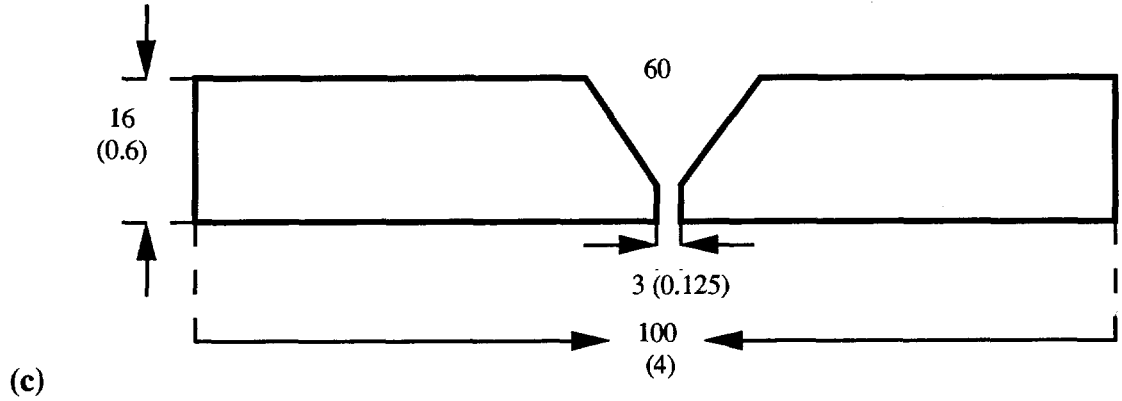

(c)

Dimensions: mm (in.)
Not to Scale

Figure 1: The groove geometries for GTA and GMA welds. (a) GTA weld for CVN test samples, (b) GTA weld for tensile test samples and (c) GMA welds for CVN test samples.

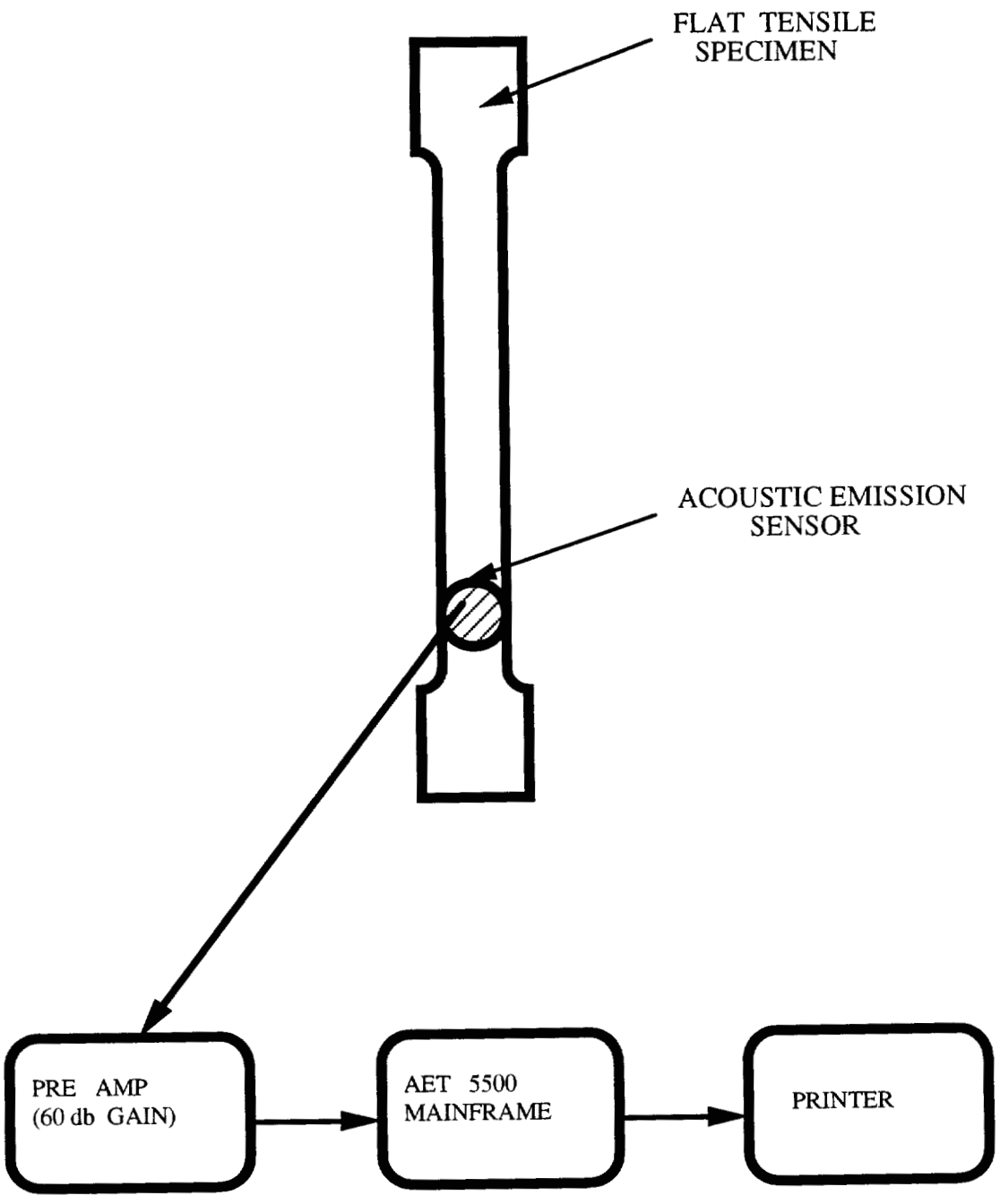

Figure 2: Schematic diagram showing the acoustic emission testing setup.

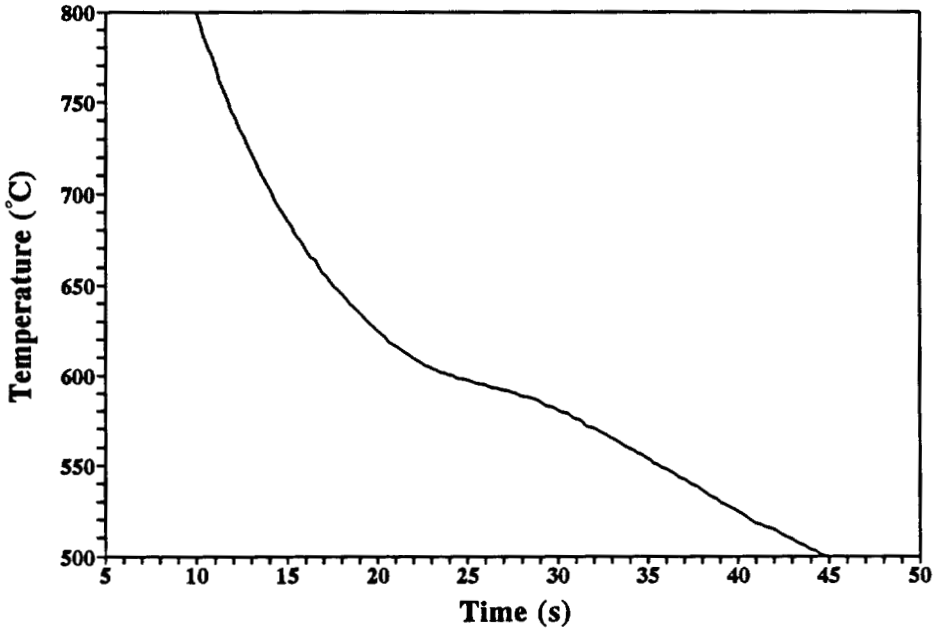

(a)

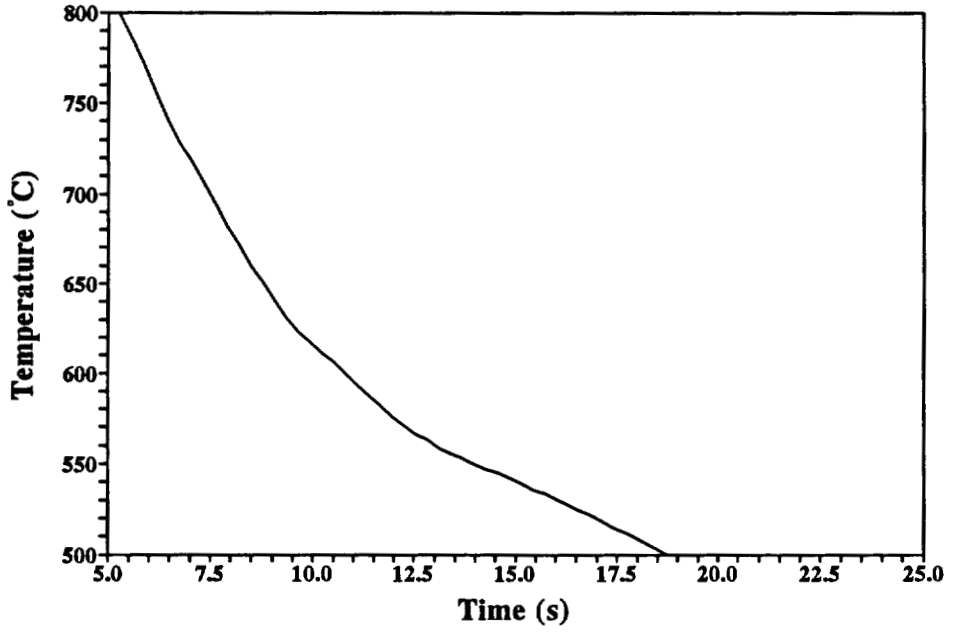

(b)

Figure 3: Cooling curve for GTA weld metal deposited on 12 mm (0.5 in.) thick plate at, (a) 3.5 kJ/mm (90 kJ/in.) and (b) at 2 kJ/mm (51 kJ/in.).

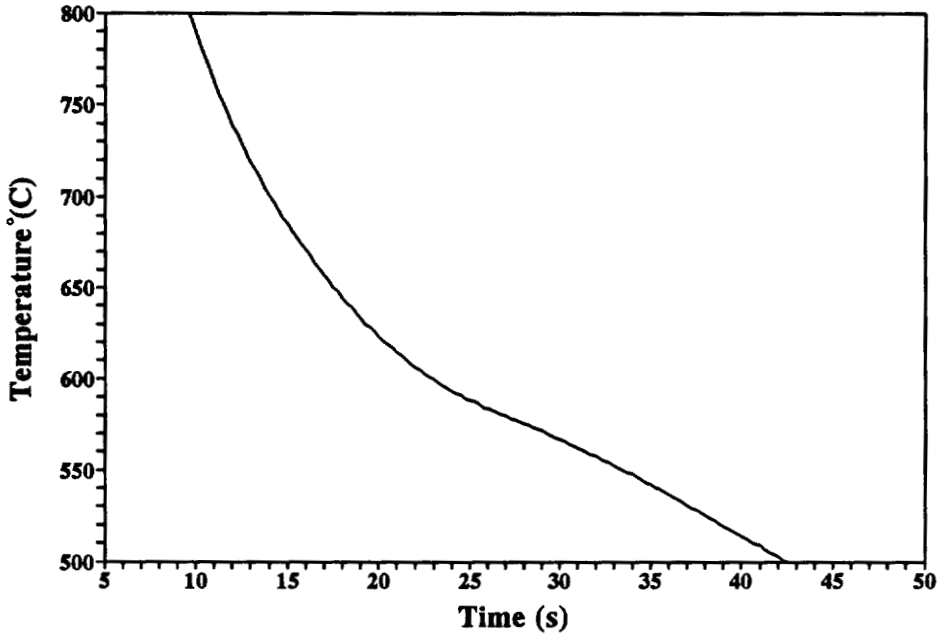

(a)

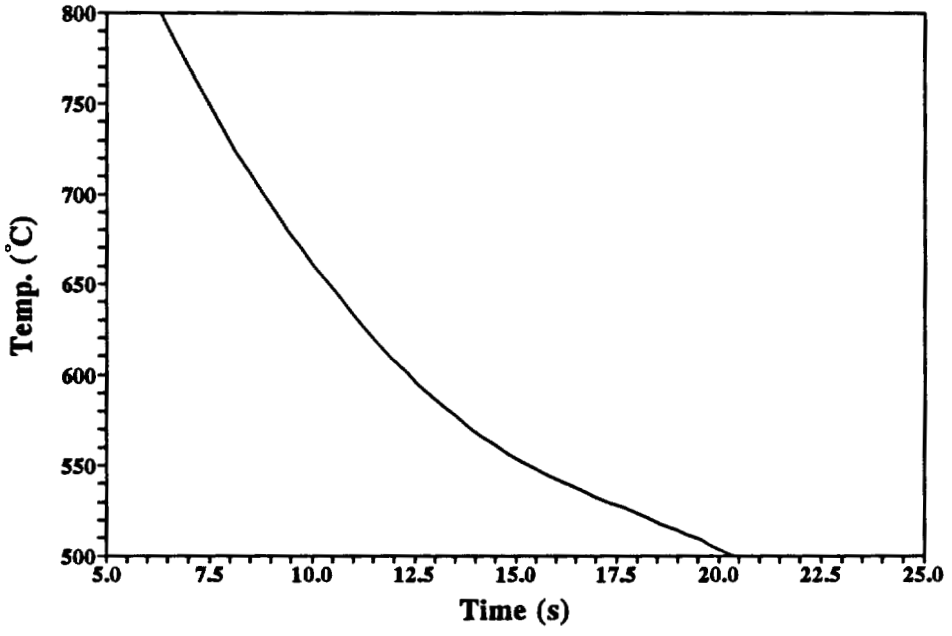

(b)

Figure 4: Cooling curve for GMA weld metal deposited on 16 mm (0.6 in.) thick plate at (a) 2.5 kJ/mm (90 kJ/in.) with 150°C (300°F) preheat and (b) at 2 kJ/mm (51 kJ/in.) with no preheat.

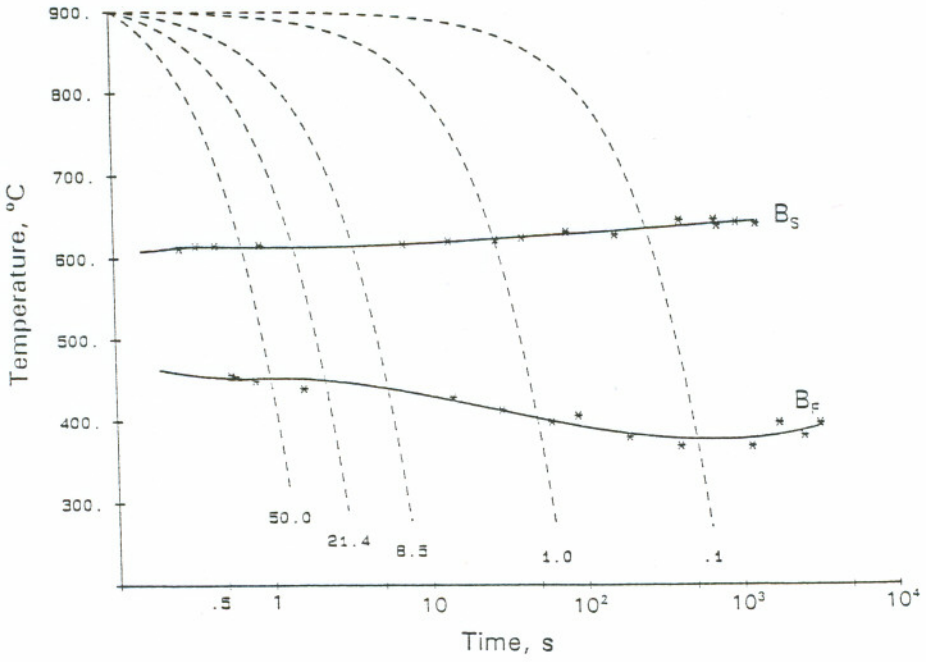

Figure 5: CCT diagram for GTA weld metal of Alloy 5 deposited at 3.5 kJ/mm (90 kJ/in.) heat input on matching base plate with Ar-5%CO_2 shielding gas, determined using 10 and 6 mm diameter weld metal samples.

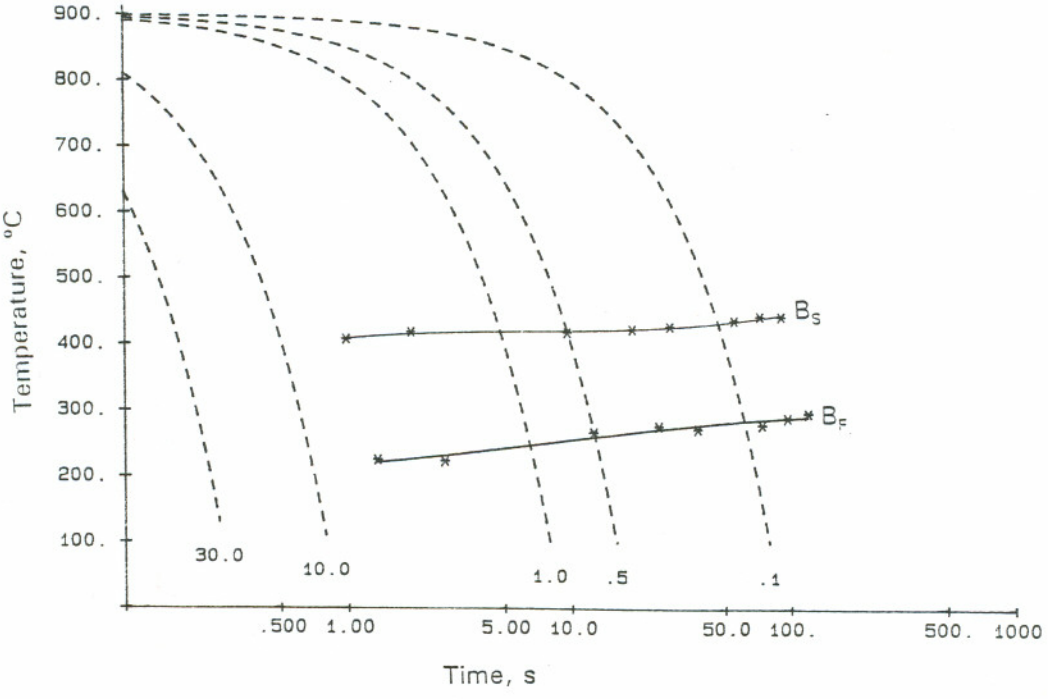

Figure 6: CCT diagram for GTA weld metal of Alloy 16 deposited at 3.5 kJ/mm (90 kJ/in.) heat input on matching base plate with Ar-5%CO_2 shielding gas, determined using 10 mm diameter weld metal samples.

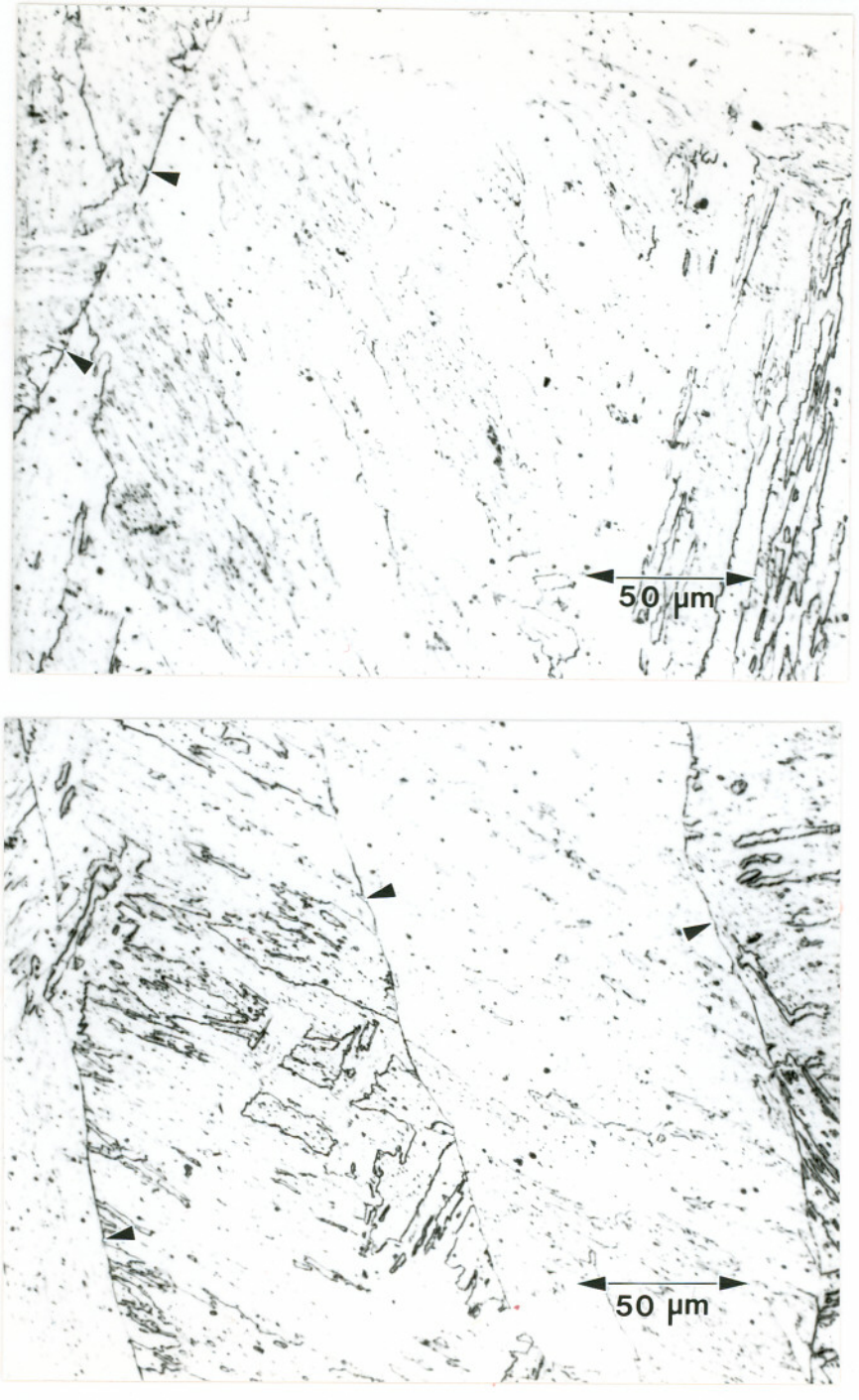

(a)

(b)

Figure 7: Optical micrographs of the GTA weld metal of Alloy 7 deposited on matching base plate with Ar-5%CO_2 shielding gas at (a) 3.5 kJ/mm (90 kJ/in.) and (b) 2 kJ/mm (51 kJ/in.) heat input, showing the reduction in the size of prior austenite grains. Arrows indicate the prior austenite grain boundaries. Etchant 2% nital.

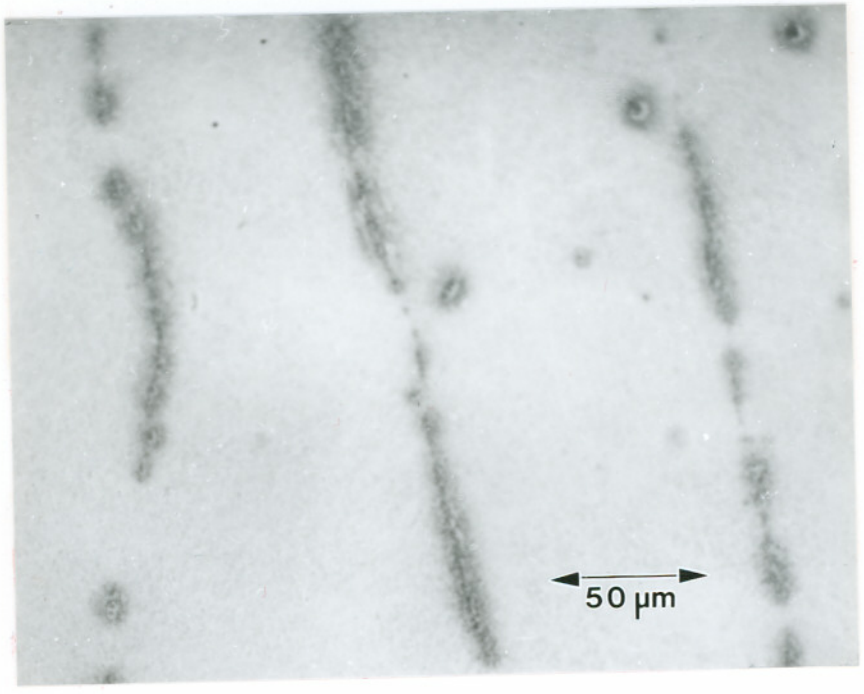

Figure 8: Optical micrograph of the GTA weld metal of Alloy 15 deposited at 3.5 kJ/mm (90 kJ/in.) heat input on matching base plate with Ar-5%CO_2 shielding gas, showing the borocarbides at the prior austenite grain boundaries, indicated by the arrows. Magnification 400X, Lepera's etchant.

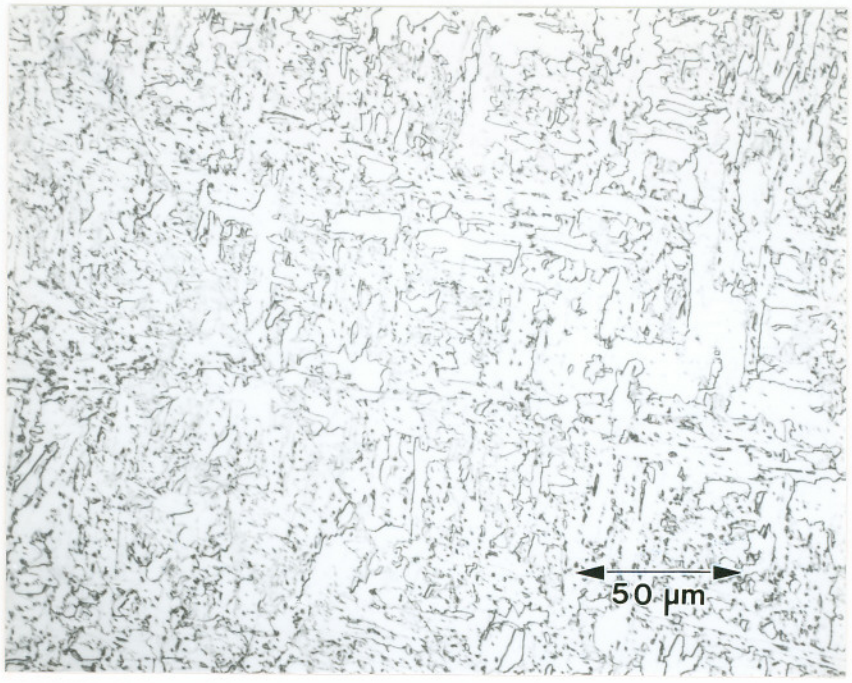

(a)

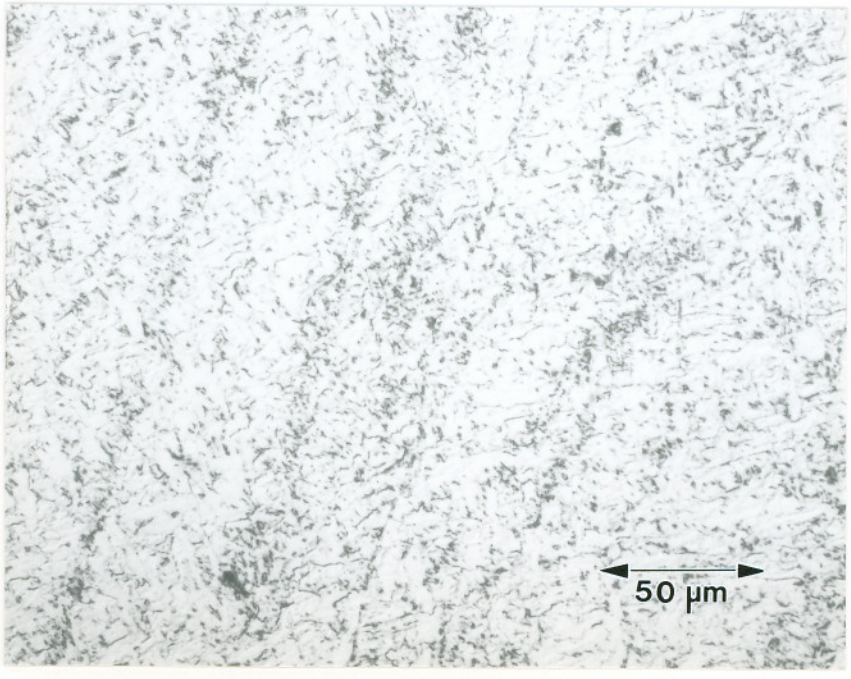

(b)

Figure 9: Optical micrographs of the GMA weld metal of Alloy 11 deposited at 2.5 kJ/mm (64 kJ/in.) heat input on HSLA-100 base plate with Ar-5%CO_2 shielding gas; (a) last pass, (b) reheated region.

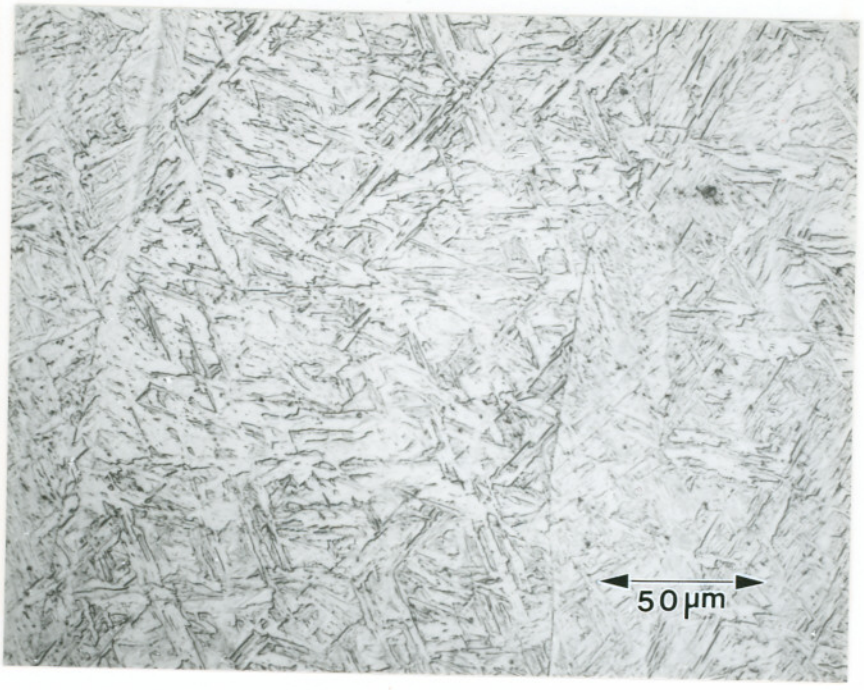

(a)

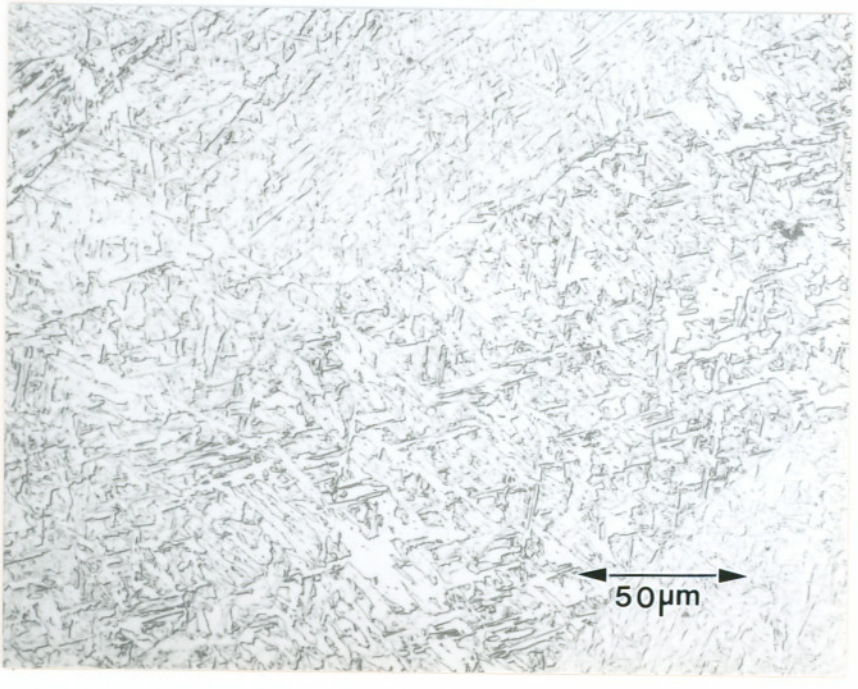

(b)

Figure 10: Optical micrographs of the GMA weld metal of Alloy 11 deposited at 1.8 kJ/mm (48 kJ/in.) heat input on HSLA-100 base plate with Ar-5%CO_2 shielding gas; (a) last pass, (b) reheated region.

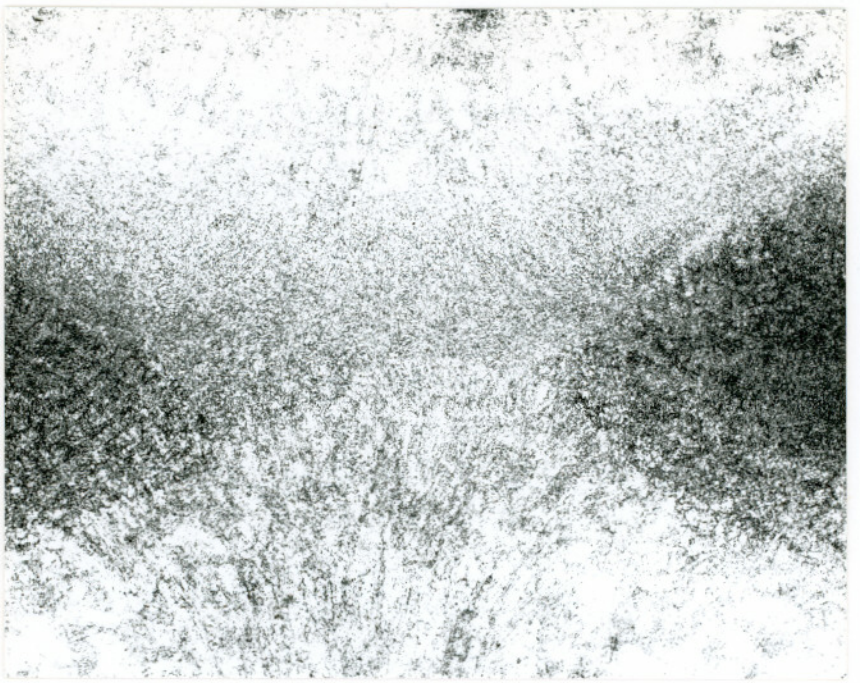

Figure 11: Optical macrograph of the GTA weld metal of Alloy 7 deposited at 3.5 kJ/mm (90 kJ/in.) heat input on matching base plate with Ar-5%CO_2 shielding gas, showing the region reheated above Ar_3.

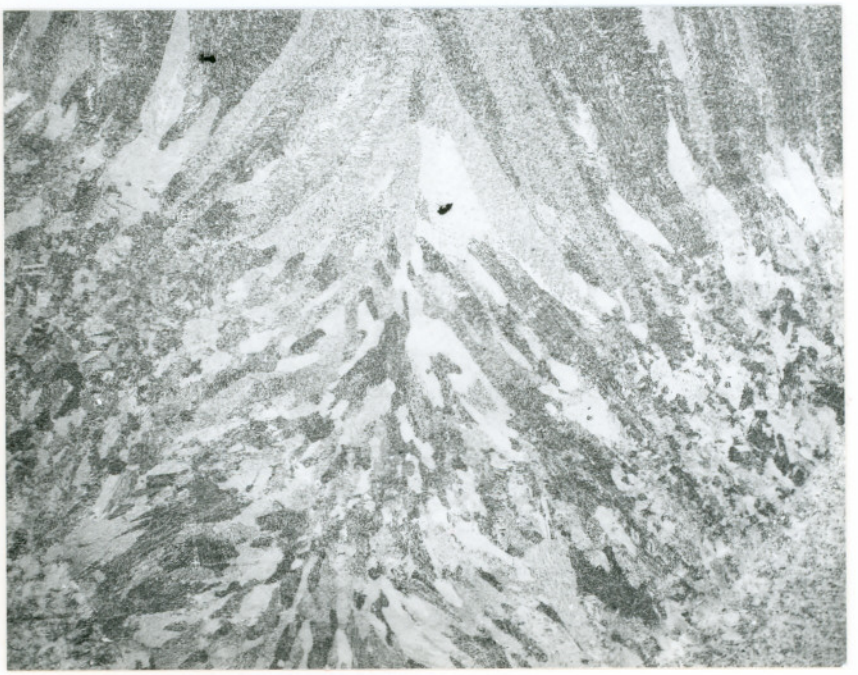

Figure 12: Optical macrograph of the GMA weld metal of Alloy 11 deposited at 2.5 kJ/mm (64 kJ/in.) heat input on HSLA-100 base plate with Ar-5%CO_2 shielding gas, showing the region reheated above Ar_3.

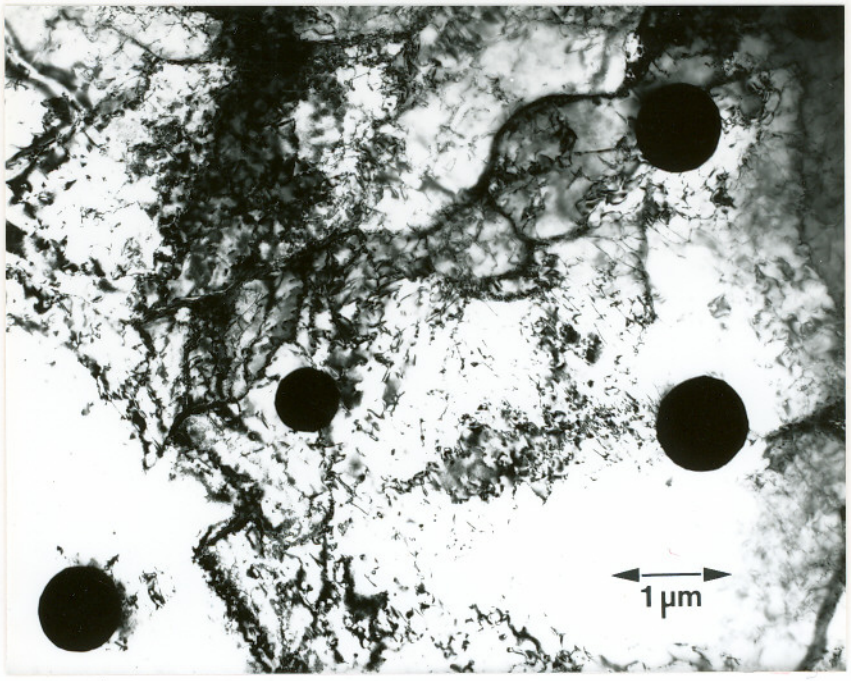

(a)

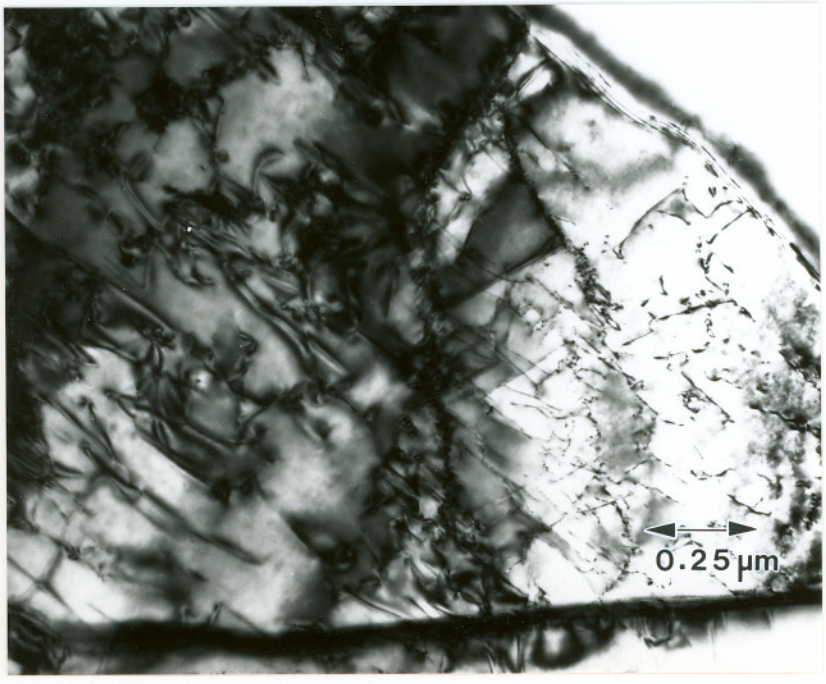

(b)

Figure 13: Transmission electron micrographs of the GTA weld metal of Alloy 1 deposited at 3.5 kJ/mm (90 kJ/in.) heat input on matching base plate with Ar-5%CO_2 shielding gas, showing the granular bainite microstructure, (a) shows weld metal inclusions.

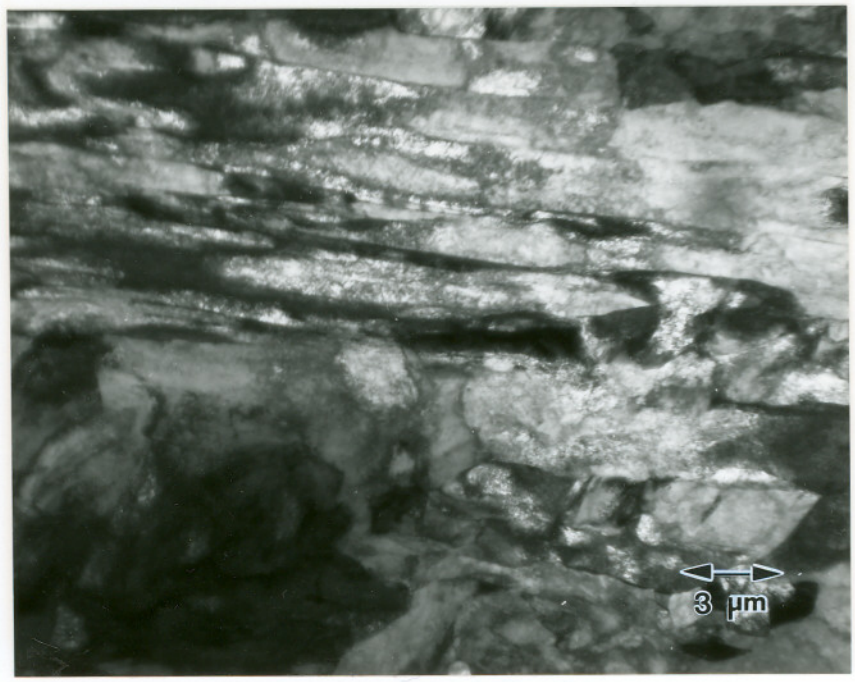

(a) Alloy 5

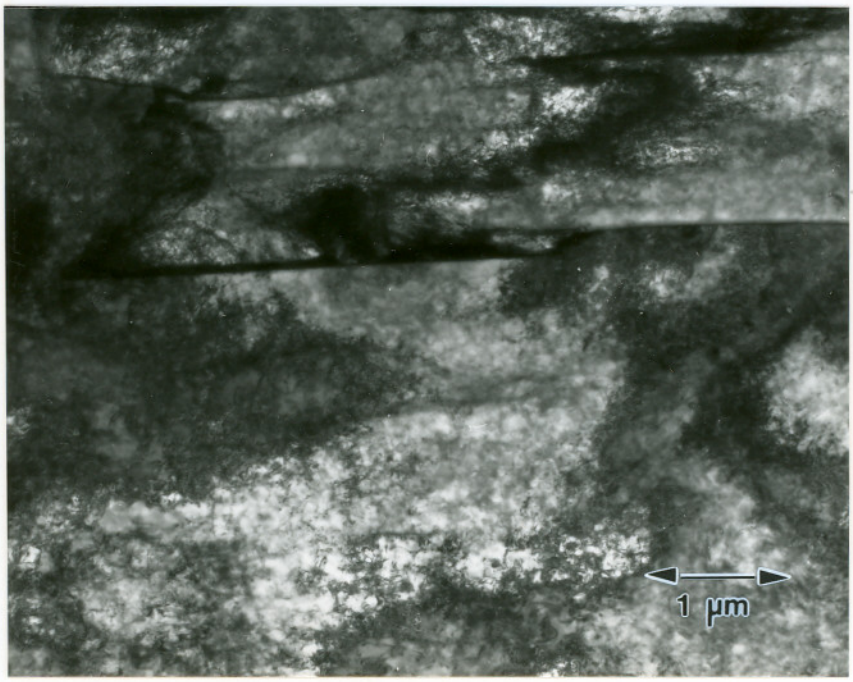

(b) Alloy 6

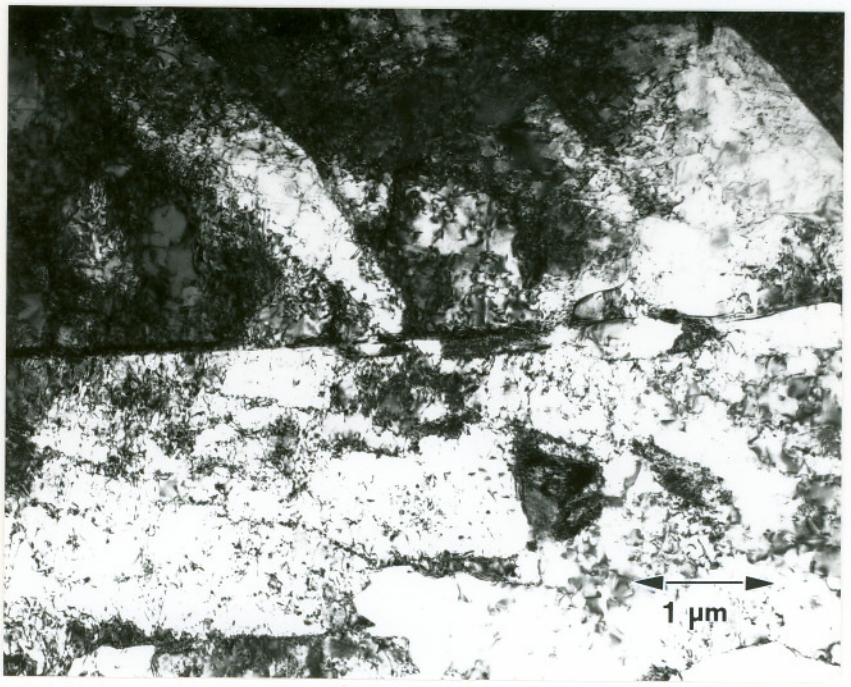

(c) Alloy 8

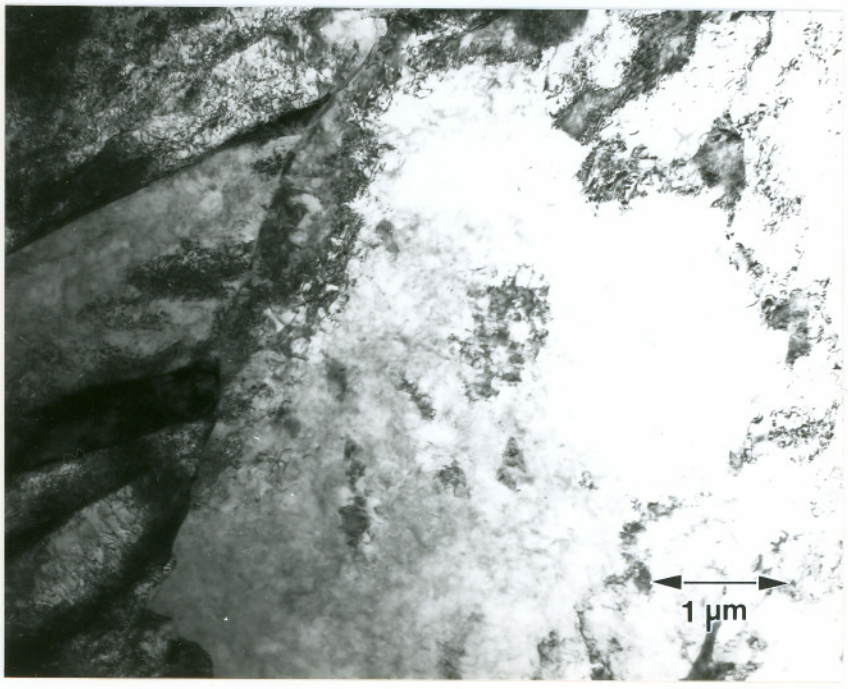

(d) Alloy 9

Figure 14: Transmission electron micrographs of the GTA weld metal of Alloys 5, 6, 8 and 9 deposited at 3.5 kJ/mm (90 kJ/in.) heat input on matching base plate with Ar-5%CO_2 shielding gas, showing mixed morphology.

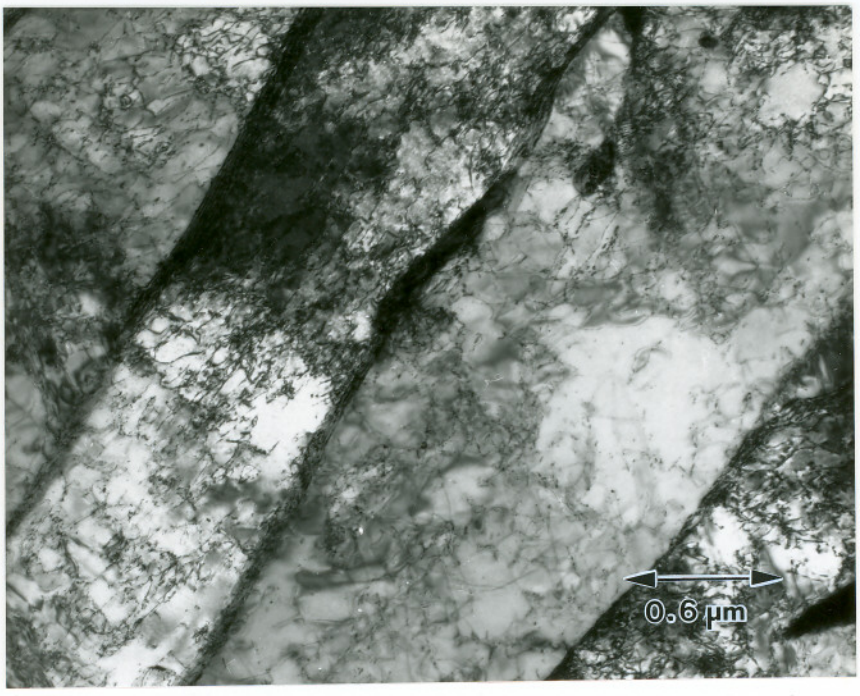

(a) Alloy 4

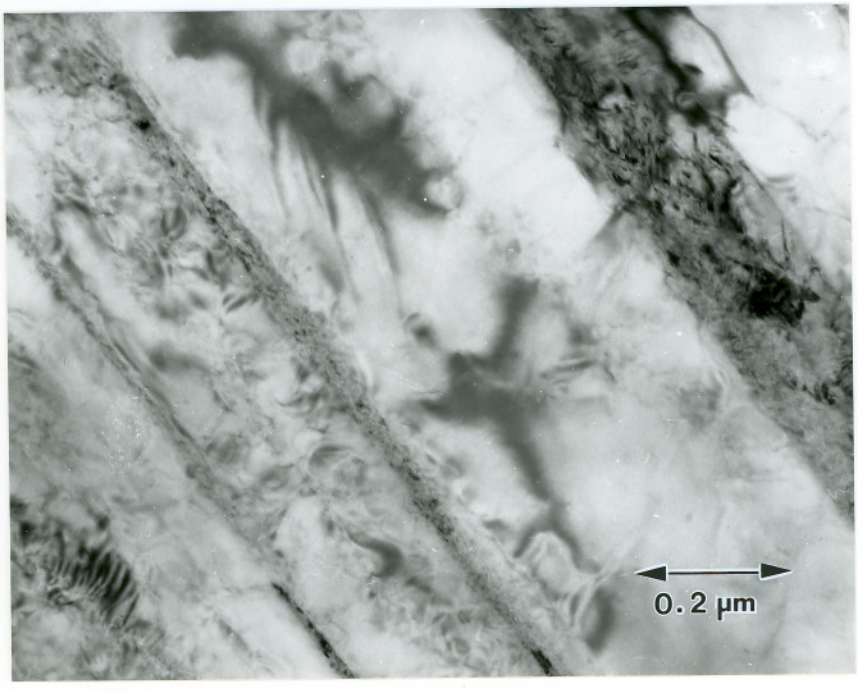

(b) Alloy 7

Figure 15: Transmission electron micrographs of the GTA weld metal of (a) Alloy 4 and (b) Alloy 7, deposited at 3.5 kJ/mm (90 kJ/in.) heat input on matching base plates with Ar-5%CO_2 shielding gas, showing the carbide free bainite microstructure. Arrows indicate the lath boundaries.

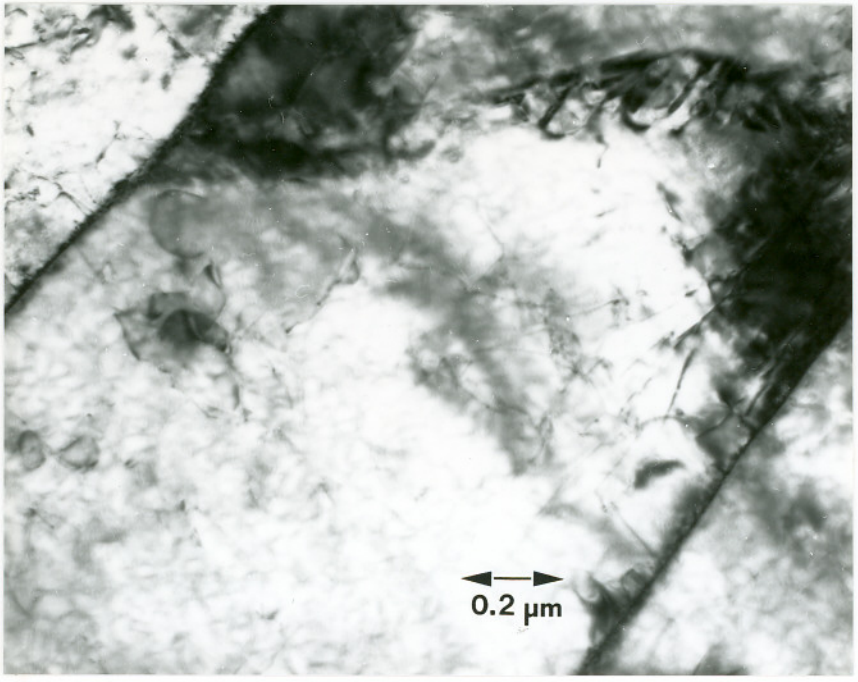

(a)

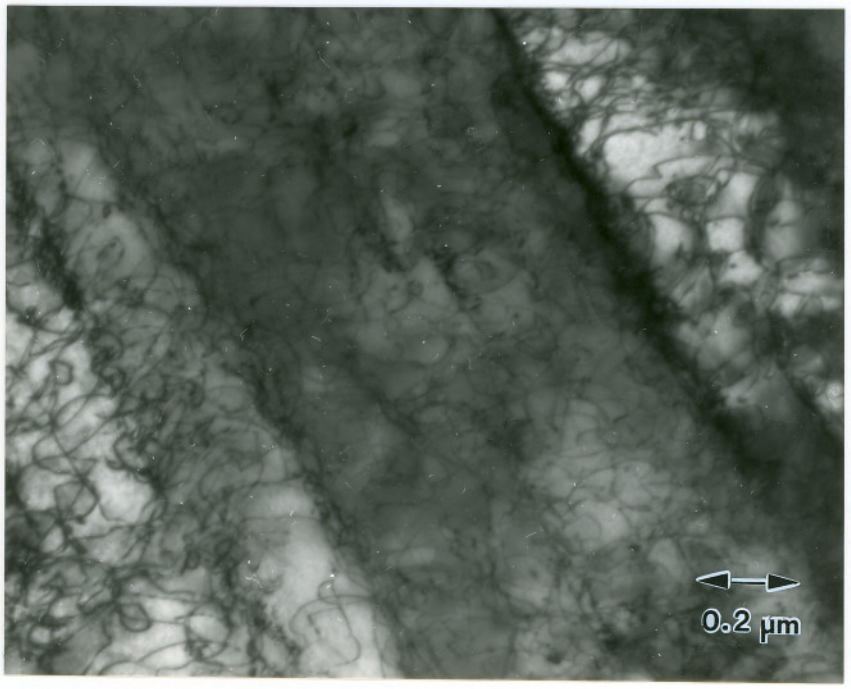

(b)

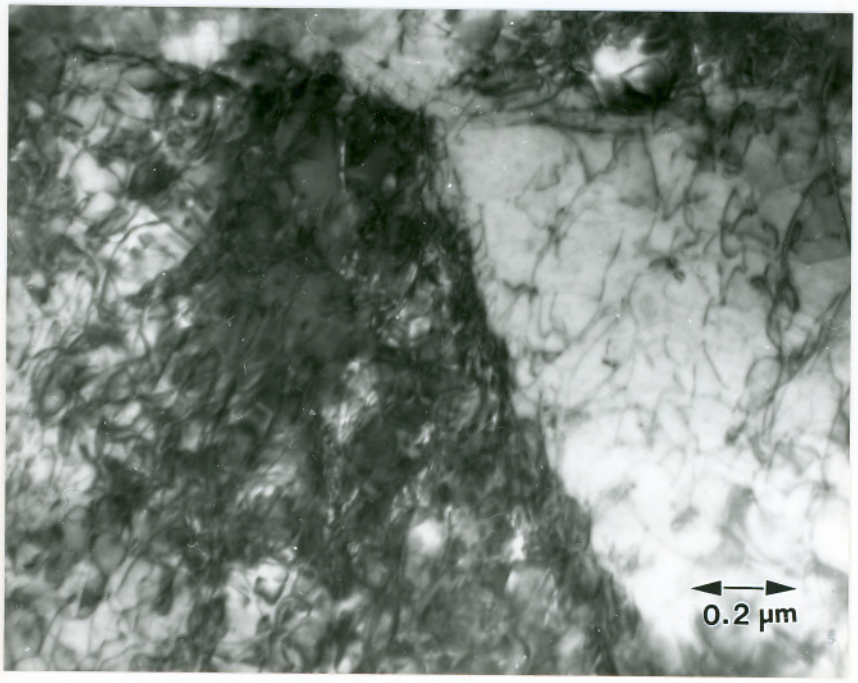

(c)

Figure 16: Transmission electron micrographs of the GTA weld metal deposited at 3.5 kJ/mm (90 kJ/in.) heat input on matching base plates with Ar-5%CO_2 shielding gas showing; (a) the sharp lath boundaries in Alloy 4, (b) diffuse lath boundaries in the lathy region of Alloy 5 weld metal and (c) cellular dislocation tangles in the granular region of Alloy 5 weld metal.

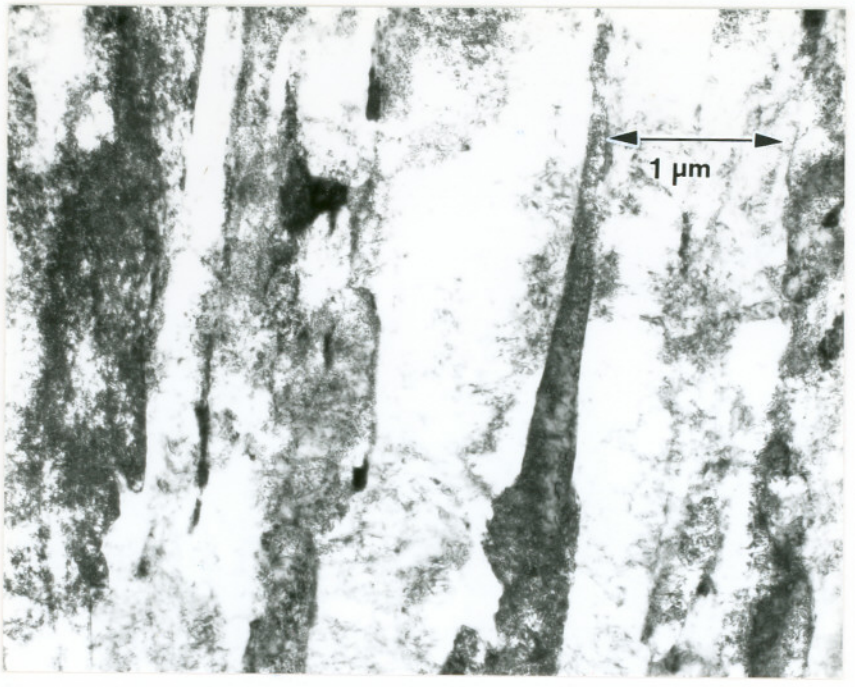

(a)

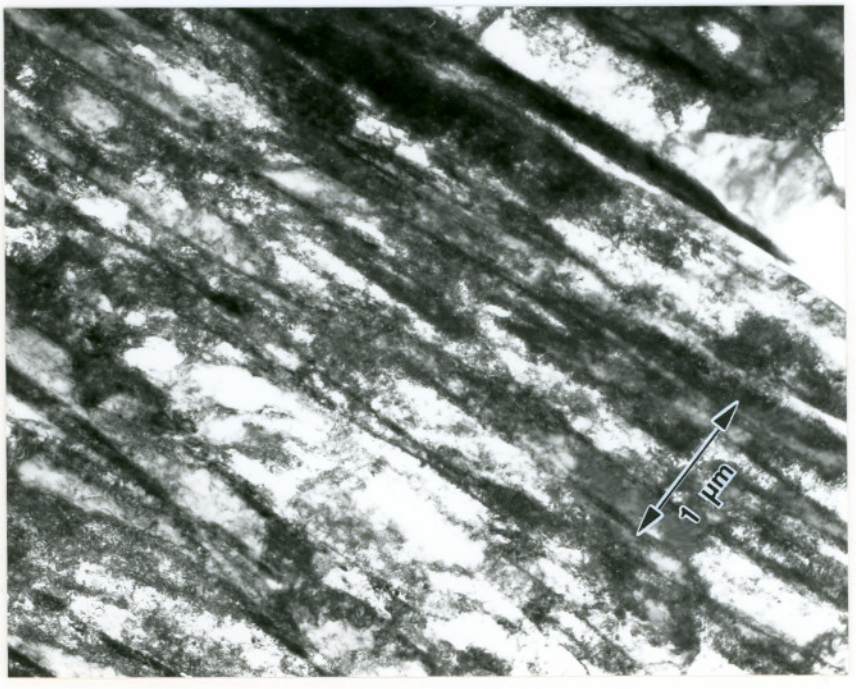

(b)

Figure 17: Transmission electron micrographs of the GTA weld metal of Alloy 7 deposited on matching base plates with Ar-5%CO_2 shielding gas (a) at 3.5 kJ/mm (90 kJ/in.) and (b) at 2 kJ/mm (51 kJ/in.) heat input, showing the finer lath width of the 2 kJ/mm weld metal. Arrows indicate the lath boundaries.

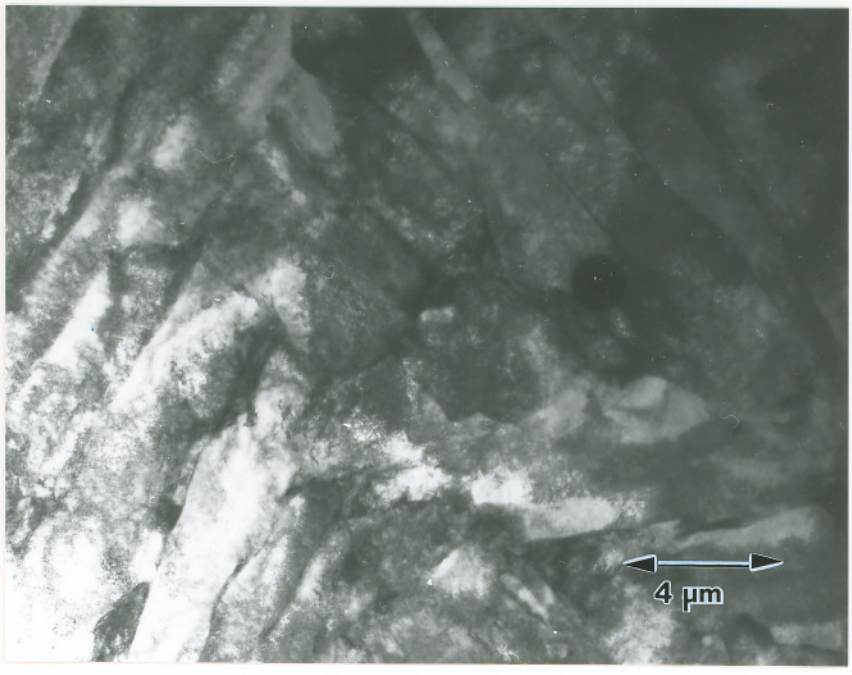

(a)

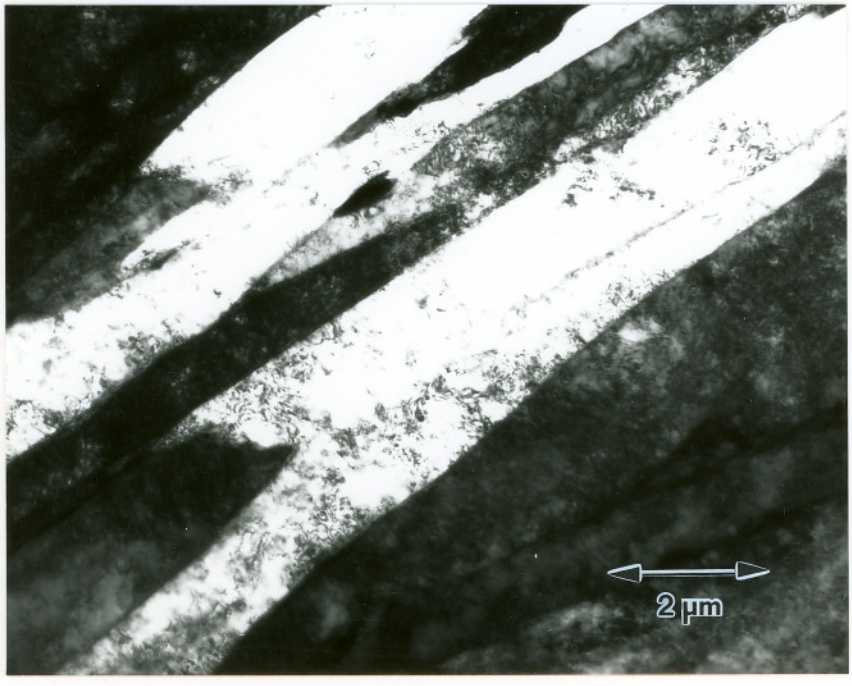

(b)

Figure 18: Transmission electron micrographs of the last pass of GMA weld metal of Alloy 11 deposited at 1.8 kJ/mm (48 kJ/in.) heat input on HSLA-100 base plates with Ar-5%CO_2 shielding; showing (a) the packets and (b) laths within the packets. Arrows indicate packet and lath boundaries.

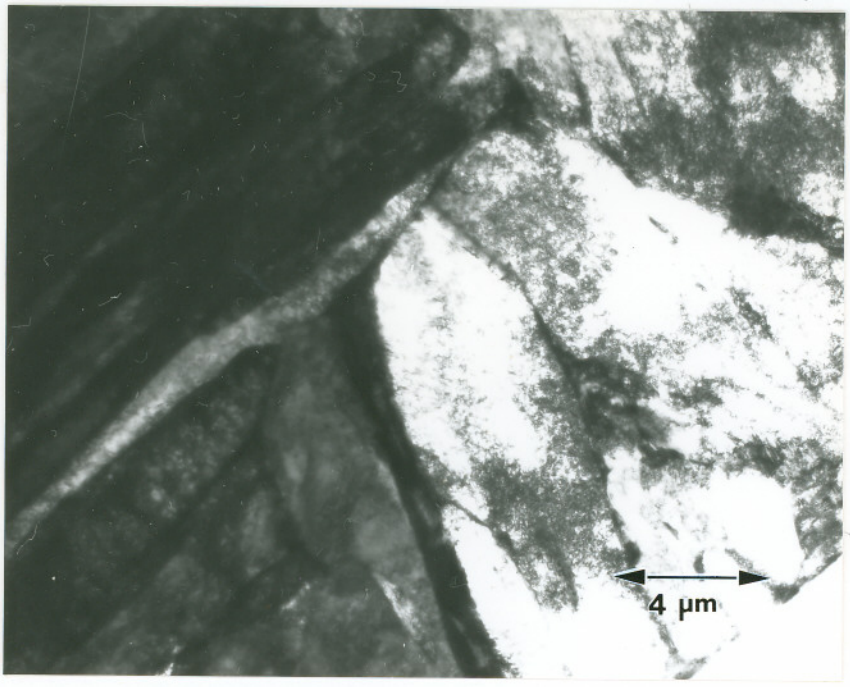

(a)

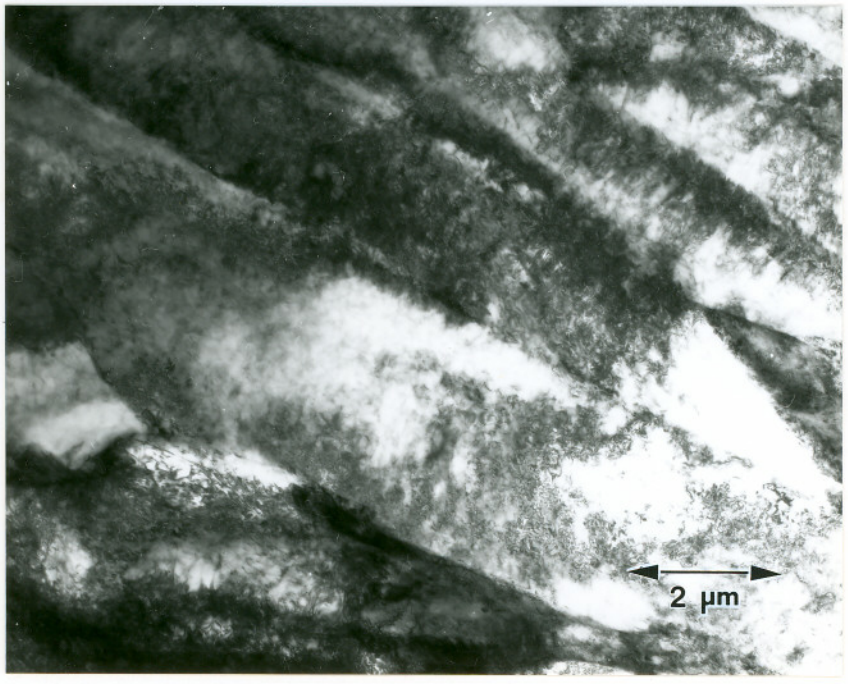

(b)

Figure 19: Transmission electron micrographs of the last pass of GMA weld metal of Alloy 11 deposited at 2.5 kJ/mm (64 kJ/in.) heat input on HSLA-100 base plates with Ar-5%CO_2 shielding gas showing; (a) the packets and (b) laths within the packets. Arrows indicate packet and lath boundaries.

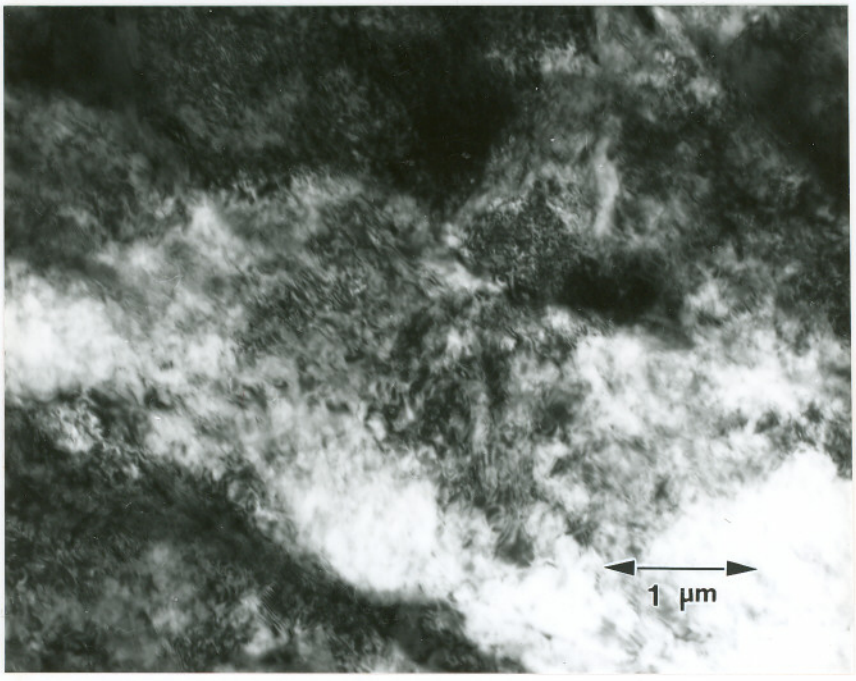

(a)

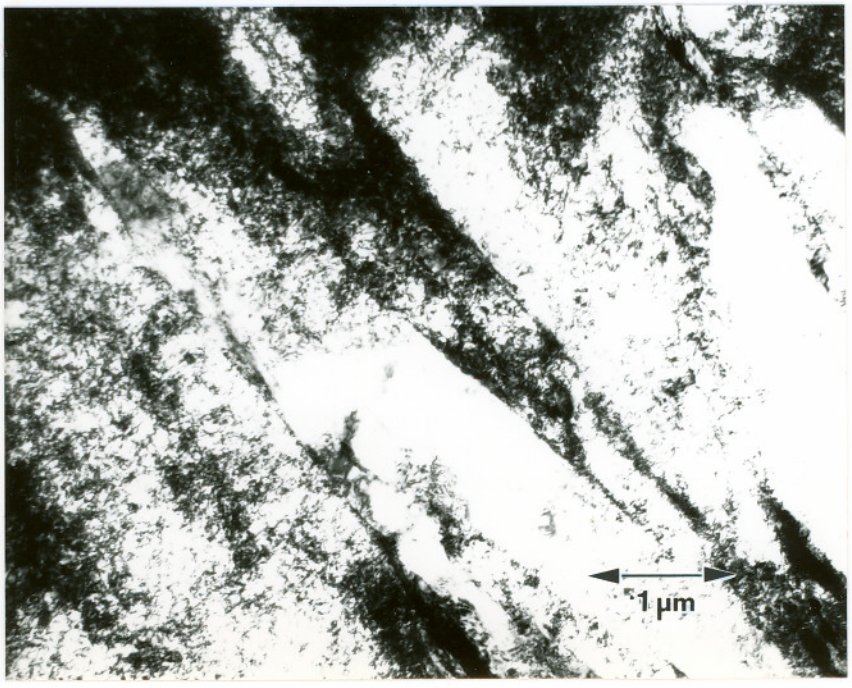

(b)

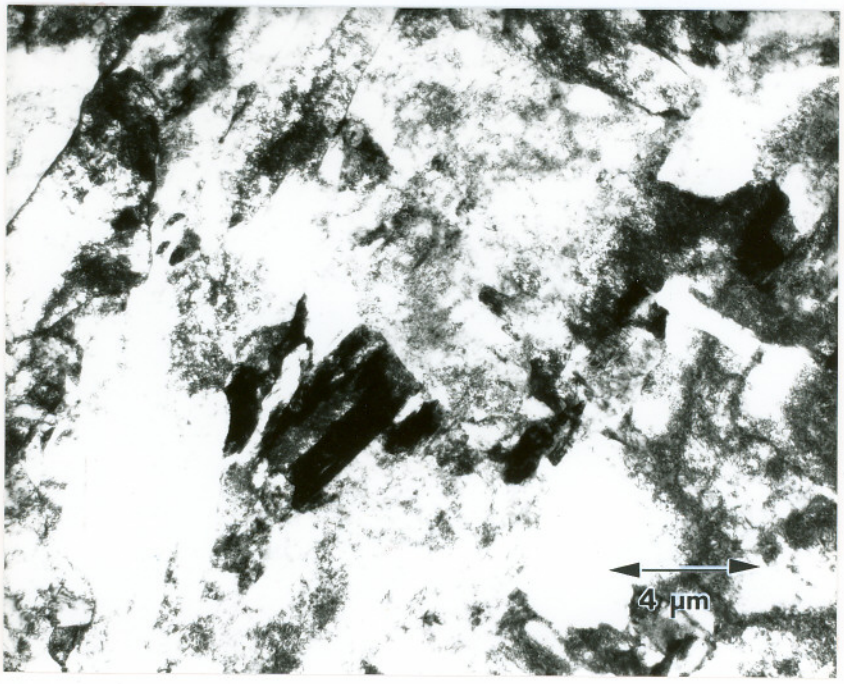

(c)

Figure 20: Transmission electron micrographs of the reheated region of GMA weld metal of Alloy 11 deposited at 2.5 kJ/mm (64 kJ/in.) heat input on HSLA-100 base plates with Ar-5%CO_2 shielding showing; (a) mixed morphology, (b) region containing laths and (c) granular region. Arrows indicate lath boundaries

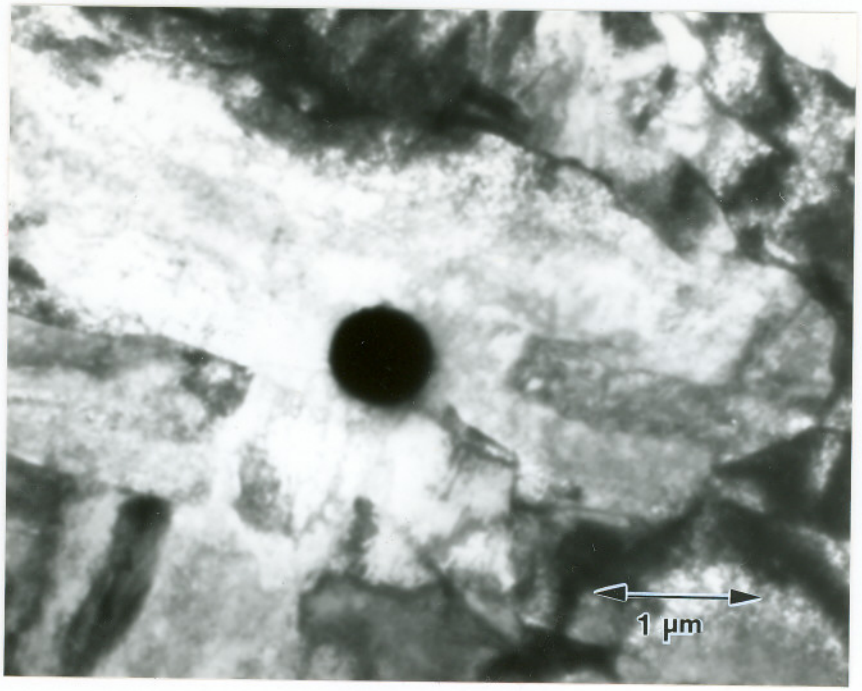

(a)

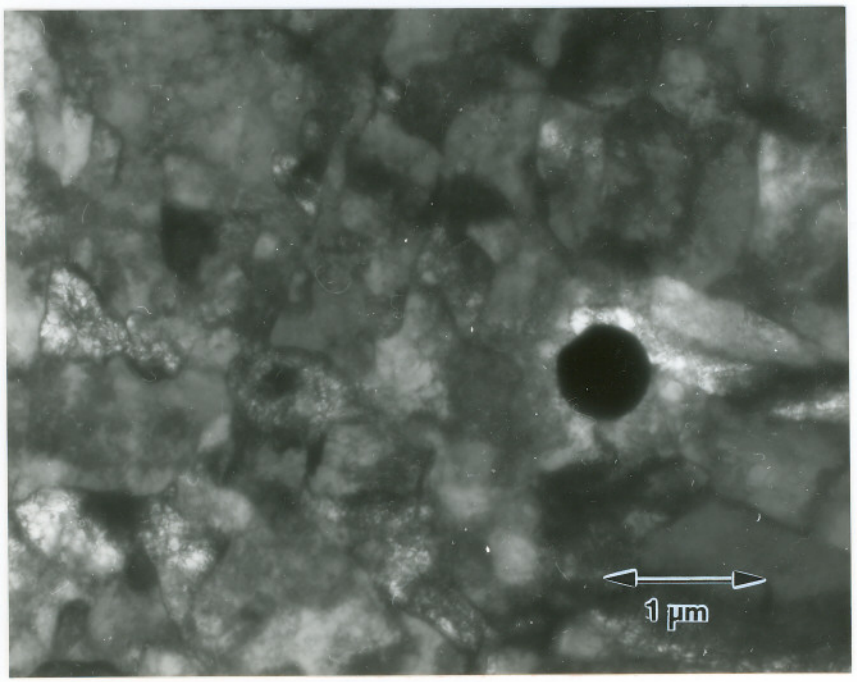

(b)

Figure 21: Transmission electron micrographs of the GTA weld metal of Alloy 5 deposited at 3.5 kJ/mm (90 kJ/in.) heat input on matching base plate with Ar-5%CO_2 shielding gas showing; (a) inclusion associated with ferrite nucleation, and (b) inclusion not associated with ferrite nucleation. Arrows indicate the boundaries of the ferrite.

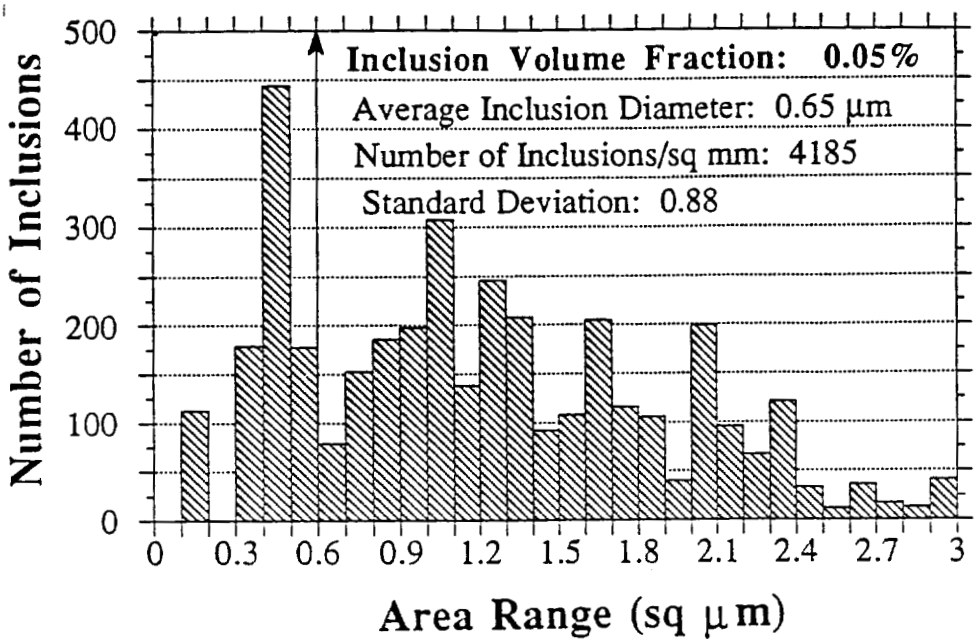

(a)

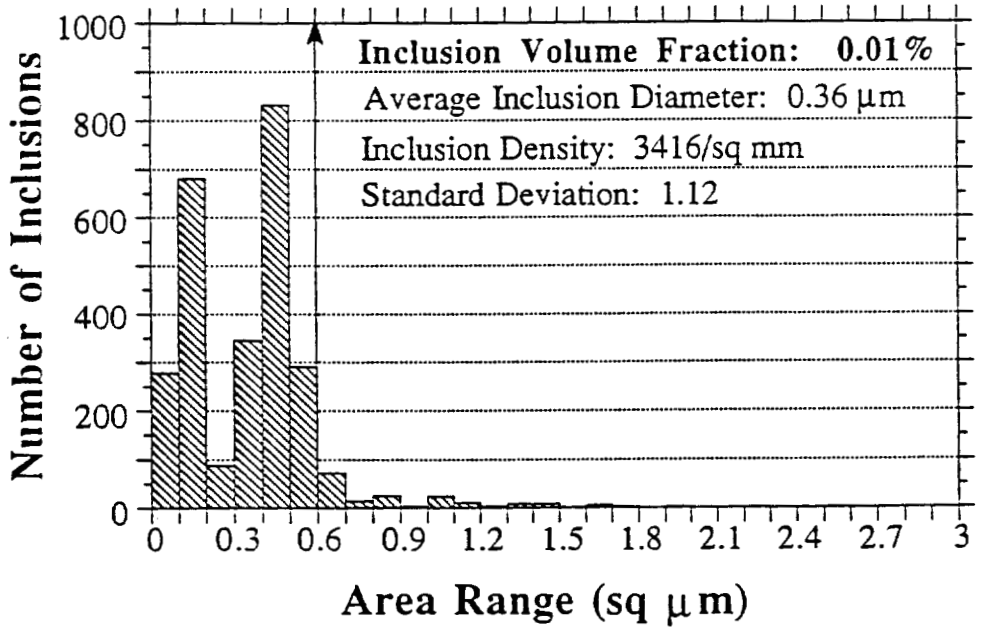

(b)

Figure 22: Inclusion size distribution for the GTA weld metal of Alloy 7 deposited at 3.5 kJ/mm (90 kJ/in.) heat input on matching base plate; (a) Ar-5%CO_2 shielding gas and (b) Ar-25%He shielding gas.

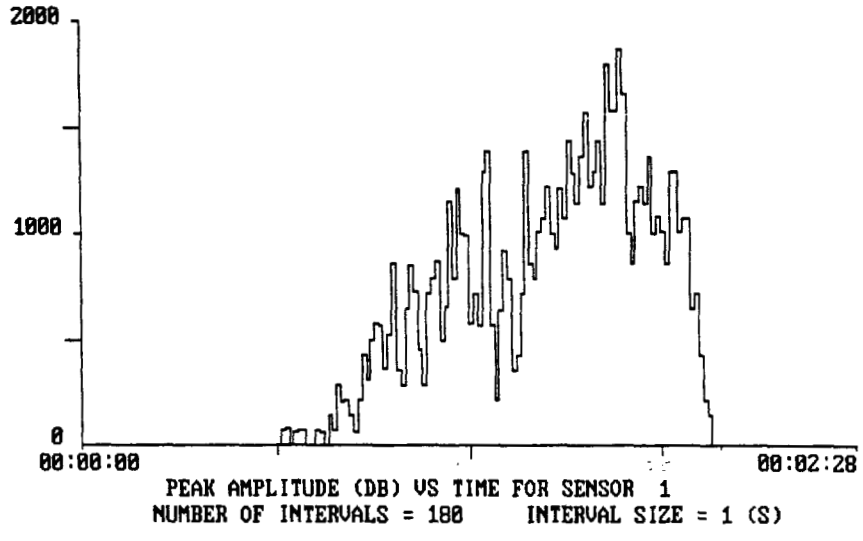

(a)

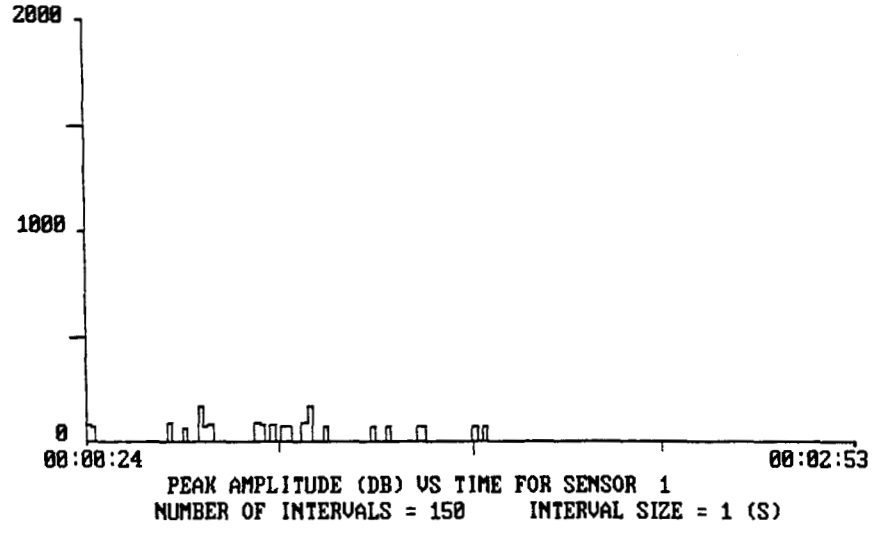

(b)

Figure 23: Acoustic emission data from the flat tensile tests the GTA weld metal of Alloy 8 deposited at 3.5 kJ/mm (90 kJ/in.) heat input on matching base plate showing Peak Amplitude vs Time for; (a) Weld metal deposited with Ar-5%CO_2 shielding gas and (b) Weld metal deposited with Ar-25%He shielding gas.

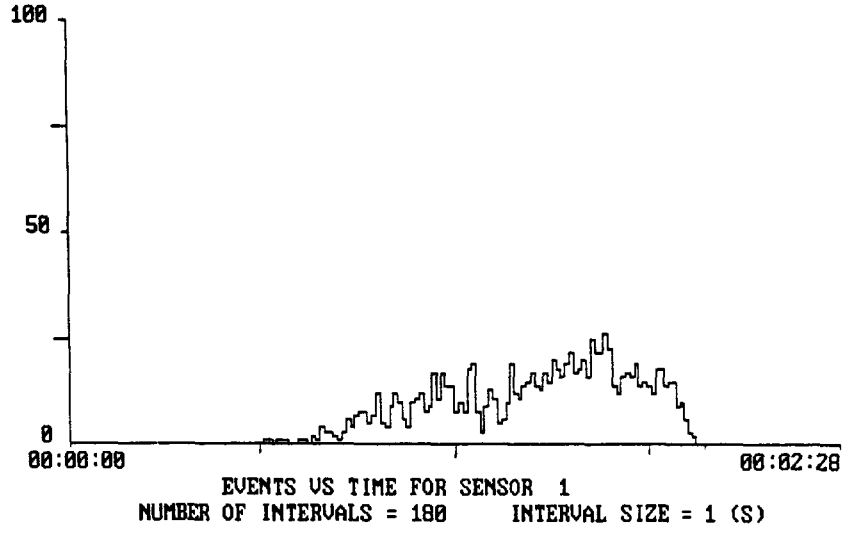

(a)

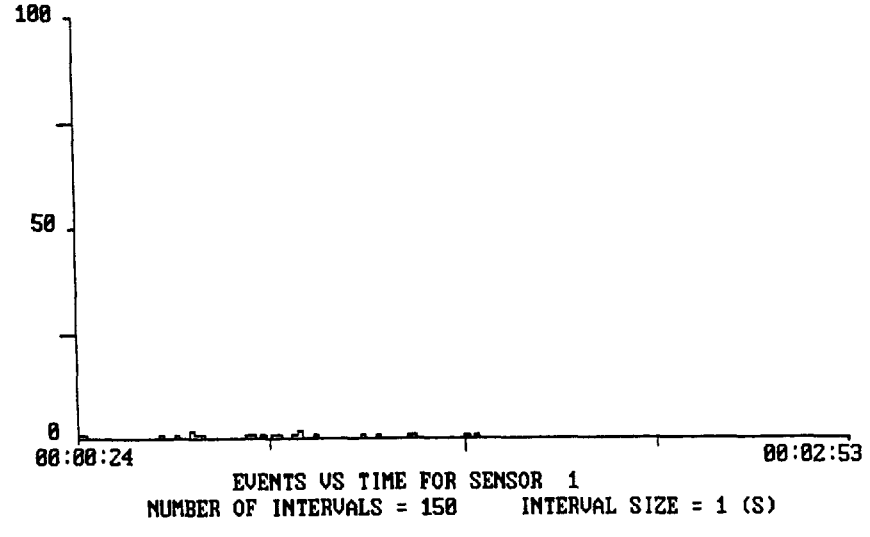

(b)

Figure 24: Acoustic emission data from the flat tensile tests the GTA weld metal of Alloy 8 deposited at 3.5 kJ/mm (90 kJ/in.) heat input on matching base plate showing number of Events vs Time for; (a) Weld metal deposited with Ar-5%CO_2 shielding gas and (b) Weld metal deposited with Ar-25%He shielding gas.

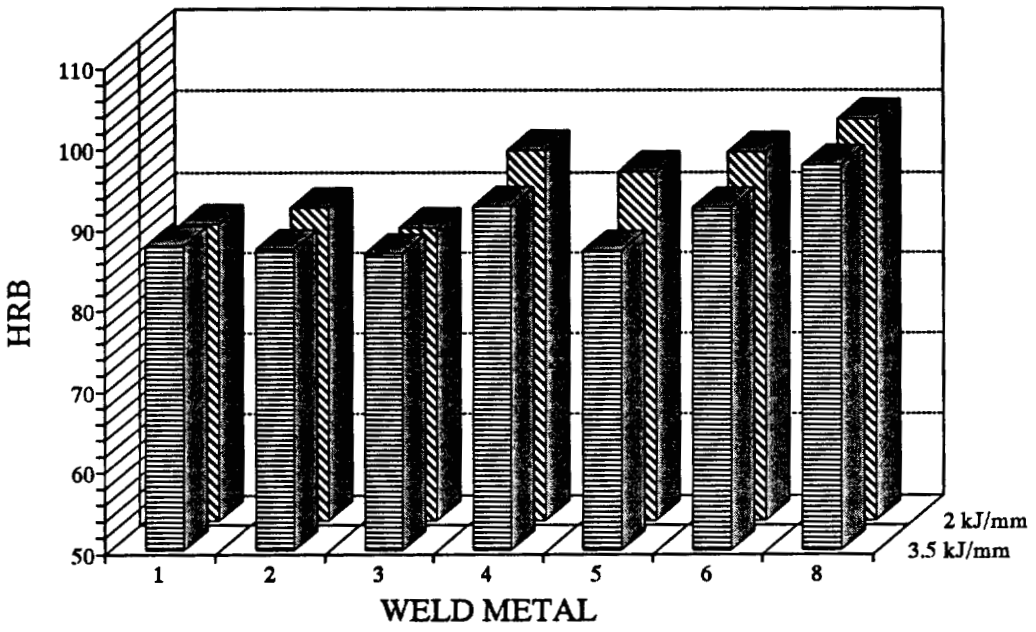

(a) Alloys 1-6 and 8

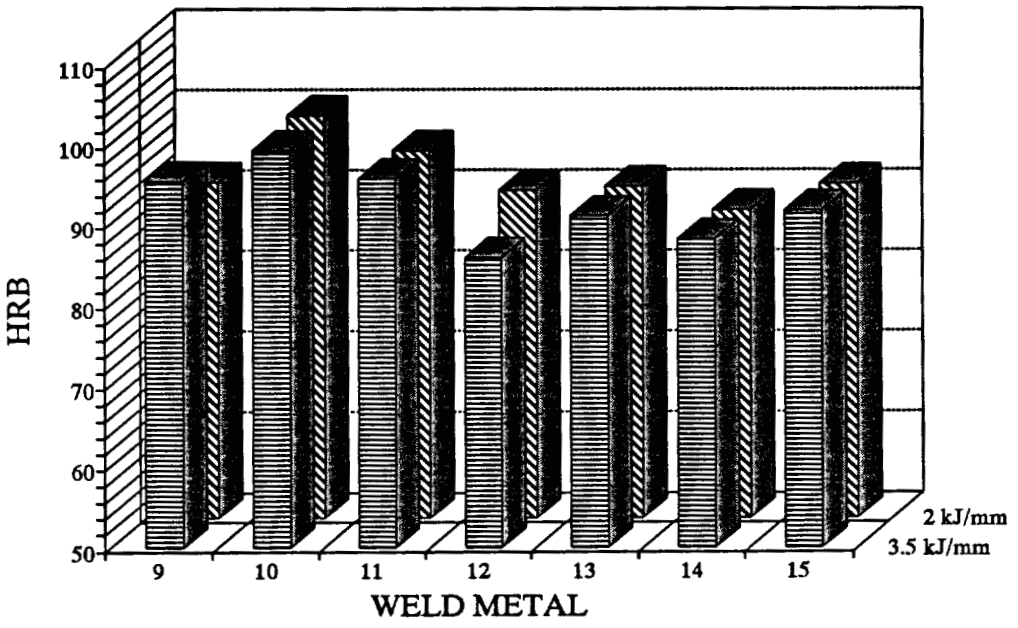

(b) Alloys 9-15

Figure 25: Comparison hardness values for the GTA weld metal of the Alloys deposited on matching base plate at 3.5 kJ/mm (90 kJ/in.) and 2 kJ/mm (51 kJ/in.) heat input with Ar-5%CO_2 shielding gas; (a) Alloys 1 to 6 and 8, (b) Alloys 9 to 15.

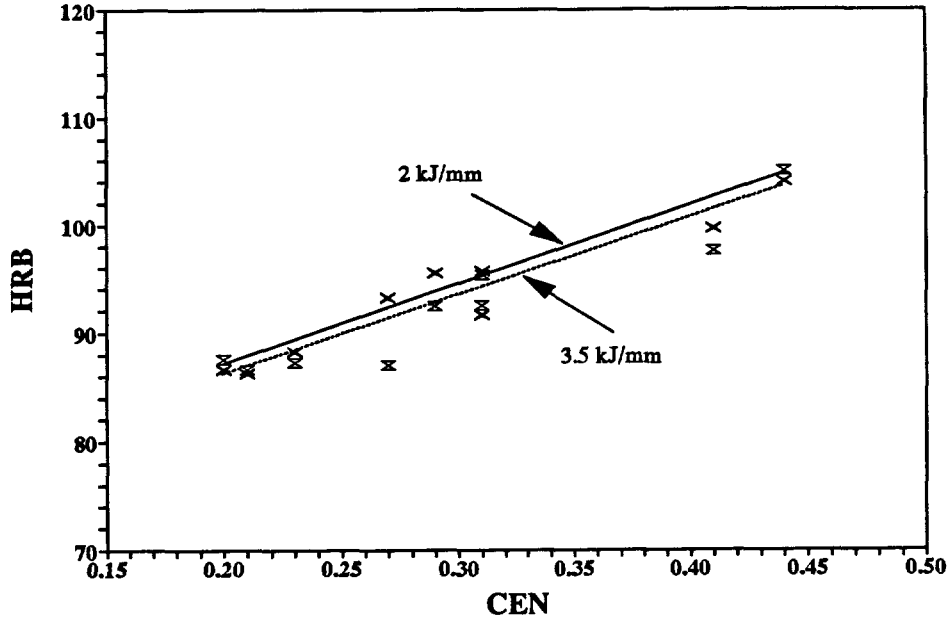

Figure 26: Variation of hardness with Yurioka's CEN values of the GTA weld metal deposited on matching base plate at 3.5 kJ/mm (90 kJ/in.) and 2 kJ/mm (51 kJ/in.) heat input with Ar-5%CO_2 shielding gas.

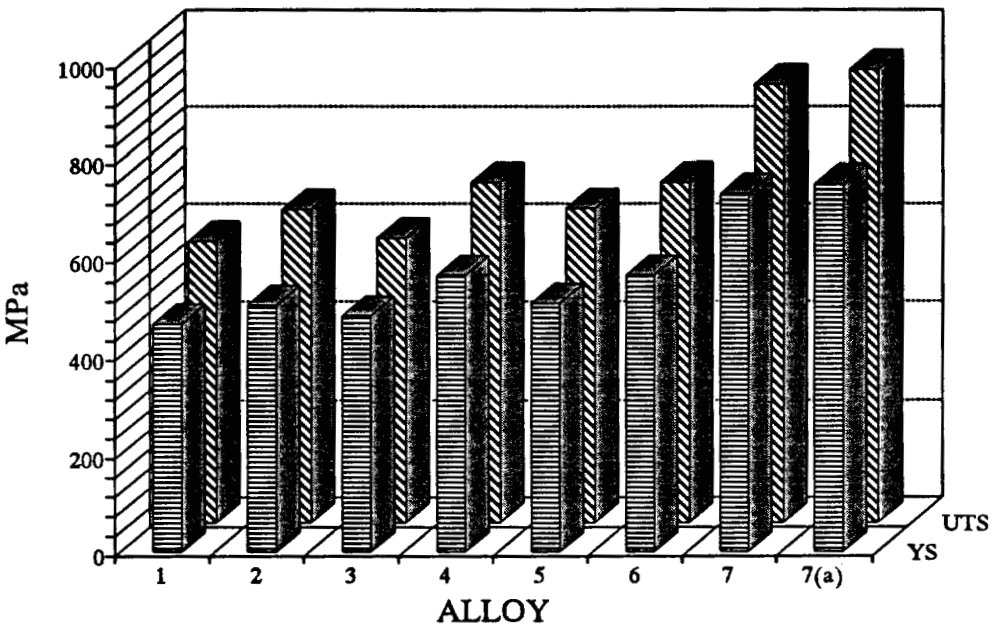

(a) Alloys 1-8

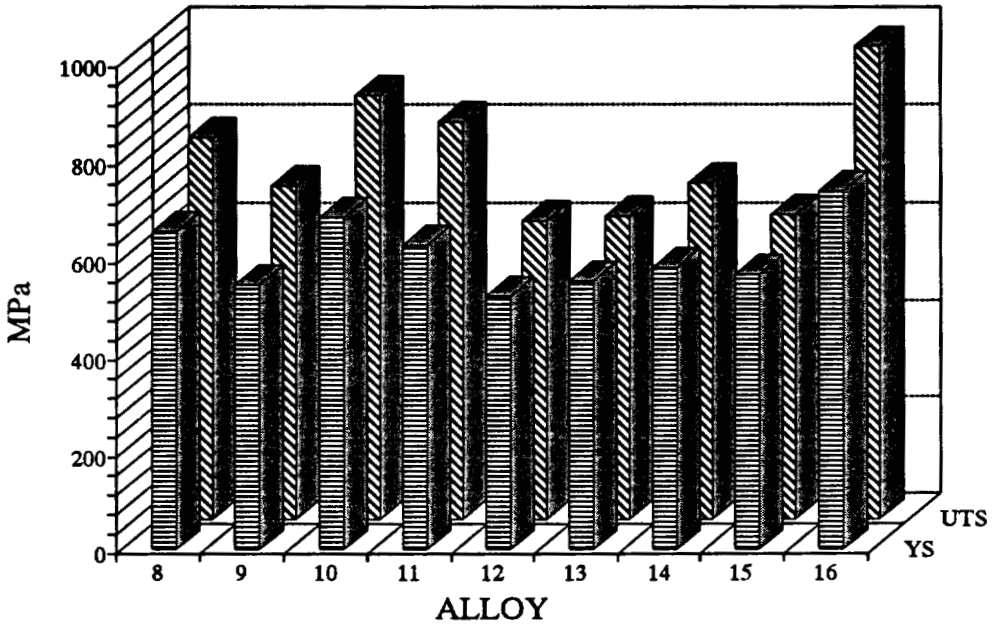

(b) Alloys 9-16

Figure 27: Tensile properties of the GTA weld metal deposited at 3.5 kJ/mm (90 kJ/in.) heat input with Ar-5%CO_2 shielding gas on matching base plate; (a) Alloys 1 through 8 and (b) Alloys 9 through 16. 7(a) is Alloy 7 filler metal on HSLA-100 base plate.

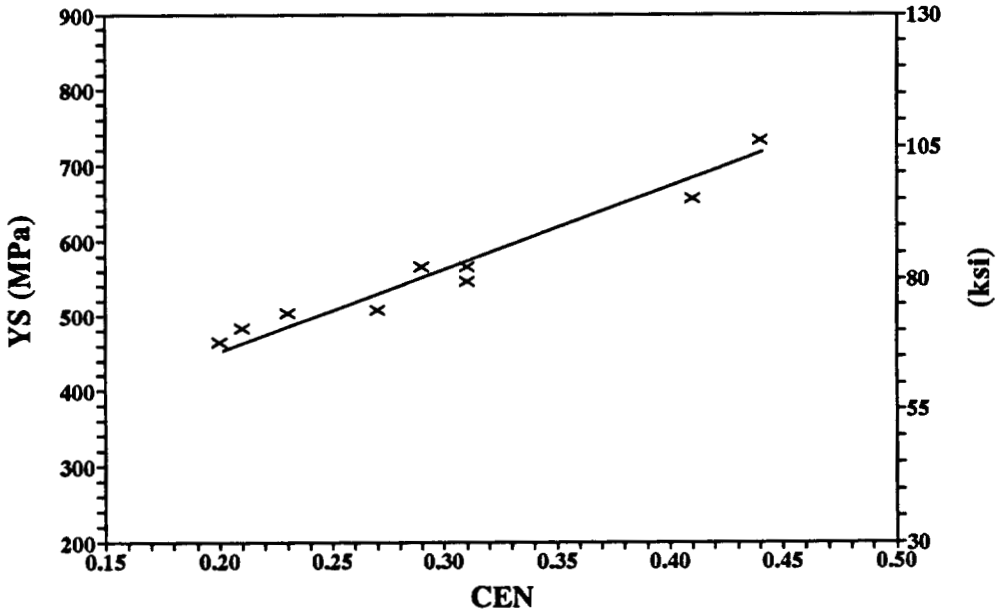

Figure 28: Variation of yield strength with Yurioka's CEN values of the GTA weld metal deposited on matching base plate at 3.5 kJ/mm (90 kJ/in.) heat input with Ar-5%CO_2 shielding gas.

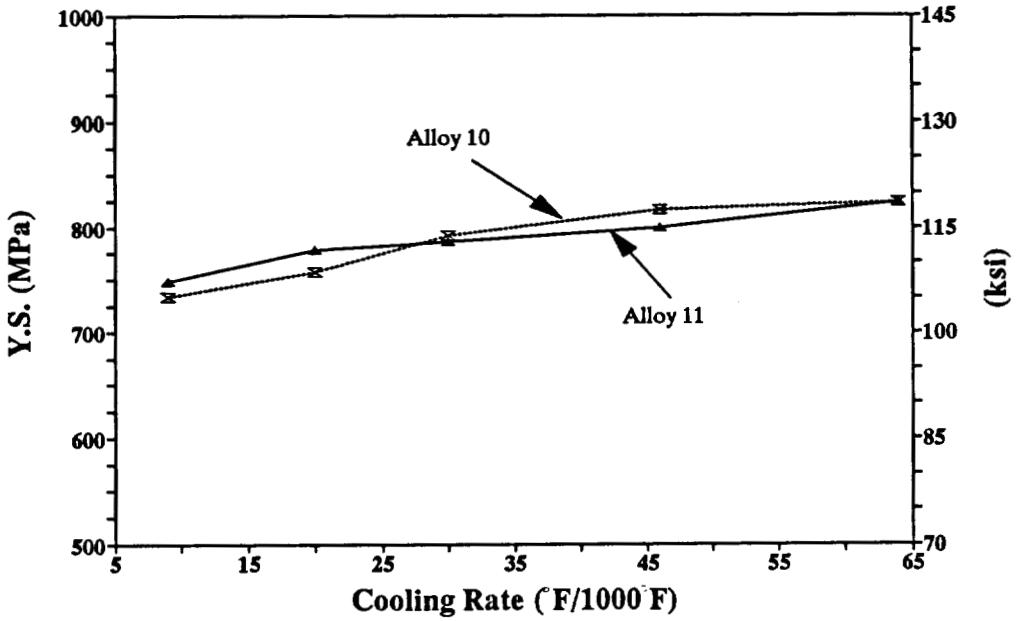

Figure 29: Variation in yield strength of the GMA weld metal of Alloys 10 and 11 deposited on HY-100 base plate with Ar-5%CO_2 shielding gas with change in cooling rate (Electric Boat Data).

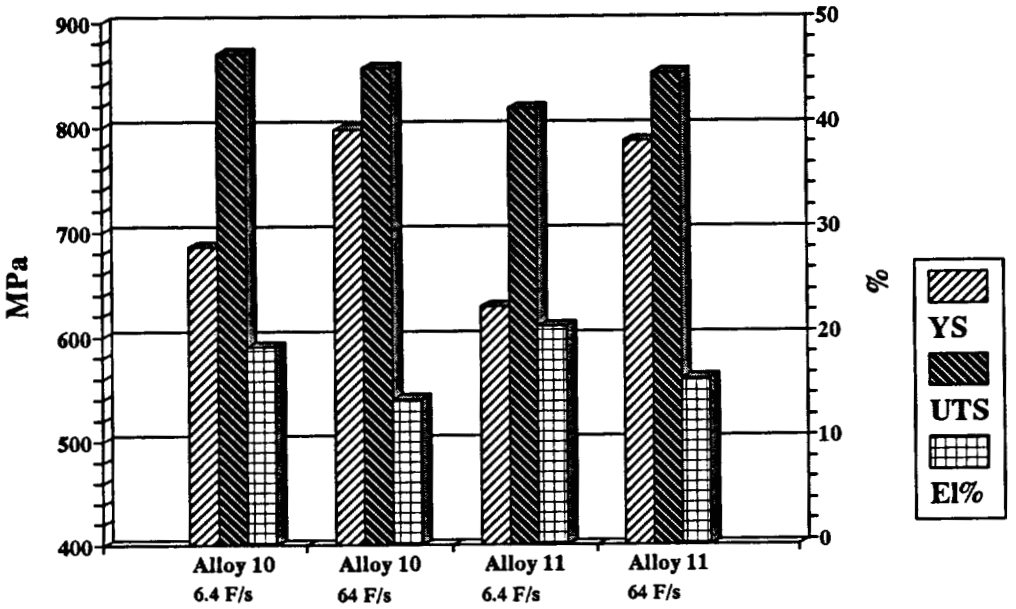

Figure 30: Change in yield strength of the GMA weld metal of Alloys 10 and 11 deposited at 1.33 kJ/mm (34 kJ/in.) and 3.2 kJ/mm (82.5 kJ/in.) with Ar-5%CO_2 shielding gas on HY-100 base plate (ESAB Data).

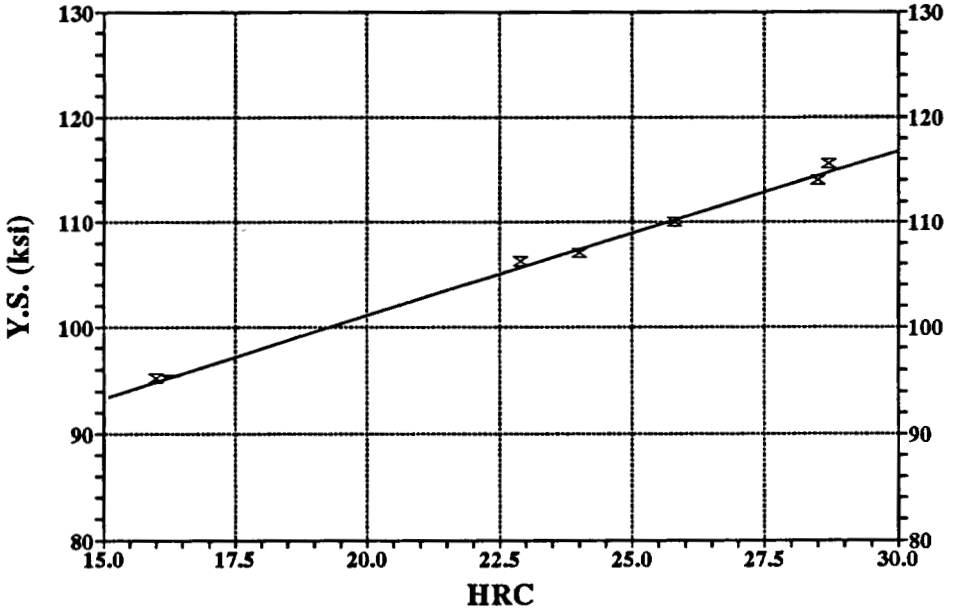

Figure 31: Variation of yield strength of the GTA weld metal deposited at 3.5 kJ/mm (90 kJ/in.) with Ar-5%CO_2 shielding gas on matching base plates with Rockwell C hardness (HRC).

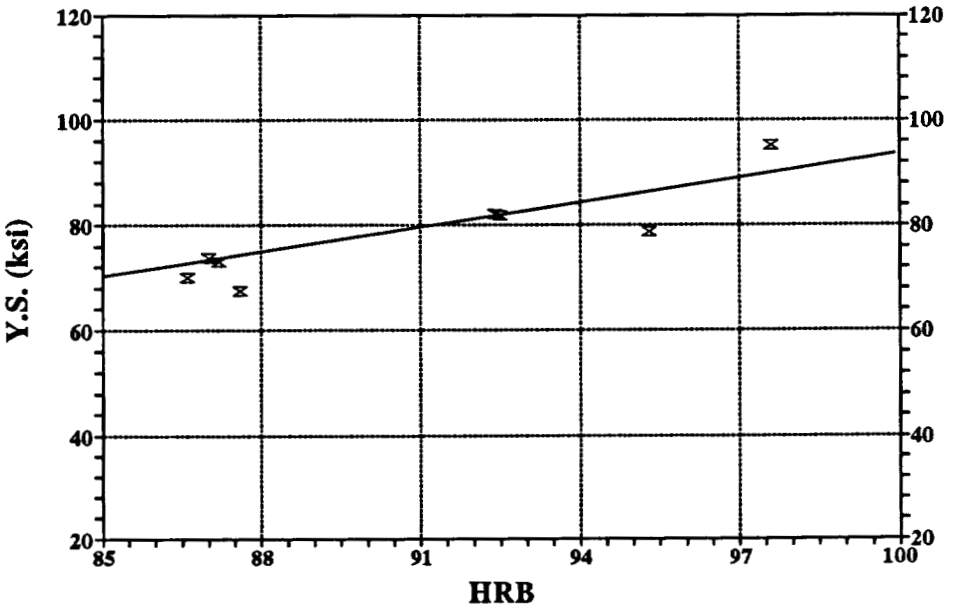

Figure 32: Variation of yield strength of the GTA weld metal deposited at 3.5 kJ/mm (90 kJ/in.) with Ar-5%CO_2 shielding gas on matching base plates with Rockwell B hardness (HRB).

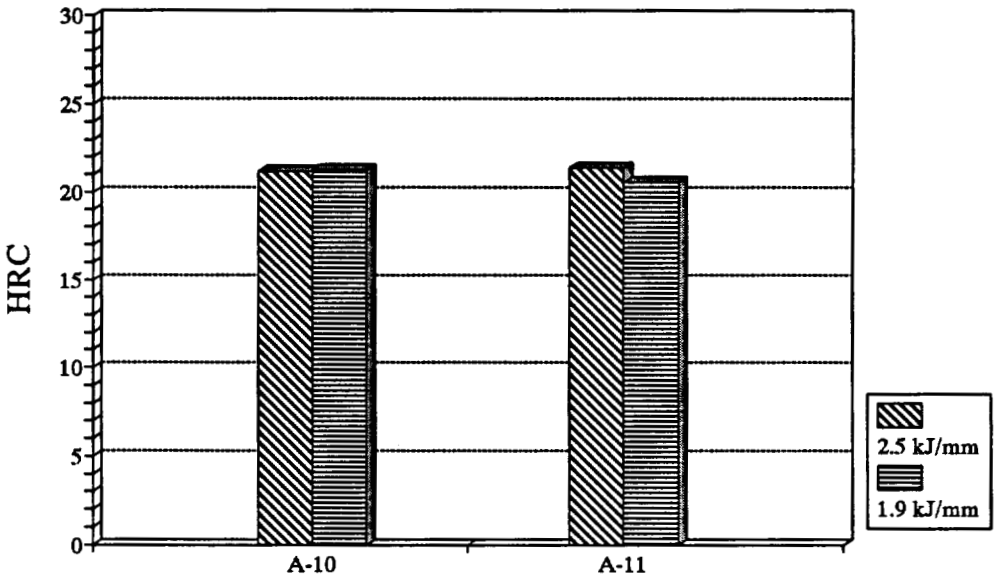

Figure 33: Comparison hardness values for the GMA weld metal of Alloys 10 and 11 deposited at 2.5 kJ/mm (64 kJ/in.) and 1.8 kJ/mm (48 kJ/in.) heat input with Ar-5%CO_2 shielding gas on HSLA-100 base plate .

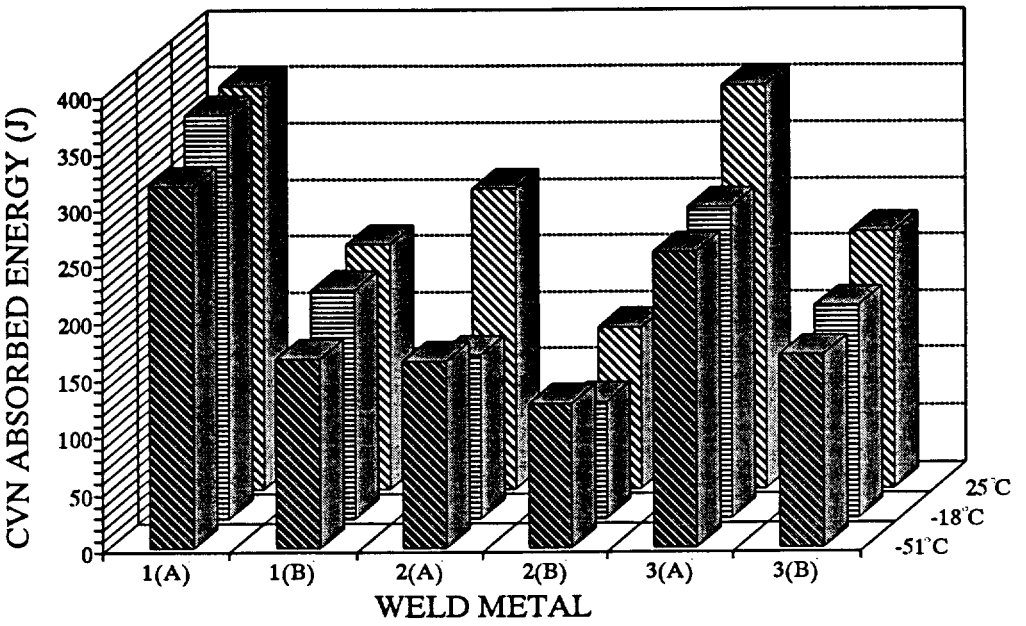

(a) Alloys 1-3

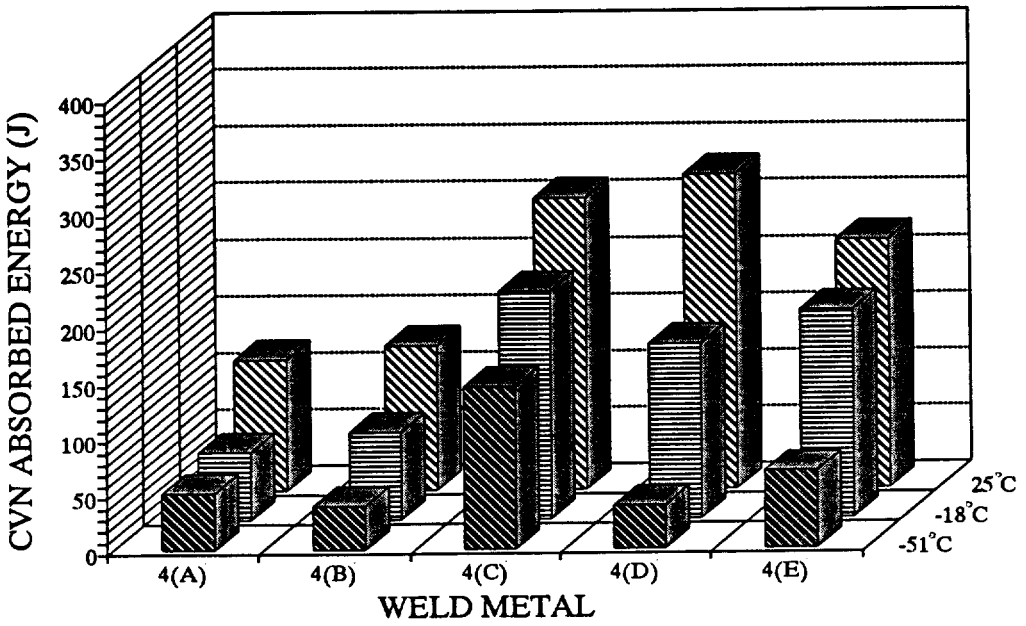

(b) Alloy 4

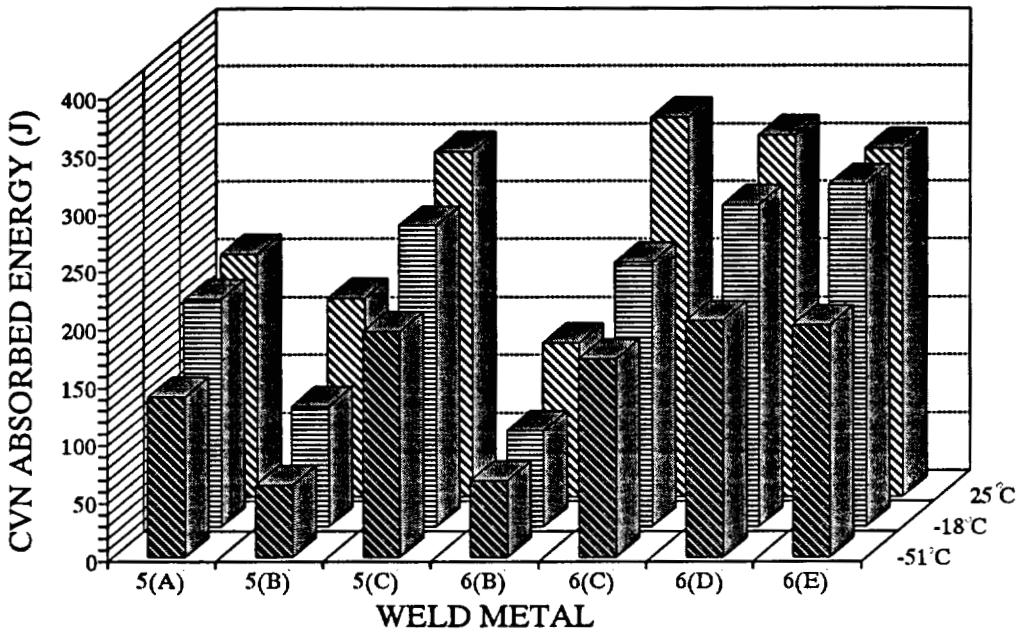

(c) Alloys 5 and 6

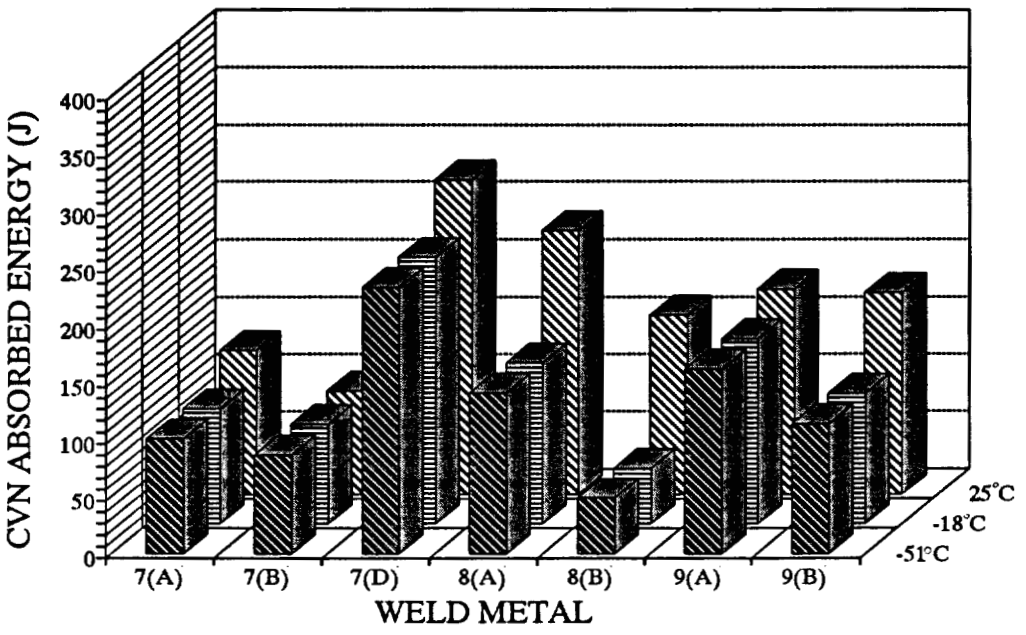

(d) Alloys 7-9

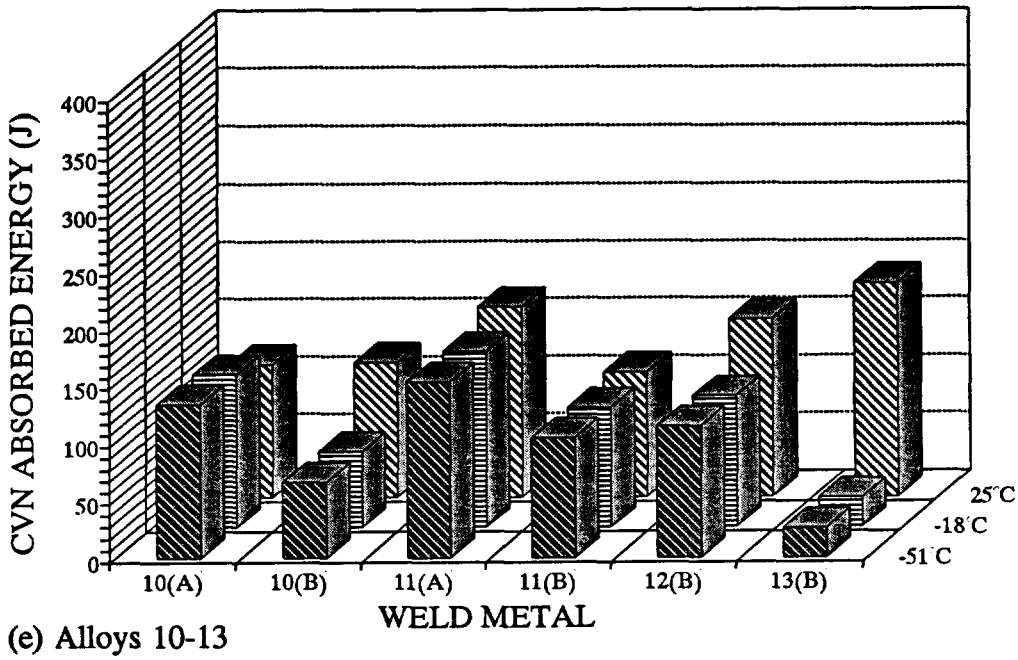

(e) Alloys 10-13

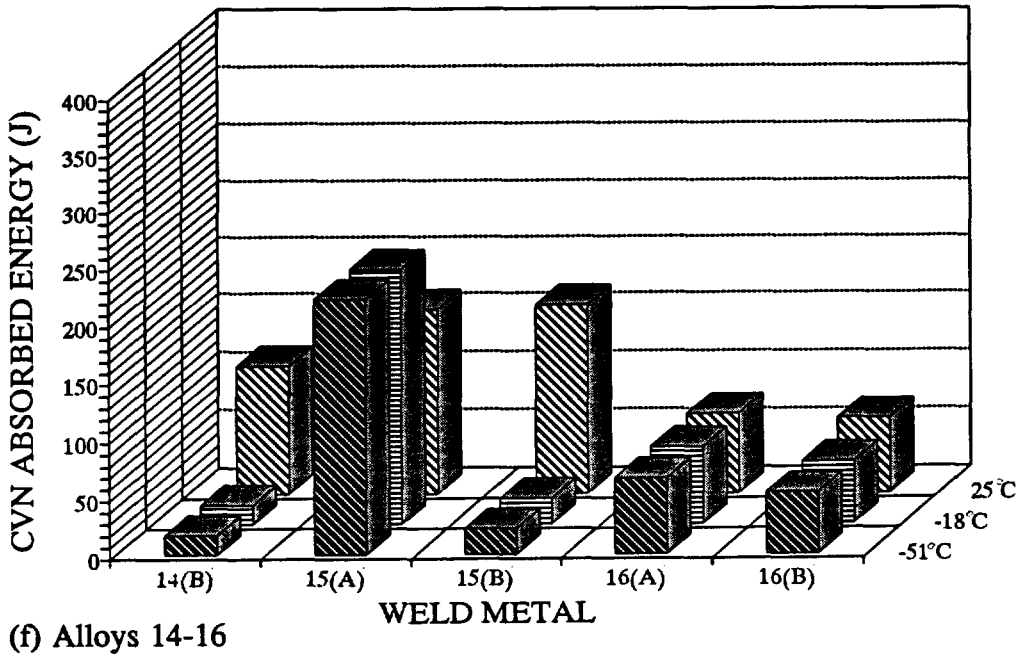

(f) Alloys 14-16

Figure 34: CVN toughness values of the GTA weld metal deposited at 3.5 kJ/mm (90 kJ/in.) 2 kJ/mm (51 kJ/in.) with Ar-5%CO_2 shielding gas on matching base plates. (A) 2 kJ/mm, Ar-5%CO_2. (B) 3.5 kJ/mm, Ar-5%CO_2. (C) 3.2 kJ/mm, Ar. (D) 3.5 kJ/mm, Ar-25%He. (E) 3.2 kJ/mm, Ar-25%He.

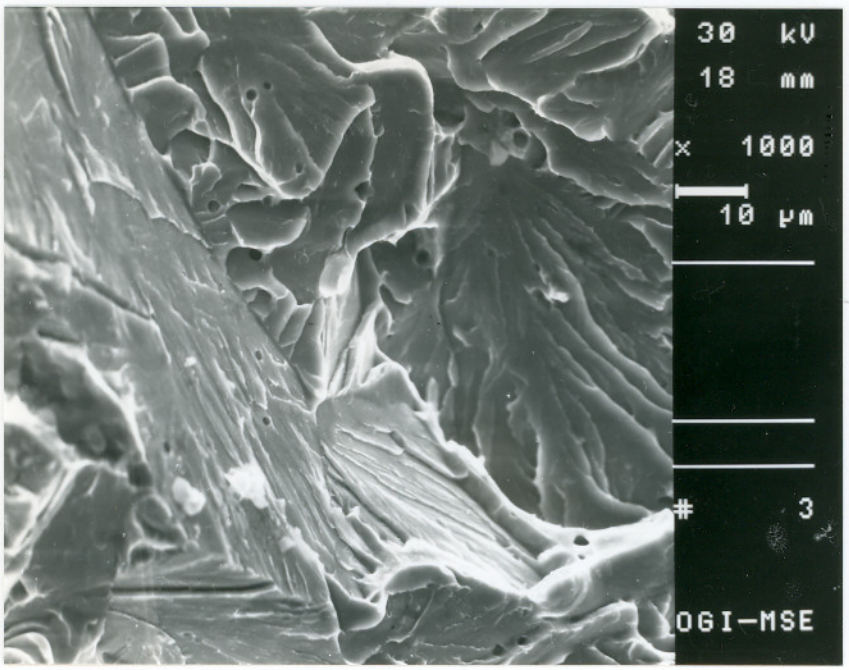

(a) Ar-5%CO_2 shielding gas

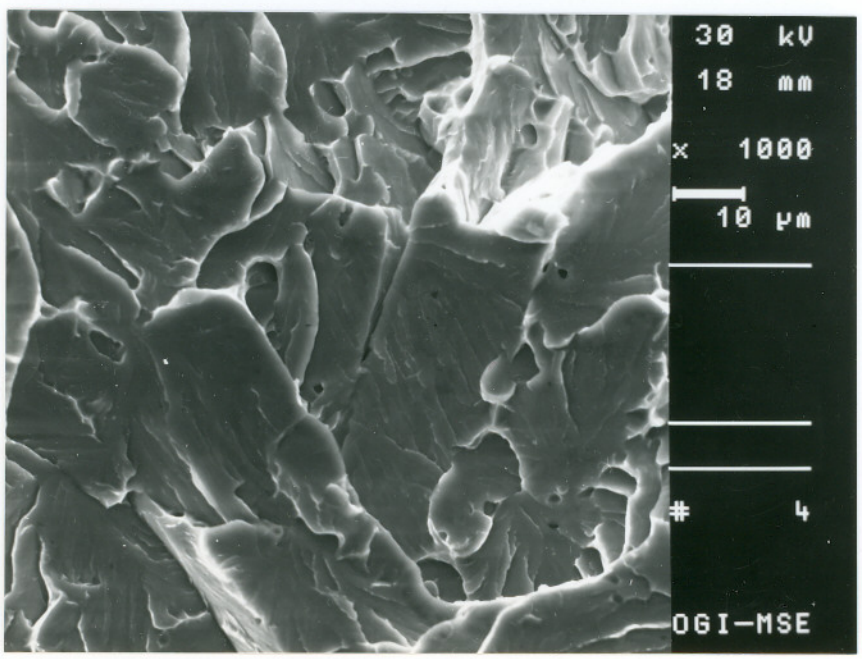

(b) Ar-25%He shielding gas

Figure 35: SEM fractographs of the broken CVN samples of GTA weld metal of Alloy 4 deposited at 3.5 kJ/mm (90 kJ/in.) heat input on matching base plate and tested at -51°C (-60°F). (a)With Ar-5%CO_2 shielding gas and (b) with Ar-25%He shielding gas.

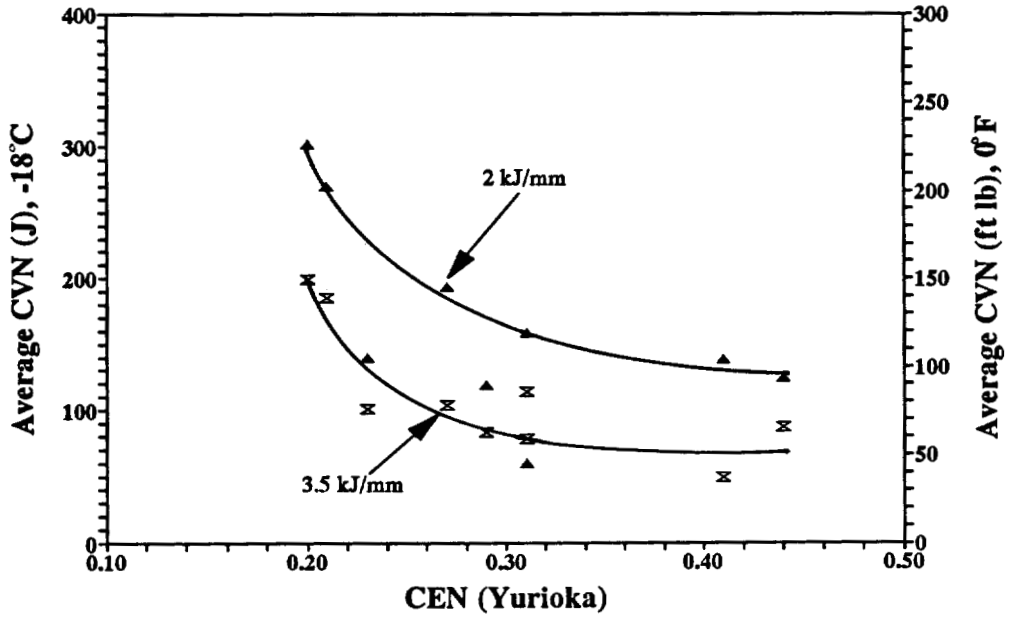

(a)

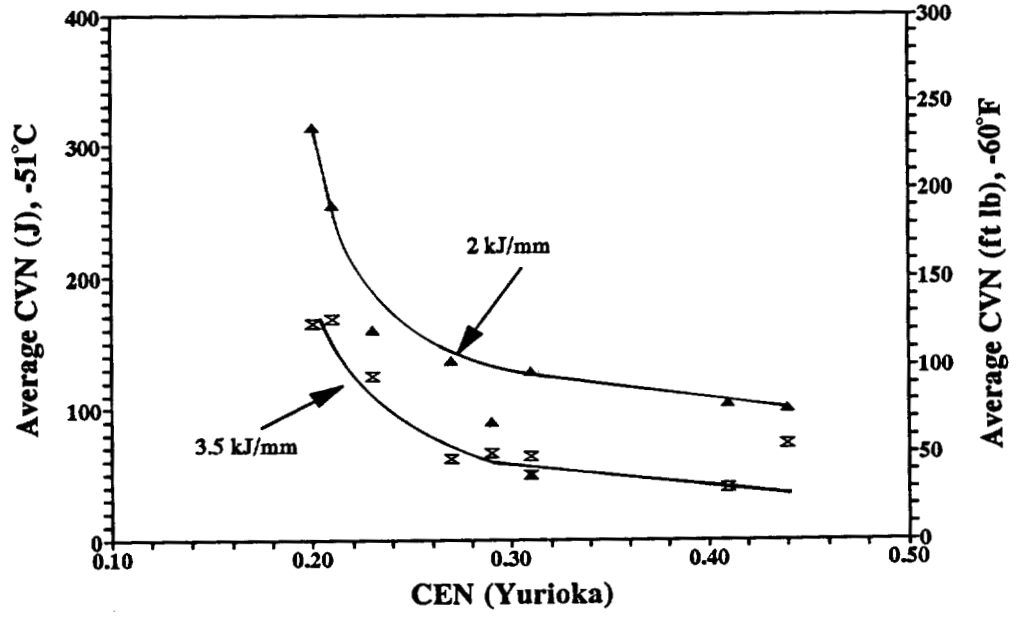

(b)

Figure 36: Variation of the average CVN absorbed energy values of the GTA weld metal, deposited on matching base plate with Ar-5%CO_2 shielding gas at 3.5 kJ/mm (90 kJ/in.) and 2 kJ/mm (51 kJ/in.) heat input with Yurioka's CEN values; (a) at -18°C (0°F) and (b) at -51°C (-60°F).

(a)

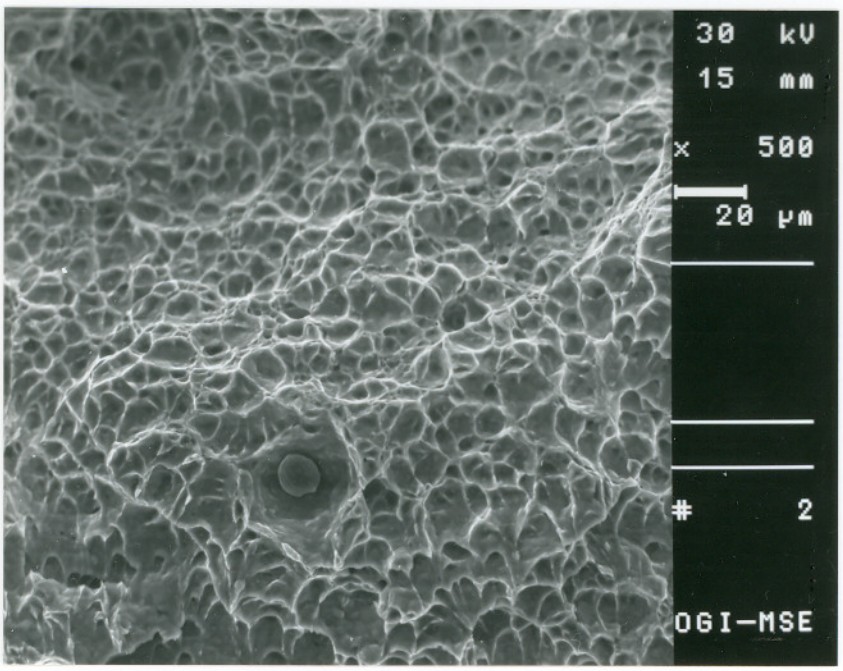

(b)

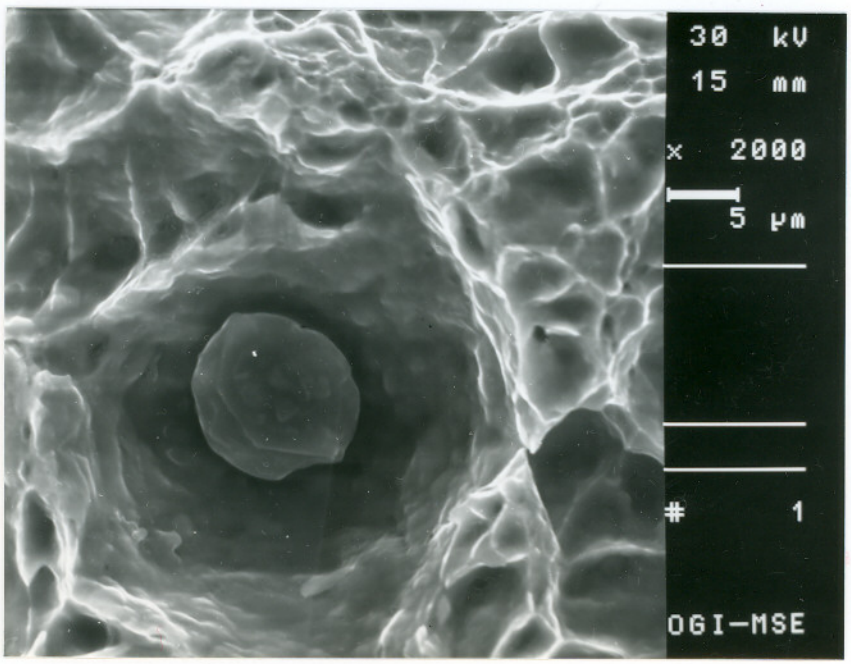

Figure 37: SEM fractographs of the broken CVN samples of GTA weld metal of Alloy 7 deposited at 3.5 kJ/mm (90 kJ/in.) heat input on matching base plate with Ar-5%CO_2 shielding gas and tested at -51°C (-60°F).

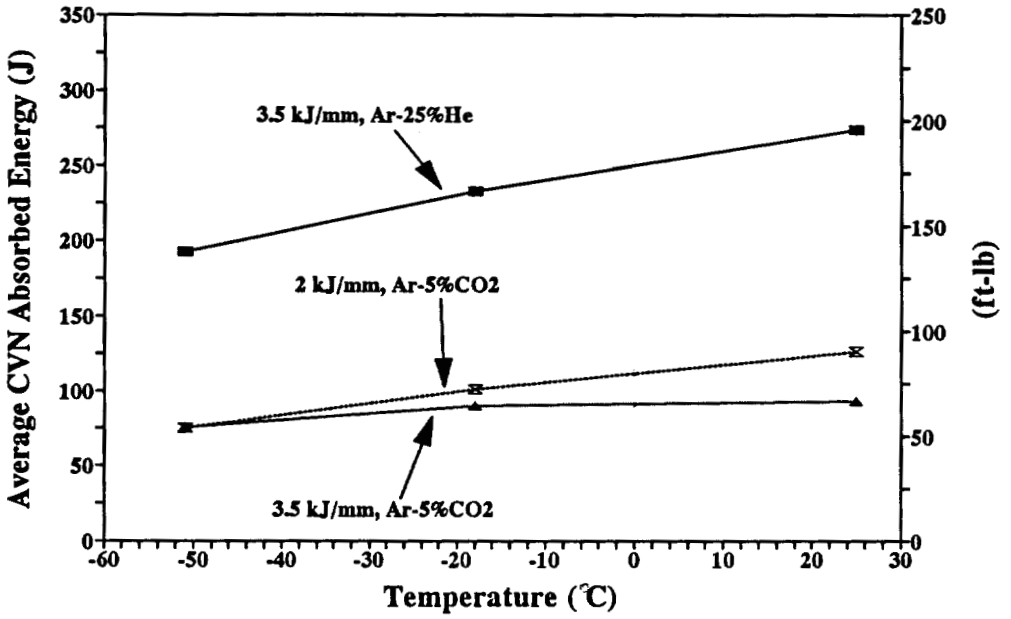

Figure 38: Comparison of CVN absorbed energy values of GTA weld metal of Alloy 7 deposited at 2 kJ/mm (51 kJ/in.) and 3.5 kJ/mm (90 kJ/in.) heat input with Ar-5%CO_2 shielding gas and 3.5 kJ/mm (90 kJ/in.) heat input with Ar-25%He shielding gas on matching base plate.

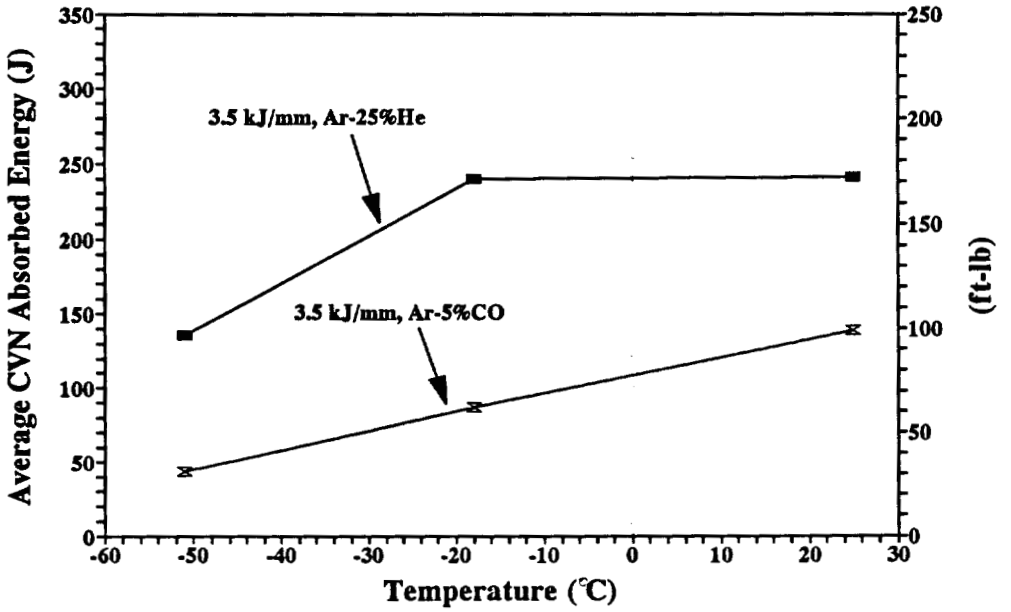

Figure 39: Comparison of CVN absorbed energy values of GTA weld metal of Alloy 7 deposited on HSLA-100 base plate at 3.5 kJ/mm (90 kJ/in.) heat input with Ar-5%CO_2 and Ar-25%He shielding gases.

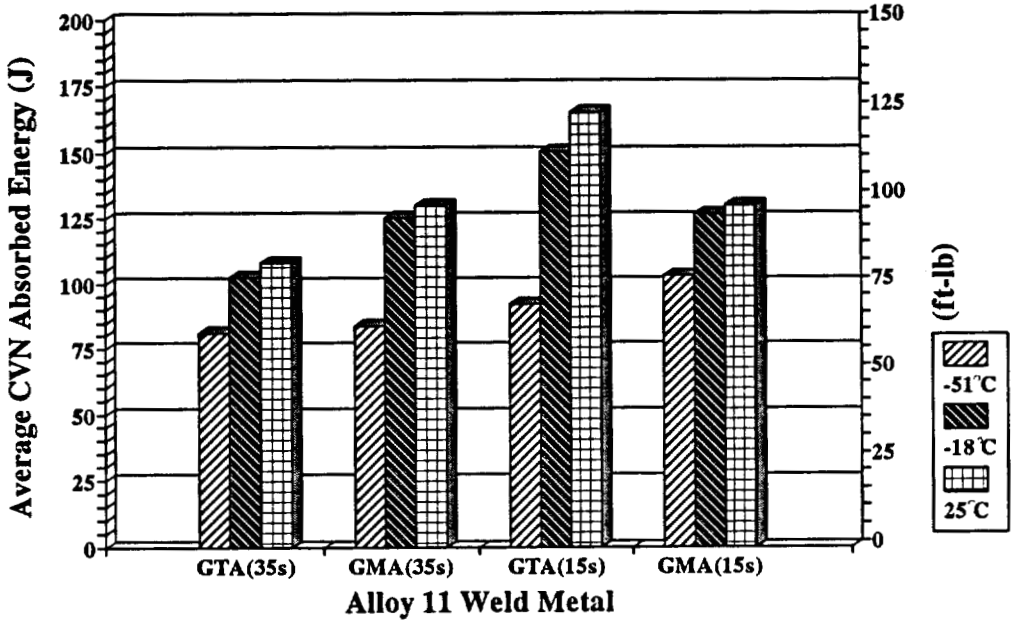

Figure 40: Comparison of CVN absorbed energy values of GTA and GMA weld metal of Alloy 11 with identical cooling rates deposited with Ar-5%CO_2 shielding gas.

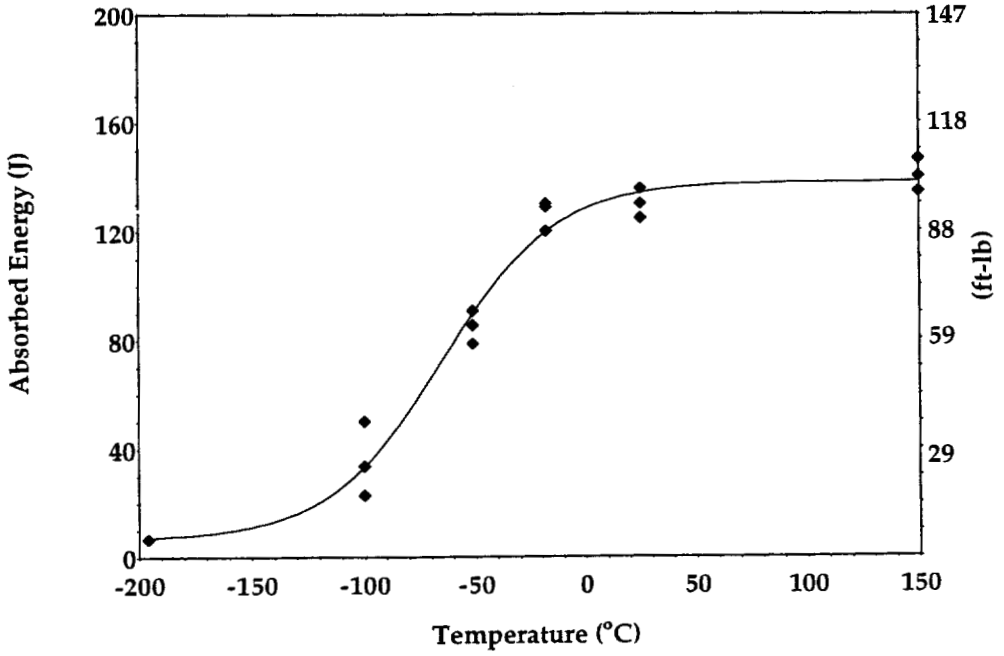

Figure 41: Ductile to brittle transition curve for the GMA weld metal of Alloy 11 deposited at 2.5 kJ/mm (64 kJ/in.) heat input with Ar-5%CO_2 shielding gas on HSLA-100 base plate.

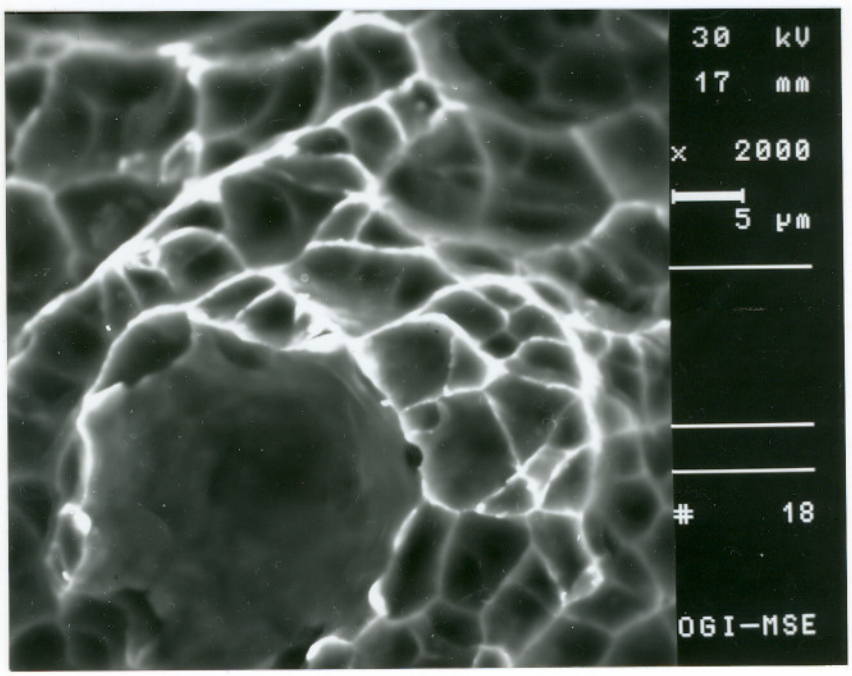

Figure 42: SEM fractograph of the CVN samples of GMA weld metal of Alloy 11 deposited at 2.5 kJ/mm (64 kJ/in.) heat input with Ar-5%CO_2 shielding gas on HSLA-100 base plate, tested at -18°C (0°F).

(a)

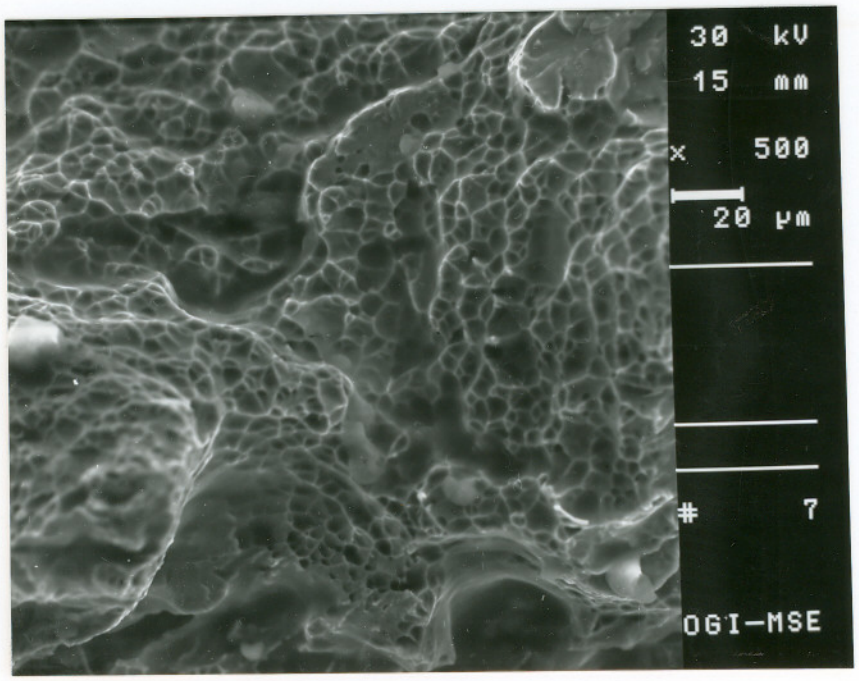

(b)

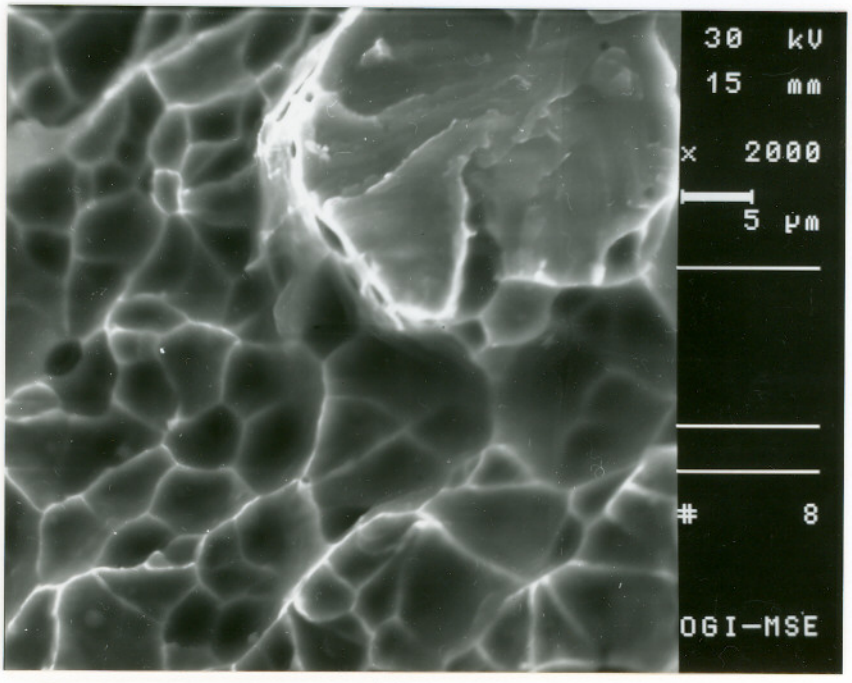

Figure 43: SEM fractographs of the CVN samples of GMA weld metal of Alloy 11 deposited at 2.5 kJ/mm (64 kJ/in.) heat input with Ar-5%CO_2 shielding gas on HSLA-100 base plate, tested at -51°C (-60°F).

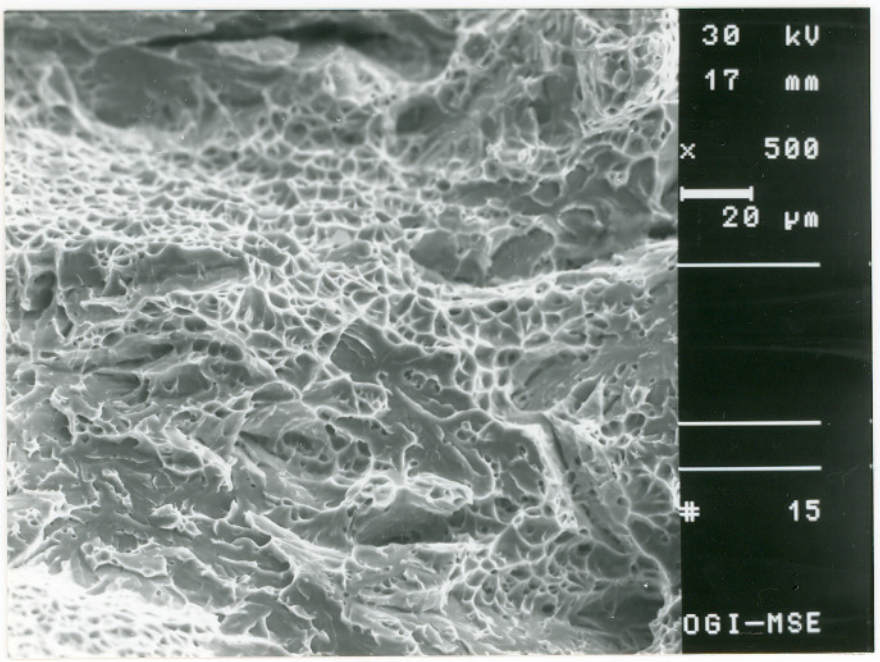

(a)

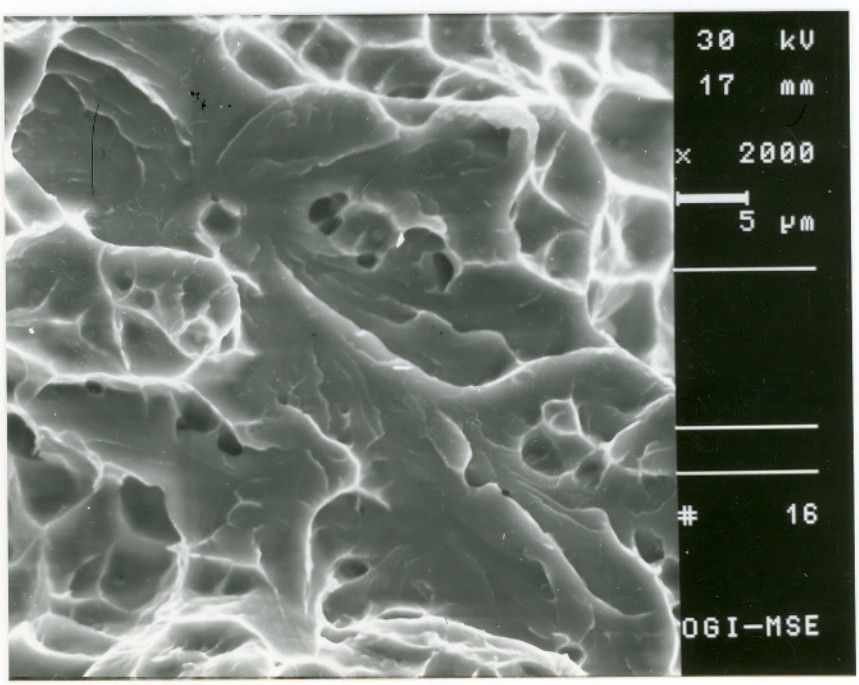

(b)

Figure 44: SEM fractographs of the CVN samples of GMA weld metal of Alloy 11 deposited at 2.5 kJ/mm (64 kJ/in.) heat input with Ar-5%CO_2 shielding gas on HSLA-100 base plate, tested at -100°C (-148°F).

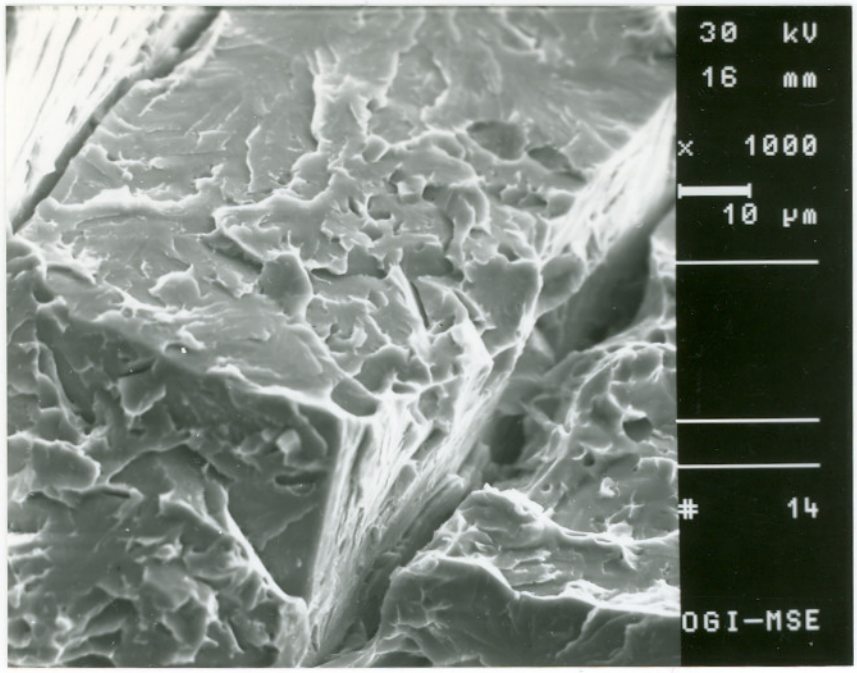

Figure 45: SEM fractograph of the CVN samples of GMA weld metal of Alloy 11 deposited at 2.5 kJ/mm (64 kJ/in.) heat input with Ar-5%CO_2 shielding gas on HSLA-100 base plate, tested at -189°C (-372°F).

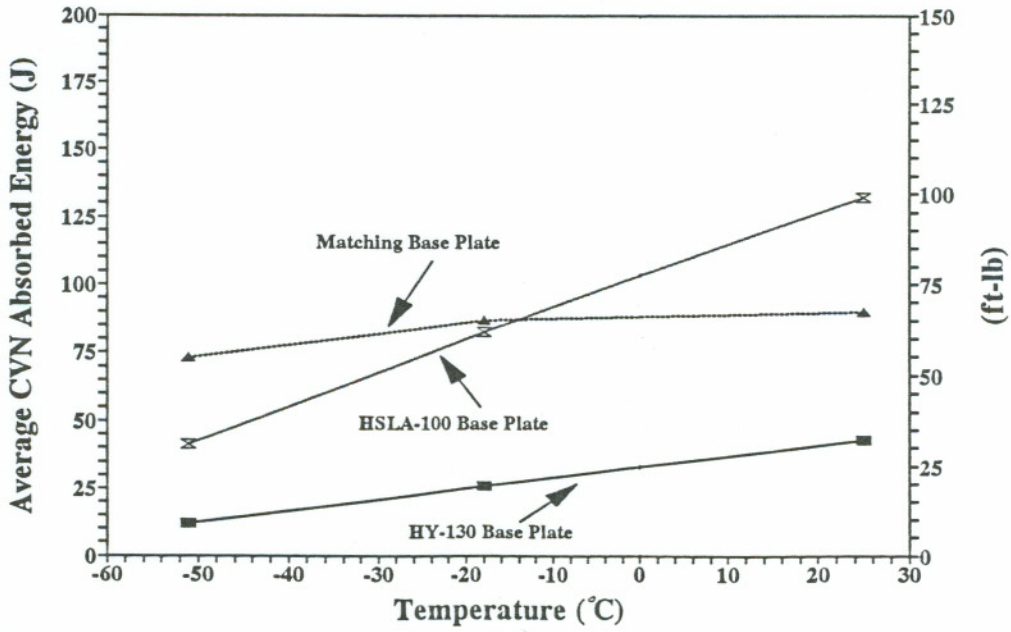

Figure 46: Comparison of CVN absorbed energy values of GTA weld metal of Alloy 7 deposited at 3.5 kJ/mm (90 kJ/in.) heat input with Ar-5%CO_2 shielding gas on HSLA-100, HY-130 and matching base plates.

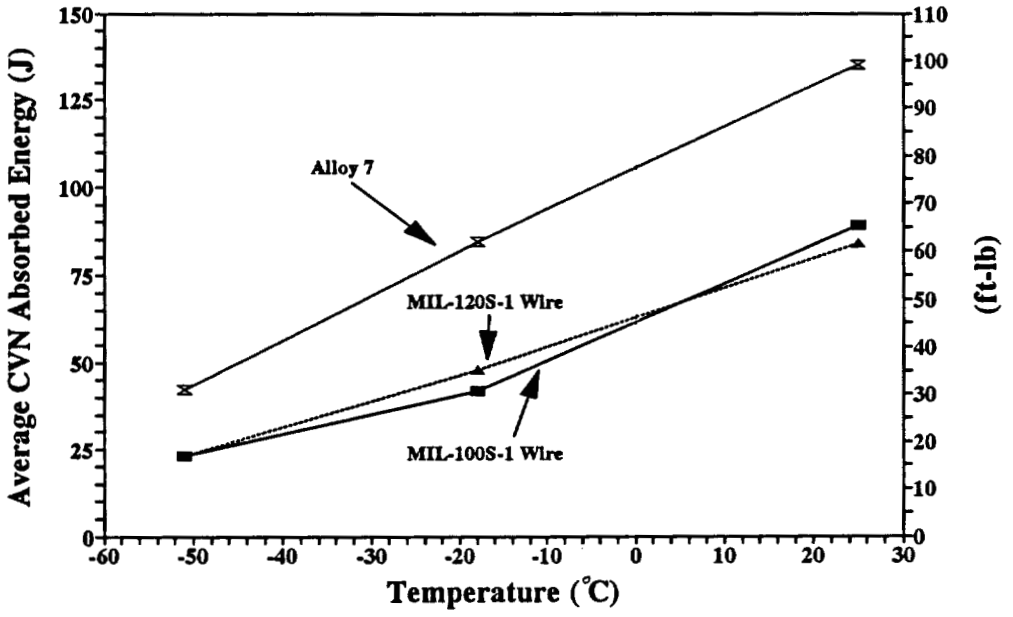

Figure 47: Comparison of CVN absorbed energy values of GTA weld metal of Alloy 7 with that of MIL-100S-1 and MIL-120S-1 type commercial wires deposited at 3.5 kJ/mm (90 kJ/in.) heat input with Ar-5%CO_2 shielding gas on HSLA-100 base plate.

(a)

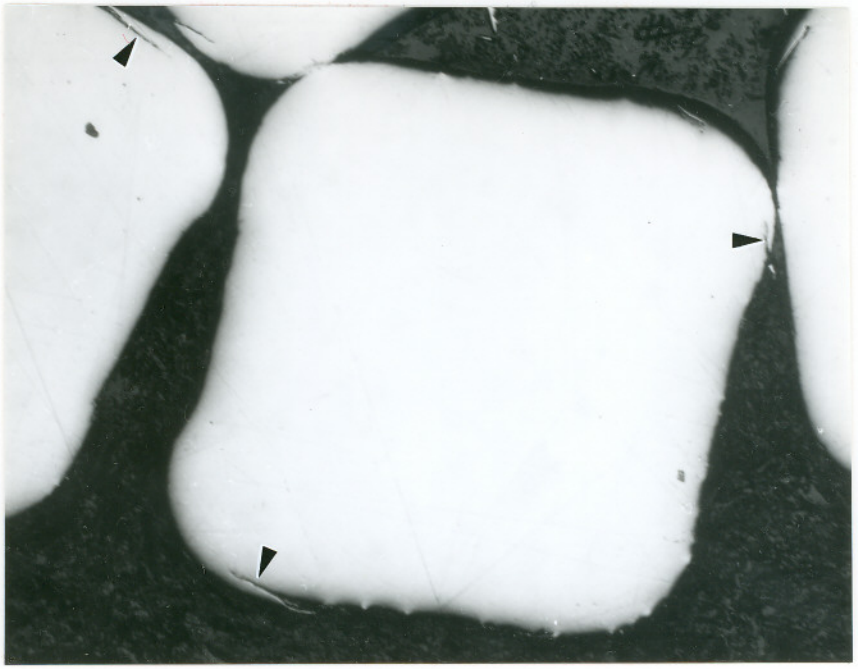

(b)

Figure 48: Optical micrographs of a plane polished unetched sample of the Alloy 7 wire, showing the cavities where wire drawing lubricant is trapped. Arrows indicate the cavities.

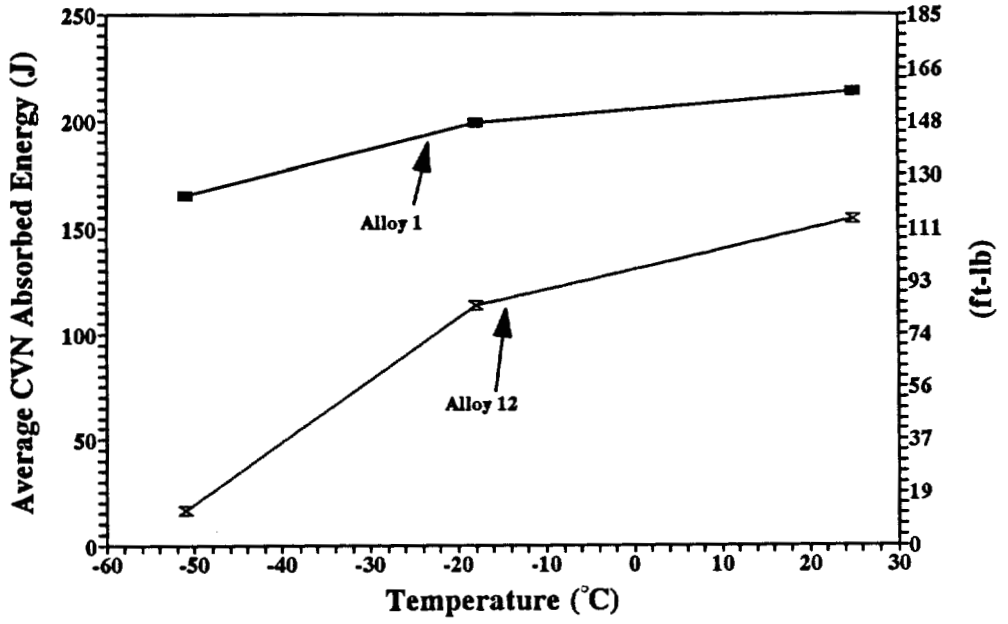

(a)

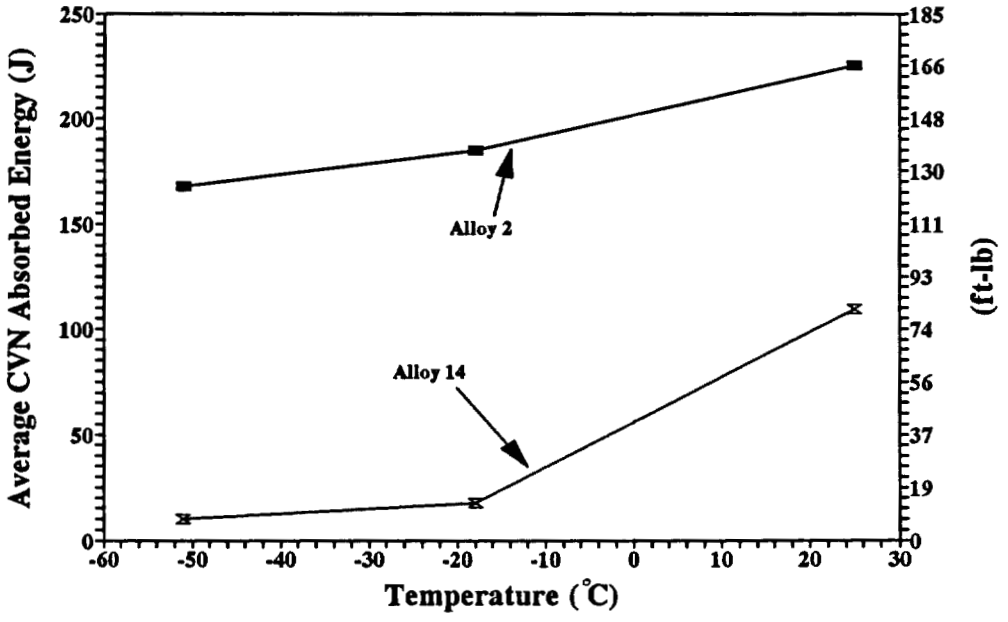

(b)

Figure 49: Comparison of CVN absorbed energy values of GTA weld metal of (a) Alloy 1 with that of Alloy 12 and (b) Alloy 2 with that of Alloy 14 deposited at 3.5 kJ/mm (90 kJ/in.) heat input with Ar-5%CO_2 shielding gas on matching base plate. Showing the deleterious effect of excessive boron on CVN toughness.

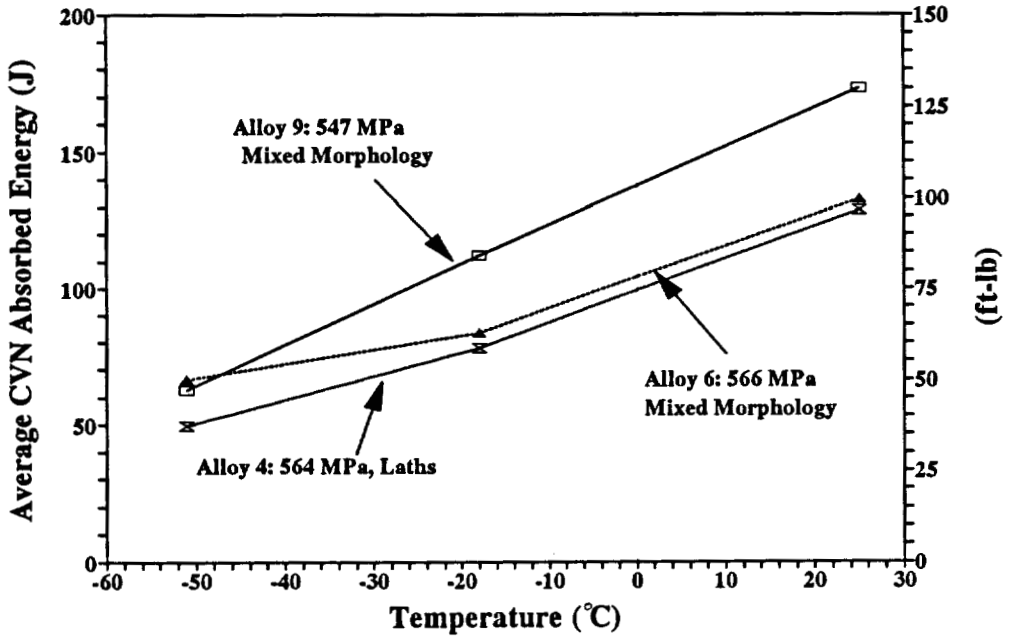

Figure 50: Comparison of CVN absorbed energy values of GTA weld metal of Alloys 4, 6 and 9 deposited at 3.5 kJ/mm (90 kJ/in.) heat input with Ar-5%CO_2 shielding gas on matching base plate. Showing that laths did not have an effect on toughness.

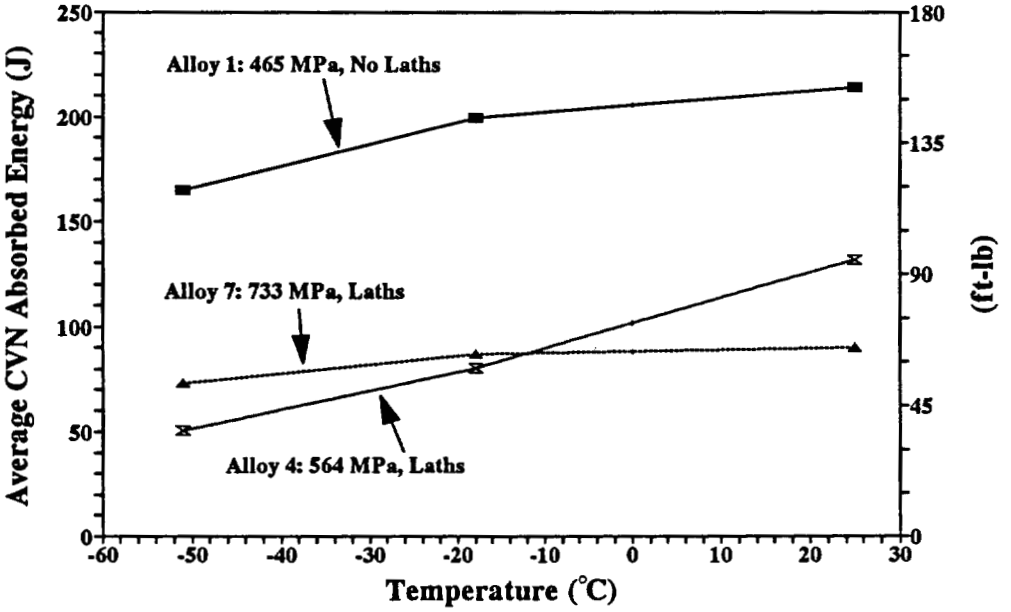

Figure 51: Comparison of CVN absorbed energy values of GTA weld metal of Alloys 1, 4 and 7 deposited at 3.5 kJ/mm (90 kJ/in.) heat input with Ar-5%CO_2 shielding gas on matching base plate. Showing that laths did not have an effect on toughness.

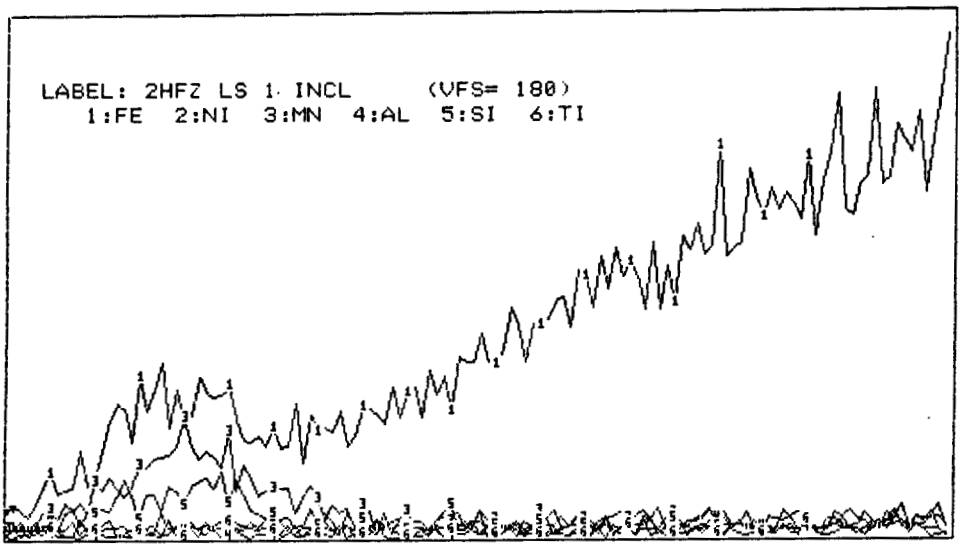

Figure 52: Results of the EDAX analysis of an inclusion in the GTA weld metal of Alloy 7 deposited at 3.5 kJ/in (90 kJ/in.) heat input with Ar-5%CO_2 shielding gas on matching base plate.

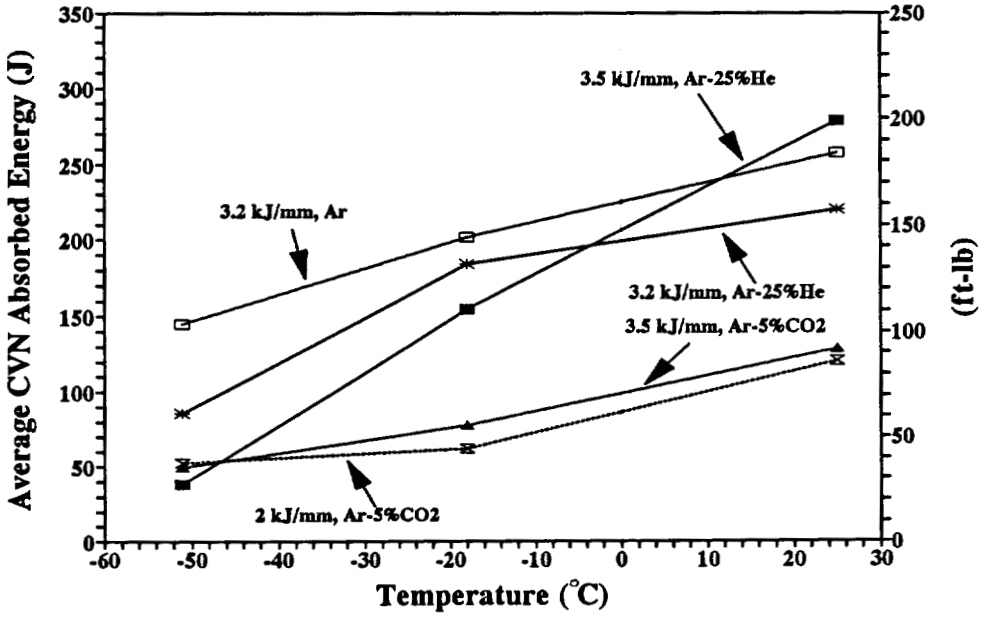

Figure 53: Comparison of CVN absorbed energy values of GTA weld metal of Alloy 4 deposited on matching base plate at 3.5 kJ/mm (90 kJ/in.) and 2 kJ/mm (51 kJ/in.) heat input with Ar-5%CO_2 shielding gas, at 3.2 kJ/mm (82 kJ/in.) with Ar and Ar-25%He shielding gas and at 3.5 kJ/mm (90 kJ/in.) heat input with Ar-25%He shielding gas.

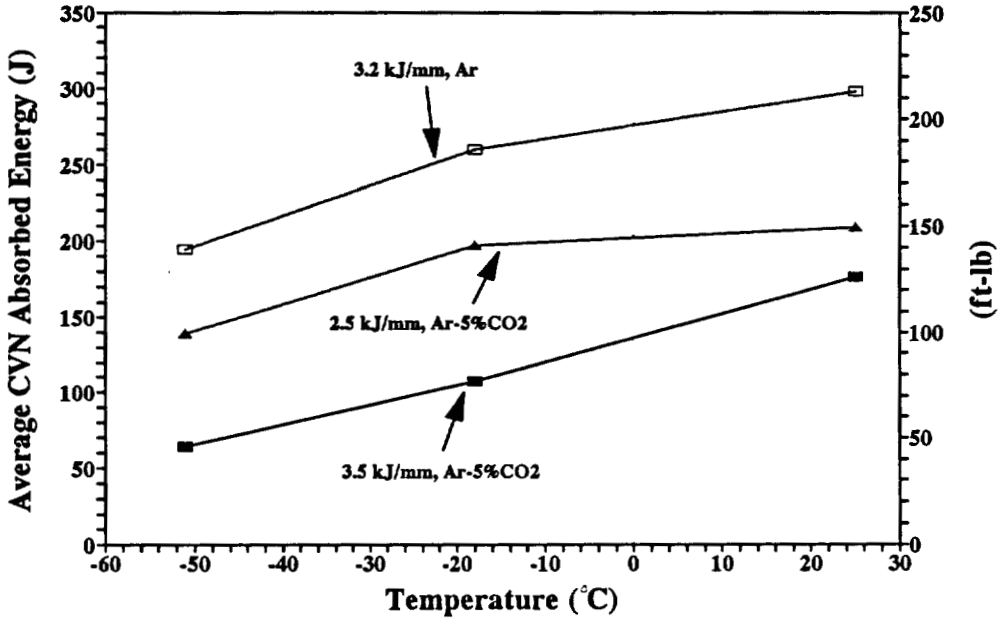

Figure 54: Comparison of CVN absorbed energy values of GTA weld metal of Alloy 5 deposited on matching base plate at 3.5 kJ/mm (90 kJ/in.) and 2 kJ/mm (51 kJ/in.) heat input with Ar-5%CO_2 shielding gas and at 3.2 kJ/mm (82 kJ/in.) with Ar shielding gas.

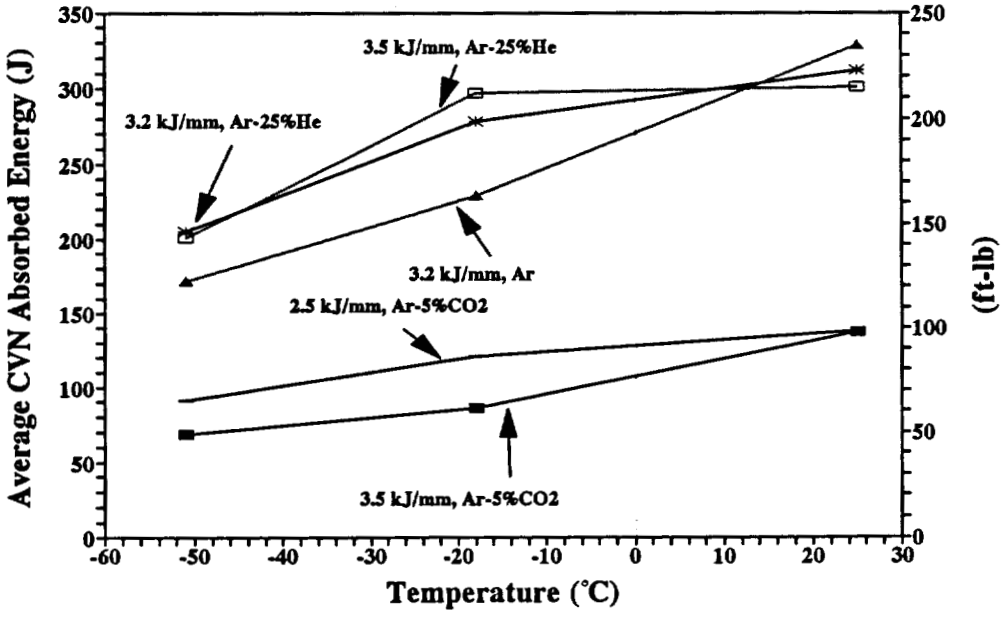

Figure 55: Comparison of CVN absorbed energy values of GTA weld metal of Alloy 6 deposited on matching base plate at 3.5 kJ/mm (90 kJ/in.) and 2 kJ/mm (51 kJ/in.) heat input with Ar-5%CO_2 shielding gas, at 3.2 kJ/mm (82 kJ/in.) with Ar and Ar-25%He shielding gas and at 3.5 kJ/mm (90 kJ/in.) heat input with Ar-25%He shielding gas.

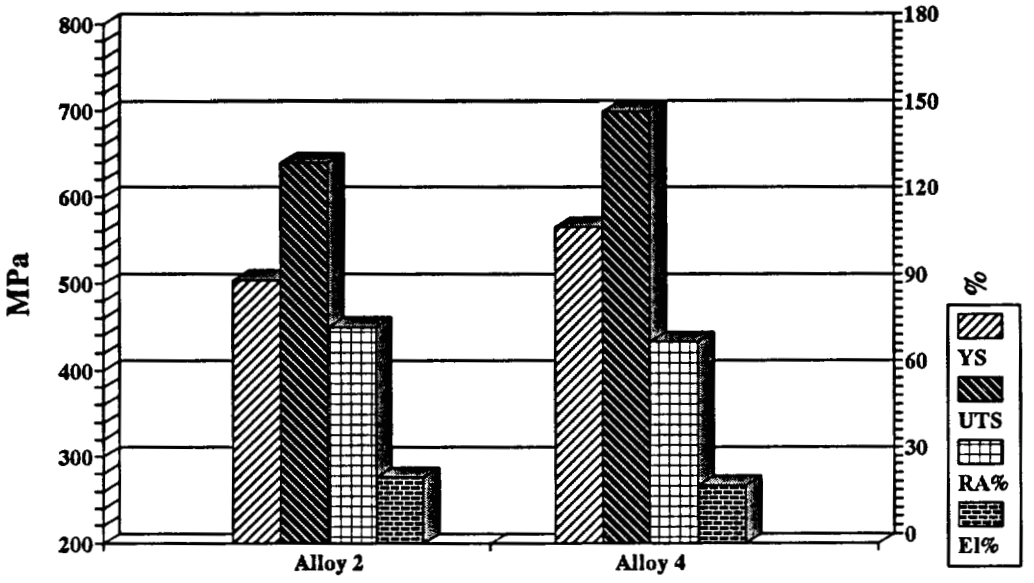

(a)

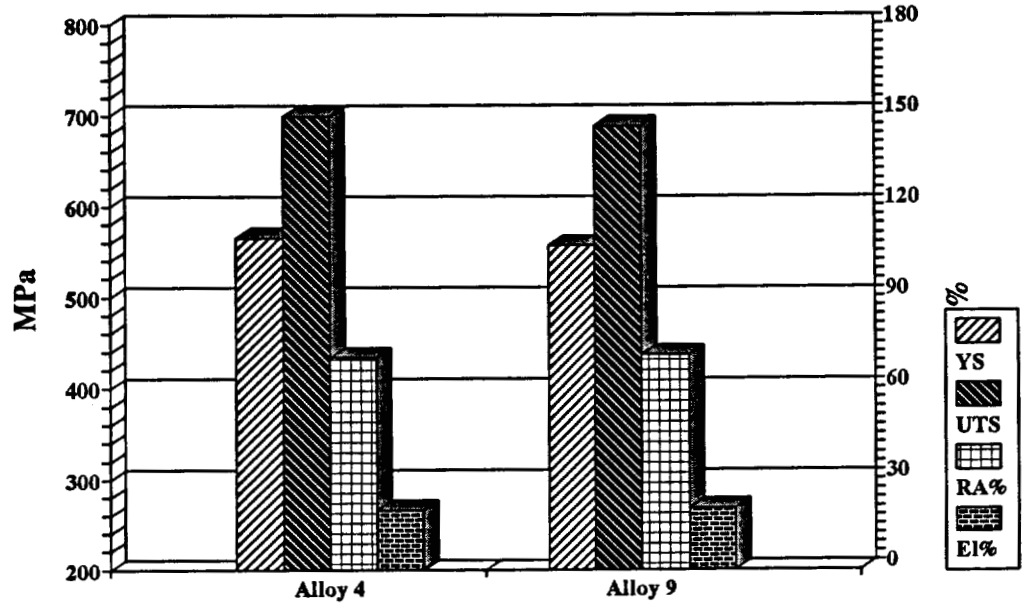

(b)

Figure 56: Comparison of the yield strengths of GTA weld metal deposited at 3.5 kJ/mm (90 kJ/in.) heat input with Ar-5%CO_2 shielding gas on matching base plate (a) Alloy 2 with that of 4, and (b) Alloy 4 with that of 9,. Showing the effect of carbon.

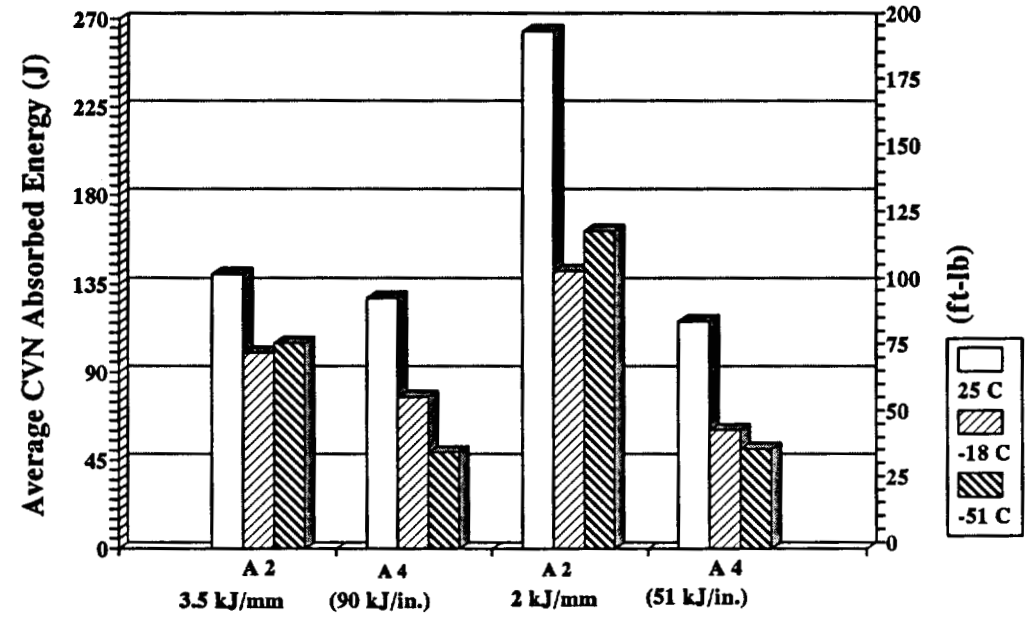

(a)

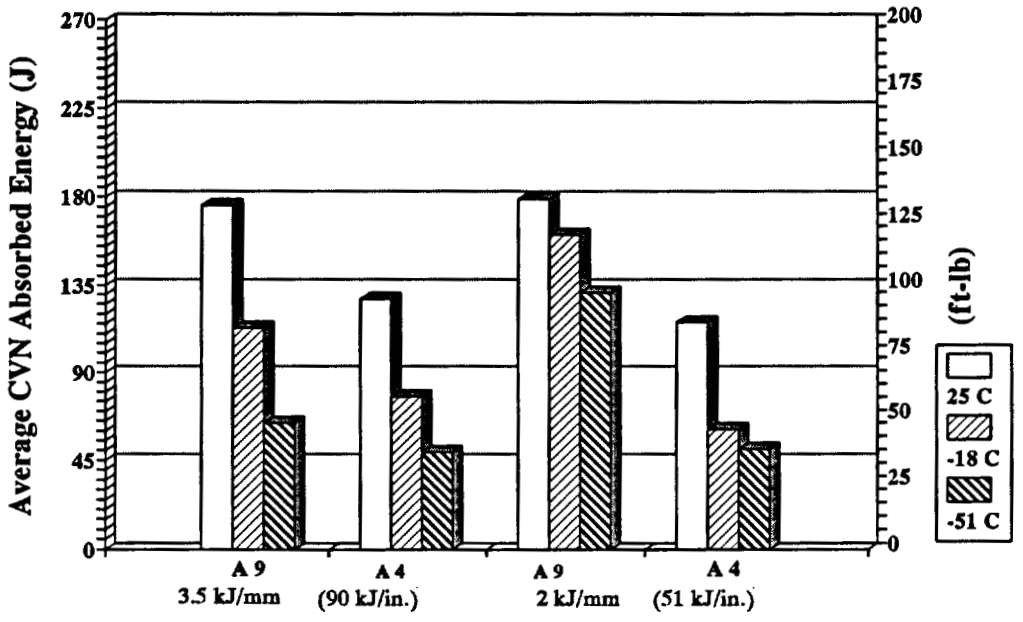

(b)

Figure 57: Comparison of the CVN absorbed energy values of GTA weld metal deposited at 3.5 kJ/mm (90 kJ/in.) heat input with Ar-5%CO_2 shielding gas on matching base plate (a) Alloys 2 and 4, and (b) Alloys 4 and 9. Showing the effect of carbon

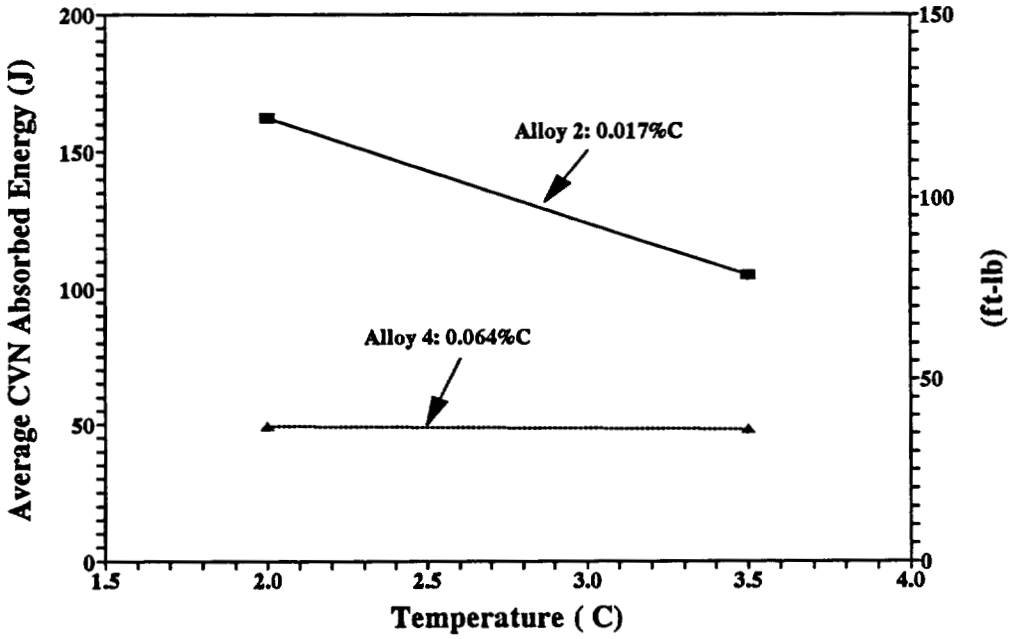

Figure 58: Effect of heat input on the CVN absorbed energy values of GTA weld metal of Alloys 2 with low carbon and Alloy 4 with high carbon deposited on matching base plate with Ar-5%CO_2 shielding gas.

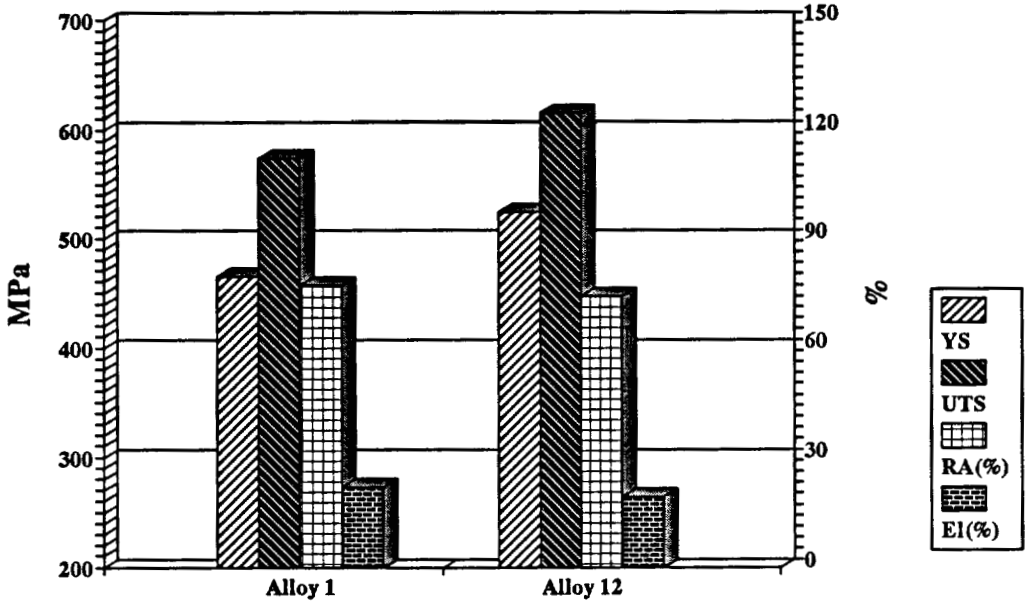

(a)

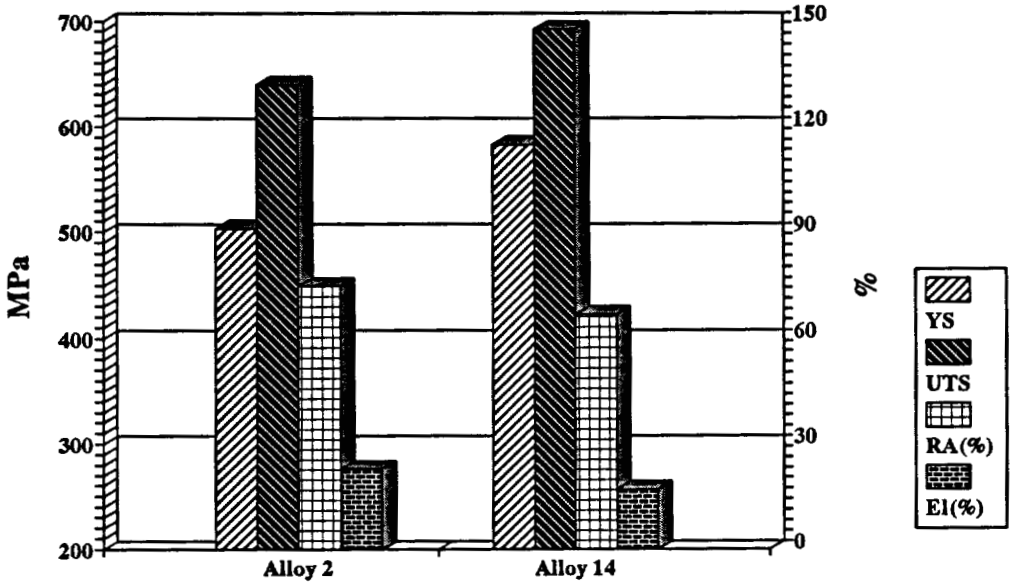

(b)

Figure 59: Comparison of the yield strengths of GTA weld metal deposited at 3.5 kJ/mm (90 kJ/in.) heat input with Ar-5%CO_2 shielding gas on matching base plate (a) Alloy 1 with that of 12, and Alloy 2 with that of 14. Showing the effect of boron.

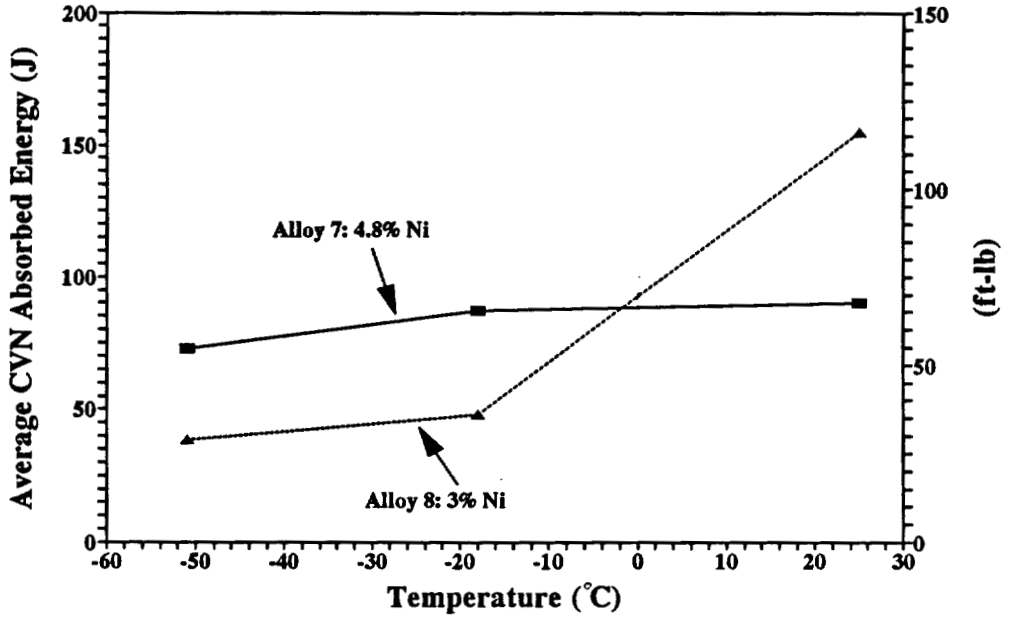

(a)

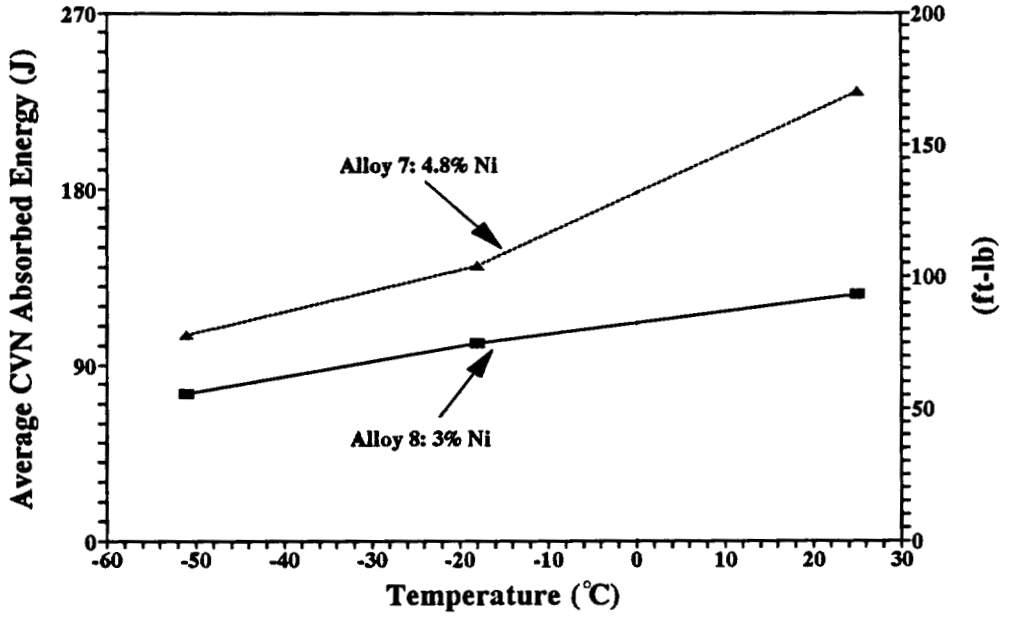

(b)

Figure 60: Comparison of the CVN absorbed energy values of GTA weld metal of Alloys 7 and 8 deposited with Ar-5%CO_2 shielding gas on matching base plate at (a) 3.5 kJ/mm (90 kJ/in.) and (b) 2 kJ/mm (51 kJ/in.)heat input. Showing the effect of Ni on toughness.

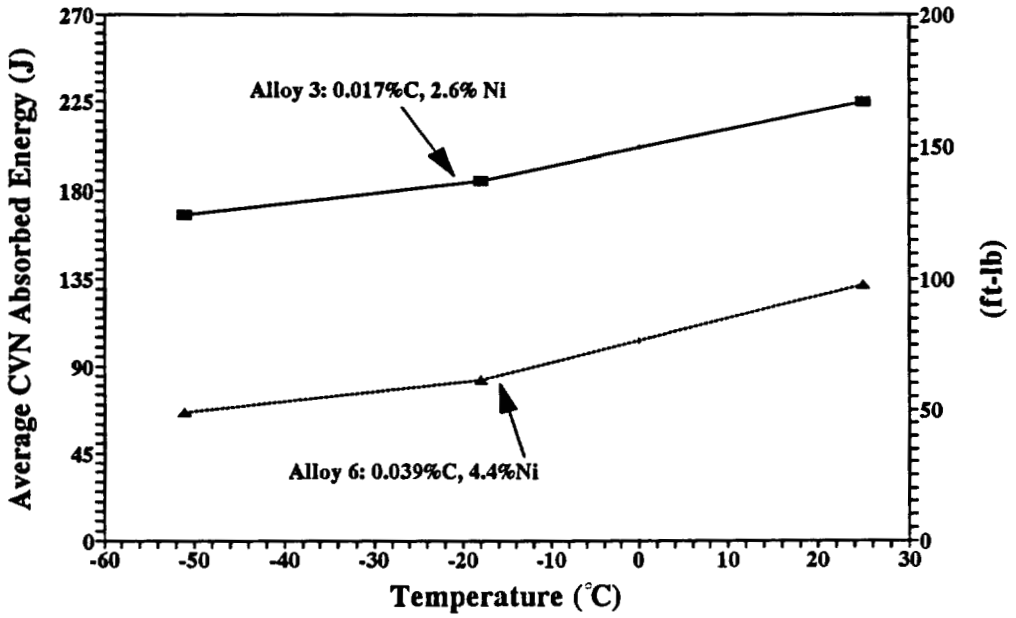

Figure 61: Comparison of the CVN absorbed energy values of GTA weld metal of Alloys 3 and 6 deposited at 3.5 kJ/mm (90 kJ/in.) heat input with Ar-5%CO_2 shielding gas on matching base plate. Showing the combined effect of Ni and C on toughness.

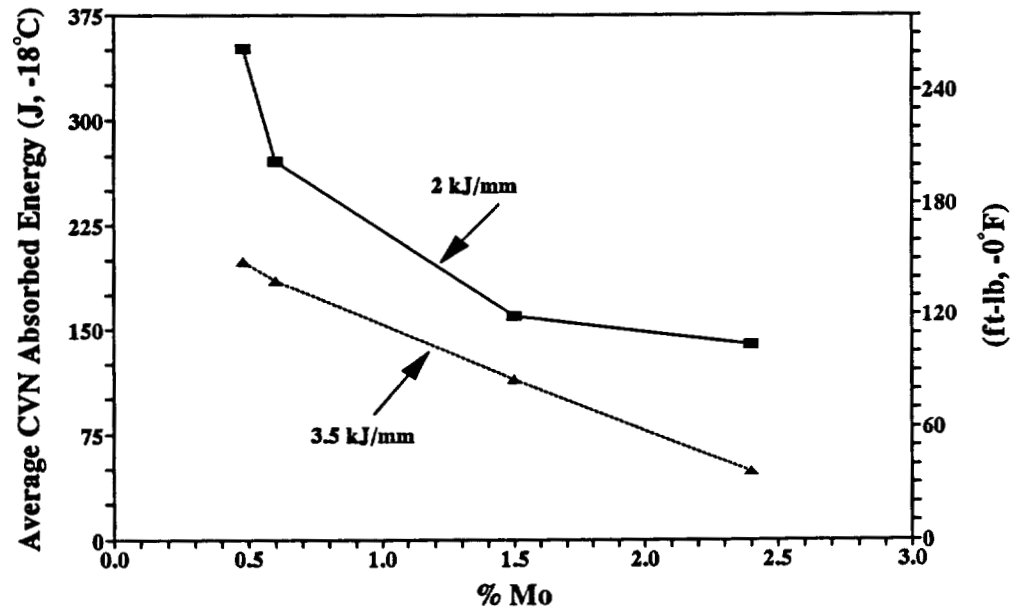

Figure 62: Comparison of the CVN absorbed energy values of GTA weld metal of Alloys 1, 3, 8 and 9 deposited at 3.5 kJ/mm (90 kJ/in.) heat input with Ar-5%CO_2 shielding gas on matching base plate. Showing the effect of Mo on toughness.

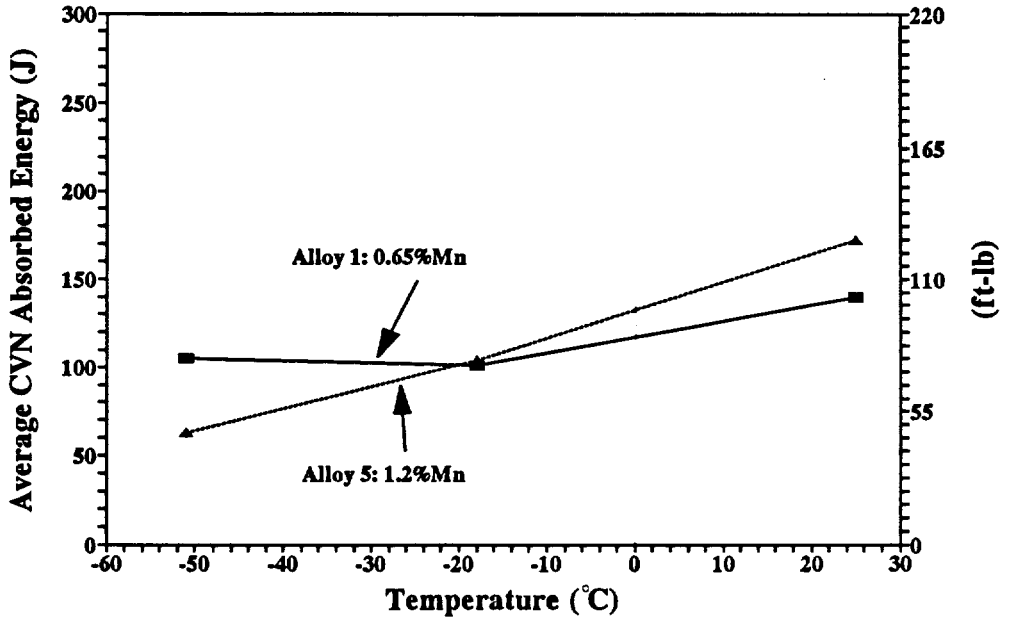

(a)

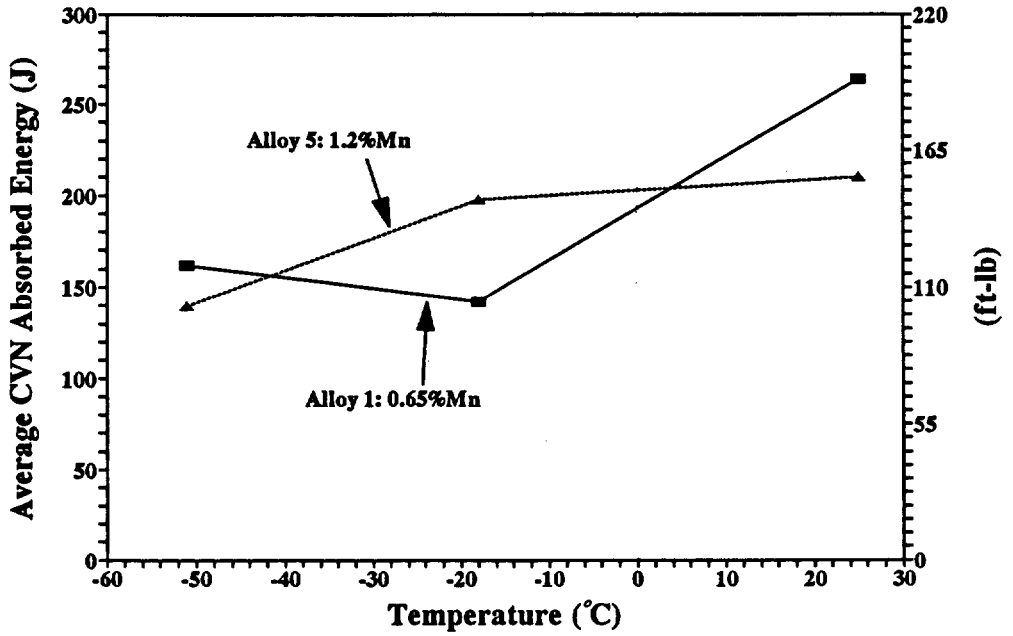

(b)

Figure 63: Comparison of the CVN absorbed energy values of GTA weld metal of Alloy 1 with those of Alloy 5 deposited on matching base plate with Ar-5%CO_2 shielding gas at (a) 3.5 kJ/mm (90 kJ/in.) and (b) 2 kJ/mm (51 kJ/in.)heat input. Showing the effect of Mn on toughness.

Appendix I:

Hardness Values of GTA Weld Metal of Alloys 4-7 Deposited on Matching Base Plates at 3.2 kJ/mm (82 kJ/in.) and 3.5 kJ/mm (90 kJ/in.) Heat Input with Ar and Ar-25%He Shielding Gases.

ALLOY	SHIELDING GAS	HEAT INPUT kJ/in (kJ/mm)	HARDNESS	AVERAGE
4	Ar	3.2 (82)	94, 92, 93.5, 93, 95, 94.5	93.7 (HRB)
4	Ar-25%He	3.2 (82)	92.5, 94, 93, 92, 91, 93	92.6 (HRB)
4	Ar-25%He	3.5 (90)	95, 93, 91.5, 90, 91, 94.5	92.5 (HRB)
5	Ar	3.2 (82)	86, 89, 89.5, 89, 89, 87	88.25 (HRB)
6	Ar	3.2 (82)	96, 95, 96.5, 94, 95, 95, 95, 93	94.9 (HRB)
6	Ar-25%He	3.2 (82)	95, 94, 93.5, 96.5, 95, 96, 95	95 (HRB)
6	Ar-25%He	3.5 (90)	90, 95, 91, 93, 92, 93.5, 92.5	92.4 (HRB)
7	Ar	3.2 (82)	21, 21, 21, 21.5, 20, 22.5, 22	21.3 (HRC)
7	Ar-25%He	3.2 (82)	22, 23, 21.5, 21, 20.5, 21, 21, 20.5	21.3 (HRC)
7	Ar-25%He	3.5 (90)	21.5, 22, 22.5, 23, 21.5	22.1 (HRC)

Appendix II

Hardness Values of GTA Weld Metal of Alloy 7 and Commercial MIL-100s-1 and MIL-120s-1 type Filler Wires Deposited on HSLA-100 and HY-130 Base Plates at 3.5 kJ/mm (90 kJ/in.) Heat Input.

FILLER METAL	BASE PLATE	SHIELDING GAS	HARDNESS	AVERAGE
Alloy 7	HSLA-100	Ar-5%CO_2	25, 26, 27, 26, 25, 26, 27, 26, 25	25.8 (HRC)
Alloy 7	HSLA-100	Ar-25%He	23.5, 26, 27, 28, 26, 24, 25, 24, 25	28.4 (HRC)
Alloy 7	HY-130	Ar-5%CO_2	33, 33, 33, 34, 31, 34, 33, 33, 31	32.7 (HRC)
Alloy 7	HY-130	Ar-25%He	33, 30, 31, 31, 30.5, 31, 30, 31, 30	30.8 (HRC)
MIL-100s-1	HSLA-100	Ar-5%CO_2	93.5, 96, 95, 94.5, 97, 93.5, 95, 94	94.8 (HRB)
MIL-120s-1	HSLA-100	Ar-5%CO_2	99.5, 101, 99.5, 98, 99, 99.5, 100, 100.5, 101, 98, 99.5, 98	99.4 (HRB)

BIOGRAPHICAL NOTE

The Author was born November 9, 1955, in New Delhi, India. He received a Bachelor of Technology degree in Metallurgy in 1978 from the Institute of Technology, Banaras Hindu University, Varanasi, India, and a Master of Science degree in Metallurgy in 1984 from the Indian Institute of Technology, Madras, India. He worked in the Ship Building and Offshore Oil Well Platform Fabrication Industry for six years and was a lecturer at the Regional Engineering College, Tiruchirapalli, India. He joined the then Oregon Graduate Center in Fall 1989 and completed the requirements for his Ph.D. degree in Materials Science and Engineering in January 1996. At the conclusion of this chapter of his life the author will like to quote the following words by Anees Jung:

"The seekers of truth climb the high hills in the hope of finding something permanent, something unchanging upon which to depend. Little do they realize that the journey is all there is."